New Insights into the Regulated Differentiation of Intercalated Cells in Mouse Kidney from Ae1 (Slc4a1) Deficient Mice

---

Dissertation

zur

Erlangung der naturwissenschaftlichen Doktorwürde

(Dr. sc. nat.)

vorgelegt der

Mathematisch-naturwissenschaftlichen Fakultät

der

Universität Zürich

von

Nicole Beate Kampik

aus Deutschland

Promotionskomitee

Prof. Dr. med. Carsten A. Wagner (Vorsitz und Leitung der Dissertation)

Prof. Dr. sc. nat. Jürg Biber

Prof. Dr. med. Johannes Loffing

Prof. Dr. med. Robert J. Unwin

Zürich, 2012

INDEX

ZUSAMMENFASSUNG

Die Niere der Säugetiere ist ein lebenswichtiges Organ, das eine Vielfalt von unterschiedlichen regulatorischen Funktionen erfüllt, wie z.B. die Aufrechterhaltung des systemischen Wasser-, Elektrolyte- und Säure-Basen Haushalts. Das renale Sammelrohrsystem setzt sich aus mindestens drei verschiedenen Zelltypen zusammen, die für die Feinabstimmung des finalen Urins verantwortlich sind. Dabei übernehmen die Hauptzellen (HZ) die Regulation von Wasser und Elektrolyten, wohingegen verschiedenen Arten von interkalierenden Schaltzellen (SZ) die Ausscheidung und Rückgewinnung von Säure-Basen Äquivalenten zukommt. Wie die Namensgebung andeutet, repräsentieren die Hauptzellen den am häufigsten vorkommenden Zelltypus im renalen Sammelrohrsystem und sind gelegentlich mit unterschiedlichen Typen von Schaltzellen (Typ A-SZ, Typ B-SZ) durchsetzt. Neben markanten Unterschieden in ihrer ultrastrukturellen Morphologie können die verschiedenen Zellen des renalen Sammelrohrs relativ einfach anhand von immunologischen Markern unterschieden werden. In der vorliegenden Studie werden Hauptzellen daher anhand eines immunologischen Nachweises des Wasserkanals Aqp2 (Aquaporin 2) identifiziert. Desweiteren werden die Säure sezernierenden Typ A-SZ von den Bikarbonat sezernierenden Typ B-SZ unterschieden, da diese beiden Typen am häufigsten im Sammelrohr vorkommen und bisher am ausführlichsten beschrieben wurden. Der immunologische Nachweis der V-ATPase (Protonenpumpe, a4 und B1 Untereinheit) dient im Allgemeinen als gemeinsamer Marker für Typen von Schaltzellen. Ferner gibt die subzelluläre Lokalisierung der V-ATPase Aufschluss über den Typus der SZ. Jedoch können die beiden Haupttypen der Schaltzellen eindeutig anhand der immunologischen Marker Ae1 (Anionen Austauscher 1, Slc4a1) für Typ A-SZ und Pds (Pendrin) für Typ B-SZ identifiziert werden.

Intensive Studien der letzten zwanzig Jahre haben stetig dazu beigetragen die komplexen Prozesse induktiver und reziproker Signalwege der metanephrischen Nierenentwicklung zu entschlüsseln und zu verstehen. Auch das ausgereifte gesunde Organ wurde bisher intensiv studiert und charakterisiert. Leider ist nur sehr wenig über die Abläufe, Signalwege und genetischen Programme bekannt, die für eine regulierte Enddifferenzierung und Reifung des sich entwickelnden Organs wichtig sind. Glücklicherweise haben einige kürzlich veröffentliche Studien an verschiedenen Modellorganismen ein wenig Licht ins Dunkel gebracht. Verschiedene Modulatoren aus den p53 und Notch Signalwegen, sowie die Transkriptionsfaktoren Foxi1 und Cp2l1 konnten letztendlich in Zusammenhang mit der terminalen Differenzierung des renalen Sammelrohrsystems gebracht werden.

Menschen und Mäuse, denen Ae1 in der Niere fehlt, entwickeln eine distale renale tubuläre Azidose (dRTA). Es ist bekannt, dass Störungen des Säure-Basen Haushalts eine adaptive Antwort der Niere induzieren, die auch eine morphologische Umwandlung des Nephron und Sammelrohrsystem zur Folge hat. In diesem Sinne führt eine chronische Säurebelastung zur Reduktion von Bikarbonat sezernierenden Typ B-SZ und gleichzeitigem Anstieg der Säure sezernierenden Typ A-SZ, wobei die individuelle und Zelltyp charakteristische Expression molekularer Marker (z.B. Ae1, Pds) unverändert bleibt. Interessanterweise konnte in der vorliegenden Studie eine ungewöhnliche Expression der Marker Pds und Aqp2 in den inneren medullären Sammelrohren von Ae1 defizienten Nieren mittels Immunfluoreszenz beobachtet werden. Hier wurde eine erhöhte Zahl an Pds exprimierenden Zellen sowie Aqp2/Pds coexprimierende Zellen im Nierenmark von Ae1 Knockout (KO) Tieren beobachtet. Dies steht im krassen Gegensatz zu Ae1 Wildtyp (WT) Nieren, bei denen eine Expression von Pds im Nierenmark nicht mehr vorkommt. Desweiteren konnten veränderte Expressionsmuster der Transkriptionsfaktoren Foxi1 und Cp2l1 in Ae1 defizienten Mausnieren festgestellt werden.

Gleichfalls wurde eine veränderte Expression von molekularen Markern der Schaltzellen in einer Nierenbiopsie eines Patienten mit der AE1 Mutation S613F beobachtet. Bei Untersuchungen zweier weiterer Mausmodelle mit unvollständiger dRTA (Knockout von Atp6v1b1 oder Rhcg) konnten derartige Veränderungen der Differenzierung von Zellen des Sammelrohres jedoch nicht festgestellt werden. Ein ähnlich negatives Ergebnis, in Bezug auf die terminale Differenzierung von Sammelrohrzellen, wurde in Nieren von Mäusen mit induzierter chronischer metabolischer Azidose über 8 Wochen gefunden. Daher kann geschlussfolgert werden, dass nicht die begleitende Azidose (dRTA) verantwortlich für die beschriebene abnorme Differenzierung des Sammelrohrs in Ae1 KO Mäusen ist, sondern das physische Fehlen von Ae1 *per se*.

Die vorliegende Studie bietet daher einige neue und interessante Erkenntnisse im Hinblick auf die terminale Differenzierung des renalen Sammelrohrsystems, die für die normale Entwicklung bzw. Regulation dieses Nephronabschnittes von Bedeutung sind. Es konnte gezeigt werden, dass die Transkriptionsfaktoren Foxi1 und Cp2l1 in unterschiedlichen Zelltypen des renalen Sammelrohrsystems exprimiert sind, was auf eine Modulation der terminalen Differenzierung durch benachbarte Zellen hindeutet. Im Einklang mit seiner Funktion als Regulator der Transkription verschiedener molekularer SZ Marker, wurde Foxi1 hauptsächlich in V-ATPase exprimierenden Schaltzellen gefunden. Cp2l1 hingegen wurde hauptsächlich in Aqp2 exprimierenden Hauptzellen detektiert, obwohl ein Fehlen von Cp2l1 auch in einem kompletten Verlust von renalen Schaltzellenmarkern (V-ATPase, Ae1, Pds) resultiert. Die Notch regulierte Signalkaskade scheint die Entwicklung der verschiedenen Zelllinien im renalen Sammelrohr der Maus zu dirigieren, vermutlich durch laterale Inhibition. Während eine Aktivierung von Notch die Präsenz von Hauptzellen in der Niere fördert, führt eine Inaktivierung von Notch zur Differenzierung von Nebenzellen.

Unter Einbeziehung der Beobachtungen an der sich entwickelnden Haut von Amphibien, der beschriebenen Resultate aus verschiedenen Mausmodellen und der

Resultate der vorliegenden Arbeit kann daher ein neues Modell für die terminale Differenzierung von Sammelrohrzellen in der Mausniere vorgeschlagen werden. Dementsprechend führt eine Aktivierung von Notch, vermutlich durch p53, zur Differenzierung von Hauptzellen aus renalen Vorläuferzellen und der Aktivierung von Cp2l1. Gleichzeitig führt die Aktivierung von Cp2l1 zur Inaktivierung von Notch in benachbarten Zellen, wodurch wiederum eine Aktivierung von Foxi1 erfolgt, welches eine Differenzierung der Schaltzellen fördert. Die Expression von Cp2l1 im Nierenmark von Ae1 KO Mäusen war gestört. Dies könnte darauf hinweisen, dass eine reziproke Interaktion oder Feedback-Schleife von Cp2l1 mit einem anderen unbekannten Schlüsselmolekül und Signalweg, oder eine negative Autoregulation von Cp2l1, im weiteren Verlauf erforderlich ist. Diesem Modell fehlt ein weiteres Schlüsselmolekül, das die Differenzierung eines bestimmten Typs von Schaltzellen interaktiv regulieren kann, da Foxi1 sowohl die Transkription von Ae1 als auch Pds reguliert. Die Ergebnisse der vorliegenden Studie unterstützen die Annahme, dass es sich bei diesem Schlüsselmolekül um den Cl^-/HCO_3^- Austauscher Ae1 selbst handeln könnte oder Ae1 damit interagiert. Zumindest scheint die Präsenz von Ae1 eine wichtige Rolle bei der Aufrechterhaltung eines bestimmten Typus der Schaltzellen zu spielen, da die Expression von Pds und Aqp2 im inneren Mark Ae1 defizienter Nieren gestört ist. Diese Hypothese wird auch dadurch gestützt, dass zuerst V-ATPase und Ae1 exprimierende Zellen in der embryonalen Niere detektiert werden und erst später Pds positive Zellen. Das bedeutet, dass sich Typ A-SZ in der zeitlichen Abfolge vor den Typ B-SZ entwickeln. Ae1 oder ein auf Ae1 basierender Multi-Protein Komplex (z.B. mit CaII) könnte also das vorangehende Modell komplettieren. Demzufolge würde eine Aktivierung von Foxi1 zur Expression von Ae1 in Typ A-SZ führen. Dies wiederum könnte eine reziproke Interaktion von Ae1 allein oder einem Ae1-Multi-Protein Komplex mit Foxi1 oder einem anderen unbekannten Molekül induzieren, um die Differenzierung von benachbarten Typ B-SZ im weiteren Verlauf zu regulieren und gleichzeitig den Typus der A-SZ in der Effektorzelle aufrechtzuerhalten.

SUMMARY

The mammalian kidney is an essential organ that serves a variety of distinct regulatory functions, such as maintenance of systemic water, electrolyte and acid-base homeostasis. The fine tuning of the final urine takes place in the renal collecting duct (CD) system, which consists of at least 3 different types of cells. The principal cells (PC) are mostly responsible for renal water and electrolyte handling, while several types of intercalated cells (IC) regulate the excretion and recovery of acid-base equivalents. As indicated by their name, principal cells represent the major CD cell type and are occasionally interspersed with distinct types of intercalated cells (type A-IC, type B-IC). Besides their marked ultrastructural morphologic differences, cells of the renal CD are easily distinguished by immunologic markers. Hence, the present study focuses on the identification of PCs by the immunologic presence of the water channel aquaporin 2 (Aqp2). Furthermore, acid secretory type A-ICs are distinguished from bicarbonate secretory type B-ICs, since these two types of ICs represent the most abundant and best characterized IC phenotype. The immunologic presence and subcellular localization of the V-ATPase (a4 and B1 subunit) is a common marker for the IC phenotype. However, the two major types of ICs are best distinguished using the immunologic markers anion exchanger 1 (Ae1, Slc4a1) for type A-ICs and pendrin (Pds) for type B-ICs.

The complex processes of inductive and reciprocal signalling required for initial metanephric kidney development were intensively studied over the past two decades steadily improving our basic understanding of nephrogenesis. Similarly, the adult and healthy organ is relatively well studied and characterized. However, the signalling events and regulatory genetic networks necessary for terminal differentiation and maturation of the developing kidney are still a black box as only very little is known. Lately, few studies with different model organisms shed some light into the dark and revealed a role for transcriptional regulators of the p53 and Notch signalling pathway,

as well as the transcription factors Foxi1 and Cp2l1 in terminal differentiation of the renal CD system.

Humans and mice deficient for renal Ae1 develop distal renal tubular acidosis (dRTA). Acid-base disturbances are known to induce adaptive responses in the kidney involving the remodelling of the nephron and collecting duct system. In addition, chronic acid challenges promote the reduction in number of base secretory type B-ICs, while the relative abundance of type A-ICs increases concomitantly. Nevertheless, the individual characteristics of the IC phenotype are preserved under these circumstances. However, in kidneys of mice with Ae1 deficiency related dRTA, an abnormal expression of Pds and Aqp2 was detected in the inner medullary collecting ducts by immunofluorescence. In contrast to wildtype (WT) mouse kidneys, Pds expressing cells and unusual Aqp2/Pds coexpressing cells were increased in abundance in the inner medulla of Ae1 knockout (KO) mice. Furthermore, the expression pattern of the transcription factors Foxi1 and Cp2l1 was altered in Ae1 deficient mouse kidneys.

Consistent with the abnormal expression of CD cell marker in Ae1 deficient inner medullary collecting ducts, we found an altered expression of molecular IC markers in a renal biopsy of a patient with the AE1 S613F mutation.

Investigations of two mouse models with incomplete dRTA (Atp6v1b1 deficiency and Rhcg deficiency) did not show any signs of abnormal CD cell differentiation. Likewise, chronic metabolic acidosis induced for eight weeks in wildtype mice did not alter the terminal differentiation of renal CD cells in mice. Hence, the accompanying dRTA or acidosis is most likely not responsible for the observed abnormal CD cell differentiation of Ae1 deficient mice, but the physical lack of Ae1 *per se*.

The present study provides some interesting and unexpected new aspects regarding the terminal differentiation of the renal CD system. Surprisingly, we localized the transcription factors Foxi1 and Cp2l1 in distinct cell types of the renal CD system, suggesting a modulation of the terminal differentiation of adjacent cells. Consistent

with its regulatory role in molecular IC markers, Foxi1 was localized in V-ATPase expressing ICs. However, Cp2l1 was mostly observed in Aqp2 expressing PCs, although Cp2l1 deficiency results in loss of characteristic molecular markers (Ae1, V-ATPase) of renal ICs. Notch signalling seems to determine the cell lineage of renal CDs in mouse, probably by lateral inhibition. While activated Notch favours the presence of PCs, inactivated Notch promotes the differentiation of renal ICs. Considering observations from amphibian skin development, other mouse models and results from the present study, we suggest the following new model of terminal CD cell differentiation in mouse kidney. Activation of Notch, probably by p53, leads to the differentiation of PCs from renal precursor and may activate Cp2l1. Active Cp2l1 might promote the inactivation of Notch in adjacent cells, which in turn activates Foxi1 and IC differentiation. Cp2l1 was abnormally expressed in the renal inner medulla of Ae1 deficient mice. Therefore, a reciprocal interaction or feedback loop of Cp2l1 with another combinatorial unknown key molecule and signalling pathway or by sequential negative autoregulation seems necessary. However, another key regulatory molecule that determines the type of ICs is missing in this model. We provide data that suggest the Cl^-/HCO_3^- exchanger Ae1 as a required key protein in the induction or maintenance of terminal differentiation of renal ICs. During embryonic kidney development, V-ATPase and Ae1 expression are detected before Pds, suggesting that A-ICs differentiate before type B-ICs. Completing the proposed model, Ae1 itself or a multiprotein-Ae1 complex (i.e. with CaII) might reciprocally interact with Foxi1 or (an)other transcriptional regulator(s). Hence, activated Foxi1 would primarily favour the differentiation of type A-ICs, which are characterized by their expression of Ae1. The multi-protein complex or Ae1 alone might than reciprocally interact with Foxi1 or another unknown molecule, which in turn regulates the differentiation of neighbouring type B-ICs and simultaneously maintains the A-IC phenotype in the effector cell.

1. INTRODUCTION

Multicellular organisms have the ability to maintain their systemic pH within narrow ranges, despite constant local and systemic changes of acid and base equivalents due to metabolic and catabolic processes. A stable *milieu interieur* is essential to ensure an optimal (working) environment for all chemical and bio-physical processes in the organism. In humans, the pH of most extracellular fluids ranges from 7.35 – 7.45 and is tightly regulated by two buffering systems, the volatile and non-volatile buffers. By definition, buffers are substances in aqueous solutions that are able to reversibly accept or donate hydrogen ions (H^+) and thus stabilize a given pH. In mammals systemic pH is maintained by non-volatile buffers like calcium carbonate, phosphate, hemoglobine and other proteins, uric acid and ammonium. However, the most important buffer system is the volatile carbon dioxide/bicarbonate buffering system, which is enabled by the action of the lungs and kidneys. The constant exhalation of carbon dioxide (CO_2) by the lungs and the renal regulation of bicarbonate (HCO_3^-) makes this buffer pair a powerful and theoretically infinite, open buffering system.

The pH dependency on the pCO_2/HCO_3^- ratio is described by the Henderson-Hasselbalch equation (Eqn. 1). Accordingly, changes in blood pH are caused by shifts in the partial pressure of CO_2 (pCO_2) in blood, or by variations of blood bicarbonate concentrations.

Eqn. 1 $$pH = 6.1 + \log \frac{[HCO_3^-]}{0.03 \times pCO_2}$$

Carbon dioxide is a waste product of cell respiration and reacts slowly with water to form carbonic acid, which rapidly dissociates to a proton and bicarbonate (Eqn. 2). The hydration reaction is usually accelerated and catalyzed by isoforms of the enzyme carbonic anhydrase.

Eqn. 2 $CO_2 + H_2O \Leftrightarrow H_2CO_3 \Leftrightarrow H^+ + HCO_3^-$

In mammals volatile CO_2 is a huge source of daily acid production (15,000 mmol CO_2/day) [1]. However, since the lungs continuously remove this potential acid by regulated exhalation, this amount is less relevant in healthy individuals. Importantly, dietary metabolism and daily loss of base equivalents into stool lead to the accumulation of non-volatile acids (70 mmol/day) [1], which essentially consume plasma bicarbonate and thus need to be removed from the body. Here, the kidneys play the essential role in the removal of this daily load of non-volatile acids by recovering virtually all filtered bicarbonate as well as generating new bicarbonate. The kidneys generate new bicarbonate in two ways: the secretion of protons along with titratable acids (i.e. phosphate, citrate) and the synthesis and excretion of ammonium.

2. MAMMALIAN KIDNEY STRUCTURE AND DEVELOPMENT

2.1 Organization of the mature mammalian Kidney

The mammalian kidney is a paired organ fulfilling a variety of essential functions. Besides the removal and excretion of metabolic waste products from the blood, it plays a central role in systemic acid-base balance, as well as maintaining salt and water homeostasis thereby regulating systemic blood pressure. The functional unit of the kidney is the nephron, which is organized in different segments (Fig. 2.1). In humans, each kidney consists of 800.000 – 1.200.000 nephrons, whereas in mouse approximately 11.000 nephrons are present [1, 2]. Each nephron begins with a glomerulum, which is a network of blood capillaries and podocytes that filter blood. The glomerulum is surrounded by the Bowman capsule that extends into an epithelial tubular structure (renal tubule) and finally connects to the collecting duct system (CDS). The nephron is subdivided into three domains, the proximal tubule (PT), the loop of Henle (LOH) and the distal tubule (DT). Based on ultrastructural and functional properties these domains are further distinguished into the early PT, the proximal convoluted and straight tubule, thin descending and ascending limbs of LOH, thick ascending limb of LOH, as well as distal convoluted tubule (DCT) and connecting tubule (CNT). Likewise, the renal collecting duct system shows a segmental organization and cortical collecting duct (CCD), outer medullary collecting duct (OMCD) and inner medullary collecting duct (IMCD) are distinguished.

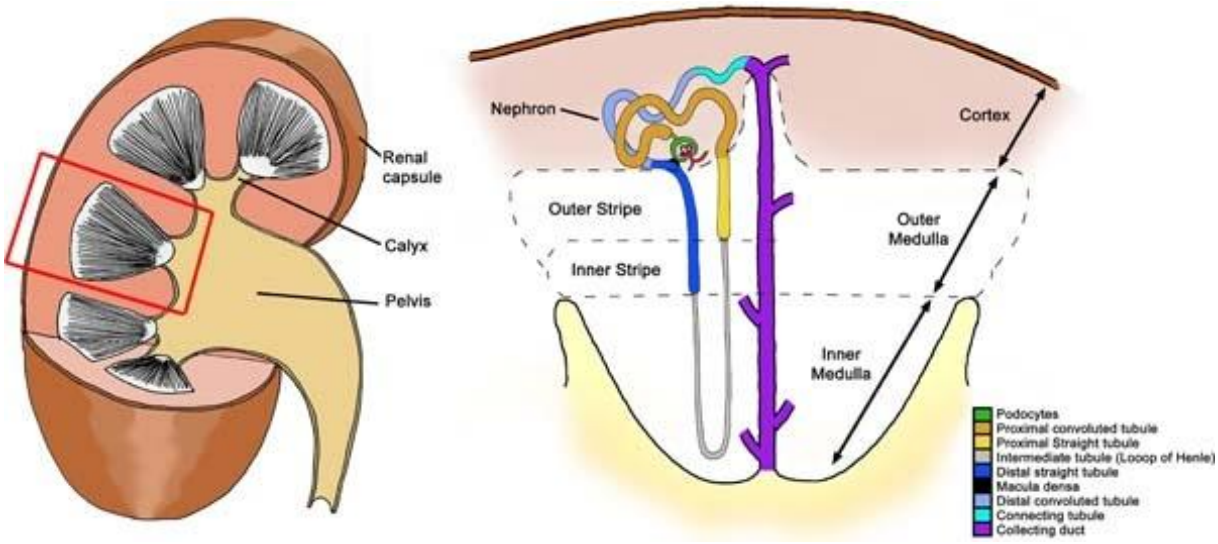

Fig. 2.1 Structure of the mammalian kidney, taken from [2]. Each kidney is surrounded by a fibrous renal capsule. The kidney is organized into the peripheral renal cortex and the renal medulla, which is arranged in multiple pyramidal structures. The tip of each pyramid (papilla) ends into minor and major calyces that empty into the renal pelvis. The renal pelvis is connected to the ureter which transmits the urine into the bladder. Image enlargement shows segmental organization of the nephron and collecting duct [2].

2.2 Development of the mammalian Kidney

The development of the mammalian kidney (metanephros) is unique, as it origins from two distinct embryonic precursor populations, the metanephric mesenchymal blastema and the ureteric bud epithelia [3]. Hence, morphogenetic and functional development of the kidney requires complex inductive interactions of the distinct precursor populations and their differentiation pathways are tightly regulated in time and space by different geneproducts. Among them are transcription factors, protooncogenes, growth factors, signalling molecules, and receptors. However, kidney morphogenesis is also dependent on cell adhesion molecule complexes (CAM) and their associations with the cytoskleleton, extracellular matrix (ECM) glycoproteins and ECM receptors like the integrins, as well as ECM degrading proteases [4]. Mammalian kidney development is further characterized by the formation of a more complex organ in three successive phases: the rudimentary pronephros, the transitory

mesonephros, and the permanent metanephros. In mammals and birds, the pronephros and mesonephros are transient structures, which degenerate or become modified to serve as a part of the male genital tract [5], while the metanephros differentiates into the permanent kidney. However, the pronephros is the functional filtering unit in larvae of amphibians and fish, while the mesonephros is the functional kidney in adults [6]. Thus, the three kidney forms of amniotes reflect the evolutionary development of the kidney approved by conserved genetic programming among different species [7].

The metanephros is the most complex structure and displays the functional kidney of adult mammals and birds. The development of the mammalian metanephric kidney is initiated at week 4-5 in humans and embryonic day 8.5 (E8.5) in mice [2, 4]. It begins with the formation of the pronephric duct (Wolffian duct) and mesonephric tubules from the intermediate mesoderm (Fig. 2.2). As they fuse and migrate into the adjacent metanephrogenic mesenchyme (MM), the ureteric bud (UB) emerges at the tip.

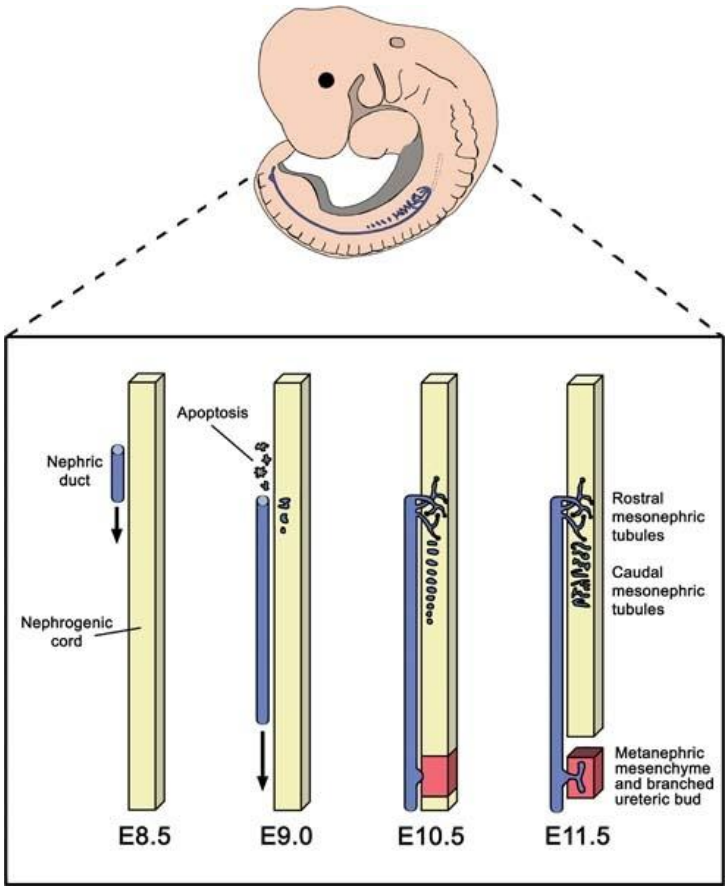

Fig. 2.2 Initiation of kidney development in mouse, taken from [2]. In mouse, kidney development starts at E8.5 with the formation of the nephric (Wolffian) duct primordium (blue) from the nephrogenic cord (intermediate mesoderm, yellow). Caudal nephric duct precursors grow towards the cloaca, while rostral cells become apoptotic. The extending nephric duct induces the formation of mesonephric tubules in the adjacent mesoderm. Rostral mesonephric tubules fuse to the nephric duct, while the ureteric bud (UB) emerges from the nephric duct near the cloaca at E10.5. The UB invades into a specialized population of nephrogenic cord cells (red), the metanephric mesenchyme (MM). Reciprocal inductive interactions between UB and MM lead to repeated branching of UB and the formation of metanephric nephrons from MM (not shown).

Reciprocal inductive interactions between the UB and MM are the key events of mammalian nephrogenesis (Fig. 2.3) and accompanied by the sequential activation of gene expression from several different gene families [6]. The MM induces a repetitive branching morphogenesis of the UB, which gives rise to the collecting system. Simultaneously, the invading UB induces a mesenchymal to epithelial transition (MET) of the MM, forming metanephric nephrons in a stereotypic sequence of morphological stages (Fig. 2.3) [8].

2.3 Formation of the Nephron

The epithelial segments of the nephron, which comprises the glomerulum, proximal tubule, loop of Henle and the distal tubule (distal convoluted tubule and connecting tubule) arise from the metanephric mesenchymal blastema. Nephron development requires a series of events which is defined by morphological stages and can be divided into different steps: 1) condensation, 2) epithelialisation, 3) early morphogenesis and 4) tubule maturation [9]. Upon ureteric bud induction, cells of the MM start to condensate around the advancing UB, forming a 4-5-cell thick layer, the cap condensate (Fig. 2.3). A cluster of cap condensate cells near the UB ampulla and the adjacent branch starts to polarize as they undergo mesenchymal to epithelial transformation. These cells separate from the cap condensate and reorganize in a pretubular aggregate to form a renal vesicle. Pluripotent precursor cells within the renal vesicle give rise to all type of glomerular and tubular epithelial cells. Nephron segmentation into globular and tubular domains is induced by the formation of two clefts within the renal vesicle. Firstly, a comma-shaped body forms with the invagination of a lower cleft (vascular cleft). Thereafter, a second upper cleft builds up the S-shaped body, which is characterized by three segments or limbs. The upper limb gives rise to the LOH and distal tubule, the middle limb to the proximal convoluted tubule and the lower limb to the glomerulum. Angioblasts invade the vascular cleft of the S-shaped body and contribute to the glomerular capillary. Finally, the distal part (upper limb) of the S-shaped body fuses to the adjacent collecting duct, completing the formation of the nephron (detailed review by [10]).

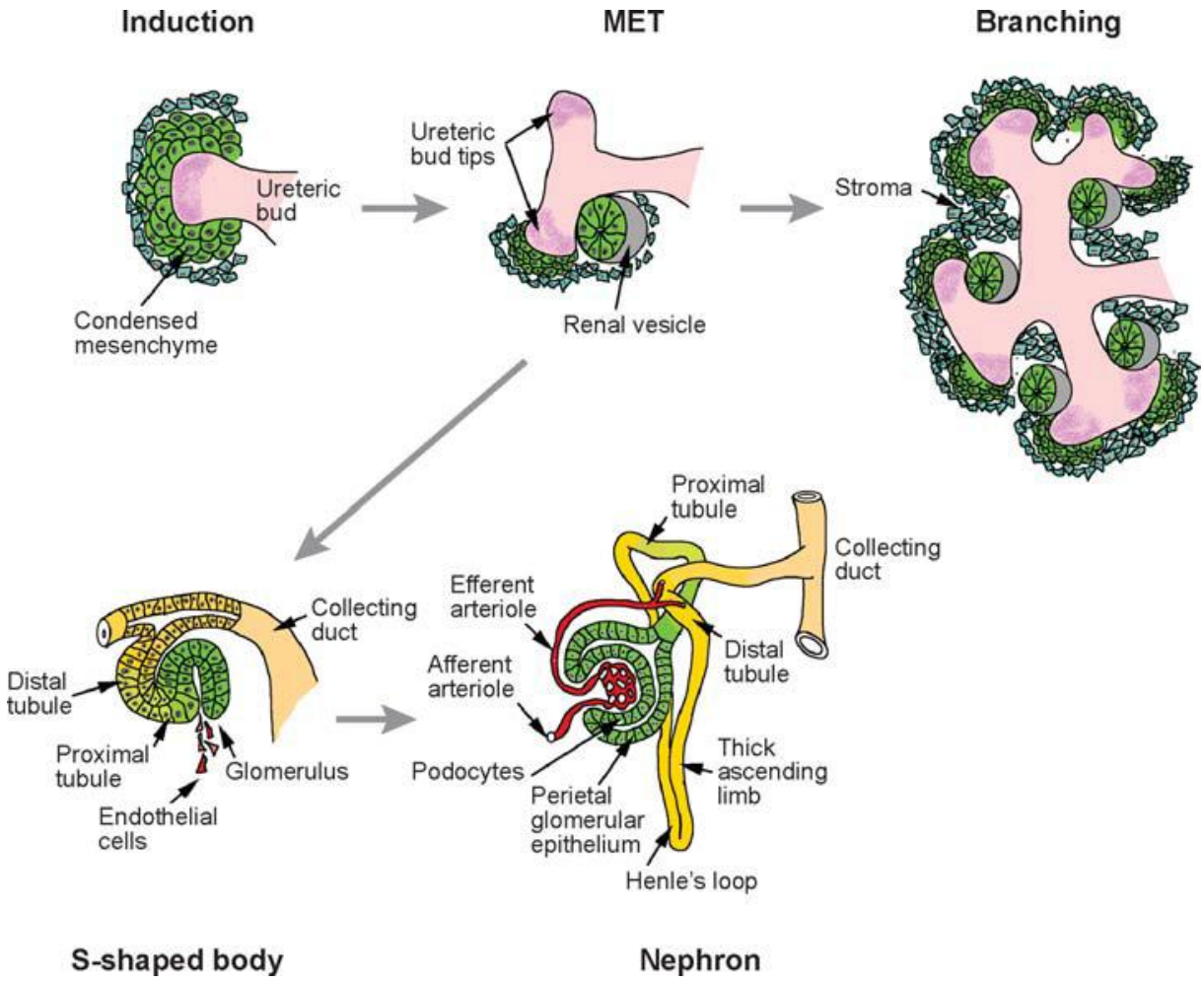

Fig. 2.3 Sequential steps of mammalian kidney development, taken from [7, 10]. Induction of the metanephric mesenchyme by the ureteric bud promotes aggregation of mesenchymal cells to form a cap condensate around its tip. A cluster of cells separates from the cap condensate and forms a renal vesicle while they polarize and undergo mesenchymal to epithelial transformation (MET). Meanwhile, unpolarized stromal mesenchyme cells migrate into the interior of the developing organ. Thereby, they influence branching morphogenesis of the ureteric bud which continues to induce nephrogenesis. Individual renal vesicles fuse to the proliferating collecting ducts. By the S-shaped body stage, the nephron is already patterned along the proximal-distal axis. Invasion of the proximal cleft by endothelial cells starts the process of glomerulogenesis [7, 10].

2.4 Formation of the renal Collecting System

The renal collecting system comprises the cortical and medullary collecting ducts, the renal calyces, the renal pelvis and the ureter. It develops from the ureteric bud by a process called branching morphogenesis while it invades the MM. Repetitive dichotomous branching events result in several generations (~15) of UB branches, which ultimately differentiate into distinct parts of the renal collecting system. The number of UB branches elaborated is considered to be a major determinant of the final number of nephrons, since the UB branch tips (ampullae) reciprocally induce discrete subsets of MM cells to undergo nephrogenesis [10]. Thus, UB branching morphogenesis might also determine the later architecture of the mature kidney [11]. Ureteric branching is completed by weeks 20-22 of gestation in humans and at E15.5 in mouse [7, 10]. Thereafter, the collecting duct system undergoes morphologic changes that result in the patterning of cortical (peripheral) and medullary (central) domains. At this stage, distinct morphologic features emerge between the cortical and medullary collecting ducts (CDs) [12]. While cortical CDs continue to undergo branching and induction of MM, medullary CDs organize into elongated, relatively unbranched linear arrays [12]. The main trunk of the UB gives rise to the mature ureter, while the early branches undergo remodelling by increased growth and dilatation to form the renal calyces and pelvis [12, 13].

2.5 Terminal Differentiation and Organization of the renal Collecting Duct System

Intensive *in vivo* and *in vitro* studies revealed many factors and molecules involved in UB outgrowth, branching morphogenesis and induction of mesenchymal to epithelial transition [14]. However, regulatory mechanisms of terminal CD system differentiation and maturation are still largely unknown. During organ development the function of the embryonic collecting duct epithelium needs to transdifferentiate from an inductive to an excretory system [15]. The architecture of the mature renal CD system is unique as it is composed of distinct cell types with highly specialized functions (see Chapter 2.6 and 3.4). Hence, the process of terminal differentiation goes along with the acquisition of functional differentiation and requires cell cycle arrest [16]. Our knowledge of the genetic programs and signals that regulate functional differentiation of the kidney has only just begun. A small number of key regulators and pathways such as the p53 and Notch signalling cascade were proposed to determine segmental nephron identity and terminal epithelial differentiation fate. Within these pathways, some transcription factors and signalling molecules (i.e. Bdkrb2, Cp2l1, Dmbt1 (Hensin), Foxi1 and Klf4) are suggested critical for the regulated differentiation of individual CD cell types. However, their hierarchical positioning within the signalling network remains to be determined. The majority of these molecules was incidentally discovered in disease models or deduced from *in vitro* studies and will be described in more detail in chapters 2.7 and 5.2.1.

The morphology of the mature renal collecting duct system in mammals is characterized by its functional, zonal and cellular heterogeneity, accounting for the functional demands of final urine processing [15]. At least three types of cells are identified based on ultrastructural features (i.e. distribution of intracellular organelles, organization of plasma membrane), molecular composition and function. Even though they are unequally distributed throughout the CD system, principal cells (PCs)

are the major cell type and responsible for water and electrolyte transport. Occasionally, the CDs are interspersed with two types of intercalated cells, type-A and type-B (A-IC, B-IC), which are involved in acid-base excretion and show a zonal distribution. In the mature mouse kidney, A-ICs are most frequently present within the outer medulla, while B-ICs are restricted to the renal cortex (Fig. 2.4) [17]. Furthermore, both types of intercalated cells are present in the late DCT and CNT [18-21]. However, based on immunologic and morphologic criteria species specific intermediate forms of intercalated cells have been described (detailed description in chapter 2.6) [22-24]. In any case, it remains controversial, whether the different ICs are truly distinct cell types or represent several configurations of the same cell [18].

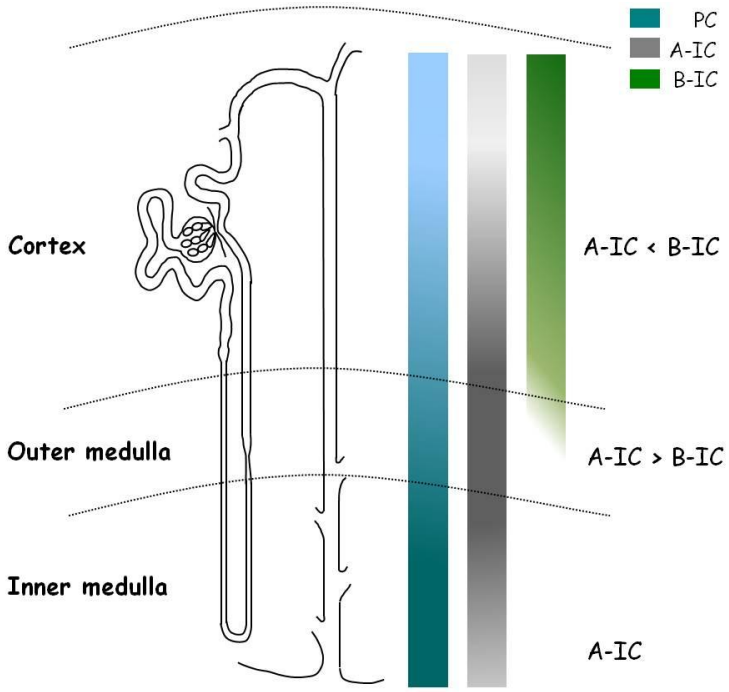

Fig. 2.4 Zonal distribution of cell populations in mouse renal collecting duct system, identified by immunologic criteria. Within the mature renal CD system, principal cells (PCs, blue bar, left) are the major cell type. However their abundance increases from the cortex towards the inner medulla. Type A-ICs (grey bar, centre) are predominantly expressed within the outer medullary CDs, whereas type B-ICs (green bar, right) are exclusively found in the renal cortex.

However, good evidence for the simultaneous differentiation of ICs from undifferentiated precursor populations in separate foci of the kidney in rodents was found [18, 25-27]. In mice, immunohistochemical identification of ICs demonstrated their contemporary appearance in the fetal connecting tubule and medullary collecting duct (MCD), while cortical collecting ducts appeared still not differentiated (Fig. 2.5, top). Hence, ICs seem to develop from distinct precursor populations which are present in both, the metanephrogenic blastema and the ureteric bud. Nevertheless, it remains speculative, whether PCs and the distinct types of ICs derive from the same or from distinct precursor populations.

In fetal rat kidneys immunologic marker identifying ICs are not detected before embryonic day 18 (E18) [18, 28]. In mice, renal IC specific proteins are detected the earliest at E13 and E14, respectively (Fig. 2.5) [25]. Consistently, cellular expression levels of transporters and other proteins adapt to the increasing functional demands. A sequential and segmental regulation of intercalated cell subtypes and differential expression of characteristic proteins (i.e. V-ATPase, CaII) were observed during tubule maturation (Fig. 2.5) [29, 30]. Soon after birth, the maturing renal tubule develops excretory and reabsorptive functionality and progressively achieves the morphology of the adult kidney by adaptive remodelling [31]. Hereby, ICs are gradually removed from the papillary surface epithelium and terminal MCDs, while their abundance increases erratically in the renal cortex and outer medulla, respectively (Fig. 2.5, bottom) [32]. Moreover, pendrin expressing B-ICs disappear completely from the entire mature MCDs and are restricted exclusively to the late DCT (DCT2), CNT, CCD, and early OMCD [21, 25-27, 31, 33]. Elimination of ICs from the developing rat MCD might involve two mechanisms. Type A-ICs seem to be extruded from the renal epithelium into the lumen, while type B-ICs become apoptotic and are phagocytosed by adjacent cells [32].

In human fetal kidney immature or undifferentiated ICs are observed as early as 8 weeks gestation, while characteristic AE1 expression is not detected before 14 weeks gestation. Moreover, Pendrin expression is observed only as late as 26 weeks gestation and solely restricted to the fetal renal cortex. Additionally and likewise in contrast to rodents, IC abundance in human fetal kidney increases progressively from the inner cortex to the inner medulla with type A-ICs being the predominant IC manifestation [27].

In outlook of the mature collecting duct epithelium, a structural and functional plasticity of the relative IC distribution has been observed as well in adaptive responses to disturbances of the *milieu interieur*. These observations raised the concept on reversal of structural and functional polarity in intercalated cells, with a definite proof still pending (detailed description in chapter 5.2.1) [17].

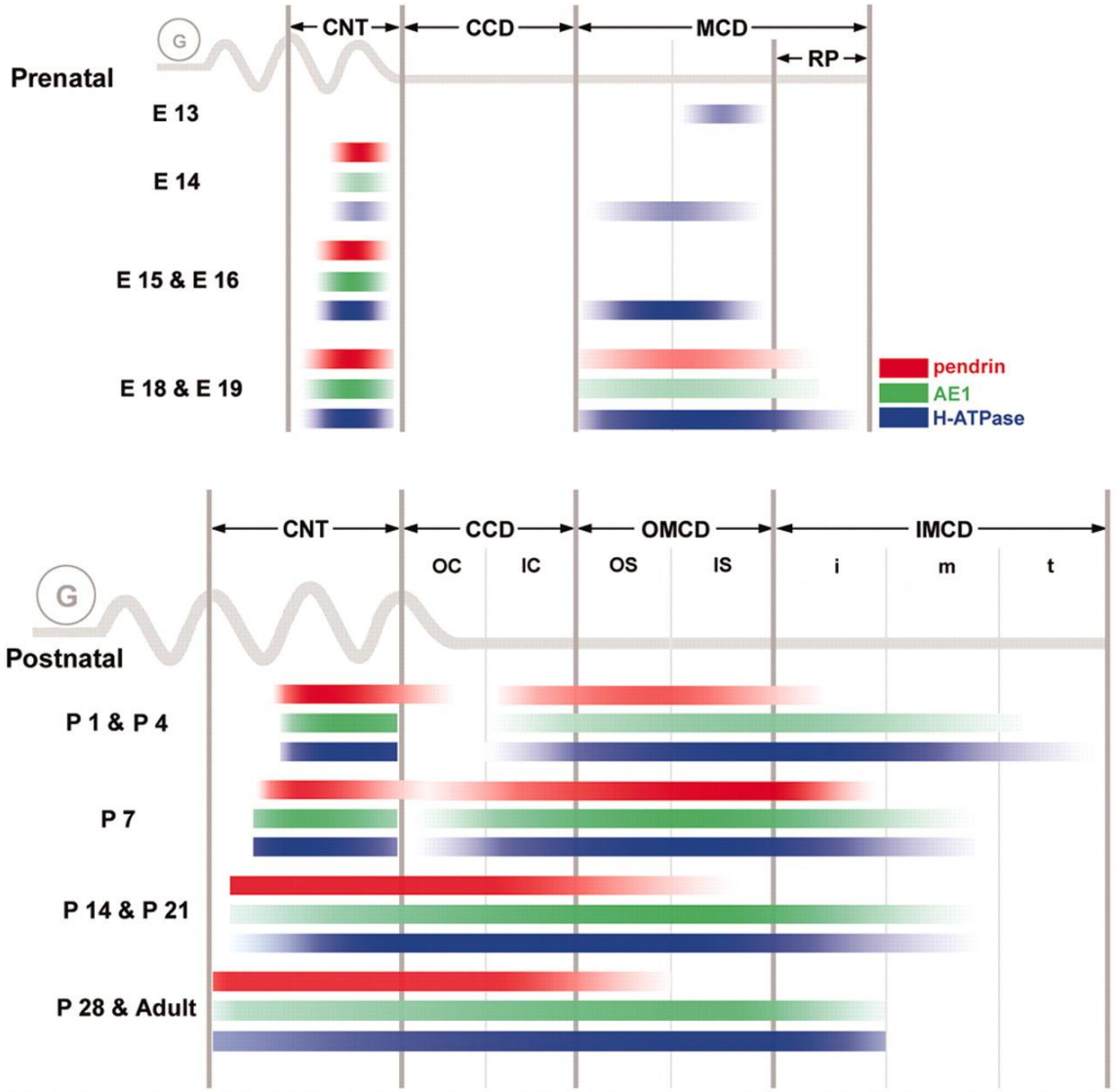

Fig. 2.5 Segmental distribution of acid-base transporters expressed in renal intercalated cells of the developing mouse, taken from [25]. E= embryonic kidney; P= postnatal kidney; RP= renal papilla; OC= outer cortex; IC= inner cortex; OS= outer stripe of outer medulla; IS= inner stripe of outer medulla; i= initial part of IMCD; t= terminal part of IMCD. It is of note, that H^+-ATPase and pendrin expressing cells are already detected in the late distal convoluted tubule (DCT2) of mouse, rat and human kidney (not shown) [21].

2.6 Architecture and Characteristics of renal Collecting Duct Cells

Intensive studies on the heterogeneous cytology of mammalian collecting ducts revealed numerous ultrastructural and molecular differences among cell types accounting for their distinct function. However, transitional changes of the structural appearances of each cell type are described all along the CD system, while molecular profiles and functional aspects remain rather constant. For the sake of simplicity, the present study focuses on the identification of principal cells and intercalated cells (type A and type B) by immunohistochemical markers.

2.6.1 Principal Cells

By light-microscopy, principal cells appear translucent while intercalated cells appear dark due to their high density of mitochondria. In higher magnification, the apical membrane of PCs consists of a prominent single cilium with few and short microvilli and microfoldings. The basal membrane forms infoldings (basal labyrinth), which appear as a characteristic basal rim, as it is devoid of any cell organelles. However, principal cells undergo gradual, from the deep cortex towards the upper third of the inner medulla, but species specific distinct morphological changes regarding the abundance of mitochondria, lysosomal organelles and basal infoldings. Subsequently, the cell size may increase drastically (rabbit, guinea pig) and the cell shape might change from polygonal to cuboidal or low columnar (rat, mouse) [17]. However, immunologically all variations of principal cells are identified by the luminal and sometimes basolateral expression of aquaporin 2 (Aqp2), (Fig. 2.6) [34, 35].

2.6.2 Intercalated Cells

As mentioned earlier, the renal CNTs and CDs are interspersed with distinct manifestations of intercalated cells. Among the diverse IC cell population, species specific differences regarding structural manifestations, protein expression profiles and cellular pattern, as well as axial changes in their zonal distribution along the CNT and CD system have been described [26, 36-39]. All these subtypes share some common features and are involved in potassium and chloride reabsorption and acid-base homeostasis [40]. The apical membrane of ICs is usually more rounded, compared to the polygonal architecture of adjacent PCs. Intercalated cells appear darker by light microscopy because of their densed cytoplasm, which contains numerous mitochondria, polysomes and tubulovesicular membrane structures. Moreover, the luminal membrane carries elaborate microfolds or microprojections and lacks the single cilium [17]. Immunologically, intercalated cells are characterized by their expression of cytosolic carbonic anhydrase II (CaII) and a vacuolar type H^+-ATPase (V-ATPase) (Fig. 2.6) [41, 42]. However, two IC manifestations are predominant and distinguished as type A and type B.

2.6.2.1 Type A-Intercalated cells

The apical cell pole of type A-ICs is usually broad and covered with elaborate microfolds and characteristic tubulovesicular structures. The apical and vesicular membrane domain is densely covered with studs. Type A-ICs are equipped with numerous mitochondria, which often arrange along the apical membrane and the nucleus shifted to the basolateral side [42]. Many microtubules and clathrin-coated vesicles are located between the tubulovesicular profile and mitochondria [17, 43]. Correspondingly, high abundance of the V-ATPase in the apical pole and membrane was demonstrated and is usually evident of type A-ICs [22, 24, 44]. The basolateral membrane of A-ICs is uncoated and devoid of V-ATPase. A kidney specific isoform of the Cl^-/HCO_3^- exchanger Ae1 (anion exchanger 1, band3, Slc4a1) is exclusively

expressed in the basolateral membrane of type A-ICs and serves as an immunologic marker (Fig. 2.6) [43, 45]. Thus, A-ICs are considered as acid secretory cells and show marked hypertrophy and hyperplasia under conditions of metabolic and respiratory acidosis and potassium depletion [17].

2.6.2.2 Type B-Intercalated cells

In many respects type B-ICs are structurally and functionally opposite to type A-ICs (as summarized in detail by [17]). Compared with type A-ICs, the apical cell pole of B-ICs is usually narrow, with few and short microvilli, while the basal pole is broad with tightly arranged deep infoldings of the membrane. B-ICs exhibit a characteristic homogeneous belt of dense vesicle-free cytoplasm, containing filamentous compounds, just below the apical membrane [42]. Thus, mitochondria usually align along the lateral membrane and vesicles are distributed throughout the remaining cytoplasm. Type B-ICs contain a large Golgi-Complex with abundant smooth endoplasmic reticulum, exhibiting clathrin-coated heads. Polyribosomes, microtubules, lysosomes and phagolysosomes are much more frequently present in B-ICs than A-ICs [17]. In contrast to type A-ICs, B-ICs usually lack apical V-ATPase expression and correspondingly apical vesicles and studs. Instead, V-ATPase and coated studs are abundant in the basolateral membrane domain [17, 42]. Lectin-immunoreactivity of the luminal membrane to peanut agglutinin (PNA) identifies B-ICs. However, a member of the Slc26 family, pendrin (Pds, Slc26a4) was finally identified as the long missing exclusive Cl^-/HCO_3^- exchanger on the luminal membrane of B-ICs [46, 47]. Thus, B-ICs serve as bicarbonate secreting cells, mirroring the action of A-ICs, allowing the fine tuning of urinary acid-base excretion [33].

2.6.2.3 Intermediate forms of Intercalated Cells

Based on morphologic criteria, intermediate variants of ICs, which cannot be attributed to type A-ICs nor type B-ICs, have been observed [17]. One manifestation of these intermediates is frequently observed in rat and mouse renal CNT and CCD and is referred to as non-A/non-B intercalated cells (non-A/non-B-IC), as they display features of both, type A-ICs and B-ICs. The non-A/non-B cells are characterized by the luminal presence of both, V-ATPase and Pds, as well as the absence of basolateral Ae1 (Fig. 2.6) [42, 46, 48]. Functionally, the equilateral expression of V-ATPase and Pds would result in the parallel secretion of H^+ and HCO_3^- in the exchange for luminal Cl^-. However, it remains controversial, whether non-A/non-B cells represent a distinct cell type or a specific activity state of B-ICs [33].

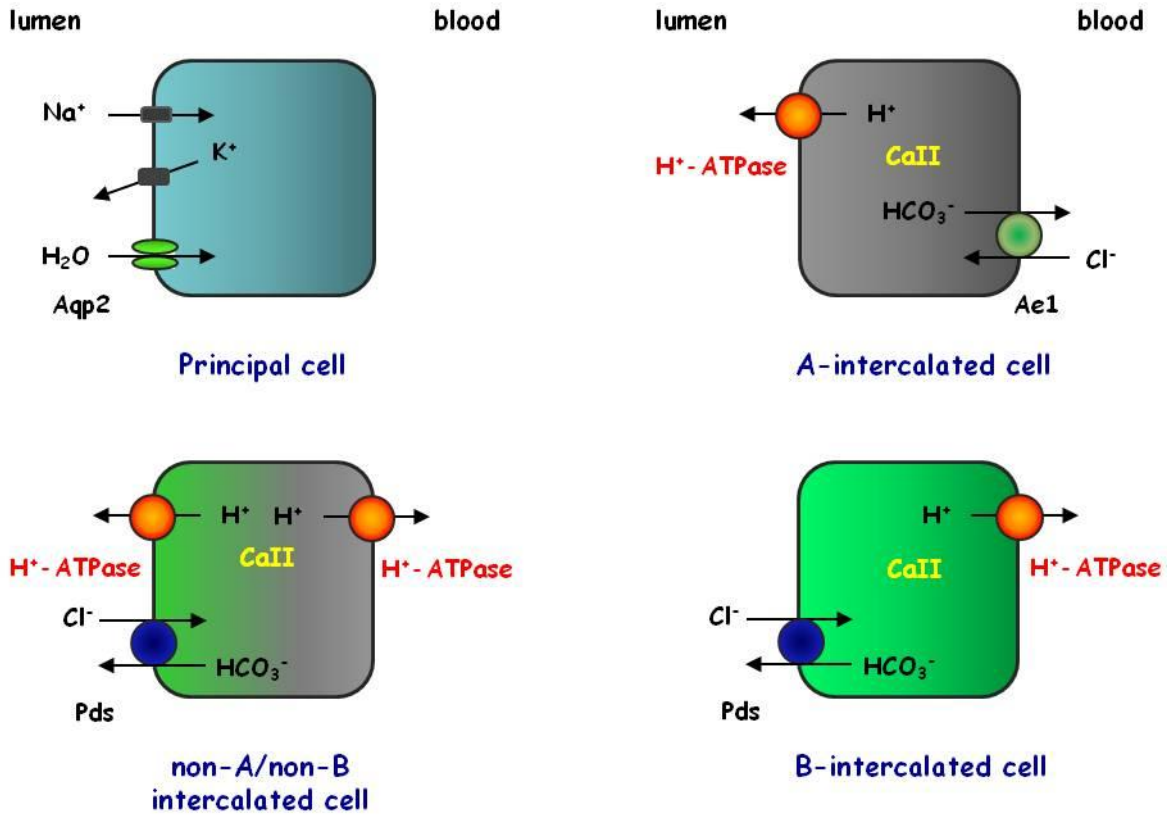

Fig. 2.6 Schematic representation of molecular collecting duct marker.

Immunohistochemically, principal cells along the CNT and CD are identified by the luminal presence of aquaporin 2 (Aqp2). Type A-intercalated cells are characterized by the luminal expression of V-ATPase (H^+-ATPase) and basolateral expression of anion exchanger 1 (Ae1). In type B-intercalated cells the V-ATPase is expressed on the basolateral membrane, while pendrin (Pds) is found on the apical side. Type non-A/non-B intercalated cells share features of both, type A-IC and type B-IC, with luminal coexpression of V-ATPase and Pds in the absence of basolateral Ae1. Moreover, some type non-A/non-B-ICs express the V-ATPase on the apical and basolateral membrane simultaneously. All types of intercalated cells express high levels of cytosolic carbonic anhydrase II (CaII).

2.7 Disturbances of terminal renal Collecting Duct Differentiation

Even though the pathways and modulators of late embryonic renal CD differentiation are largely unknown, a variety of distinct molecules were discovered and suggested to play a role in mouse CD differentiation and adaptive plasticity of the mature nephron. Among them are receptors, signalling molecules, transcription factors, enzymes and transport proteins [49]. Strong evidence for most of the regulatory molecules and pathways comes from mouse disease models and *in vitro* experiments. However, developmental studies of other model organisms, such as zebrafish (pronephros and epidermis) and *Xenopus laevis* (larval skin), are of great support, as they share structure-function similarities and conserved regulatory mechanisms with the mammalian renal CD system (Fig. 2.7) [50-53].

The differentiation of ionocytes (proton-secreting cells, PSC) in the larval epidermis of *Xenopus laevis* is probably the best available model, resembling mammalian renal intercalated cells. It has been shown recently, that two types of ionocytes are present and distributed in a "salt and pepper" fashion in the *Xenopus* larval skin. Similar to mammalian renal ICs, *Xenopus* type alpha-ionocytes (A-INCs) are characterized by the basolateral expression of ae1 and apical v-ATPase, while type beta-ionocytes (B-INCs) express apical pendrin and basolateral v-ATPase [51]. Moreover, differentiation of the ionocyte subtypes is regulated by notch activity and the downstream targets upstream binding protein 1 (ubp1) and foxi1 (Fig. 2.7) [51].

Xenopus ubp1 belongs to the family of grainyhead transcription factors (chapter 2.7.4) and shares close sequence similarities with the leader binding protein 1a (Lbp1a) of mouse and men. However, direct orthologues of ubp1 in mouse and men were not reported [51]. Additionally, based on its proposed functional role, *Xenopus* ubp1 rather resembles an orthologue of mammalian Cp2l1 (chapter 2.7.4) [51].

However, in *Xenopus* larval skin, expression of foxi1 was found in both types of ionocytes, whereas ubp1 seems to localize specifically with pendrin expressing B-INCs. Interestingly, notch activity might mediate the regulation of ubp1 and foxi1 in a dose dependent manner. Strikingly, the notch signalling pathway, as well as the transcription factors Foxi1 and Cp2l1 (mammalian orthologue of ubp1) are suggested critical determinants of mammalian renal IC differentiation.

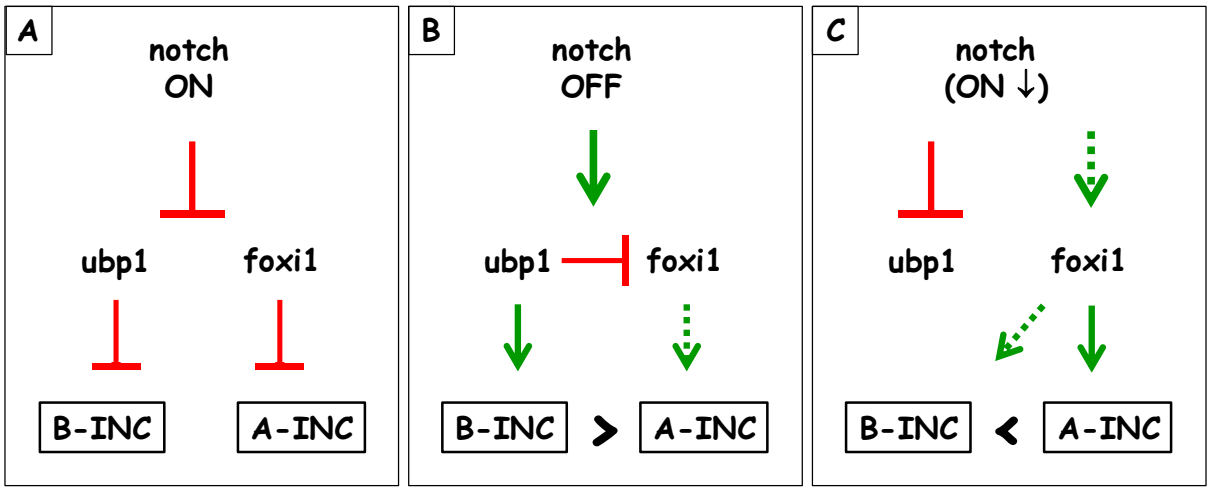

Fig. 2.7 Suggested model of *Xenopus laevis* epidermal ionocyte differentiation. The schematic model is based on the findings of [51]. **A)** Overexpression of activated notch leads to suppression of ionocyte (INC) formation, probably by inactivating ubp1 and foxi1. **B)** Inhibition of notch leads to the formation of ionocytes, presumably by activation of ubp1 and foxi1. However, B-INCs (type beta-ionocytes) are favoured over A-INCs (type alpha-ionocytes), most likely by ubp1 mediated repression of foxi1. **C)** Dose dependent effect of notch. While inactivated notch abolishes INC formation **(A)**, little amounts of activated notch lead to the formation of INCs, favouring A-INCs over B-INCs.

Similar observations were made regarding the differentiation of distinct ionocyte populations and keratinocytes in the epidermis of zebrafish embryos and larvae [52]. Cell lineage tracing experiments revealed the development of ionocytes and keratinocytes from the same precursor cell pool [54]. At least two types of ionocytes are distinguished, Na^+,K^+-ATPase-rich (NaR) cells and H^+-ATPase-rich (HR) cells. Apparently, members of the fox transcription factor family (foxi1 and foxi3) are essential in ionocyte specification [54-56]. Furthermore, the delta-notch signalling is required to inhibit ionocyte formation of neighbouring cells, thus inducing the keratinocyte phenotype by lateral inhibition. Recently, the grhl1 (grainyhead-like 1) transcription factor was discovered to play some role in ionocyte and non-keratinocyte formation, probably by negative autoregulation (Fig. 2.8) [57].

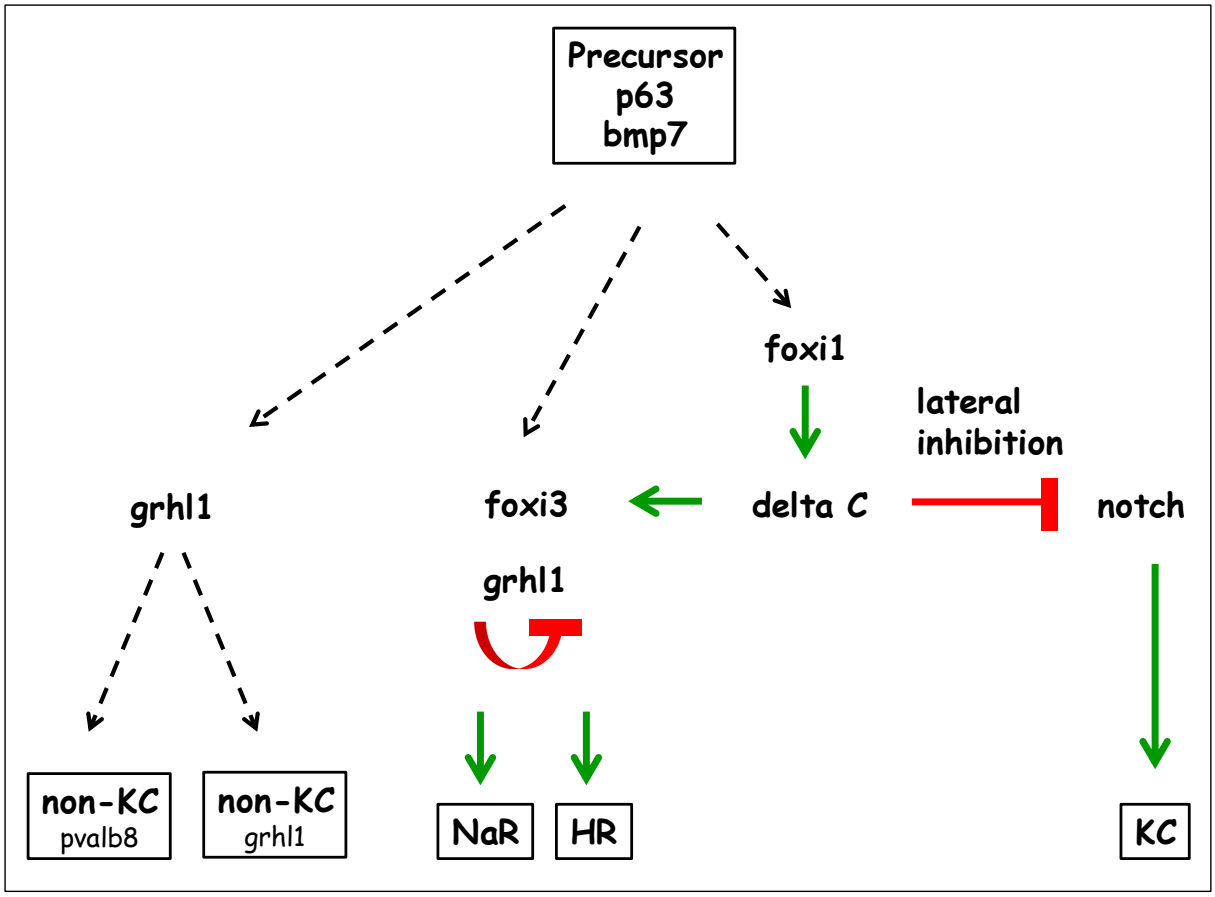

Fig. 2.8 Predicted model of epidermal cell differentiation in zebrafish larvae, modified after [56, 57]. A common pool of epidermal precursor cells (expressing p63, bmp7) give rise to distinct cell types. Hereby, foxi1 mediated activation of delta C seems to determine the cell fate of neighbouring cells. While delta C mediated induction of foxi3 gives rise to the ionocyte lineage (Na^+,K^+-ATPase-rich cells, NaR; H^+-ATPase-rich cells, HR), the activation of the delta/notch signalling pathway promotes the development of keratinocyte (KC) precursor cells by lateral inhibition. Furthermore, the induction of foxi3 and the negative autoregulation of grhl1 within the ionocyte precursor might result in the terminal differentiation of NaR and HR. In addition, the activation of grhl1 alone may lead to the development of distinct non-keratinocytes (non-KC).

2.7.1 The p53 gene family

Terminal cell differentiation inversely correlates with proliferation and thus requires cell cycle arrest and activation of a functional gene expression in the cell [16]. The tumor suppressor protein TP53 (p53) is a master regulator of transcription and central to the activation of cell cycle arrest, senescence, apoptosis, tumorogenesis, embryo development and differentiation [58, 59]. Consistently, p53 expression and activity is crucially regulated during embryonic kidney development and plays a role in transcriptional regulation of renal functional genes (RFGs) [60-62]. Briefly, in the fetal rat kidney p53 expression was detected in the differentiated zone with the onset of tubular differentiation, while it was absent in the immature nephrogenic zone [61]. The spatiotemporal distribution pattern and posttranslational modifications of p53 correlate with the expression of RFGs (i.e. Bdkrb2, Aqp2, Na^+/K^+-ATPase α1, AT_{1A}) and thus differentiated renal epithelial cells [63]. Consistently, p53 was shown to control the expression of these RFGs in distinct *in vivo* and *in vitro* models [61, 63, 64]. In addition, transcription factors (i.e. Klf4, Foxi1) involved in epithelial differentiation might be controlled directly by p53 or signalling molecules within the p53 pathway [65-67]. Interestingly, p53 deficient newborn mice exhibit severe renal cysts and hyperplasia, while p53 overexpression results in renal hypoplasia [61]. Among the p53 responsive genes the bradykinin receptor type B2 (Bdkrb2, B2R) was identified and their relationship was investigated in more detail. The bradykinin receptors are thought to mediate paracrine actions of the renal kallikrein-kinin-system (KKS), which comprises cellular growth, inflammatory response, modulation of renal blood flow and urinary sodium excretion [68, 69]. Indeed, salt stressed Bdkrb2 deficient mouse embryos develop renal CD dysplasia and die early after birth [70]. The observed renal dysgenesis might be a result of p53 mediated apoptosis of nephron progenitors and repression of terminal differentiation [71, 72]. Moreover, a combinatorial model involving the transcription factors p53, cAMP response-element binding protein (CREB), Krüppel-like factor 4 (Klf4), and the transcriptional coactivator CREB-binding protein (CBP) is proposed to cooperatively activate Bdkrb2 transcription in the

process of terminal nephron differentiation (Fig. 2.9) [13, 65, 66]. Accordingly, p53 performs a dual role in terminal epithelial differentiation by controlling cell cycle arrest and activating the transcription of renal function genes. However, whether a multi-protein complex is also required for the transcriptional regulation of other p53 targets such as Aqp2 or Na^+/K^+-ATPase is still unknown.

In addition, p73, another member of the p53 family and close homologue, was identified to control the expression of Aqp2 and Bdkrb2, independently of p53 [73]. Furthermore, p73 and p63, but not p53, might activate the Notch signalling pathway and thus influence developmental cell fate decisions [74].

All together, genes of the p53 family might promote terminal differentiation of renal epithelial cells in the CD system and eventually initiate segment-specific transcription factors and cofactors ensuring segmental identity rather than specifying a cell lineage or cell fate [66].

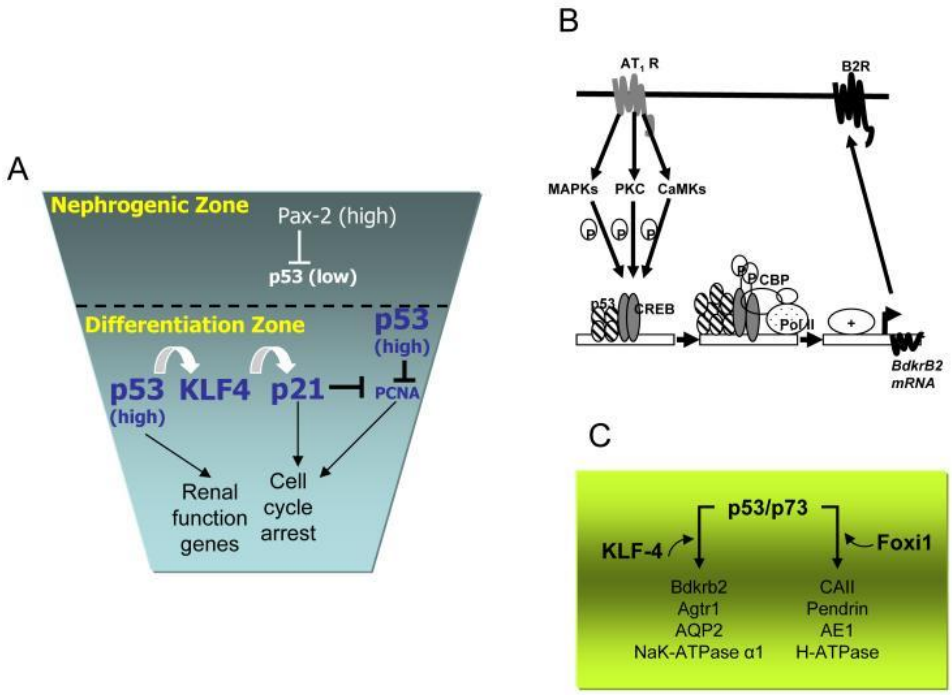

Fig. 2.9 Suggested role of p53 family in terminal nephron differentiation, taken from [66]. **A)** Terminal nephron differentiation requires p53 stabilization and enhanced DNA binding activity. In the nephrogenic zone Pax-2 represses transcription of p53. In the differentiation zone high levels of p53 suppress transcription of PCNA and induces KLF4 transcription, which in turn activates p21 expression and sustains cell cycle arrest [66]. **B)** Activation of the AT_1R by angiotensin II mediates phosphorylation of CREB, which allows interaction of CREB with p53 and the coactivator CBP, thus enhancing Bdkrb2 (B2R) transcription. CBP serves as a bridging molecule for the basal transcription machinery and as a histone acetyltransferase [66]. **C)** p53 and its homologue p73 are able to bind the promoters and activate the expression of renal function genes. However, the transcriptional activation requires additional transcription factors like KLF-4 or Foxi1 [66].

Pax-2 (paired box gene 2); PCNA (proliferating cell nuclear antigen); KLF4 (Krüppel-like factor 4); AT_1R (angiotensin II receptor type 1); CREB (cAMP response-element binding protein); CBP (CREB-binding protein); Foxi1 (Forkhead box protein I1)

2.7.2 Notch signalling pathway

The Notch signalling pathway is an evolutionary well conserved mechanism of intercellular crosstalk and a master regulator of development, cell fate determination, cell differentiation, tissue patterning, homeostasis and repair. The different actions of the Notch pathway can be broadly subdivided into three categories, which are 1) lateral inhibition, 2) lineage decisions, and 3) boundaries/inductive signalling [75]. Recent studies suggest Notch as a key regulator in renal development by establishing proximal epithelial fate during nephron segmentation and differentiation of principal cells in the renal CD system (Fig. 2.10) [76, 77].

This has been nicely demonstrated in a study by Jeong and colleagues [77]. In detail, the Notch signalling pathway was selectively disrupted in the renal CD system by a conditional KO of mind bomb 1 (Mib 1). Mib 1 is an E3 ubiquitin ligase that is necessary for endocytotic removal of Notch ligands and thus initiating Notch signalling [78]. However, inactivation of the Notch signalling pathway in the renal CD system, leads to nephrogenic diabetes insipidus due to reduced abundance of Aqp2 positive principal cells and their concomitant replacement by V-ATPase positive intercalated cells (Fig. 2.10 A) [77]. Interestingly, *Foxi1* mRNA abundance (see Chapter 2.7.3) was markedly increased in kidneys with inactivated Notch signalling. Intriguingly, constitutive activation of Notch signalling completely reverses the renal CD phenotype by restoring Aqp2 positive principal cells, virtually replacing all types of V-ATPase positive intercalated cells (Fig. 2.10 B). The constitutive activation of Notch was achieved by the introduction of the Notch intracellular domain (NCID) into the conditional Mib 1 deficiency phenotype [77]. Thus, Notch signalling critically influences the cellular heterogeneity of the mouse renal CD system.

Consistently, the Notch signalling pathway controls the mosaic pattern of multi-cilia cells and principal cells in the zebrafish pronephros by lateral inhibition [76, 79]. Furthermore, the Notch regulatory mechanism and members of the grainyhead family (see Chapter 2.7.4) most likely contribute to cell lineage determination of PSCs (proton-secreting cells) in *Xenopus laevis* and zebrafish larval skin, acting upstream of *foxi1* (Fig. 2.7, 2.8) [51].

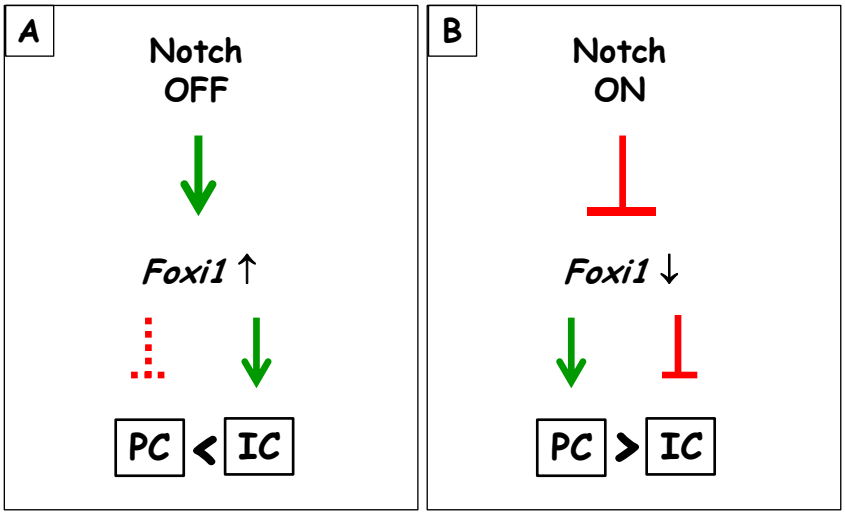

Fig. 2.10 The Notch signalling pathway determines terminal differentiation of cells in the mammalian renal collecting duct system (after [77]). **A)** Disruption of the Notch signalling pathway goes along with increased *Foxi1* mRNA expression and favours the abundance of V-ATPase positive intercalated cells (ICs) on the expense of Aqp2 positive principal cells (PCs). **B)** Constitutive activation of the Notch signalling pathway is accompanied by downregulation of *Foxi1* mRNA and results in the presence of Aqp2 positive PCs with a complete loss of V-ATPase positive ICs.

2.7.3 Foxi1 deficiency

Transcription factors are essential regulatory proteins in embryogenesis and organ development. There is a large family of forkhead box (FOX) transcription factors identified, which share homology in the forkhead box domain, a well conserved DNA binding motif of 80-100 amino acids, also known as the winged helix domain. At present, 50 FOX genes in the human genome and 44 Fox gene orthologues in mouse are identified and distinguished in 19 clades [80]. Based on phylogenetic criteria, a common nomenclature using alphabetic letters for distinct Fox classes (FOXA – FOXS) is agreed. The FOX transcription factors play important roles in embryo and organ development, cell cycle control, growth, differentiation, longevity and cancerogenesis in a variety of distinct species [81].

At least two Fox genes are involved in early kidney development, Foxd1 and Foxc1 [10]. Another member Foxi1 was found to be expressed in distal tubules of fetal kidneys of later developmental stages and in the adult kidney [82], particularly in ICs of the renal CDs [83]. Furthermore, Foxi1 expression was detected in the mouse inner ear and epididymis [84-86]. Analysis of the Foxi1 consensus binding sequence identified potential target genes expressed in the renal distal tubule, among them are *Pds*, *Ae1*, *Ae4* and the *a4* and *B1 subunits of the V-ATPase* [82, 83, 85, 87]. Consistently, mice deficient for Foxi1 develop distal renal tubular acidosis (dRTA), most evidently due to the loss of acid-base regulating proteins in renal ICs, such as Pds, Ae1, Ae4 and the B1 subunit of the V-ATPase [83]. Interestingly, renal collecting ducts of Foxi1 KO mice are composed of only a single cell type that is equally positive for the PC marker Aqp2 and the IC marker CaII, instead of distinct populations of ICs and PCs (Fig. 2.11). Likewise, ultrastructural analysis of the CD system confirmed a lack of normal ICs in Foxi1 null mutants. Instead of, a cell type neither displaying clear features of ICs nor strictly PC characteristics was found. Hence, all these data suggest Foxi1 as a critical factor regulating the correct and functional patterning of the renal CD epithelium. Whether Foxi1 is a direct or indirect regulator is still not known.

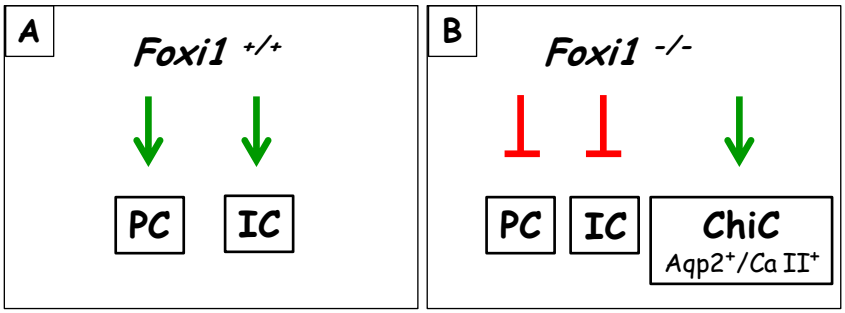

Fig. 2.11 Relationship of Foxi1 and terminal differentiation of mouse renal collecting duct cells (after [83]). **A)** The renal collecting duct (CD) of healthy mice consists of principal cells (PCs) and types of intercalated cells (ICs). **B)** However, PCs and ICs are absent in the renal CD system of Foxi1 deficient mice and replaced by a chimeric cell (ChiC) type, coexpressing aquaporin 2 (Aqp2) and carbonic anhydrase II (CaII).

2.7.4 Cp2l1 deficiency

The family of LSF (late SV40 factor), also referred to as CP2 (CCAAT-binding protein 2 on α-globin) related proteins comprises an ancient and evolutionary well conserved family of transcription factors which are rather ubiquitously expressed and usually transcriptional activators [88]. The LSF family consists of two branches, the LSF/CP2 subfamily and the grainyhead (GRH) subfamily. In the human and mouse genome three LSF-subfamily genes are identified, of which one is LBP-9/CRTR-1 (Leader binding protein 9, CP2-related transcriptional repressor-1) also known as TCFCP2L1/CP2L1 (Transcription factor CP2-like1). CP2L1 is exceptional among the LSF-subfamily, as it is rather expressed in specific tissue and acts as a general repressor instead of activator [89]. In general, members of the grainyhead gene family play fundamental roles in the development and morphogenesis of epithelial tissues in a wide variety of species. Murine *Cp2l1* is characteristically expressed in the developing duct epithelium of exocrine glands including the salivary glands and in kidney [89, 90]. In detail, spatio-temporal *Cp2l1* expression in the fetal mouse kidney is differentially regulated in both, the nephrogenic and ureteric bud derived epithelia (Fig. 2.12). However, in the postnatal maturing kidney, *Cp2l1* expression becomes restricted to the DCT, CNT, CCD and OMCD.

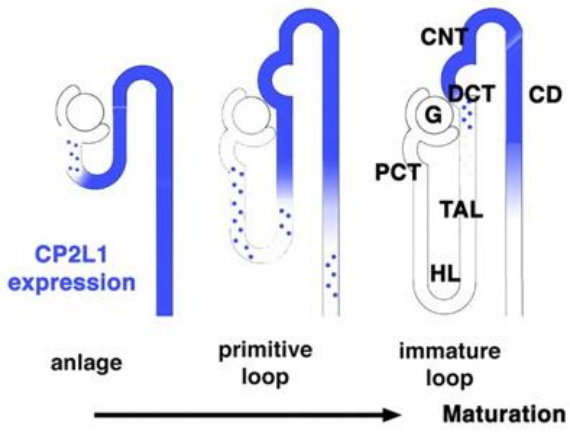

Fig. 2.12 Differential expression of Cp2l1 in the developing mouse kidney, taken from [90].

Developmental maturation of functional salivary gland and renal distal tubule epithelium was defective in Cp2l1 deficient mouse embryos [90]. In particular, Cp2l1 depleted kidneys lack the expression of *Clcnkb*, *Gk-6* and *Fxyd2c*, genes which are characteristically present in the TAL, CNT and DCT, respectively. Moreover, mRNA expression of *Atp6v1b1*, *Ae1* and *Pds* was completely absent in Cp2l1 deficient kidneys (Fig. 2.13). Unfortunately, more detailed characterization of the renal CD morphology is missing, as well as data assessing the acid-base homeostasis in these mice, despite the observation of a mild urinary concentrating defect. Anyhow, Cp2l1 deficiency in mice correlates with incomplete renal CD differentiation, strongly affecting the characteristic structure and function of ICs. However, regulatory pathways and mechanisms involving transcriptional control of Cp2l1 are still missing.

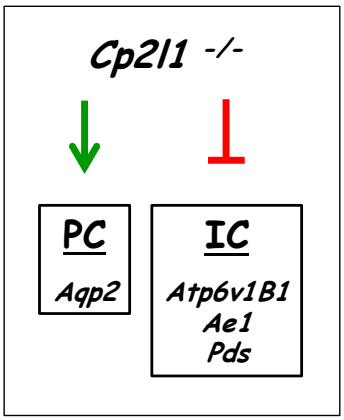

Fig. 2.13 Correlation of *Cp2l1* deficiency with the expression of genes usually present in mouse renal collecting duct cells (after [90]). Loss of *Cp2l1* in kidneys of mice does not alter the mRNA expression of aquaporin 2 (*Aqp2*), a marker for principal cells (PCs). However, *Cp2l1* deficiency goes along with the absence of *Atp6v1B1*, *Ae1* and *Pds* mRNA, usually expressed by types of intercalated cells (ICs).

2.7.5 Dmbt1 (Hensin) deficiency

Besides the importance of regulatory transcription factors and signalling molecules, another group of proteins, namely integrins and extracellular matrix (ECM) proteins, play a role in terminal differentiation of renal epithelial cells. Initially discovered in cultured epithelial cells derived from rabbit kidney, the ECM protein hensin is proposed crucial for terminal differentiation of renal intercalated cells and the hypothesized transdifferentiation of types of ICs upon acid-base disturbances (chapter 5.2) [91-93]. Hensin is expressed during embryonic development and with species differences in the expression levels in pancreas, intestine, gallbladder, salivary glands and nasal/olfactory/vomeronasal epithelium [94]. It has been described previously by different investigators and thus is known, beside other names, also as Dmbt1 (deleted in malignant brain tumors 1) or muclin (mucin-like glycoprotein). However, it has been reported, that hensin is synthesized and secreted to the extracellular matrix as a monomer or polymer. The polymerization of hensin seems to mediate interconversion of type B-ICs to type A-ICs and requires the presence of at least 3 additional proteins (galectin 3, cis-trans peptidyl prolyl isomerase and integrin αvβ1) [95-98].

Recently, a mouse model with conditional deletion of hensin from renal intercalated cells was investigated [99]. The mice were reported to lack renal type A-ICs all along the CD system and consequently develop complete dRTA due to renal bicarbonate wasting. Essentially, type B-ICs were preserved in the renal cortex of the mutant mice, while a novel IC phenotype was discovered in the inner medulla. Here, the authors found an uncertain type of ICs, which displays the ultrastructural characteristics of type B-ICs but lacks pendrin expresssion. This novel cell type is suggested to be the progenitor of medullary type A-ICs. In the same study, another mouse model with a conditional deletion of integrin β1 from renal ICs was compared, since integrin β1 was suggested critical for hensin polymerization and deposition to the ECM. Accordingly, a phenotype similar to that of hensin deficient mice was observed. However, despite intensive studies, a putative molecular mechanism of hensin mediating renal IC

differentiation has never been suggested. Nevertheless, hensin was very recently integrated into an oversimplified schematic model of intercalated cell differentiation (Fig. 2.14) [100].

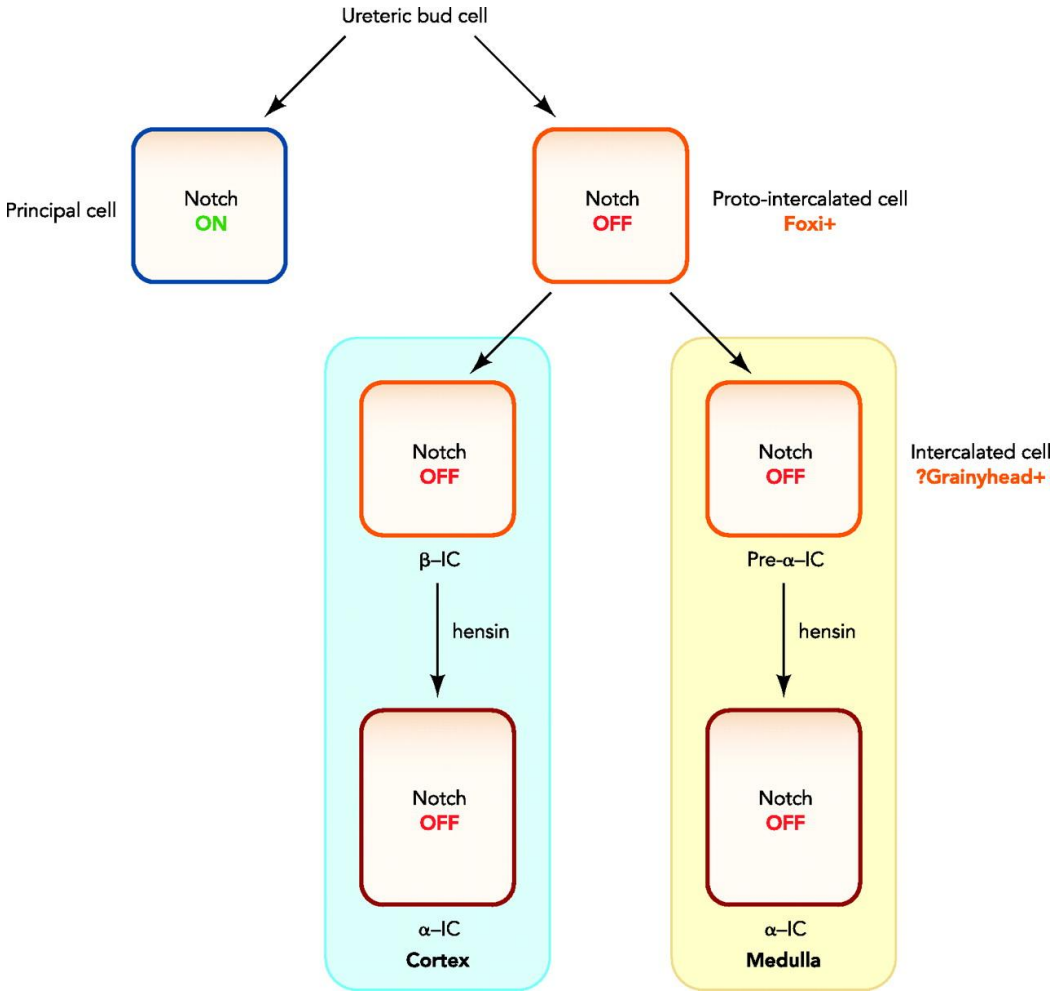

Fig. 2.14 Proposed model for renal intercalated cell differentiation, taken from [100].

2.7.6 Carbonic anhydrase II deficiency

Besides transcription factors and signalling molecules the presence of the enzyme carbonic anhydrase II (CaII) was found to be a critical determinant of terminal IC differentiation. Renal ICs express high levels of the cytosolic enzyme CaII which catalyzes the rapid conversion of CO_2 and water to H_2CO_3. CaII deficiency in mouse and men is known to cause distal renal tubular acidosis (dRTA). Moreover, ICs of the CCD and particularly MCD are severely reduced and replaced by PCs in kidneys of CaII deficient mice (Fig. 2.15) [101, 102]. Another study showed that the phenomenon of IC depletion in CaII deficient mice develops during late postnatal maturation of the kidney [103]. In detail, a remodelling of the MCD favouring PC abundance on the expense of ICs was only detectable after 3 weeks of life. These observations suggest that the presence or absence of CaII directly influences the cell type diversity in the renal CD.

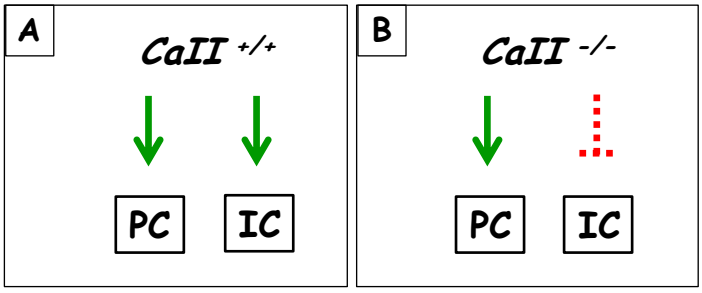

Fig. 2.15 Carbonic anhydrase II (CaII) deficiency leads to depletion of intercalated cells (ICs) in mouse kidney (after [101-103]). Detailed description in text.

Notably, chronic pharmacologic inhibition of CaII with acetazolamide in rats was shown to induce distinct remodelling of the renal CD system [104]. Here, type A-IC abundance in the renal CCD was increased with a corresponding decrease in type B-ICs, without affecting the ratio of total IC to PC. Furthermore, the relative number of type A-ICs in the outer medulla was increased on the expense of PCs. In addition, the size of ICs in CCD and OMCD was markedly increased. In contrast, A-ICs were strongly reduced in the inner medulla of acetazolamide treated rats, but not completely absent as it was reported for CaII deficient mice. These data are consistent with the concept of adaptive nephron plasticity (see Chapter 5.2.1).

3. RENAL ACID-BASE TRANSPORT

The kidneys ability to produce acidic urine is an important mechanism to adapt to intermediate and chronic imbalances in systemic acid-base homeostasis. Renal excretion of acids is enabled by three regulatory pathways along the nephron: 1) reabsorption of filtered HCO_3^- in the proximal tubule, 2) ammoniagenesis and excretion of ammonia and titratable acids, and 3) excretion of excess protons in the distal nephron.

3.1 Renal bicarbonate handling

Bicarbonate in the blood is freely filtered in the renal glomerulum and thus needs to be recovered from the renal tubular lumen to prevent loss into the urine. The proximal tubule is the main site of renal HCO_3^- reabsorption, accounting for 80% [105, 106]. As illustrated in Fig. 3.1, luminal HCO_3^- and H^+ are converted to CO_2 and H_2O by the action of the membrane bound carbonic anhydrase IV (CAIV). Carbon dioxide enters the proximal tubule cell rapidly by diffusion where it is once more combined with H_2O to form HCO_3^- and H^+. This intracellular hydration is catalyzed by carbonic anhydrase II (CAII), which is a soluble isoform. While the H^+ exits the cell to the luminal site, mostly in exchange for Na^+, via the Na^+/H^+ exchanger NHE3, the formed HCO_3^- is cotransported together with Na^+ to the blood by the basolateral Na^+/ HCO_3^- cotransporter NBCe1.

The remaining 20 % of luminal HCO_3^- are finally reabsorbed in the thick ascending limb of the loop of Henle [107] and the distal tubule [108].

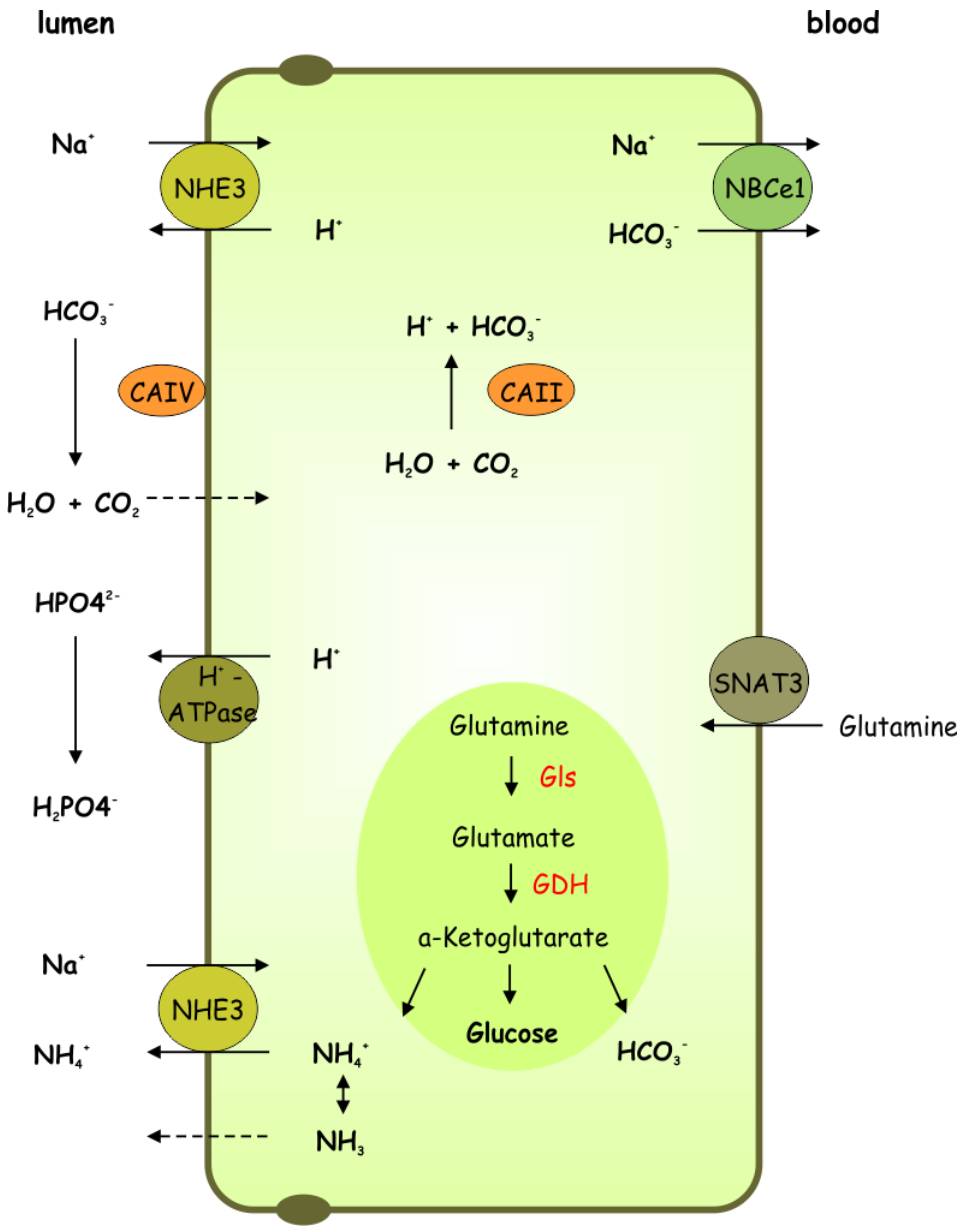

Fig. 3.1 Bicarbonate reabsorption in proximal tubule (adapted after [1]), detailed description in text.

3.2 Ammoniagenesis

Beside the recovery of bicarbonate from the urine, the kidneys are able to generate new bicarbonate from the synthesis of ammonium (NH_4^+). Ammonium is primarily produced from glutamine in mitochondria of the proximal tubule (Fig. 3.1) [109]. Glutamine, provided by the liver due to amino acid break down, enters the proximal tubule cells mostly by the Na^+ coupled cotransporter SNAT3 [110]. Inside the mitochondria, glutamine is cleaved to glutamate and ammonium (NH_4^+) by glutaminase. Glutamate is then further converted to α-ketoglutarate and a second NH_4^+ by glutamate dehydrogenase (GDH). Ammonium inside the cell dissociates into H^+ and gaseous NH_3, which diffuses into the tubular lumen, where it binds again to H^+ and is trapped as NH_4^+. The protons are consumed to form glucose from α-ketoglutarate, thus generating bicarbonate. Ammonium might also be secreted into the lumen by the apical Na^+/H^+ exchanger NHE3, replacing the H^+ as the preferred substrate. Along the different parts of the loop of Henle (LOH), ammonium is secreted and primarily reabsorbed in the thick ascending limb (TAL). This leads to the accumulation of NH_4^+ in the interstitium of the outer medulla, partially favouring non-ionic diffusion of NH_3 into the lumen of the medullary collecting ducts, where it is excreted to the final urine along with H^+.

As recently discovered, ammonia secretion in the inner medullary collecting duct, is not only passive, but mediated by the Na^+/K^+-ATPase and the Rhesus glycoproteins RhBG and RhCG [111-114]. These specialized transporters are predominantly present in principal cells and type-A intercalated cells of the collecting ducts [112] (Fig. 3.2). Mice deficient for Rhcg display an incomplete form of distal renal tubular acidosis (dRTA), due to insufficient NH_3 excretion to the urine, indicating its relevance (see chapter 7.1.2) [114].

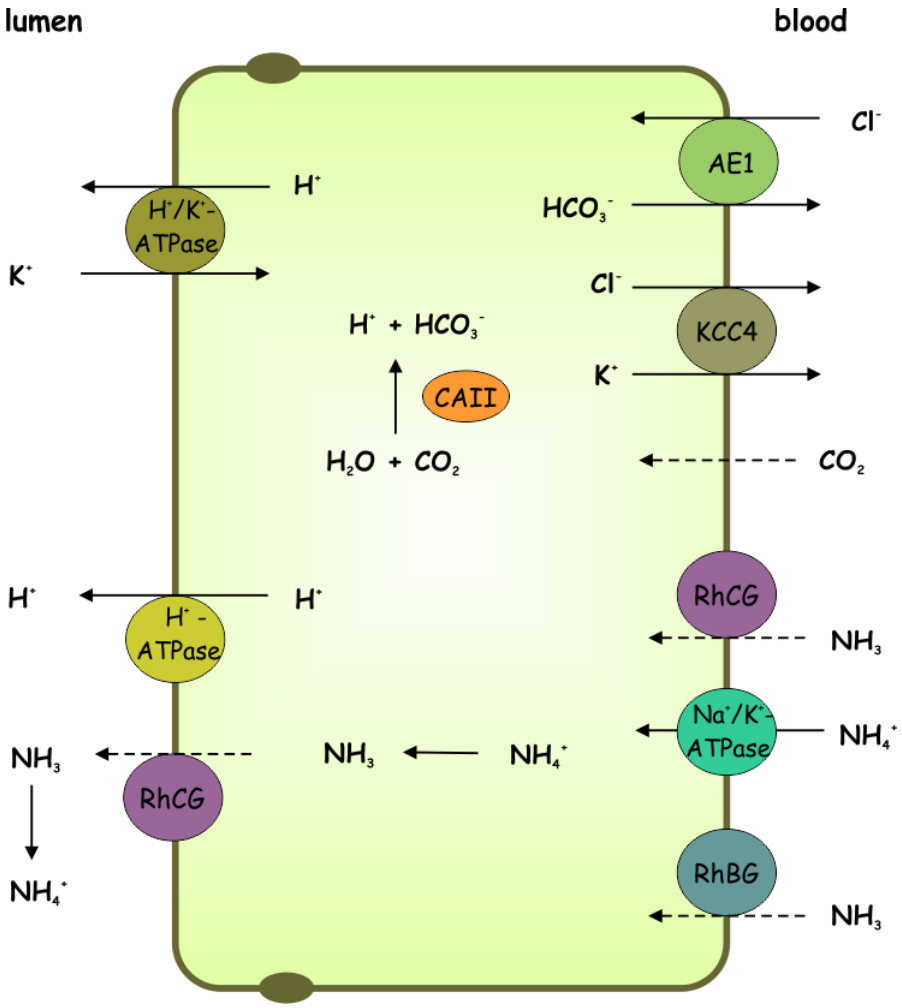

Fig. 3.2 Ammonia excretion in type-A intercalated cell of renal collecting duct (adapted after [109]), detailed description in text.

3.3 Renal use of titratable acids

Protons excreted with the urine are not only bound as NH_4^+, but are also bound to other buffers, the so called titratable acids (TA). By definition, titratable acidity describes the amount of acid required to titrate the urine buffers from the plasma pH to urine pH [115]. The most important urinary titratable acids are phosphate (Fig. 3.1) and creatinine. However, other organic salts such as sulfate, citrate, lactate, pyruvate and urate also contribute to urinary buffering and thus, titratable acidity. The term net acid excretion (NAE) describes the sum of titratable acids and NH_4^+ minus the urinary HCO_3^- concentration in the urine (Eqn. 3) [1].

Eqn. 3 $NAE = (TA + NH_4^+) - HCO_3^-$

3.4 Acid-base transport in the distal nephron

While the proximal tubule plays a major role in the *de novo* generation and reabsorption of bicarbonate, the distal tubule and the collecting ducts are the site of urinary fine tuning and final acidification [116]. Today, the distal convoluted tubule (DCT), the connecting tubule (CNT) and the initial collecting tubule (ICT) are taken together as the classical distal tubule, even though they display significant cell heterogeneity. The collecting ducts (CD) are distinguished in cortical collecting ducts (CCD), outer medullary collecting ducts (OMCD) and inner medullary collecting ducts (IMCD). As already described, the collecting ducts are comprised of at least three different cell types, principal cells, type-A and type-B intercalated cells. The principal cells are responsible for salt and water homeostasis. Type-A intercalated cells are acid secretory cells, since they secrete protons into the urine and transport bicarbonate into the blood. A-ICs are characterized by the luminal expression of the V-ATPase and basolateral expression of the Cl^-/HCO_3^- exchanger AE1 (SLC4A1, Band 3) (Fig. 2.6, 3.3).

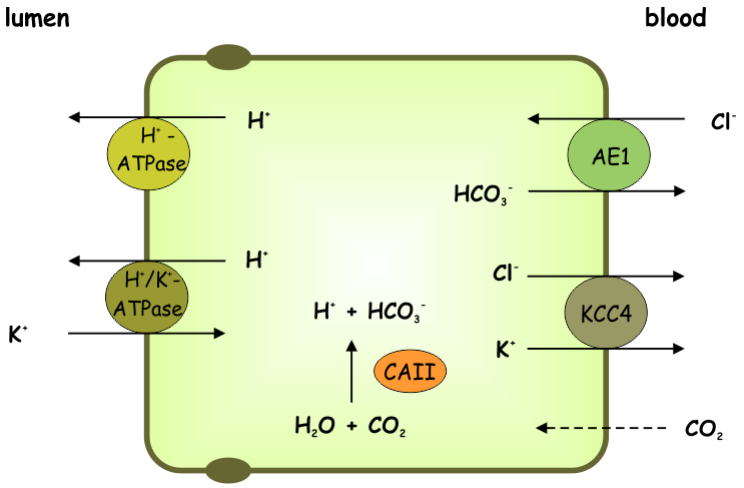

Fig. 3.3 Model of type-A intercalated cell (A-IC) without NH_3/NH_4^+ pathway, adapted from [116], detailed description in text.

Type-B intercalated cells (B-ICs) are bicarbonate secreting cells and show opposite features of type A-ICs with the luminal expression of the Cl^-/HCO_3^- exchanger pendrin (SLC26A4, PDS) and the basolateral presence of V-ATPase (Fig. 2.6, 3.4).

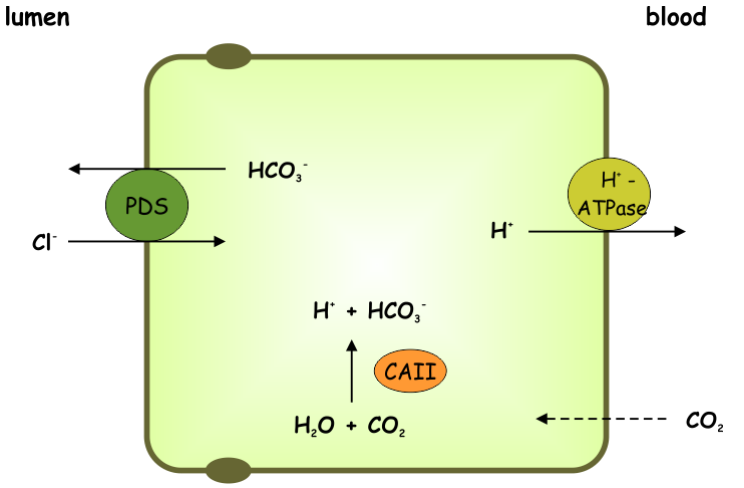

Fig. 3.4 Model of type-B intercalated cell (B-IC), adapted from [116], detailed description in text.

However, proton and bicarbonate excretion by the collecting ducts is strongly dependent on the presence of NH_3 and titratable acids in the urine and is influenced by different factors, such as systemic acid-base and electrolyte status, several hormones and nutrition [116, 117].

4. DISTURBANCES OF ACID-BASE HOMEOSTASIS

Systemic and renal acid-base regulation is influenced by a multitude of physiologic and pathophysiologic factors including respiration, nutrition and physical activity, as well as medication and various epithelial transporter disorders. Clinically, acidosis defines a blood pH lower than 7.35, while alkalosis exists with a blood pH higher than 7.45. Typically, four basal pH disturbances of different origin (Tab. 4.1) are distinguished: 1) respiratory acidosis, 2) respiratory alkalosis, 3) metabolic acidosis, and 4) metabolic alkalosis. In general, respiratory derived acid-base disturbances are primarily caused by alterations in blood pCO_2 due to inappropriate pulmonary ventilation. In contrast, metabolically derived pH imbalances are usually caused by accumulation or loss of non-volatile acids and therefore changes in blood HCO_3^- concentration. Furthermore, metabolically derived pH disturbances may be distinguished in extrarenal and renal origin. Extrarenal metabolic pH disturbances might be caused by nutrition (i.e. high protein content), diarrhoea and excessive sports. However, systemic pH imbalances might also arise because of renal tubular dysfunction. In any case, the body tries to restore systemic pH as close to normal by acute and long-term regulatory mechanisms.

Tab. 4.1 Clinical types of acid-base disturbances, modified after [1]

Disturbance	Symptom	Response
Respiratory acidosis	↑ pCO_2	↑ HCO_3^-
Respiratory alkalosis	↓ pCO_2	↓ HCO_3^-
Metabolic acidosis	↓ HCO_3^-	↓ pCO_2
Metabolic alkalosis	↑ HCO_3^-	↑ pCO_2

Clinically, determination of the serum anion gap helps to identify the cause of metabolic acidosis [118]. The anion gap is a calculated value, given by subtraction of the major anions [HCO_3^-] and [Cl^-] from the major cation [Na^+] (Eqn. 4).

Eqn. 4 Anion Gap = $[Na^+] - ([HCO_3^-] + [Cl^-])$

Thus, the anion gap is usually a positive value (12 ± 4 meq/l), reflecting the quantity of anions which are not balanced by cations [119]. The result of the anion gap is classified as high or normal and allows the following interpretations. A high anion gap acidosis may be observed in the presence of additional metabolic acids consuming bicarbonate (i.e. lactic acidosis, ketoacids) or in renal failure, when the kidneys do not sufficiently reabsorb bicarbonate or secrete acids. Normal anion gap acidosis, also called hyperchloremic acidosis, goes along with the loss of bicarbonate compensated by an equivalent increase in serum chloride concentration. This form is usually caused by renal tubular acidosis, diarrhoea and ingestion of ammoniumchloride or hydrochloric acid.

4.1 Respiratory acidosis

Respiratory acidosis occurs during insufficient alveolar ventilation (hypoventilation) and leads to increased arterial pCO_2 levels (hypercapnia) which is initially corrected by HCO_3^- buffering from the extracellular fluid. On the long term, the kidneys need to correct the distorted blood [HCO_3^-/CO_2] by reabsorbing all filtered HCO_3^- and enhancing the generation and secretion of all available acids by upregulating renal acid-base transporters [120, 121].

4.2 Respiratory alkalosis

Hypocapnia describes a state of low arterial pCO_2 levels caused by alveolar hyperventilation. This leads to respiratory alkalosis and fall in plasma [HCO_3^-]. Chronic hypocapnia further decreases extracellular fluid [HCO_3^-] as a result of reduced renal net acid excretion [120, 121].

4.3 Metabolic acidosis

Metabolic acidosis is a severe acid-base imbalance that may be caused by numerous factors, such as starvation, diarrhoea, intoxication or disease complications like diabetic ketoacidosis. Acute metabolic acidosis, lasting up to several days, is much more common than chronic forms [122]. However, the immediate compensatory response to metabolic acidosis is an increase in alveolar ventilation, thus exhaling more CO_2. This is usually achieved by enhancing the respiratory tidal volume and frequency. However, the final correction of plasma [HCO_3^-/CO_2] needs to be established by the kidney. Thus, renal excretion of H^+ and HCO_3^- reabsorption is maximally upregulated. Additionally, ammoniagenesis and final excretion of NH_4^+ increases markedly and becomes the main H^+ extrusion pathway. Detailed adaptive responses of the kidney to acid loads will be discussed later on (chapter 5).

4.4 Metabolic alkalosis

Two conditions may lead to metabolic alkalosis, namely the loss of hydrogen ions (i.e. by vomiting) or the inappropriate increase in plasma [HCO_3^-] (i.e. abuse of steroids and diuretics). Likewise to metabolic acidosis, the respiratory system responds and adapts immediately to metabolically derived alkalosis. Here, the respiratory frequency slows down significantly, leading to the accumulation of pCO_2 in the blood. Again, the kidney is responsible for the final and persistent correction. During metabolic alkalosis, acid secretion and bicarbonate reabsorption by the kidney is markedly reduced. Moreover, type B-ICs of the renal cortical collecting ducts may even switch from net H^+ secretion to HCO_3^- secretion [1, 123].

4.5 Renal tubular acidosis

Impaired renal acidification leads to renal tubular acidosis (RTA), a form of metabolic acidosis with hyperchloremic anion gap in the setting of normal glomerular filtration [124]. Generally, acquired or inherited RTA may develop either because of insufficient proximal bicarbonate reabsorption or due to inadequate distal urinary acidification. However, based on the clinical symptoms and the underlying functional defect, four different types of RTA are distinguished: type 1 classic distal (dRTA), type 2 proximal (pRTA), type 3 combined proximal and distal RTA, and type 4 distal-like hypoaldosteronism (hyperkalemic dRTA) [125, 126].

4.5.1 Type 1 RTA

Distal renal tubular acidosis (dRTA) is characterised by the renal inability to acidify the urine, leading to metabolic acidosis with variable severity of accompanying hypokalemia, hypercalciuria and hypocitraturia. The underlying defect is usually an acquired or inherited form of impaired acid secretion by type A-ICs of the renal collecting ducts. The impact of inadequate urine acidification might result in spontaneous systemic metabolic acidosis (complete dRTA) or metabolic acidosis after an imposed acid load (incomplete dRTA) [127]. Therapeutically, adequate bicarbonate supplementation is sufficient to restore plasma bicarbonate to near normal levels. The oral application of potassium citrate is favoured over sodium bicarbonate, as it simultaneously treats the accompanying and often life-threatening hypokalemia [128].

Primary familial dRTA is caused by mutations of epithelial transporters essentially expressed in renal type A-ICs. In dependence of the mutation and the affected transporter respectively, autosomal- dominant and –recessive forms of dRTA are known (Tab. 4.2) [126, 127]. Most commonly, loss of function mutations of the Cl^- /HCO_3^- exchanger AE1 or the V-ATPase were identified in patients with primary familial dRTA [129-134].

However, dRTA frequently also develops as a secondary disorder, often in consequence of autoimmune diseases such as Sjögren`s syndrome [135-138].

Tab. 4.2 Subtypes and features of inherited dRTA, adapted from [126].

dRTA Inheritance	Age at Presentation	Clinical Features	Transporter
Dominant	Adulthood	mild/compensated Metabolic Acidosis Hypokalemia (variable) Hypercalciuria Hypocitraturia Nephrolithiasis Nephrocalcinosis sometimes Rickets/ Osteomalacia Secondary Erythrocytosis	AE1 (SLC4A1)
Recessive	Childhood	Metabolic acidosis with Hemolytic Anemia	AE1 (SLC4A1)
Recessive	Infancy/ Childhood	early onset bilateral sensorineural hearing loss Metabolic Acidosis early Nephrocalcinosis growth retardation Rickets	B1 subunit of V-ATPase (ATP6V1B1)
Recessive	Infancy/ Childhood	as above with later onset of hearing loss or no deafness	a4 subunit of V-ATPase (ATP6V0A4)

4.5.2 Type 2 RTA

Proximal renal tubular acidosis (pRTA) is usually caused by defective proximal tubule bicarbonate reabsorption with intact distal acidification. This leads to excessive loss of bicarbonate by the kidney and subsequent metabolic acidosis with hypokalemia [139]. Primary isolated pRTA is a rare disorder and associated with dominant and recessive inherited mutations in the Na^+/HCO_3^- cotransporter NBCe1 (SLC4A4) (Fig. 3.1). Since NBCe1 is also expressed in the eye, pRTA might come along with ocular abnormalities [140].

4.5.3 Type 3 RTA

Type 3 RTA is caused by carbonic anhydrase II (CAII) deficiency and combines proximal and distal RTA features. It is characterized by reduced proximal bicarbonate reabsorption and distal inability to acidify the urine despite systemic acidosis [141]. CAII plays an important role in bone and central nervous system (CNS) metabolism. Therefore, CAII malfunction frequently leads to osteopetrosis, cerebral calcification, and mental retardation [142, 143].

4.5.4 Type 4 RTA

Type 4 RTA is actually a primary disorder in renal electrolyte handling with secondary normal anion gap acidosis. In general, renal aldosterone deficiency or resistance are thought to be the underlying defect. Thus, hyperkalemia and hyperchloremia are unique characteristics of type 4 RTA. The mild metabolic acidosis develops secondary to the hyperkalemia, which induces an intracellular alkalosis impairing renal proximal NH_4^+ generation and excretion [144].

5. RENAL ADAPTATION TO SYSTEMIC ACIDOSIS

Systemic acidosis requires compensatory responses of the kidney function increasing the capacity of acid-base and electrolyte handling with cellular reorganization and even remodelling of the nephron [145-148]. Furthermore, the body has other mechanisms that contribute to renal compensatory regulation of acid-base imbalance, such as increase of glomerular filtration rate (GFR) [1], hormones that directly stimulate kidney function (angiotensin II, endothelin) [149, 150] and hormones (i.e. parathyroid hormone, vitamin D) affecting bone resorption and thus recruitment of additional non-carbonate buffers [151, 152].

5.1 Adaptation of proximal renal tubule

In response to metabolic acidosis the renal proximal tubule undergoes a set of adaptations to maximally recover filtered bicarbonate [153] and generate new bicarbonate to buffer excess systemic acids. Increased acid loads enhance the capacity of proximal bicarbonate reabsorption by modulating the activity and/or abundance of apical and basolateral transport mechanisms [154]. The apically located Na^+/H^+ exchanger NHE3 plays a crucial role in transcellular bicarbonate reabsorption (Fig. 3.1) and enhanced transport activity, as well as increase in its abundance in the proximal tubule and TAL during metabolic acidosis have been demonstrated [154-157]. Furthermore, the V-ATPase is an important apical H^+ extrusion pathway, accounting for up to 40% of sodium independent bicarbonate transport, which is rapidly regulated by pCO_2 and pH [158, 159]. Moreover, acidic pH modulates basolateral Na^+/HCO_3^- cotransport mediated by NBCe1 and increases the abundance of transporter at the cell membrane [160-163]. In turn, mutations of NBCe1 lead to proximal renal tubular acidosis (chapter 4.5.2) [164, 165].

However, effective renal acid buffering requires *de novo* generation of additional bicarbonate by the synthesis and excretion of ammonium and excess acids. Ammonium is enzymatically generated from the amino acid glutamine in renal proximal tubule cells (Fig. 3.1). During metabolic acidosis, the excretion and synthesis of ammonium is highly upregulated [166] involving the supply and uptake of glutamine into renal tubular cells [167].

Additionally, the kidney increases the excretion of titratable acids, mainly phosphate (Fig. 3.1). In the proximal tubule, two unrelated gene families (SLC20 and SLC34) of phosphate transporters are expressed [168, 169]. Transport activity and abundance of members of the SLC34 family were found to be regulated upon acid-base disturbances [170]. In response to metabolic acidosis elevated levels of phosphate are excreted into the urine, where it combines with excess protons acting as a titratable acid. Since elevated circulating phosphate is partially released from bone mass, chronic systemic acidosis may lead to osteoamalacia or osteopetrosis, as well as nephrocalcinosis and nephrolithiasis [171].

5.2 Adaptation of distal renal tubule

The renal response to metabolic acidosis does not only require adaptations of the proximal tubule, but also of the distal nephron. The importance of the final urinary acidification and fine tuning by the distal nephron is also highlighted by the dysfunction of numerous transporters leading to dRTA. Within the collecting duct, the vacuolar type H^+-ATPase (V-ATPase) is the major protein responsible for H^+ secretion into urine. It is differentially expressed in all types of intercalated cells and thus involved in mediating renal net H^+ secretion and HCO_3^- generation or H^+ reabsorption and net HCO_3^- secretion (Fig. 2.6) [133]. The V-ATPase is a heteromultimeric complex, consisting of 13 different subunits which are assembled in two domains (Fig. 5.1) [172]. Some of the identified subunits are almost exclusively expressed in the kidney among them are the a4 (ATP6V0A4) and B1 (ATP6V1B1)

subunits. As indicated in Fig. 2.6, 3.3 and 3.4, the plasma membrane location of the V-ATPase in intercalated cells (IC) is strongly dependent on the type of IC. Interestingly, acid-base disturbances do not seem to alter the mRNA or protein expression levels of renal V-ATPases, but trigger its redistribution within the cell [40]. While acidosis promotes the insertion of the proton pump into the cell membrane from a subplasma membrane pool of V-ATPase vesicles, alkalosis drives the retrieval of V-ATPase from the membrane into the submembrane vesicular pool [147]. In addition, acid-base disturbances regulate the protein abundance of the Cl^-/HCO_3^- exchangers Ae1 and Pds (Fig. 2.6). Acid-loads were shown to increase the protein abundance of Ae1 and decreases Pds, whereas alkali-loads decrease Ae1 abundance and increase Pds [173].

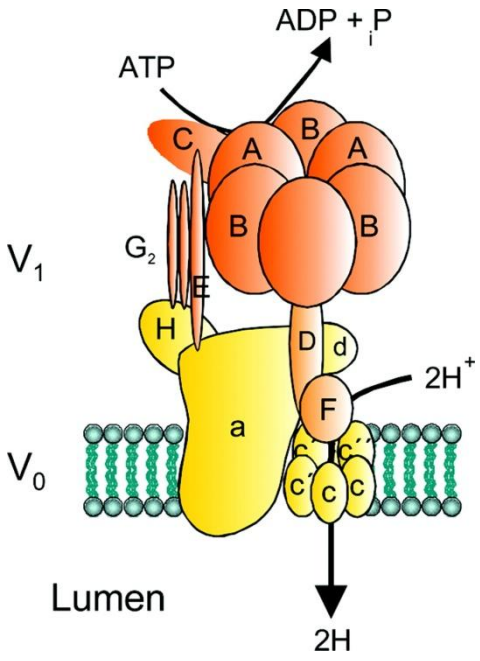

Fig. 5.1 Structural model of vacuolar type H^+-ATPase (V-ATPase), taken from [172].

5.2.1 Adaptive plasticity of distal renal tubule

In addition to acid-base related changes of the cellular protein composition and localization, acute and especially long-term acid-base imbalances are accompanied by changes in the relative number and axial distribution of renal type A-ICs and B-ICs [104, 145, 146]. It has been observed that the relative number of type A-ICs increases dramatically in rodents receiving chronic oral acid loads. Strikingly, the relative number of type B-ICs decreases at the same time, while the ratio of total ICs to PCs is not changed [173, 174]. The opposite phenomenon is true for rodents receiving chronic alkali loads, since the relative number of type B-ICs increases on the expense of type A-ICs. These empiric data raised several hypotheses, which are:

1) IC progenitors might exist in the CD epithelium and become activated upon acid-base perturbations [175-177].

2) Terminally differentiated ICs proliferate or become apoptotic upon prolonged functional request [138, 146, 178, 179].

3) The concept of the plasticity of functional epithelial polarity was raised, a process where type B-ICs might convert into type A-ICs or *vice versa*. Moreover, type B-ICs are postulated precursors of type A-ICs [91, 174, 180].

Since then, several studies have been performed testing either idea. Accordingly, circulating (i.e. haematopoietic stem and progenitor cells, HSPCs) or tissue specific residual progenitor cells giving rise to new differentiated renal epithelial cells seem rather important for postinjury repair. Furthermore, the notion of proliferation or apoptosis of terminally differentiated cells upon exogenous stimuli (i.e. acid-base or electrolyte disturbances) is more tempting than the concept of adaptational reversal of functional epithelial polarity. In fact, the latter theory was never proofed convincingly.

5.2.2 Gdf15 is involved in early adaptive proliferation of renal type A-IC

Recently, the growth differentiation factor 15 (Gdf15), a member of the transforming growth factor-β (TGF-β) superfamily was found to be involved in the proliferation of type A-ICs during early adaptation of the kidney to metabolic acidosis [146]. The murine orthologue Gdf15 is also designated as macrophage inhibitory cytokine-1 (MIC-1), prostate-derived factor (PDF), placental TGF-β (PTGF-β), placental bone morphogenetic protein (PLAB) and non-steroidal anti inflammatory drug-activated gene-1 (NAG-1), reflecting its pleiotropic functions [181]. As typically reported for TGF-β superfamily members, Gdf15 is a multifunctional acting factor and involved in the control of embryonic development and pregnancy, osteogenic and haematopoietic development, cellular responses to stress stimuli, inflammation and tissue repair after acute injury.

During protein synthesis, Gdf15 undergoes extensive peptide processing leading to several manifestations, such as signal-peptide, propeptide, and mature peptide, which are associated with distinct molecular mechanisms (Fig. 5.2) [181]. The biological active mature protein is a secreted dimer, serving multiple autocrine and paracrine actions upon a multitude of stimuli (detailed review by [181]).

In the mature mouse kidney, low mRNA expression levels all along the nephron were reported under basal conditions [146]. However, *Gdf15* mRNA levels increased readily with induction of metabolic acidosis in the CNT, CCD and mostly OMCD. After 3 days of acid load, *Gdf15* mRNA was maximally increased and declined with prolonged acidosis. Strikingly, the time-course of *Gdf15* mRNA regulation upon acid loading matched the relative proliferation rates of type A-ICs. Moreover, acidotic Gdf15 deficient mice showed a reduced and delayed proliferation rate of type A-ICs [146].

Interestingly, the early proliferation of type A-ICs of acidotic mice was shown to be dependent on the regulation of the cell-cycle regulatory protein Cyclin D1, which is a downstream target of the phosphatidylinositol-3 kinase (PI3K)/Akt/mammalian target of rapamycin (mTOR) signalling pathway. Consistently, the cell-cycle regulatory

proteins p53 and cyclin D1/D3 were abnormally regulated in Gdf15 KO mice. The molecular action of Gdf15 in renal CD differentiation remains uncertain. However, a putative role in controlling the orientation of the mitotic spindle by Gdf15 is suggested. Hence, this study [146] demonstrated nicely, that metabolic acidosis induces the proliferation of terminally differentiated type A-IC population in the renal OMCD of mice. Notably, proliferation markers were rarely detected in PCs or type B-ICs. In addition, the data indicate that p53, Gdf15 and the PI3K/Akt/mTOR regulatory pathway are required for the acute proliferation event. However, detailed investigation of the interactive mechanisms is needed.

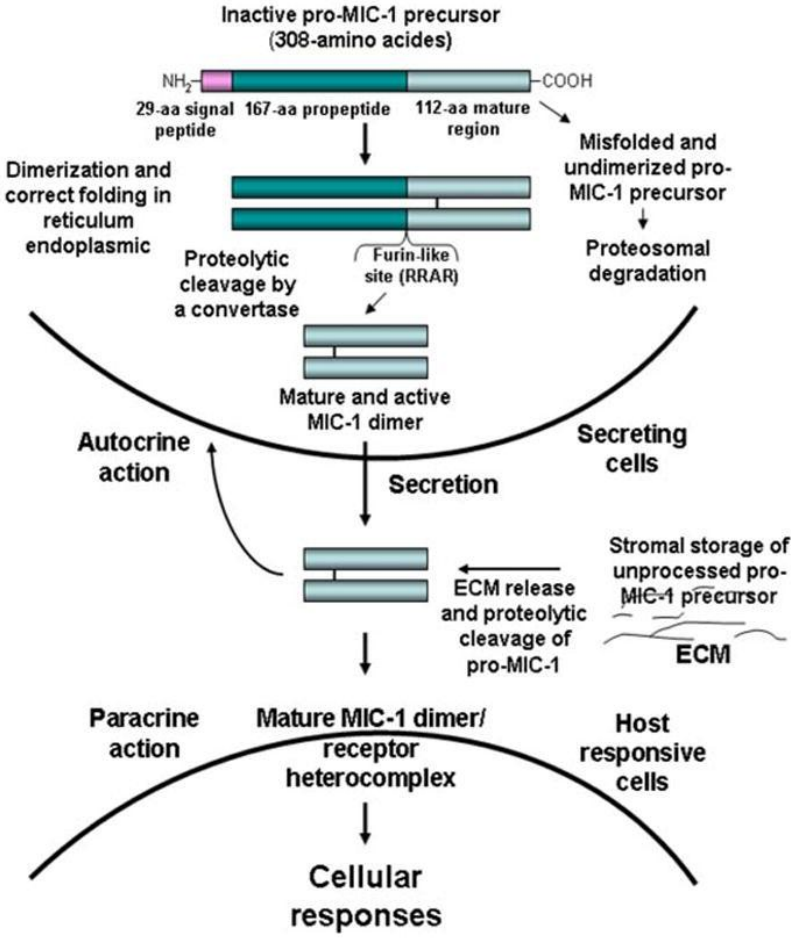

Fig. 5.2 Illustration of cellular processing, secretion and storage of Mic-1 (Gdf15), taken from [181]. The biologically active mature Mic-1 protein is a secreted dimer and induces distinct autocrine and paracrine actions upon various stimuli.

6. BICARBONATE TRANSPORTER

At present, two evolutionary unrelated gene families encoding for bicarbonate transporting proteins were identified in humans, the SLC4 (solute carrier 4) family of anion exchangers (AE) and the SLC26 family of sulfate permease anion transporters [182]. The gene products of either family display distinct phylogenetic relationships with differences in their tissue and subcellular distribution, as well as substrate preference, transport mode and regulatory mechanisms. Deficiencies in some of the members of both families lead to hereditary diseases affecting different organ functions and thus display characteristic phenotypes [127].

6.1 The SLC4 Family

In humans, the SLC4 (solute carrier 4) family of Cl^-/HCO_3^- exchangers consists of ten members with distinct phylogenetic relationships. They are distinguished by their transport mechanism and preferred substrate and thus belong to at least three different major clades (Fig. 6.1) [183]. The Na^+-independent and electroneutral Cl^-/HCO_3^- exchangers SLC4A1 (AE1), SLC4A2 (AE2), and SLC4A3 (AE3). The Na^+-dependent electrogenic HCO_3^- cotransporter SLC4A4 (NBCe1) and SLC4A5 (NBCe2), and the Na^+-dependent electroneutral HCO_3^- cotransporter SLC4A7 (NBCn1) and SLC4A10 (NBCn2), as well as the $Na^+/ HCO_3^-/Cl^-$ exchanger SLC4A8 (NDCBE). SLC4A9 (AE4) does also belong to the Na^+ dependent clade but its transport function and substrate preference are still unresolved. SLC4A11 (BTR1) belongs to the third major clade, since it shares similarities with borate transporters of plants, and fungi. However, its transport mechanism and anion preferences remain elusive.

SLC4 homologues were identified in genomes of many different organisms, such as marine bacteria, plants, fungi, marine invertebrates, insects, and a variety of vertebrate and mammalian species [183].

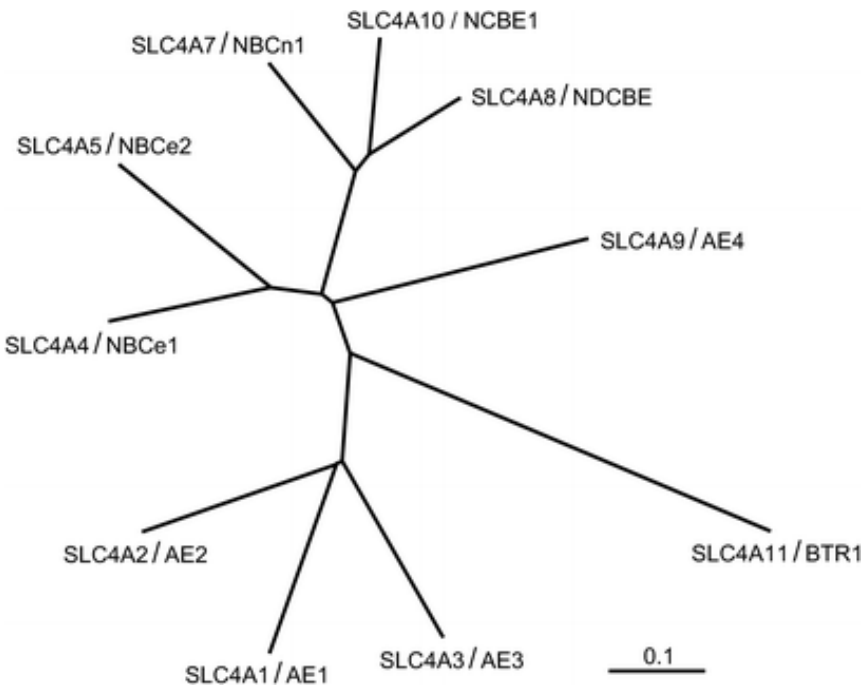

Fig. 6.1 Phylogenetic tree of human SLC4 family, taken from [183].

Members of the SLC4 family are crucial for several physiologic processes in mammals, such as the carriage of CO_2 from tissue to lungs, epithelial secretion and reabsorption of acid-base equivalents (e.g. in the kidney, stomach and pancreas), reabsorption of NaCl (e.g. ileum and proximal colon) as well as regulation of cell volume and intracellular pH in almost every cell of the body [183].

All SLC4 polypeptides share three common structural domains and features. They have a remarkably long intracellular hydrophilic N-terminal domain consisting of 400-700 amino acids, followed by a polytopic transmembrane domain of ~500 amino acids, which spans the membrane 10-14 times, and a short cytoplasmic C-terminal domain of 30-100 amino acids [184]. The predicted topology and structure of SLC4 transporters is mostly derived from studies of the highly abundant human erythroid AE1 protein (Fig. 6.2). Almost all *SLC4* genes express 5'- variant transcripts from alternate promoters, thus generating different polypeptide isoforms with distinct N-terminal domains.

6.1.1 Electroneutral Anion Exchangers

Among the SLC4 family, three members (AE1, AE2 and AE3) belong to the clade of electroneutral and Na^+-independent Cl^-/HCO_3^- exchangers. As they mediate the 1:1 exchange of monovalent anions from opposing sites of the plasma membrane, they are also referred to as anion exchangers (AEs). Their preferred substrates are Cl^- and HCO_3^-, but they can also transport OH^-. In addition, AE1 was shown to mediate the exchange of SO_4^{2-} and H^+ for Cl^- at very low rates [185]. Since the anion exchange mechanism is driven by substrate gradients, AEs can mediate influx and efflux of HCO_3^- by reversing the transport mode, but only erythroidal AE1 is known to work reversibly under physiological conditions [186]. Pharmacologically, all AEs are inhibited by the disulfonic stilbenes SITS and DIDS. However, the oxonol dye diBA5(C4) was shown to be a more potent inhibitor of AE1 than AE2, whereas polyaminosterols were found to inhibit AE2 more potently than AE1 [187].

The structure of the three AEs is highly conserved, especially within the transmembrane (TM) domains, as they share up to 56% of amino acid identity [183]. However, they are distinct in their regulation and transport activity. Interestingly, in a physiological range, AE1 activity is not modulated by pH, whereas AE2 and AE3 activity is highly sensitive to changes in pH [182, 188]. Additionally, AE2, but not AE1, was shown to be activated by hypertonicity and contributes to cell volume regulation when expressed in *Xenopus laevis* oocytes [182].

Furthermore, AE1 has a single N-glycosylation site, of yet unknown function, at the fourth extracellular loop, while AE2 and AE3 are N-glycosylated at the third extracellular TM domain [184]. However, the N-glycosylation of AE2 and AE3 had only little effects on transport activity or membrane expression [189].

The present study focuses on the relevance of Ae1 in the kidney. Notably, renal deficiency of Ae1 does not seem to induce compensatory regulation of other AEs in mouse kidney [190].

6.1.2 The Anion exchanger 1

In mammals, the anion exchanger 1 (AE1) is predominantly expressed in the plasma membrane of red blood cells (RBCs) and the basolateral membrane of renal type A-ICs (Fig. 3.3). Lower expression levels of AE1 are also present in the heart, distal colon, glomerular podocytes and other tissues [191, 192]. Homologous of mammalian AE1 were also identified in insects and amphibians [51, 193, 194]. The *AE1* gene encodes two polypeptide variants, the longer erythroid AE1 (eAE1, red cell band 3) and the shorter kidney AE1 (kAE1). In humans, kAE1 initiates at Met66 (methionine 66), while it initiates at Met79 in mice [184]. Numerous mutations of the *SLC4A1* gene have been identified in humans, but also cattle and zebrafish, which either affect the structure and function of RBCs or the kidney (Fig. 6.2) [184].

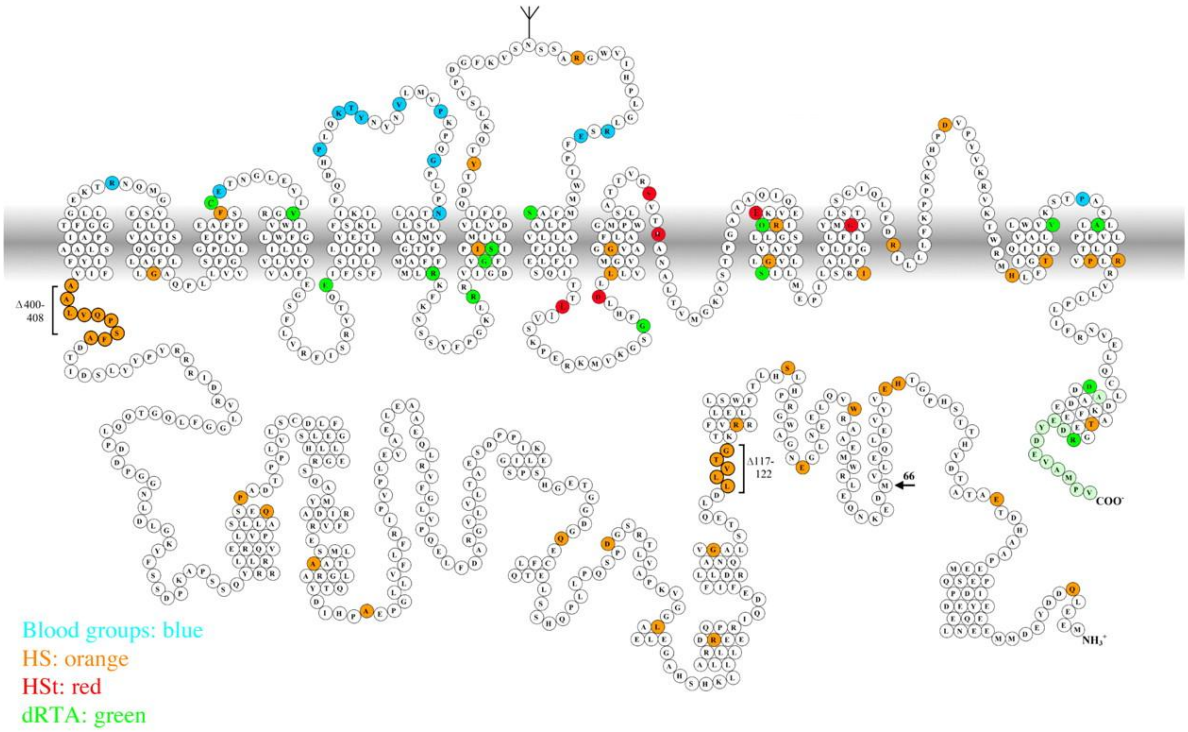

Fig. 6.2 Predicted topology model for human AE1 polypeptide, after Zhu et al. [195] taken from [184]. Polymorphisms encoding blood group antigens are highlighted in blue. Mutations (missense, nonsense, splicing and deletion) associated with hereditary spherocytic anemia and ovalocytosis (HS) are highlighted in orange, missense mutations leading to hereditary stomatocytosis (Hst) and xerocytosis are shown in red. Mutations identified in dominant and recessive distal renal tubular acidosis (dRTA) are labeled in green and terminal truncations are in lighter orange and green.

In the RBC, eAE1 is the most abundant integral membrane protein and serves, together with the action of the metalloenzyme carbonic anhydrase II (CAII), to increase the CO_2 carriage capacity of the blood and thus its removal by the lungs (Fig. 6.3). CAII was suggested to interact with the short C-terminus of eAE1 forming a pH dependent functional transport metabolon that accelerates transmembrane bicarbonate transport [196, 197].

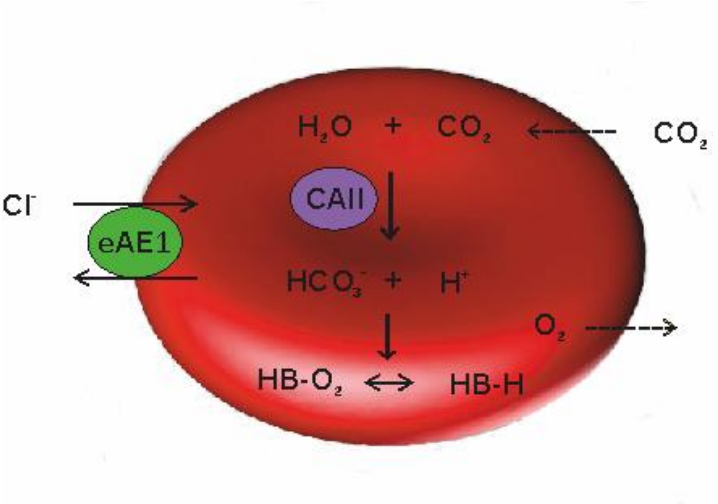

Fig. 6.3 Role of AE1 in erythroid CO_2 carriage (Jacobs-Stewart Cycle), modified from [183]. In the capillaries, CO_2 enters the erythrocyte mostly by transmembrane diffusion and probably via the water channel aquaporin 1. Soluble CA II (carbonic anhydrase II) catalyzes the rapid formation of HCO_3^- from intracellular CO_2 and H_2O. Deoxygenated hemoglobin buffers excess H^+ (Hb-H), while eAE1 releases newly generated HCO_3^- into the blood plasma in the exchange for extracellular Cl^- ("Hamburger"-Shift). The cycle is reversed in the lungs with oxygenation of hemoglobin (Hb-O_2).

Furthermore, the presence of eAE1 dimers or tetramers in the RBC membrane is known to be crucial for the stability and integrity of the membrane as it is a central part of a cytoskeletal macrocomplex (Fig. 6.4) [186]. In the RBC, the N-terminal domain of eAE1 anchors the spectrin based cytoskeleton to the plasma membrane via interaction with ankyrin. Moreover, eAE1 was shown to interact with protein 4.1 and 4.2, hemoglobin, glycolytic enzymes (aldolase, GAPDH, protein tyrosine kinase) and rhesus glycoprotein complexes [198, 199].

However, possible interactions of kAE1 with other proteins in the renal type A-ICs are less well understood and most likely different, since the kAE1 N-terminal domain lacks the first 65 amino acids in humans or 78 amino acids in mouse and therefore the ability of, for example ankyrin binding. Additionally, mutations of AE1 affecting both organs simultaneously, RBCs and kidney, are rarely seen.

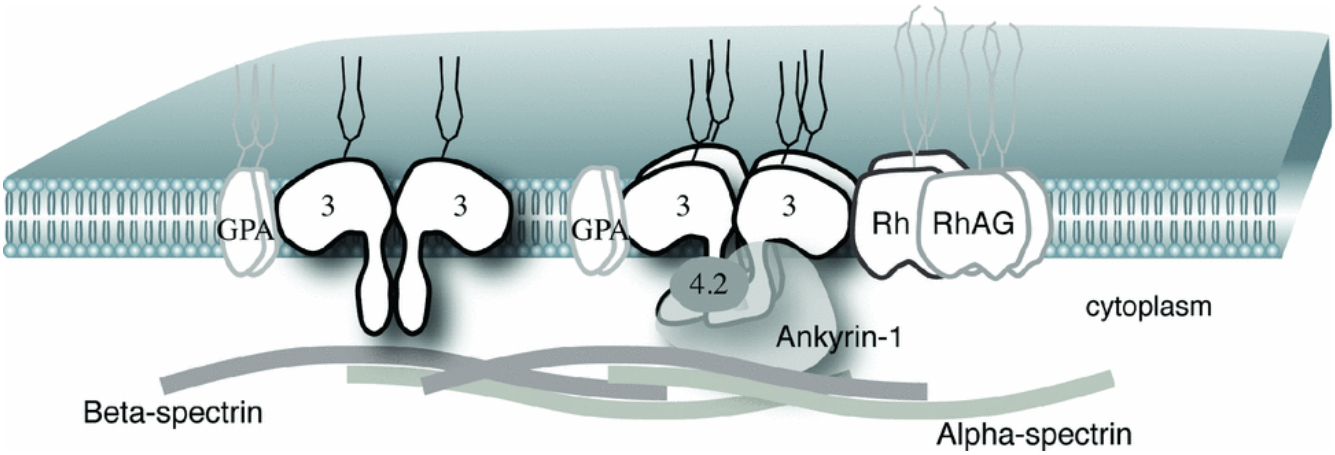

Fig. 6.4 AE1 macrocomplex in the erythroidal membrane, taken from [186]. In the RBC membrane, eAE1 (indicated as band 3) is present as dimers or tetramers, which interact with other cytoskeletal proteins forming a macrocomplex. Dimers of eAE1 bind to glycophorin A (GPA), while tetrameric eAE1 is further interacting with the rhesus glycoprotein RhAG and the cytoskeletal complex protein 4.2, ankyrin-1 and α- and β- spectrin.

Several mutations of human AE1 are identified and indicated in Fig. 6.2. They give rise to erythrocyte malformation and malfunction with haemolytic anaemia in dominant hereditary spherocytosis (HS) or stomatocytosis (Hst) with overhydrated cation-leak syndrome, or affect the kidney function leading to primary dRTA [200]. Notably, mutations leading to HS are distributed throughout the whole transporter, while Hst mutations are restricted to the first part of the second half of the TM domain and dRTA associated mutations are spread within the TM domain and the C-terminal tail. Since the *SLC4A1* gene generates at least two tissue specific products, mutations affecting both organs simultaneously are rarely seen. However, dominantly inherited mutations affecting the RBCs might be recessively inherited for renal defects [186] and dominantly inherited RBC mutants are associated with 50% expression of the wildtype allele, which seems to be sufficient for normal renal function [200]. Additionally, some dRTA associated AE1 mutations are rescued by chaperones like glycophorin A (GPA), which are expressed in RBCs or heterologous expression systems, but not in kidney [201-203].

In the kidney, kAE1 is abundantly expressed at the basolateral membrane of type A-ICs Fig. 2.6, 3.2, 3.3). Together with apical H^+ secretion, kAE1 is required for the acidification of the final urine, as it is the major basolateral bicarbonate extruder. Deficiency for kAE1 in man, mouse and cattle leads to dominant or recessive forms of dRTA. Among humans, mutations such as kAE1 R589 (H, C, S), S613F and R901X were identified in dominant dRTA, while G701D, S773P and S667F cause recessive forms. Several *in vitro* studies of dRTA associated AE1 mutants try to explain their pathogenicity and give rise to possible mechanisms involved in renal AE1 biosynthesis and targeting. Interestingly, the dominant negative kAE1 R901X mutation was shown to be mistargeted to the apical membrane or retained intracellularly in MDCK cells [204, 205]. Similarly, expression of dominant negative kAE1 R589H and S613F in polarized MDCK cells showed the retention of the protein within the ER (endoplasmatic reticulum) as well, where it can dimerize with the wild-type kAE1 and thus prevent its trafficking to the surface [206]. However, when expressed in *Xenopus* oocytes, kAE1 R589H retains partial activity and surface expression [207], which might be due to incubation with lower temperature (temperature-sensitive folding mutation), or the presence of different trafficking, signalling and folding chaperones in *Xenopus* derived cells [200]. Anyhow, in a renal biopsy from a patient with dominant kAE1 R589H associated dRTA and superimposed pyelonephritis and nephrocalcinosis, a reduced number of intercalated cells was observed, with preserved expression of V-ATPase, but absence of detectable kAE1 [208]. In contrast, analysis of a renal biopsy from a patient with the dominant kAE1 S613F mutation, showed reduced number and size of ICs, with an exclusively cytosolic expression of kAE1 [138].

6.2 The SLC26 Family

The SLC26 family of anion exchangers consists of ten members that play critical roles in a variety of physiological processes, such as skeletal development, synthesis of thyroid hormone, transepithelial Na^+-Cl^- transport, renal bicarbonate excretion and pancreatic bicarbonate secretion [209]. Accordingly, SLC26 transporters are very distinct in their expression pattern. Moreover, they transport a variety of monovalent and divalent anions, including sulfate, chloride, iodide, formate, oxalate, hydroxyl ion, and bicarbonate with variable transport specificity [209].

Within the kidney, several SLC26 members are expressed along the renal tubule (i.e. SLC26A1, SLC26A4, SLC26A7) [209-211]. However, the present study focuses exclusively on the Cl^-/HCO_3^- exchanger Pendrin (SLC26A4).

6.2.1 Pendrin

Pendrin (PDS, SLC26A4) is expressed in the inner ear, thyroid gland, and the kidney and transports chloride, bicarbonate, and iodide [33, 209]. In humans, mutations of PDS are associated with Pendred Syndrome, which is clinically characterized by hypothyroidism and goiter, as well as sensorineural deafness [33]. In the kidney, Pds is exclusively expressed on the luminal membrane of bicarbonate secreting type B-ICs and type non-A/non-B ICs of the CD system (chapter 3.4, Fig. 2.6 and 3.4). As described in chapter 2.5, Pds expressing cells are restricted to the renal cortex of adult kidneys (Fig. 2.4, 2.5). However, during renal development Pds expressing cells derive from both, the MM and UB pool of progenitor cells (Fig. 2.5).

The expression of Pds in mouse kidney and inner ear was shown to depend on the transcriptional activation by the forkhead box protein Foxi1 (chapter 2.7.3). In adult rodent kidneys Pds expression is highly regulated by systemic acid-base status (chapter 4.4, 5.2, and 5.2.1) and systemic chloride levels (for review see [33]). However, humans and mice with genetic disruption of Pds have normal acid-base

balance under basal conditions [33, 212]. Nevertheless, two independent Pds deficient mouse models show a reduced urinary pH due to a reduced urinary buffering of H^+ by secreted HCO_3^- [212, 213]. Interestingly, the abundance of type non-A ICs, but not A-ICs, was shown to be reduced in the renal cortex of Pds KO mice [212]. Moreover, type B-ICs in Pds deficient kidneys were markedly reduced in size and their ultrastructural appearance was altered [212]. Concomitantly, a reduction of transporters involved in renal H^+/OH^- handling (i.e. V-ATPase, NBC3, Rhbg) was noted, probably attenuating a rise in intracellular and systemic pH due to the loss of Pds [212].

7. MOUSE MODELS USED IN THIS STUDY

In the present study, distinct mouse models were used to answer the question whether an acid-base disturbance *per se* or the absence of renal Ae1 would introduce the observed abnormal presence of IC marker in Ae1 deficient mice.

7.1 Mouse models with primary dRTA

As already described in detail, renal Ae1 deficiency leads to distal renal tubular acidosis (dRTA) in mouse and men. Furthermore, loss of function mutations or absence of Atp6v1b1 and Rhcg in mice was also shown to reduce the kidneys ability of maximal urinary acidification and therefore the removal of systemic excess acid. Hence, a genetic defect in one of the three proteins impairs renal IC mediated acid-base handling and thus causes primary dRTA. Therefore, Atp6v1b1 and Rhcg deficient mice serve as alternative models to investigate a possible impact of inherited dRTA on the differentiation of ICs, respectively.

7.1.1 Atp6v1b1 deficient mice

Deficiency of the B1 subunit of the V-ATPase (ATP6V1B1) leads to spontaneous dRTA in humans [214]. Nevertheless, the phenotype is different in mice, as a homozygous deficiency of the B1 subunit of the V-ATPase (Atp6v1b1) leads to incomplete dRTA [215]. Briefly, under standardized laboratory conditions and feeding with normal rodent chow B1 KO mice did not show a detectable renal acid-base disturbance. Consistently an increased abundance of the alternative B subunit (B2) of V-ATPase was detected, which might partially compensate for B1 deficiency. Anyhow, after an oral acid load these animals develop systemic acidosis, due to an insufficient urinary acidification. It seems reasonable, that the strong alkali load provided by the standard rodent chow, might help to compensate insufficient urinary acidification under basal conditions [215].

7.1.2 Rhcg deficient mice

Distal urinary acidification is a complex process, involving the coordinated secretion of protons by luminal V-ATPase and the recovery of bicarbonate to the blood by basolateral Cl^-/HCO_3^- exchanger. As already discussed, this process is limited and thus additional alternate acid extrusion pathways like titratable acids and essentially ammonium are required. Recently, the rhesus glycoprotein Rhcg was identified as an ammonia transporter in mice, rats and humans [109]. Similar to murine B1 deficiency, mice lacking Rhcg display incomplete dRTA, as unravelled by oral acid load test [114]. Again, animals under basal conditions were raised with standard rodent chow, implicating large alkali loads that may compensate for renal insufficiency. Two independently generated Rhcg KO mice are available (Marini AM, Bruxelles [114] and TIGM, USA (Bourgeois, Bounoure, Christensen, Devuyst, Wagner, unpublished data)). However, both mouse models develop incomplete dRTA with minor differences under basal conditions.

7.2 Induced chronic metabolic acidosis model

As reported above, B1 and Rhcg deficient mice are prone to develop dRTA under forced acid-base disturbances. However, Ae1 KO mice and patients with dominant mutations of kAE1 suffer chronically from complete dRTA. Experimentally induced acute and particularly chronic acid-base disturbances in rodents were observed to alter the renal CD morphology (chapter 5.2, 5.2.1 5.2.2). Thus, the observed dysregulation of CD cell markers in Ae1 deficient subjects might be a result from the chronic acid-base disturbance or from the loss of Ae1 protein in the kidney. The oral application of NH_4Cl to the food or drinking water of rodents is a common experimental approach to induce metabolic acidosis [155, 216, 217]. Even though a more than 7 days lasting treatment with NH_4Cl is already considered a chronic acid-base disturbance and sufficient to cause adaptive responses in renal CD morphology, the period of time does not compare with the lifelong deteriorating dRTA in Ae1 deficient subjects. Furthermore, an altered differentiation of CD markers was initially observed in adult (P84) Ae1 KO mice. Therefore, metabolic acidosis in C57/Bl6 wildtype mice was induced for a total of 8 weeks, starting right away after weaning at 3 to 4 weeks of life. Based on recent studies, the supplementation of equivalent amounts of NH_4Cl to the food was favoured over the addition of 0.28M NH_4Cl to the drinking water to avoid unwanted side effects by chronic dehydration of the animals [218, 219].

8. AIM OF THE STUDY

Similar to humans, Ae1 deficiency in mice is correlated with the development of complete dRTA and nephrocalcinosis, as well as dysmorphology and malfunctionality of erythrocytes [190, 200, 220]. Furthermore, a severe urinary concentrating defect associated with dysregulated renal expression and localization of the water channel Aqp2 was observed in Ae1 deficient mice [190]. Additionally, unpublished observations indicated an abnormal distribution of intercalated cell marker proteins within the renal CD system of Ae1 deficient mice. Moreover, in renal biopsies of patients carrying dRTA associated AE1 mutations (AE1R589H and AE1S613F) aberrancies of V-ATPase expressing cells in the renal CDs have been reported [138, 208].

Therefore, the major aim was to examine the role of Ae1 in collecting duct cell differentiation by addressing the following subaims:

1) Characterization and quantification of possible abnormal expression pattern of renal IC marker by immunofluorescence (IF) in Ae1 deficient mice at different developmental and mature time points of life.
2) Investigation of a possible impact of acid-base disturbance on IC differentiation, by comparing the abnormal IC marker expression in Ae1 deficient mice with expression profiles in distinct mouse models for incomplete dRTA and chronically induced metabolic acidosis (chapter 5.2.1).
3) Immunologic comparison of IC marker expression in Ae1 deficient mice and patients carrying AE1 mutations associated with dRTA.
4) Investigation of the possible impact of candidate molecules (transcription factors, signalling molecules, receptors), which have been reported to play a role in IC development and differentiation (chapter 2.7 to 2.7.6, 5.2.2), on the abnormal IC differentiation observed in Ae1 deficient mice, by IF, qRT-PCR and immunoblot.

9. MATERIAL AND METHODS

9.1 Animal experiments

Animal experiments were performed in the ZIHP (Zurich Center for Integrative Human Physiology) Core facility for Rodent physiology (ZIRP) according to the rules and guidelines of the Swiss animal welfare law and approved by the Veterinäramt Kanton Zürich, Switzerland.

Ae1 deficient mice were obtained from Luanne Petersen and Seth Alper, Boston, Massachusetts, USA [220]. B1 deficient mice were obtained from Richard P. Lifton, New Haven, Connecticut, USA [215]. Rhcg deficient mice were obtained from TIGM (Texas A&M Institute for Genomic Medicine). All transgenic strains were bred in heterozygous pairs in the in-house animal facility of the University of Zurich.

Where appropriate, time of gestation was assessed by monitoring vaginal mating plugs. Adult mice or embryos and pups were euthanized by cervical dislocation or decapitation for organ collection. Both kidneys were subsequently removed, freed from the renal capsule, cut into halves, snap frozen in liquid nitrogen (N_2) and stored at -80°C until further analysis.

C57/Bl6 male mice were obtained from Institute of Veterinary Sciences, Fuellinsdorf, Switzerland at the age of 3 to 4 weeks and exposed to an oral acid load for 8 weeks to induce chronic metabolic acidosis. The animals were housed in normal cages with tab water *ad libitum* and fed standard rodent powder chow (GLP 3433, Kliba Nafag, Switzerland). Supplementation of 2 g NH_4Cl/100 g powdered food (equivalent to 0.28 M NH_4Cl in the drinking water) for 8 weeks was given to induce chronic metabolic acidosis [170, 219]. The bodyweight of all animals was assessed weekly and the health status (indicated by the appearance of the fur and activity) was determined at least every 2 days. At the end of the experimental period, the animals were placed in metabolic cages (Tecniplast, Italy). The mice were allowed to adapt to

the new environment for 3 days before assessing metabolic parameters and collection of 24 hours urine samples under mineral oil for another 2 days.

Finally, mice were anesthetized with 1.5% Isoflurane/pressurized air and 500 µl venous blood was taken with a heparinised syringe from the *V. cava caudalis* for subsequent blood gas analysis (ABL505, Radiometer, Copenhagen). The remaining blood was centrifuged at 5,000 rpm (4°C) for 5 minutes and the obtained plasma was snap frozen in liquid N_2 for further analysis. Finishing blood sampling, 5 animals per group were perfused with phosphate buffered saline (PBS, pH 7.4) through the left ventricle to allow wash-out of residual blood. Both kidneys were subsequently removed, freed from the capsule, cut into halves and snap frozen in liquid N_2 for further analysis. Another 5 animals per group were processed for organ fixation as described in 9.2.

9.2 Fixation and cryopreservation of whole organs

Adult and juvenile mice were anesthetized with 1.5 % Isoflurane/pressurized air and perfused through the left ventricle with 10 ml preperfusate consisting of 10,000 IU Heparin-Na Solution (BBraun), 2 ml Rapidocain 1 % (Ratiopharm), 2 ml $CaCl_2$ 16 %, 2 ml 0.9 % NaCl and 2 ml Aqua destillata. Subsequently, the animal was perfusion fixed with 3 % Paraformaldehyde (PFA) in 0.1 M Na-cacodylate buffer. After 5 minutes the kidneys were removed and postfixed for an additional hour on ice in the above fixative solution. Embryos and pups were euthanized by decapitation and kidneys were subsequently removed and immersion fixed in 3 % PFA/0.1 M Na-cacodylate buffer for 1 hour at 4°C. Following fixation, the kidneys were stored at 4°C in 1% PFA/0.1 M Na-cacodylate buffer. Cryoprotection was assured by immersion in 30% Sucrose/PBS. The kidneys were then embedded in Tissue-Tek Cryomolds (VVR) and Neg-50 frozen section medium (Richard-Allan Scientifics) with liquid propane and stored at -80°C.

9.3 Immunofluorescence

Paraffin embedded human kidney biopsy sections (kind gifts of Robert Unwin, University College London, UK and Seth Alper, Beth Israel Deaconess Medical Center, Boston, MA) were dewaxed in a series of 2 x 10 min 100 % Xylol, 3 x 3 min 100 % ethanol (EtOH), 3 x 3 min 96 % EtOH, and 1 x 30 min 75 % EtOH before rehydration in PBS. Cryopreserved mouse kidneys were cut into 3-5 μm thin slices (Cryostat CM1850, Leica) and rehydrated in PBS for at least 60 minutes. Different antigen retrievals were carried out, where necessary. Paraffinized tissue sections were treated by microwaving for 4 minutes in 10 mM citric acid pH 6.0 and 1 % sodium dodecyl sulfate (SDS) in PBS for 5 minutes. Cryopreserved tissue sections were either treated with 1 % SDS/PBS for 5 minutes, 0.3 % Triton X/PBS for 15 minutes or by microwaving. Following antigen retrieval, the sections were washed in PBS for 3 x 5 minutes. Unspecific binding of antibodies was impeded by 15 minutes incubation with 1 % bovine serum albumin (BSA) in PBS. Antibodies were diluted in 0.02 % Na-azide/PBS and stored at 4°C. Primary antibodies were incubated for overnight at 4°C in a moist chamber followed by two washes with hypertonic PBS (18 g/l NaCl/PBS) and 1 x wash with PBS. Secondary antibodies containing 4',6-diamidino-2-phenylindole (DAPI) were incubated in the dark for 120 minutes at room temperature (RT) in a moist chamber followed by previously described washing-steps. The stained sections were finally embedded with Glycergel (DakoCytomation) and kept at 4°C in the dark until microscopic analysis. Photomicrographs were taken using an upright DM 5500 fluorescence microscope with AF 6000 System (Leica) including the objectives HC PL FLUOTAR 10.0x0.30 DRY, HCX PL APO 40.0X1.25 OIL and HCX PL FUOTAR 100.0X1.30 OIL. Fluorescent specimens were pictured using a DFC 360 FX monochrome camera (Leica) and chromogenic specimens were pictured by bright-field microscopy using the digital colour camera DFC 295 (Leica). Images were further analyzed and processed using the LAS AF Lite Software (Leica), Corel PHOTO-PAINT X5 and the open-source software Image J (National Institute of Health).

The following combinations of primary antibodies detecting different marker proteins were used in distinct colocalization studies to distinguish principal cells, variations of ICs, type A-ICs and type B-ICs (Tab. 9.1).

Tab. 9.1 Marker combinations in immunofluorescent colocalization studies

Species: Mouse			
1)	Aqp2	Pds	Calb1
2)	Aqp2	Ae1	Calb1
3)	Aqp2	a4	Calb1
4)	Aqp2	B1	Calb1
5)	Aqp2	CaII	Calb1

Species: Human			
1)	AQP2	PDS	AE1
2)	AQP2	PDS	a4
3)	AQP2	PDS	B1
4)	AQP2	PDS	CAII

9.5 Quantification of cells

Immunofluorescently labelled cells from at least one kidney cross section per animal and each set of antibody combination was counted (Tab. 9.1). Principal cells were identified by luminal aquaporin 2 expression. Intercalated cells were either labelled for the a4 or B1 subunit of the V-ATPase. Type B-ICs were identified by the apical presence of Pds and type A-ICs by the basolateral presence of Ae1, where appropriate. The cellular affiliation to distinct renal tubule segments was taken into account. The renal CNT, CCD, OMCD and IMCD were primarily distinguished based on morphologic criteria. Immunologic presence of cytosolic calbindin D28K (Calb1) was further used to discriminate between the CNT and CCD segment [21].

Tab. 9.2 List of Antibodies (AB) used for immunofluorescence

1° AB	Antigen/Catalog No.	dilution (mouse)	dilution (human)	Source
rabbit-anti-mouse Ae1	DCFIYEDQIRPQDREELLRALLLK	1:1,000	1:500	Own (Pineda)
guinea pig-anti-mouse Ae1	DCFIYEDQIRPQDREELLRALLLK	1:500		Own (Pineda)
rabbit-anti-mouse Pendrin	CKDPLDLMEAEMNAEELDVQDEAMRRLAS	1:1,000		Own (Pineda)
guinea pig-anti-mouse Pendrin	CKDPLDLMEAEMNAEELDVQDEAMRRLAS	1:1,000	1:250	Own (Pineda)
rabbit-anti-a4	CKFSPFSFKHILDGTAEE	1:1,500	1:500	Own (Pineda)
rabbit-anti-B1	CAQQDPASDTAL	1:1,000	1:250	Own (Pineda)
guinea pig-anti-B1	CAQQDPASDTAL	1:500		Own (Pineda)
rabbit-anti-CaII	AB1828	1:1,500	1:500	Chemicon Int.
goat-anti-Aqp2	sc9882	1:2,000	1:200	Santa Cruz
mouse-anti-Calbindin D28K	McAB 300	1:20,000		Swant
goat-anti-Foxi1	TSGVLYPREGTEV	1:200		abcam
rabbit-anti-Cp2l1	MLFWHTQPEHYNQHNSGSC	1:1,500		[90]

2° AB	Antigen/Catalog No.	dilution (mouse)	dilution (human)	Source
donkey-anti-goat IgG Alexa 647	A21447	1:1,000	1:500	Invitrogen
donkey-anti-goat IgG Alexa 488	A11055	1:1,000		Invitrogen
donkey-anti-rabbit IgG Alexa488	A21206	1:1,000	1:1,000	Invitrogen
donkey-anti-rabbit IgG Alexa594	A21207	1:1,000		Invitrogen
donkey-anti-guinea pig IgG Cy2	706-226-148	1:500		dianova
donkey-anti-guinea pig IgG Cy3	706-165-148	1:500	1:500	dianova
donkey-anti-guinea pig IgG Dylight 649	706-496-148	1:500		Jackson Immuno Lab
donkey-anti-mouse IgG Dylight 649	715-496-151	1:500		Jackson Immuno Lab
donkey-anti-mouse IgG Alexa594	A21203	1:1,000		Invitrogen
donkey-anti-mouse IgG Alexa488	A21202	1:1,000		Invitrogen
4´,6-diamidino-2-phenylindole, dilactate (DAPI, dilactate)	D3571	1:1,000	1:1,000	Invitrogen

9.6 RNA Isolation and qRT-PCR

Total RNA was isolated from half a kidney of adult mice (P30 and P84) using the RNEasy mini Kit (Qiagen). Total RNA from one kidney of mouse embryos (E18) or newborn mice (P3) was isolated using the RNEasy micro Kit (Qiagen). RNA isolation and on-column DNA digestion was performed according to the manufacturer`s protocols. Total RNA quantity was measured using a ND-1000 UV/Vis-Spectrophotometer (NanoDrop Technologies). Reverse transcription of total RNA (300 ng) was carried out using the TaqMan Reverse Transcription Kit (Applied Biosystems). Quantitative real-time PCR (qRT-PCR) was performed with an ABI PRISM 7700 sequence detection system (Applied Biosystems) using TaqMan Universal PCR Master Mix (Applied Biosystems). Specific primers for the genes of interest were designed using the online-tool Primer3 (http://frodo.wi.mit.edu/primer3/) and tested by conventional PCR to generate the expected amplification products. Oligonucleotide probes conjugated to the reporter dye FAM at the 5' end and the quencher TAMRA at the 3' end were obtained from Microsynth, Switzerland. The mRNA expression levels of genes of interest were firstly normalized to the expression levels of the housekeeping gene *hypoxanthine-guanine-phosphoribosyltransferase* (*Hprt*). Secondly, the normalized values were calculated in percentage and statistical analysis was performed, respectively.

Reverse Transcription		
Step	Temperature	time
1	25°C	10 min
2	40°C	30 min
3	95°C	5 min
4	4°C	hold

Real Time RT-PCR			
Step	Temperature	time	cycle
1	50°C	2 min	
2	95°C	10 min	
3	95°C	15 sec	40
4	60°C	1 min	
5	4°C	hold	

Tab. 9.3 List of primer and Taqman probes used for qRT-PCR

Gene	Accession No.	forward primer
Hprt	NM_013556	5'- TTATCAGACTGAAGAGCTACTGTAATGATC -3'
Aqp2	NM_009699	5'- TGGTGCTGTGCATCTTTGCCT -3'
Slc4a1 (Ae1)	NM_011403	5'- AGGACCTGGTGTTGCCAGAG -3'
Slc26a4 (Pds)	NM_011867	5'- GCCTTTGGGATAAGCAACGTC -3'
Cp2l1	NM_023755	5'- ATGCTGTTCTGGCACACGCAGC -3'
Foxi1	NM_023907	5'- AAGAAGGTGCCCCGAGATG -3'
Klf4	NM_010637	5'- CTGCCAGACCAGATGCAGT -3'
Bdkrb2	NM_009747	5'- ATGCCCTGCTCCTGGAAGCTACT -3'
Gdf15	NM_011819	5'- AGAGGACTCGAACTCAGAACCAAG -3'
Rhcg	NM_019799	5'- GTTGGAGAAGAAGCGCAAGAA -3'
Atp6v1b1 (B1)	NM_134157	5'- AGGACAGTGTGCAGCGTCAAT -3'
Hensin (Dmbt1)	NM_007769.2	5'- GCTCTTTCACCTCAACATCCA -3'

Gene	Accession No.	reverse primer
Hprt	NM_013556	5'- TTACCAGTGTCAATTATATCTTCAACAATC -3'
Aqp2	NM_009699	5'- ACTTGCCAGTGACAACTGCTG -3'
Slc4a1 (Ae1)	NM_011403	5'- CGGTTATGCGCCATGGA -3'
Slc26a4 (Pds)	NM_011867	5'- CAACGATGGCAACATCACA -3'
Cp2l1	NM_023755	5'- TCTCAGGAGATAGCTGCGGCTC -3'
Foxi1	NM_023907	5'- TCTTCTCACAGTTAGGGTCCAGAGT -3'
Klf4	NM_010637	5'- TGGTATAGGTTTTGCCACAGC -3'
Bdkrb2	NM_009747	5'- AGATCTCGGCCACAGTGCAGCTG -3'
Gdf15	NM_011819	5'- TTGACGCGGAGTAGCAGCTGGC -3'
Rhcg	NM_019799	5'- CGAAGACCATGGCGTGTACA -3'
Atp6v1b1 (B1)	NM_134157	5'- CCTGAACAATGGCCTTGGTC -3'
Hensin (Dmbt1)	NM_007769.2	5'- GCTGGCTTGCATGTGATTT -3'

Gene	Accession No.	oligonucleotide (Taqman probe)
Hprt	NM_013556	5'-TGAGAGATCATCTCCACCAATAACTTTTATGTCCC -3'
Aqp2	NM_009699	5'- ACCTCCTTGGGATCTATTTCACCG -3'
Slc4a1 (Ae1)	NM_011403	5'- ACCTGAGGCTCCGCATGTCGACTATACC -3'
Slc26a4 (Pds)	NM_011867	5'- TGGATTTTTCTCCTGTTTTGTGGCTACCACT -3'
Cp2l1	NM_023755	5'- TGGCAGCTACTTGCGTGATGTGCTGGC -3'
Foxi1	NM_023907	5'- ACGACCCAGGCAAAGGGAATTACTG -3'
Klf4	NM_010637	5'- TCTCTCCATTATCAAGAGCTCATGCCA -3'
Bdkrb2	NM_009747	5'- GCCTCCTTTGGCATCGAAATGTTC -3'
Gdf15	NM_011819	5'- TGTCCGGATACTCAGTCCAGAGGTGAGA -3'
Rhcg	NM_019799	5'- TTACTATCGCTACCCGAGCTTCCAG -3'
Atp6v1b1 (B1)	NM_134157	5'- CCCAGTATGCTGAGATTGTCAACTTTACCCTCC -3'
Hensin (Dmbt1)	NM_007769.2	5'- TGACAATAACACCACCAATCTCCCTTTGTGAGT -3'

9.7 Protein Isolation

Crude membrane and cytosolic proteins were extracted from half a kidney of adult mice (P30 and P84). In detail, the organ was minced on ice and homogenized in 200 µl of ice cold resuspension buffer (200 mM Mannitol, 80 mM Hepes, 41 mM KOH, pH 7.5 supplemented with 1 tablet/10 ml Complete Mini Protease Inhibitor Cocktail, Roche) using a Polytron homogenizer (0.5 mm diameter at 20,000 rpm for 1 minute at 4°C). The homogenate was further sonicated on ice before centrifugation at 2,000 rpm for 20 minutes at 4°C. The resulting supernatant was transferred into a prechilled tube and further centrifuged at 41,000 rpm for 1 hour at 4°C. After ultracentrifugation the supernatant (cytosolic proteins) was transferred into a fresh prechilled tube, while the pellet (crude membrane proteins) was resuspended in 50 µl of ice cold resuspension buffer. Protein concentration was measured using the Bio-Rad *DC* Protein Assay according to manufacturer recommendations.

In order to obtain total cell lysates, confluent cell monolayers, grown on 6 well plates (Nunclon Surface, nunc), were washed with ice-cold PBS (without Ca^{++}, Mg^{++}, Gibco) at 4°C and scraped into a prechilled 1.5 ml Eppendorf tube. The cell suspension was centrifuged at 2,000 rpm for 5 minutes at 4°C and the supernatant was removed. Subsequently, the densed cell pellet was lysed by addition of 50 µl RIPA buffer (20 mM Tris-HCl pH 7.5, 150 mM NaCl, 1 mM Na_2EDTA, 1 mM EGTA, 1% NP-40, 1% Na-deoxycholate, supplemented with 1 x Protease inhibitor cocktail (Sigma) and 2 mM PMSF) and vigorous pipetting. The crude cell lysate was centrifuged at 10,000 rpm for 10 minutes at 4°C and the supernatant (total cell lysate) was transferred into a fresh tube. Protein concentration was measured using the Bio-Rad Protein Assay following manufacturer recommendations.

9.8 Nuclear protein extraction

Buffer A (hypotonic lysis buffer)
10 mM Tris-Cl, pH 8.0
150 mM NaCl
10 mM $MgCl_2$

Homogenization buffer (HB)	
0.27 M Sucrose	in 1x Buffer A
2 mM EDTA, pH 8.0	
0.1 % NP-40	
1 mM PMSF	
0.5 mM DTT	
Protease Inhibitor Cocktail (1 tablet/10 ml, Sigma)	

Nuclear extraction buffer (NEB)
10 mM Tris-Cl, pH 8.0
1 mM EDTA, pH 8.0
400 mM NaCl
1 mM DTT
1 mM PMSF

Sucrose Cushion (SC)	
30 % w/v Sucrose	in 1x Buffer A
2 mM EDTA, pH 8.0	

Nuclear proteins were extracted from half a kidney of adult mice (P30 and P84). The tissue was minced and subsequently homogenized on ice in 2 ml of ice cold homogenization buffer (HB) using a Polytron homogenizer (0.5 mm diameter at 20,000 rpm) for 1 minute. Prior to homogenization, a 3 ml layer of sucrose cushion (SC) was prepared in a 15 ml Sarstedt tube on ice. The homogenate was smoothly transferred to the 15 ml tube overlaying the SC and centrifuged at 2,000 rpm for 15 minutes at 4°C. Subsequently, the supernatant was removed and the densed pellet of nuclei was washed with ice cold PBS and centrifuged again. Following removal of PBS,

the pelleted nuclei were resuspended in 1 volume of ice cold nuclear extraction buffer (NEB) transferred to a prechilled tube and incubated for 15 minutes on ice while vortexing every 5 minutes. Afterwards the samples were centrifuged at 13,200 rpm at 4°C for 15 minutes and the supernatant (nuclear extracts) was transferred into a fresh prechilled tube. Protein concentration was determined using the Bio-Rad Protein Assay according to manufacturer recommendations.

9.9 Immunoblotting

For immunoblotting 20 μg of crude membrane, or cytosolic protein extracts, or total cell lysate, or 5 μg of nuclear protein extracts were solubilized in Laemmli buffer, seperated by SDS-PAGE and stained with Coomassie Blue or blotted on a PVDF membrane (Immobilon-P, Millipore). Washing steps were carried out using TBS-T (Tris buffered saline, 0.1 % Tween 20) and unspecific binding of the antibodies was impaired using 5 % non-fat dry milk/TBS-T. Antibodies were diluted according to Tab. 9.4 in 1 % non-fat dry milk/TBS-T. Primary antibodies were incubated overnight at 4°C, while secondary antibodies were incubated for 2 hours at RT. Immunoreactive signals were detected by chemiluminescence (Immobilon Western Substrates, Millipore) using a DIANA III-chemiluminescence detection system (Raytest). Densitometry of the respective signals was quantified using the AIDA software (Advanced Image Data Analyzer, Raytest) and normalized to β-actin intensity or Coomassie Blue staining as indicated.

Tab. 9.4 List of Antibodies (AB) used for immunoblotting

1° AB	Antigen/Catalog No.	dilution	Source
guinea pig-anti-Ae1	DCFIYEDQIRPQDREELLRALLLK	1:500	Own (Pineda)
rabbit-anti-pendrin	CKDPLDLMEAEMNAEELDVQDEAMRRLAS	1:1,000	Own (Pineda)
rabbit-anti-B1	CAQQDPASDTAL	1:1,000	Own (Pineda)
rabbit-anti-AQP2	AQP2 C-term	1:3,000	Loffing, J.
goat-anti-Foxi1	TSGVLYPREGTEV	1:250	abcam
goat-anti-Gdf15	sc46248	1:1,500	Santa Cruz
mouse-anti-β actin	A5441	1:10,000	Sigma

2° AB	Antigen/Catalog No.	dilution	Source
anti-rabbit IgG, AP	S3731	1:5,000	Promega
anti-rabbit IgG, HRP	NA9341	1:10,000	Amersham
anti-guinea pig IgG, AP	A5062	1:5,000	Sigma
anti-mouse IgG, AP	S3721	1:5,000	Promega
anti-mouse IgG, HRP	NA931	1:10,000	Amersham
donkey-anti-goat IgG, AP	V1151	1:5,000	Promega

9.10 Blood and Urine Analysis

Blood pH, blood gas (pCO_2, pO_2), and blood electrolyte concentrations (Na^+, K^+, Cl^-, Ca^{++}) were analyzed using an ABL 505 blood gas analysator (Radiometer, Kopenhagen) and performed on heparinised venous blood as described earlier (chapter 9.1). Creatinine in urine was measured according to Jaffe`s method [221]. Urinary ammonium was measured following Berthelot`s protocol [222]. Plasma and urinary Urea levels were measured using diacetyl monoxime [223] and inorganic phosphate was determined using acid ammonium molybdate [224]. The urinary electrolytes were normalized to urinary creatinine and represented as mean ± SEM (standard error of the mean).

9.11 Cell culture and transient transfection

Hek293T cells (P8-10) were grown on 75 cm^2 flask (Greiner) in complete growth medium (DMEM with L-Glutamine (PAA), supplemented with 1 mM L-Glutamine (Lonza), 1 mM NEAA (Non-Essential-Amino-Acids (Lonza), and 10% FCS (fetal calf serum, Gibco)) at 37°C with 5% CO_2 atmosphere. Cells were passaged when they reached 80% confluency and split in a 1:15 ratio for general maintenance. Prior to trypsinization with 0.1 mM Trypsin-EDTA (Sigma), the monolayer was washed twice with prewarmed PBS (without Ca^{++}, Mg^{++}, Gibco). Trypsinization was stopped by addition of complete growth medium and cell suspension was centrifuged at 1,000 rpm for 1 minute. The supernatant was removed and the cell pellet was gently resuspended in complete growth medium. Transient transfections were carried out using Lipofectamine 2000 (Invitrogen) following manufacturer recommendations. Briefly, 2^6 cells/well were seeded on Poly-L-Lysine (Sigma) coated (15 minutes at RT) 6 well plates (Greiner) in complete growth medium. After 24 hours the growth medium was replaced by serum-free reduced medium (Opti-Mem, Gibco) and cells were transfected with 1 μg Foxi1 plasmid DNA (ImaGenes IRAVp968C0115D, Acc.No. BC007475). In case of untransfected cells, the plasmid DNA was replaced by equivalent amounts of sterile distilled water. Cells were harvested 48 hours after transfection and total cell lysates were prepared as described in chapter 9.7. Plasmid DNA was purified from a liquid bacteria culture using the Fast Plasmid Kit (Eppendorf).

9.12 Statistical Analysis

All data are presented as mean ± SEM (standard error of the mean). Statistical Analysis was performed with GraphPad Prism Software 5.0 and the unpaired *t*-test or one way ANOVA with Tukey post-test were done where appropriate. Only results with $p \leq 0.05$ were considered statistically significant.

10. RESULTS

As already mentioned, a urinary concentrating defect correlating with Aqp2 dysregulation was observed in adult Ae1 deficient mice, in addition to erythroidal defects and severe dRTA [190]. Furthermore, preliminary unpublished observations indicated the abnormal expression of renal IC marker proteins involved in acid-base homeostasis. Therefore, colocalization studies using specific antibodies targeting the a4 and B1 subunits of the V-ATPase, Pds, Ae1, CaII and Aqp2 were performed. As described earlier, carbonic anhydrase II is strongly expressed in renal ICs and therefore commonly used as a general marker [41, 42]. However, in the present study a strong CaII expression was additionally found in Aqp2 positive cells of the CNT and early CCD in kidneys of murine and human origin (data not shown). Hence, CaII did not proof a specific marker for renal ICs in general and these data will not be further considered. Therefore, as shown in Fig. 2.6 renal principal cells were identified by the presence of Aqp2 ($Aqp2^+$), while V-ATPase ($B1^+$, $a4^+$, $V\text{-}ATPase^+$) labelling identified types of intercalated cells in general. Furthermore, Ae1 ($Ae1^+$) expression specified type A-ICs, where appropriate, while Pds (Pds^+) labelling determined type B-ICs. The number of cells positive or negative for either marker was assessed and statistically analyzed with respect to the segmental distribution. Within the CD system four different segments (CNT, CCD, OMCD and IMCD) were primarily distinguished based on morphologic criteria. Moreover, simultaneous immunologic localization of the Calcium binding protein Calbindin D28K (Calb1) helped to discriminate between the CNT and CCD segments. No further information was gathered by Calb1 staining and therefore these data will not be presented.

10.1 Intercalated cells of the mature Ae1 deficient mouse kidney are abnormally differentiated

Investigation of the mature kidney of juvenile (P30) and adult (P84) Ae1 deficient mice revealed unusual expression of pendrin in inner medullary collecting ducts. Moreover, mRNA expression levels as well as protein abundance and expression pattern of candidate regulatory molecules involved in terminal differentiation of the renal collecting duct were found to be abnormally regulated in kidneys of P30 and P84 Ae1 KO mice. However, kidney development and maturation seemed unaffected in Ae1 deficient animals.

10.1.1 Pendrin is abnormally expressed in the inner medulla of adult Ae1 deficient mouse kidney

In the healthy adult kidney, pendrin expression identifies type B-ICs and is usually restricted to the renal cortex, (Fig. 10.1). In contrast to wild-type (WT), Pds expression was still present in the renal inner medulla of adult (P84, postnatal day 84) Ae1 knock-out (KO) mice (Fig. 10.2). Moreover, Pds in the inner medulla was unusually coexpressed with the PC marker Aqp2. Interestingly, Pds expression in the renal cortex (CNT and CCD) of adult Ae1 KO mice appeared normal, indicating a cortical preservation of the type B-IC phenotype. Nevertheless, quantification of individually labelled cells revealed an altered cellular distribution in distinct renal segments of Ae1 KO mice compared to WT (Fig. 10.3). The marker combination used in this colocalization study distinguishes only between principal cells ($Aqp2^+$) and type B-ICs (Pds^+), thus other variations of ICs are represented in the population of unlabelled (none) cells. Consistent with the chronic dRTA, the relative number of Pds^+ cells is significantly reduced in the CNT and CCD of Ae1 KO mice with a concomitant increase in $Aqp2^+$ cells (Fig. 10.3A, B). Furthermore, unusually $Aqp2^+/Pds^+$ colabelled cells were detected in the renal OMCD (Fig. 10.3C), probably at the expense of unlabelled (none) cells. Moreover, the relative abundance of both, Pds^+ and

Aqp2^{+}/Pds^{+} cells respectively, is significantly increased in IMCDs of Ae1 deficient mice, with a simultaneous reduction of unlabeled cells (Fig. 10.3D).

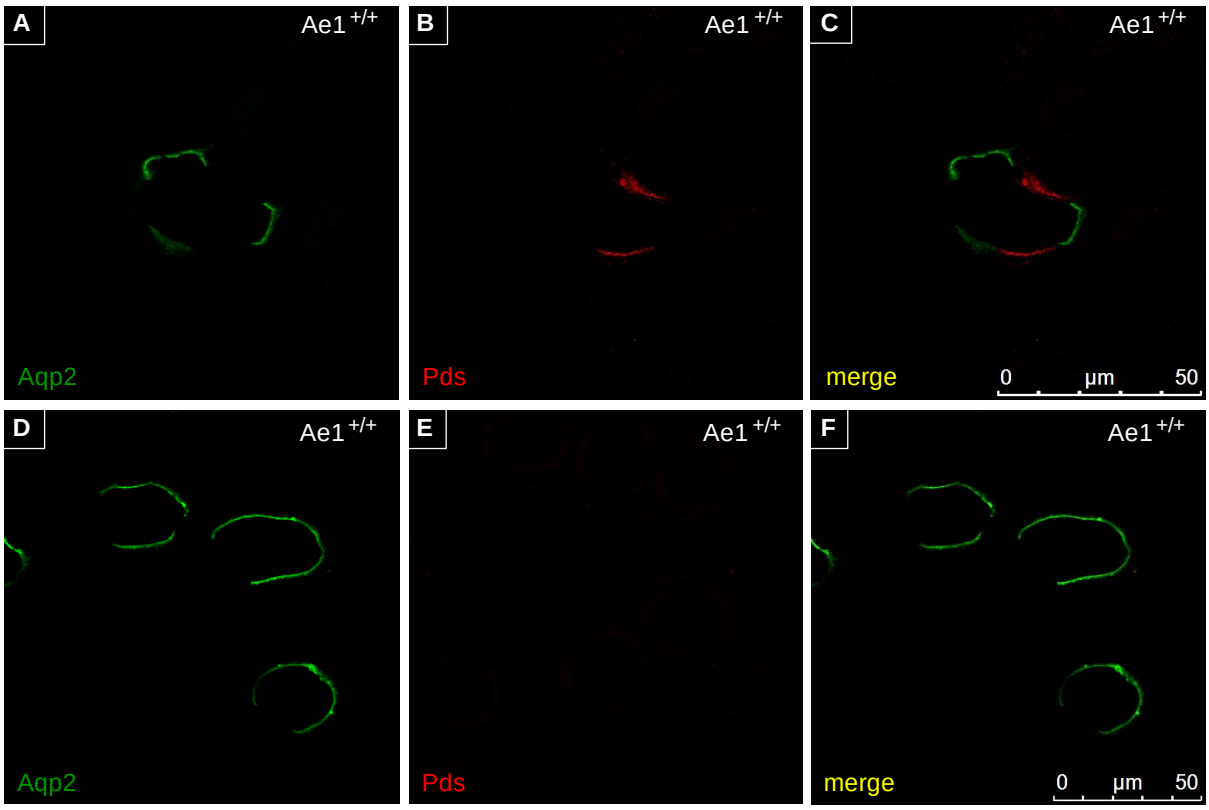

Fig. 10.1 Immunologic localization of Pds in adult (P84) Ae1$^{+/+}$ mouse kidney. **A-C)** Representative photomicrographs from renal cortex (CCD). **D-F)** Representative photomicrographs from renal inner medulla (IMCD). **A, D)** Individual Aqp2 (aquaporin 2) expression in renal CCD and IMCD identifies principal cells. **B)** In the CCD, Pds (pendrin) localizes to the luminal membrane of Aqp2 negative cells, identifying B-ICs. **E)** In adult WT mouse kidney, Pds is absent from the inner medulla. **C, F)** merge. Magnification 400x.

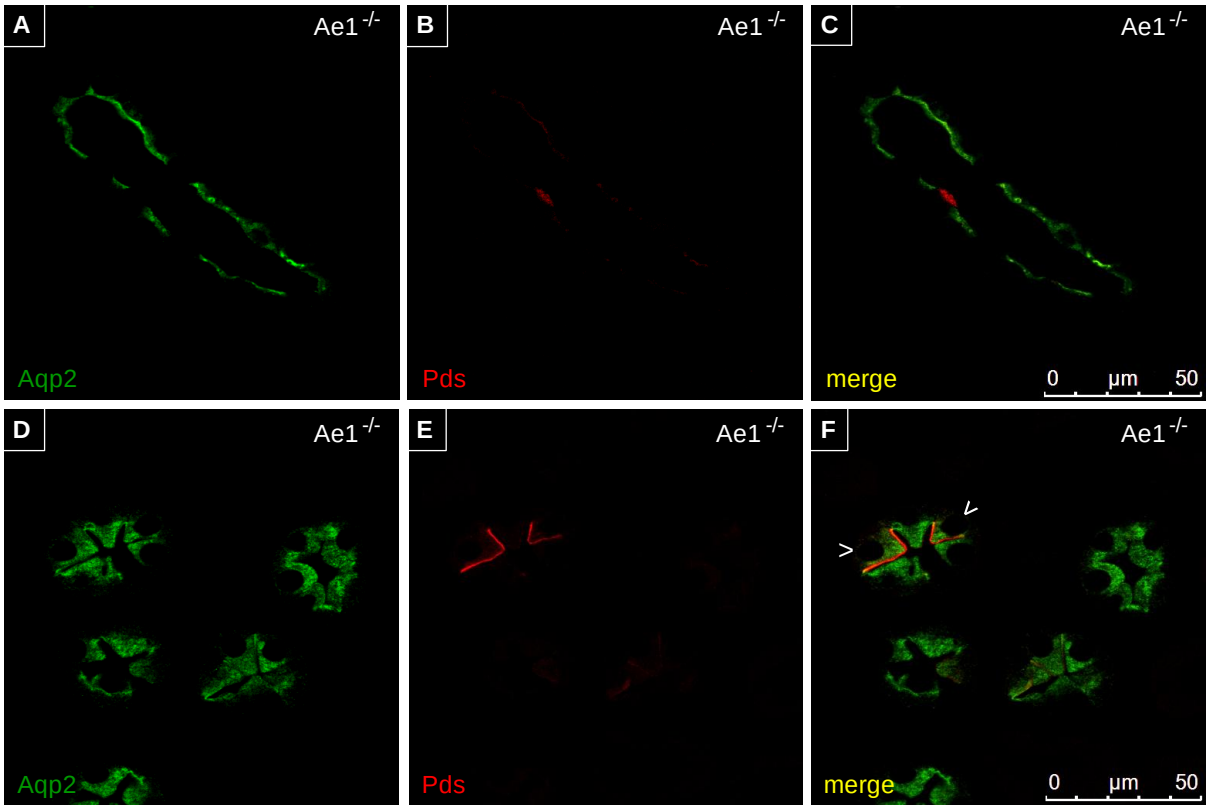

Fig. 10.2 Immunologic localization of Aqp2 and Pds in adult (P84) Ae1$^{-/-}$ mouse kidney. **A-C)** Representative photomicrographs from renal cortex (CCD). **D-F)** Representative photomicrographs from renal inner medulla (IMCD). **A, D)** Individual Aqp2 (aquaporin 2) expression in renal CCD and IMCD identifies principal cells. **B)** In the CCD, Pds (pendrin) localizes to the luminal membrane of Aqp2 negative cells, identifying B-ICs. **C)** merge. **E)** In adult Ae1 deficient mouse kidney, Pds expression is occasionally still present on the luminal membrane of IMCD cells and even coexpressed with luminal Aqp2 expression (**F**, arrowheads). Magnification 400x.

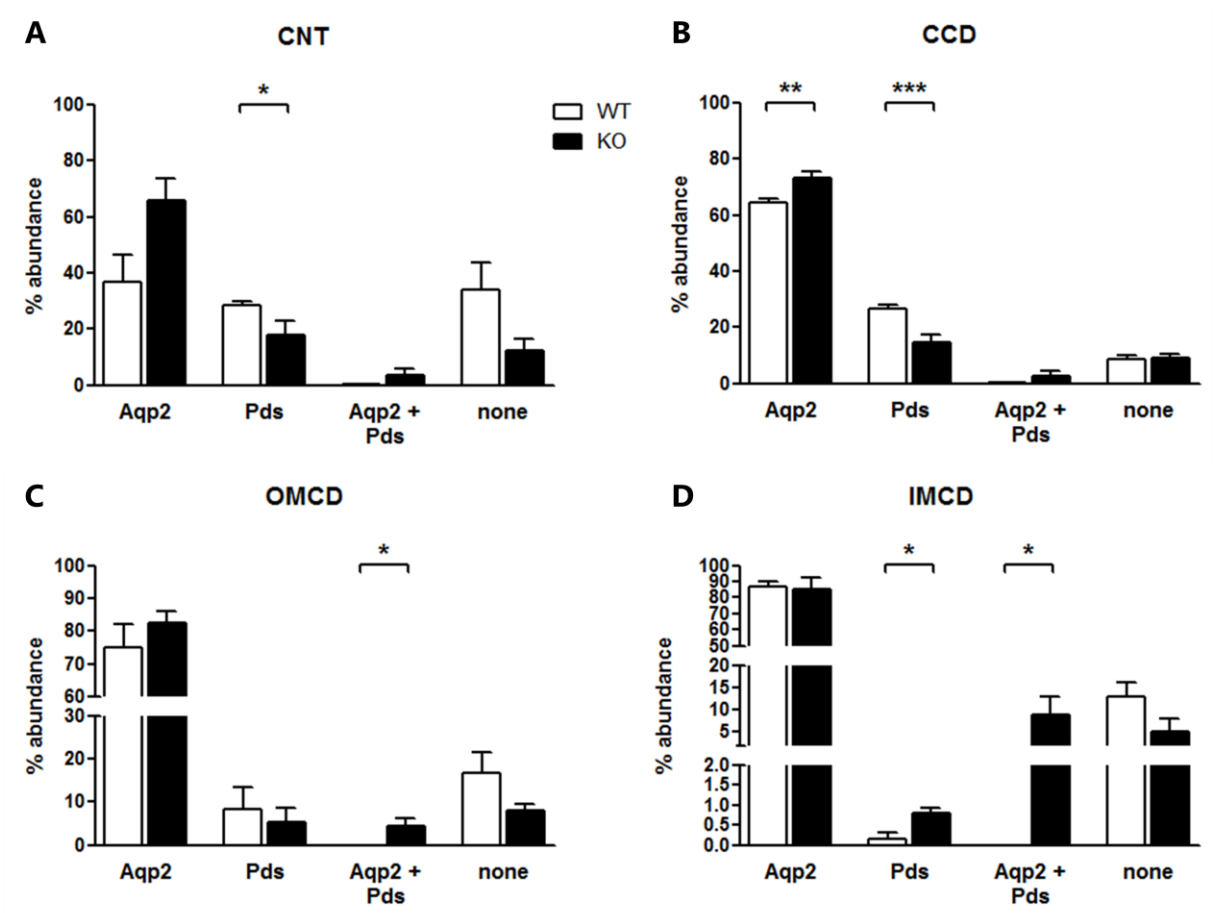

Fig. 10.3 Relative distribution of Aqp2 and Pds in adult (P84) WT and Ae1 KO mouse kidney. **A-D)** Summary of cell counts assessing the relative abundance of Aqp2 (aquaporin 2) and Pds (pendrin) positive cells in the renal CNT, CCD, OMCD and IMCD of adult (P84) Ae1 WT and KO mice. In total, 9,676 cells were counted in WT kidneys (n=7) and 5,533 cells in KO kidneys (n=4). Statistical analysis using Student`s *t*-test. * $p \leq 0.05$, ** $p \leq 0.01$, *** $p \leq 0.001$.

CNT: connecting tubule, CCD: cortical collecting duct, OMCD: outer medullary collecting duct, IMCD: inner medullary collecting duct

10.1.2 Intercalated cells in the mature kidney of juvenile (P30) Ae1 deficient mice are abnormally differentiated

Similar to adult (P84) Ae1 deficient mice, an unusual presence of Pds in cells of the mature inner medulla was observed in juvenile (P30) Ae1 KO mouse kidneys (Fig. 10.4 to 10.7). Consistently, renal medullary Pds expression was still present in Ae1 KO kidneys and in addition unusually coexpressed with Aqp2 in the IMCD (Fig. 10.6C, 10.7F, 10.8C, D). However, the relative distribution of labelled cells within the renal distal tubule was slightly different in P30 compared to P84 Ae1 KO kidney, possibly reflecting the impact of prolonged dRTA. In detail, $Aqp2^+$ cells were less abundant in the renal CNT of P30 WT and Ae1 KO mice compared to P84 CNT, while unlabelled cells were more abundant (Fig. 10.8A). Interestingly, the relative abundance of Pds^+ cells in the renal CNT was comparable at both ages. Furthermore and in contrast to P84 kidneys, there was no difference in the relative abundance of $Aqp2^+$, Pds^+ or unlabelled cells in the CNT of P30 Ae1 WT and KO kidneys. Moreover, Pds^+ cells in the renal CCD of P30 Ae1 KO mice were increased compared to P30 WT, while the relative abundance of unlabelled cells was reduced and $Aqp2^+$ cells were not altered (Fig. 10.8B). In contrast, Pds^+ cells in the renal CCD of P84 Ae1 KO animals were significantly reduced, while unlabelled cells were not altered and $Aqp2^+$ cells were increased compared to P84 WT kidneys (Fig. 10.3B). Similar to the renal CCD of P30 animals, the relative abundance of Pds^+ cells in P30 Ae1 KO OMCD was increased when compared to P30 WT OMCD and the relative numbers of unlabelled cells were decreased (Fig. 10.8C). In contrast, OMCDs of P84 Ae1 KO mice displayed unusual presence of $Aqp2^+/Pds^+$ cells compared to P84 WT, probably on the expense of unlabelled cells (Fig. 10.3C). Finally, in the renal IMCD of P30 Ae1 KO increased abundances of Pds^+ and $Aqp2^+/Pds^+$ cells were found compared to P30 WT, with an adequate reduction of $Aqp2^+$ cells (Fig. 10.8D). Likewise, Pds^+ and $Aqp2^+/Pds^+$ cells were increased in Ae1 KO IMCD of P84 mice compared to WT IMCD, but here the relative number of $Aqp2^+$ was not altered (Fig. 10.3D). The inappropriate increases in

Pds^+ and $Aqp2^+/Pds^+$ cells might rather be explained by the modestly reduced presence of unlabelled cells in P84 Ae1 KO kidneys compared to WT.

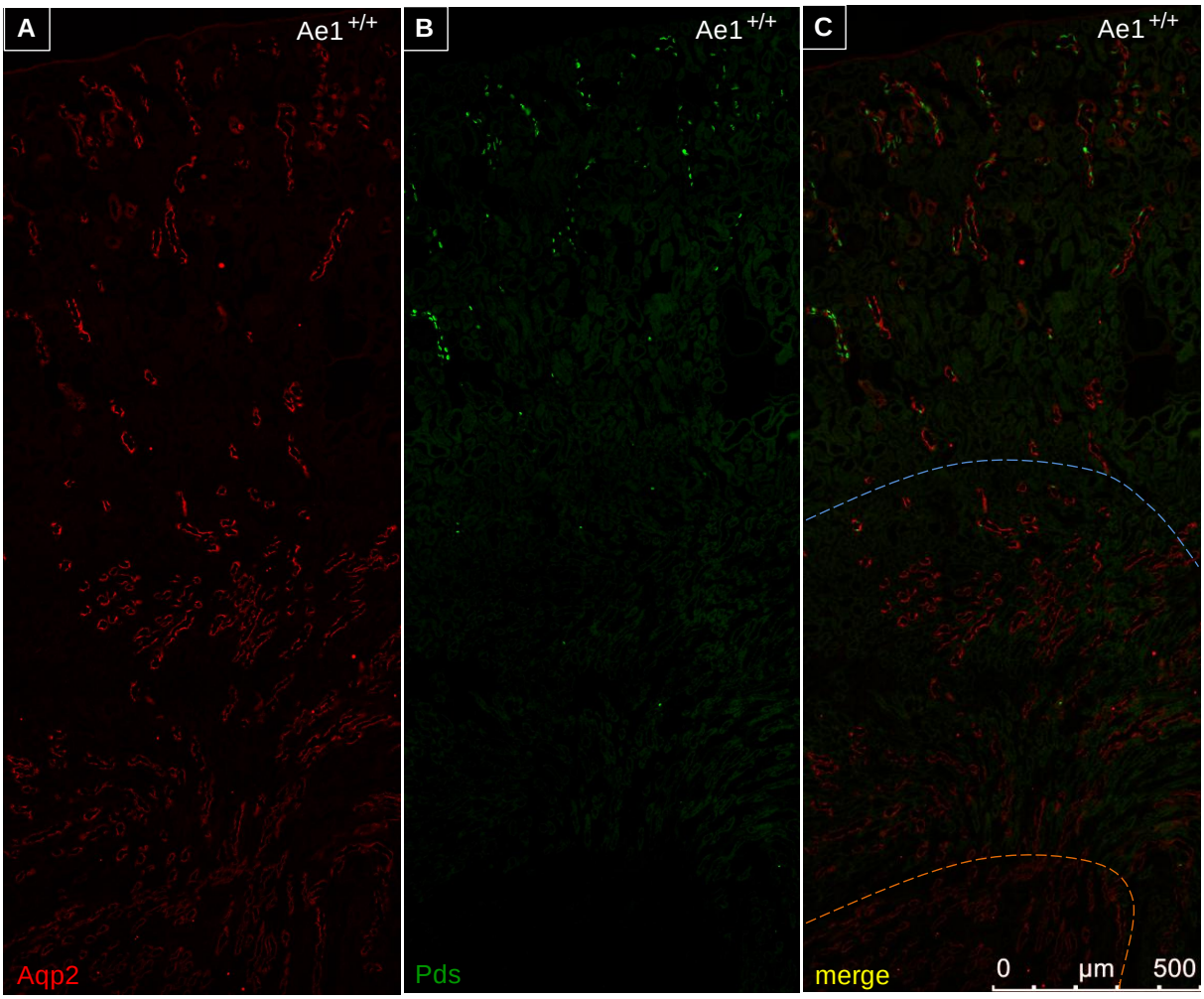

Fig. 10.4 Zonal distribution of Aqp2 and Pds expressing cells in kidney of juvenile (P30) Ae1 $^{+/+}$ mouse. **A)** Aqp 2 (aquaporin 2) is expressed along cortical and medullary collecting ducts. **B)** Pds (pendrin) expression is restricted to the renal cortex in mature kidney. **C)** merge, blue dashed line indicating cortico-medullary boundary, orange dashed line indicating medullary-papillary boundary. Magnification 400x, Tile Scan.

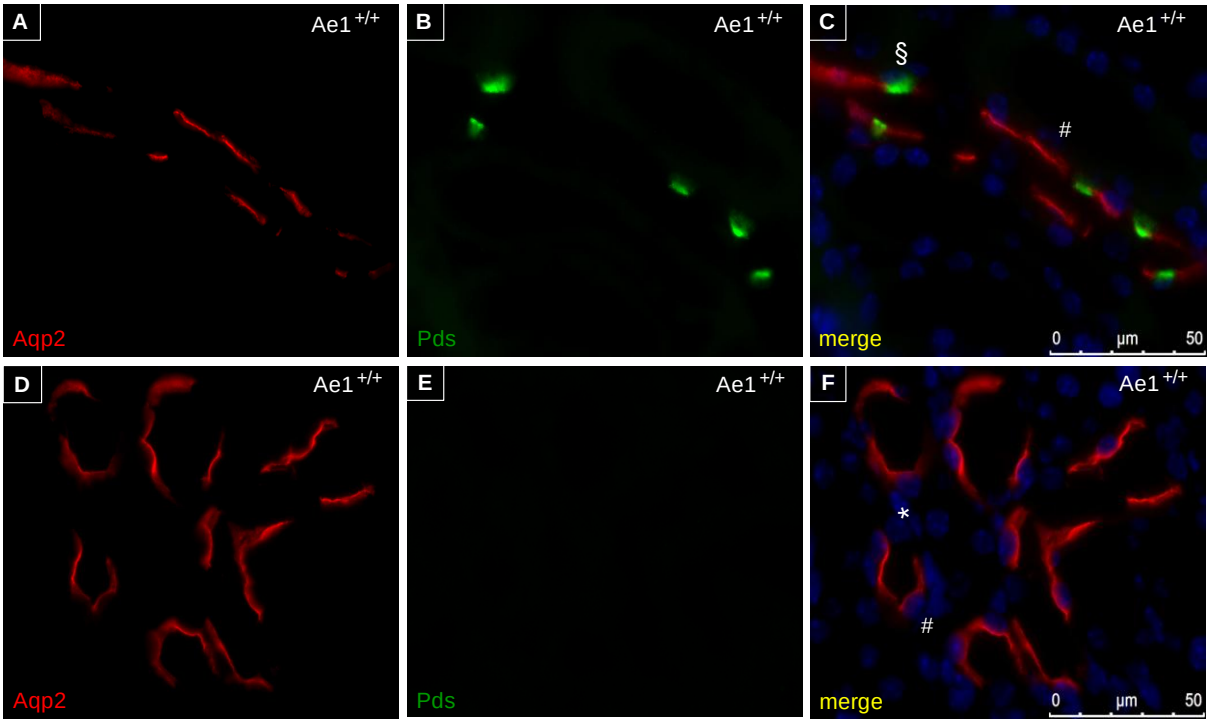

Fig. 10.5 Zonal distribution of Aqp2 and Pds expressing cells in kidney of juvenile (P30) Ae1 $^{+/+}$ mouse. Aqp2 (aquaporin 2) is expressed along cortical **(A)** and medullary **(D)** collecting ducts. Pds (pendrin) expressing cells are frequently present in the renal cortex **(B)** and absent from the medullary collecting ducts **(E)**. **C, F)** merge. Nucleic acid stained with DAPI (blue). § Pds positive cell; # Aqp2 positive cell; * Aqp2/Pds negative cell. Magnification 400x.

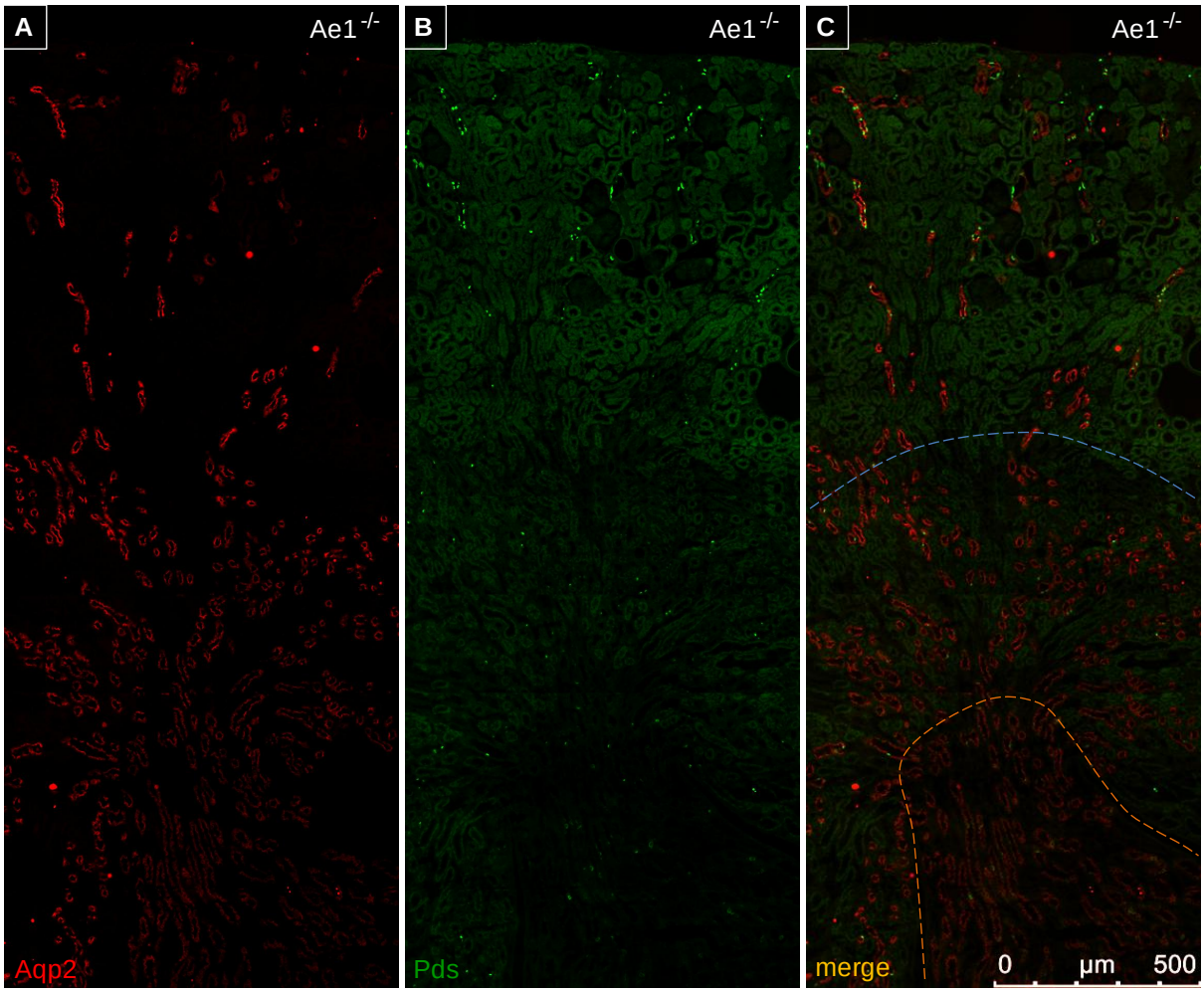

Fig. 10.6 Zonal distribution of Aqp2 and Pds expressing cells in kidney of juvenile (P30) Ae1 $^{-/-}$ mouse. **A)** Aqp 2 (aquaporin 2) is expressed along cortical and medullary collecting ducts. **B)** Pds (pendrin) expression is present in the cortex and inner medulla of the mature kidney. **C)** merge, blue dashed line indicating cortico-medullary boundary, orange dashed line indicating medullary-papillary boundary. Magnification 400x, Tile Scan.

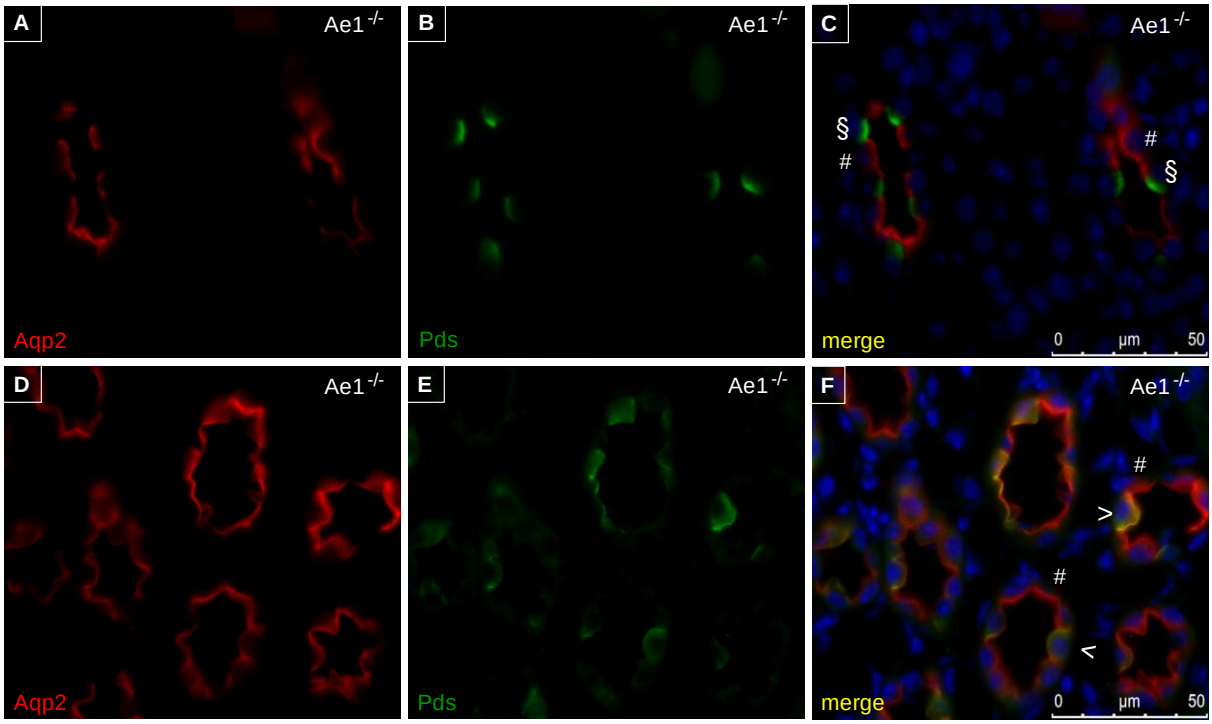

Fig. 10.7 Zonal distribution of Aqp2 and Pds expressing cells in kidney of juvenile (P30) Ae1 $^{-/-}$ mouse. Aqp2 (aquaporin 2) is expressed along cortical **(A)** and medullary **(D)** collecting ducts. Pds (pendrin) expressing cells are frequently present in the cortical **(B)** and medullary collecting ducts **(E)**. **C, F)** merge. Nucleic acid stained with DAPI (blue). § Pds positive cell; # Aqp2 positive cell; arrowhead: Aqp2/Pds positive cell. Magnification 400x.

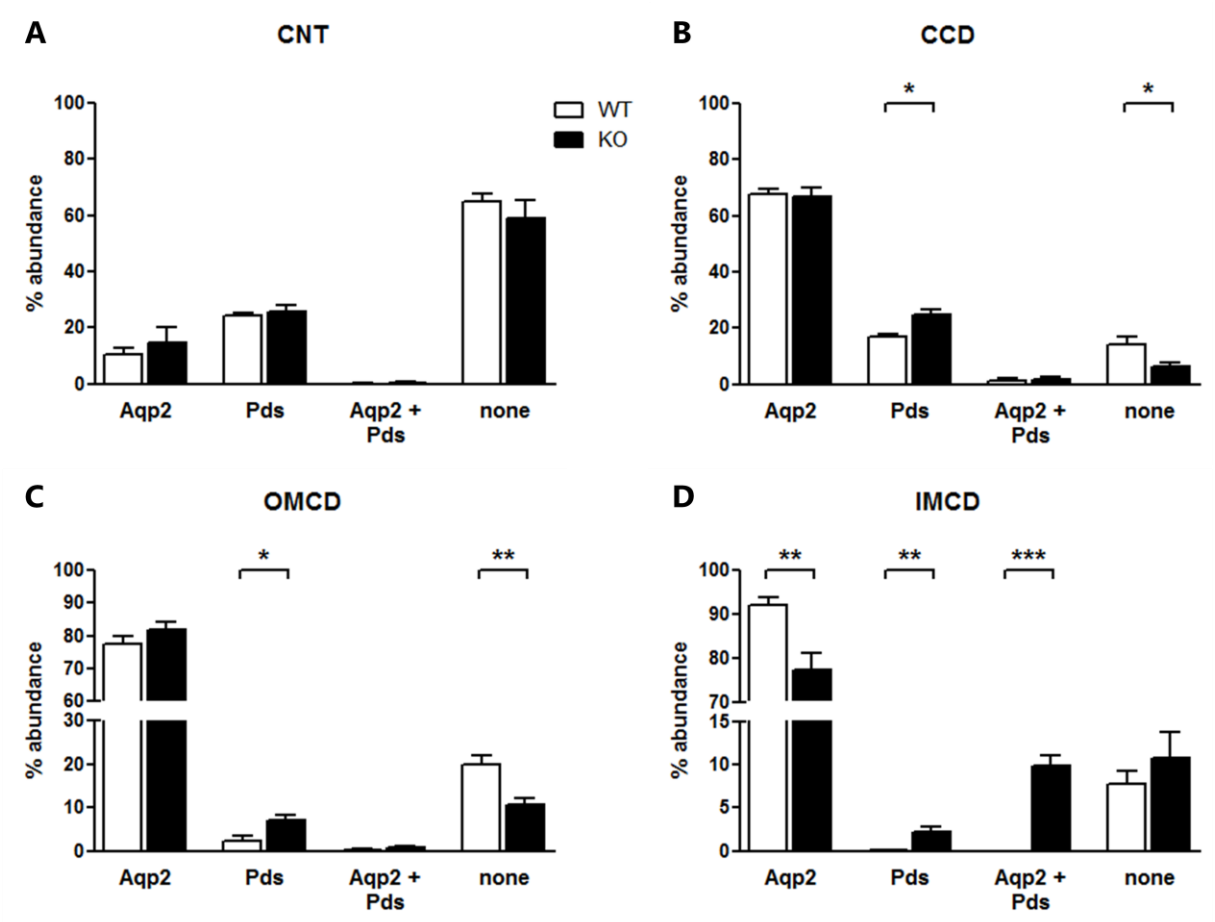

Fig. 10.8 Relative distribution of Aqp2 and Pds expressing cells in kidneys of juvenile (P30) Ae1 WT and KO mice. Summary of cell counts assessing the relative abundance of Aqp2 (aquaporin 2) and Pds (pendrin) positive cells in the renal CNT, CCD, OMCD and IMCD of juvenile (P30) Ae1 WT and KO mice. In total, 5,214 cells were counted in WT kidneys (n=5) and 5,335 cells in KO kidneys (n=5). Statistical analysis using Student`s *t*-test. * $p \leq 0.05$, ** $p \leq 0.01$, *** $p \leq 0.001$.

CNT: connecting tubule, CCD: cortical collecting duct, OMCD: outer medullary collecting duct, IMCD: inner medullary collecting duct

In order to investigate the distribution and appearance of Pds negative ICs of P30 Ae1 KO kidneys, co-immunostainings using the a4 and B1 subunits of the V-ATPase, indicating the presence of manifestations of ICs other than type B-ICs, were performed and quantified (Fig. 10.9 and 10.10). No significant differences in the relative abundance and distribution of the kidney-specific a4 subunit of V-ATPase ($a4^+$) cells were found in P30 Ae1 KO kidneys compared to WT (Fig. 10.9). However, co-staining of Aqp2 and the IC-specific B1 subunit of V-ATPase gave another impression. Here, renal inner medullary collecting ducts of P30 Ae1 KO mice showed a significant increased abundance for $Aqp2^+/B1^+$ cells with a concomitant reduction in $Aqp2^+$ cells compared to WT (Fig. 10.10D). Although alterations of $B1^+$ cell expression in the other segments did not reach significant difference, a similar trend was observed. In the renal CNT of P30 Ae1 KO mice a modest increase in $Aqp2^+/B1^+$ cells (p-value 0.0590) and reduction in unlabelled cells became apparent, while the increase in $Aqp2^+/B1^+$ cells of the CCD (p-value 0.0621) and OMCD (p-value 0.0798) was accompanied by a reduction in $Aqp2^+$ cells (Fig. 10.10A-C).

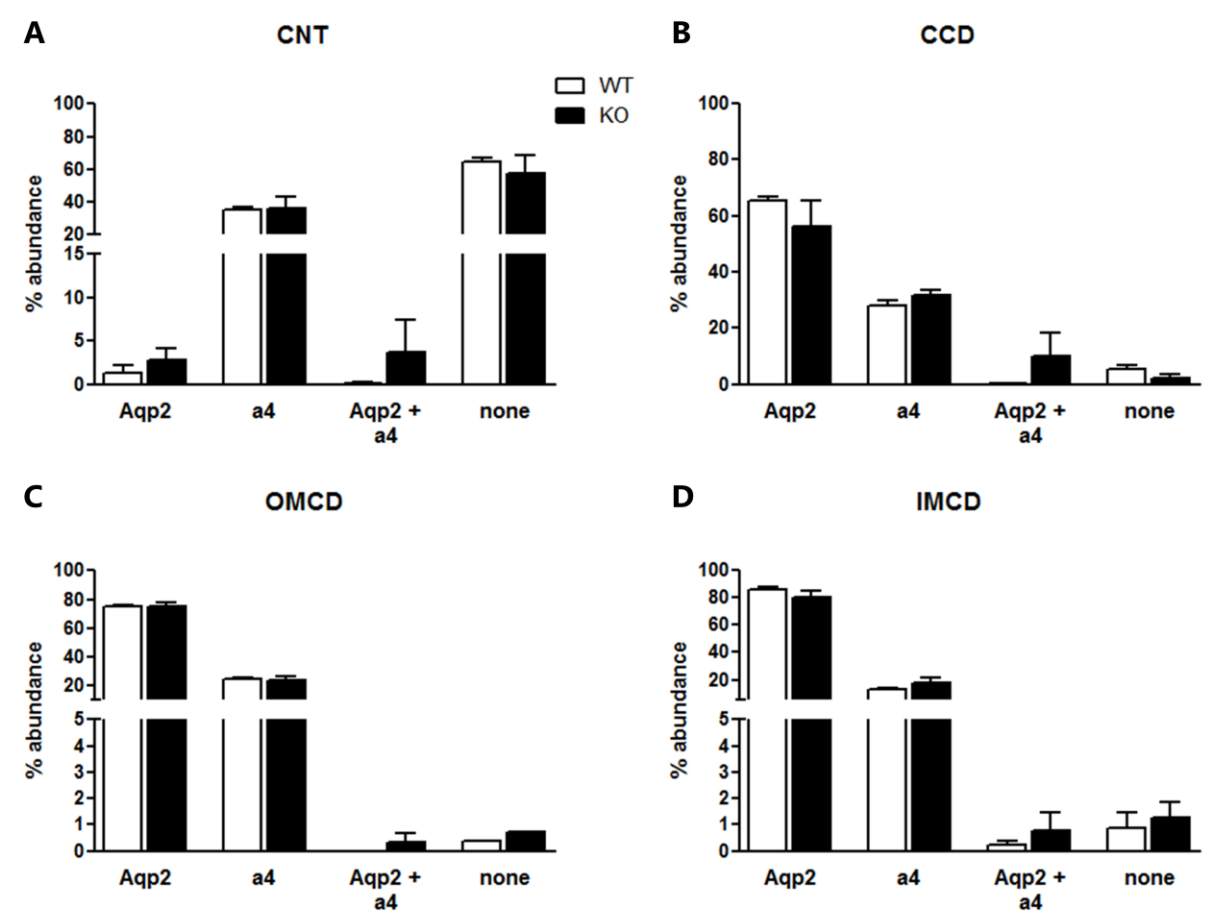

Fig. 10.9 Relative distribution of Aqp2 and a4 expressing cells in kidneys of juvenile (P30) Ae1 WT and KO mice. Summary of cell counts assessing the relative abundance of Aqp2 (aquaporin 2) and a4 (a4 subunit of V-ATPase, Atp6v0a4) positive cells in the renal CNT, CCD, OMCD and IMCD of juvenile (P30) Ae1 WT and KO mice. In total, 4,930 cells were counted in WT kidneys (n=5) and 5,094 cells in KO kidneys (n=5). Statistical analysis using Student`s *t*-test. * $p \leq 0.05$, ** $p \leq 0.01$, *** $p \leq 0.001$.

CNT: connecting tubule, CCD: cortical collecting duct, OMCD: outer medullary collecting duct, IMCD: inner medullary collecting duct

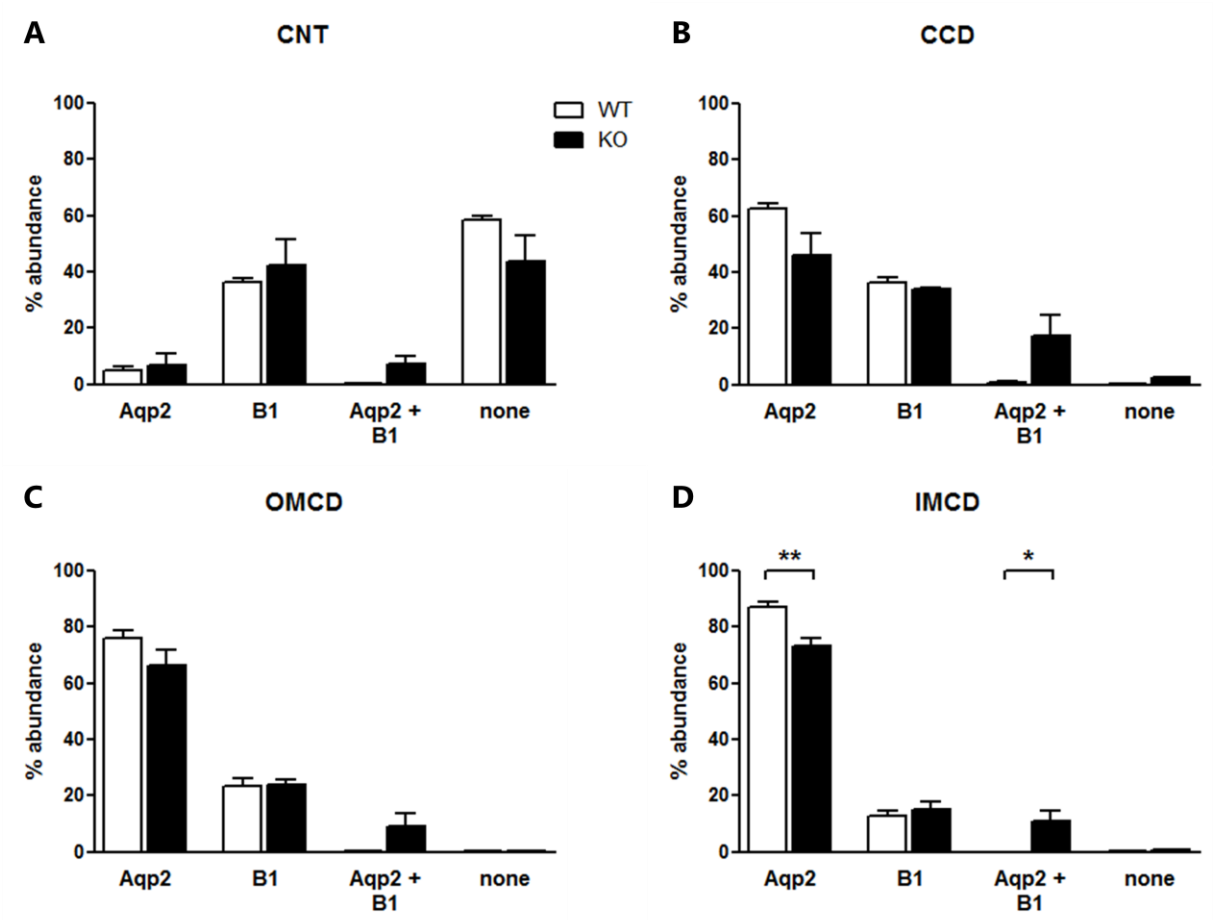

Fig. 10.10 Relative distribution of Aqp2 and B1 subunit of V-ATPase (Atp6v1b1) expressing cells in kidneys of juvenile (P30) Ae1 WT and KO mice. Summary of cell counts assessing the relative abundance of Aqp2 (aquaporin 2) and B1 (B1 subunit of V-ATPase, Atp6v1b1) positive cells in the renal CNT, CCD, OMCD and IMCD of juvenile (P30) Ae1 WT and KO mice. In total, 5,619 cells were counted in WT kidneys (n=5) and 4,638 cells in KO kidneys (n=5). Statistical analysis using Student`s *t*-test.

* $p \leq 0.05$, ** $p \leq 0.01$, *** $p \leq 0.001$.

CNT: connecting tubule, CCD: cortical collecting duct, OMCD: outer medullary collecting duct, IMCD: inner medullary collecting duct

As described in chapter 2.7, some molecules and transcription factors have been identified as critical in terminal differentiation of renal CD specific cells. Among them are the transcription factors Foxi1 and Cp2l1. Even though both transcription factors were localized in renal tubular structures a detailed localization concerning their putative presence in the CD epithelium is missing. Therefore, the expression patterns of both transcription factors were investigated in more detail and preliminary results were compared between Ae1 WT and KO.

The Foxi1 protein was occasionally detected in nuclei of CD cells in P30 WT mouse kidney. Co-labelling with the B1 subunit of V-ATPase (Fig. 10.11, 10.13) and Aqp2 (Fig. 10.14, 10.16) revealed predominant expression of Foxi1 in intercalated cells and less in principal cells of the CNT, CCD, OMCD and IMCD. Quantification of cell counts showed that the majority of $Foxi1^+$ nuclei corresponded with $B1^+$ cells (Fig. 10.13, 10.16). Results obtained from cell counts suggest a relative equal distribution of $Foxi1^+/B1^+$ cells among the CNT (23.69%), CCD (26.33%) and OMCD (21.70%) segments of P30 WT mouse kidney with a similar trend in Ae1 KO animals (Fig. 10.13). However, in Ae1 WT kidney the relative abundance of $Foxi1^+/B1^+$ cells in the IMCD (15.19%) is significantly lower compared to CCD (26.33%, p-value <0.05), reflecting the expected reduced presence of ICs in the renal inner medulla compared to cortex. Similarly, in Ae1 WT kidney the presence of $Foxi1^+$ cells in the staining series with Aqp2 (Fig. 10.16) declines significantly from CNT (24.08%), CCD (18.64%), OMCD (14.72%) to IMCD (8.19%), indicating again the expected reduction of ICs along the CD system towards the papilla. Anyhow, comparing the relative distribution of Foxi1 expression in Ae1 WT and KO kidneys of P30 mice showed some small but significant differences. Individually labelled $Foxi1^+$ cells in the staining series with the B1 subunit of V-ATPase were significantly increased in IMCDs of Ae1 KO kidneys when compared to WT (Fig. 10.13D). In addition, a simultaneous but statistically not significant increase in $Foxi1^+/Aqp2^+$ cells was observed in IMCDs of Ae1 KO kidneys (Fig. 10.16D). Furthermore, individually $Foxi1^+$ and unlabelled (none) cells were significantly reduced in the CCD of P30 Ae1 KO kidneys, while $Aqp2^+/Foxi1^+$

coexpressing cells increased concomitantly (Fig. 10.16B). Hence, loss of Ae1 in kidneys of P30 mice alters the relative segmental distribution of Foxi1 in the CCD and OMCD, favouring its coexpression with the principal cell marker Aqp2.

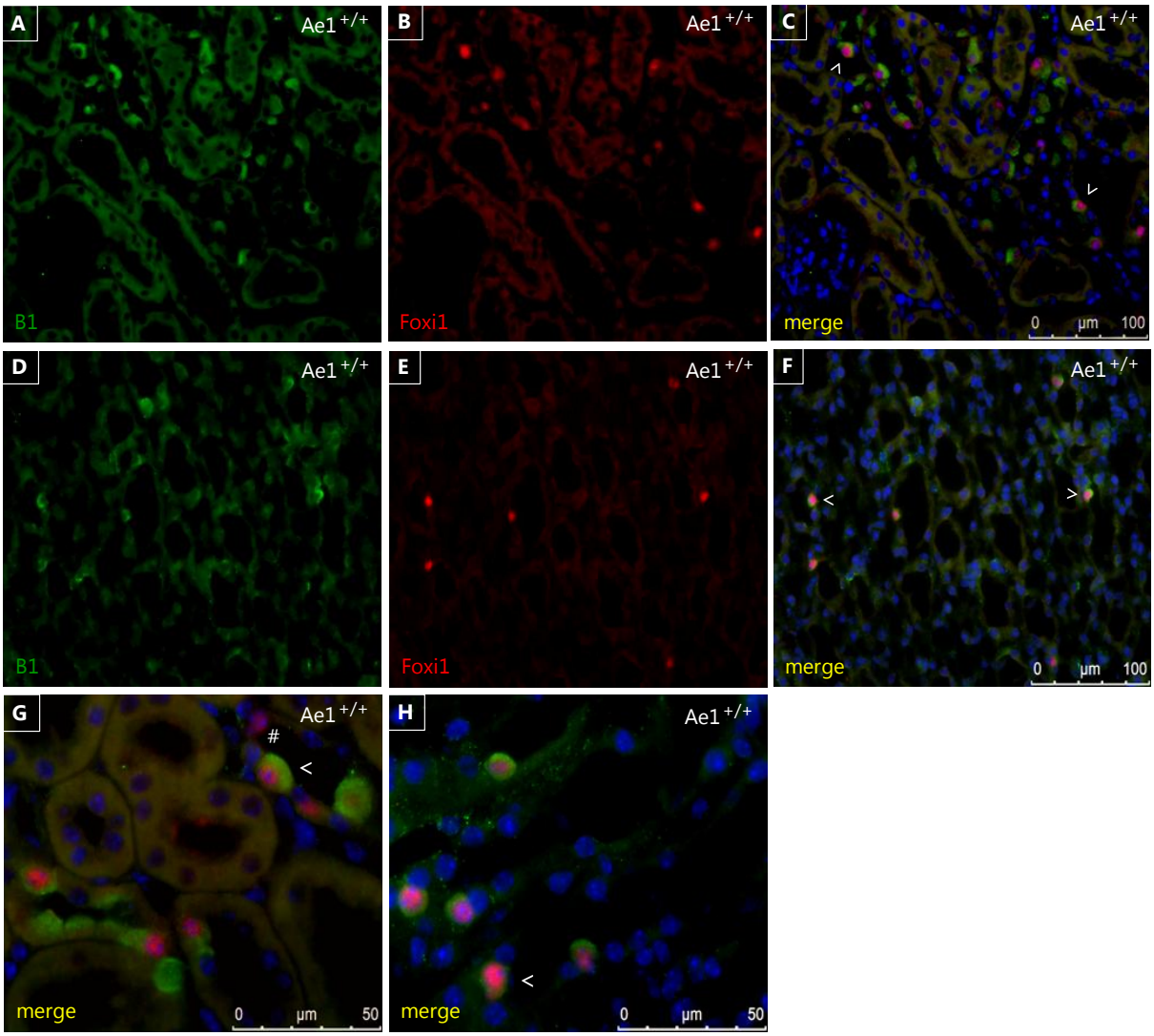

Fig. 10.11 Expression pattern of Foxi1 and B1 expressing cells in kidney of juvenile (P30) Ae1 $^{+/+}$ mouse. **A-C, G)** Renal cortex. **D-F, H)** Renal inner medulla. B1 (B1 subunit of V-ATPase, Atp6v1b1) expressing intercalated cells were frequently present in the renal cortical **(A)** and medullary **(D)** collecting ducts. Nuclear expression pattern of Foxi1 protein was detected in cortical **(B)** and medullary **(E)** tubular structures. Overlay reveals expression of Foxi1 in B1 positive and less frequently in B1 negative cells along the renal collecting ducts **(C, F, G, H)**. Nucleic acid stained with DAPI (blue). # B1 negative/Foxi1 positive cell; arrowhead: B1/Foxi1 positive cell. **A-F)** Magnification 400x. **G,H)** Magnification 1,000x.

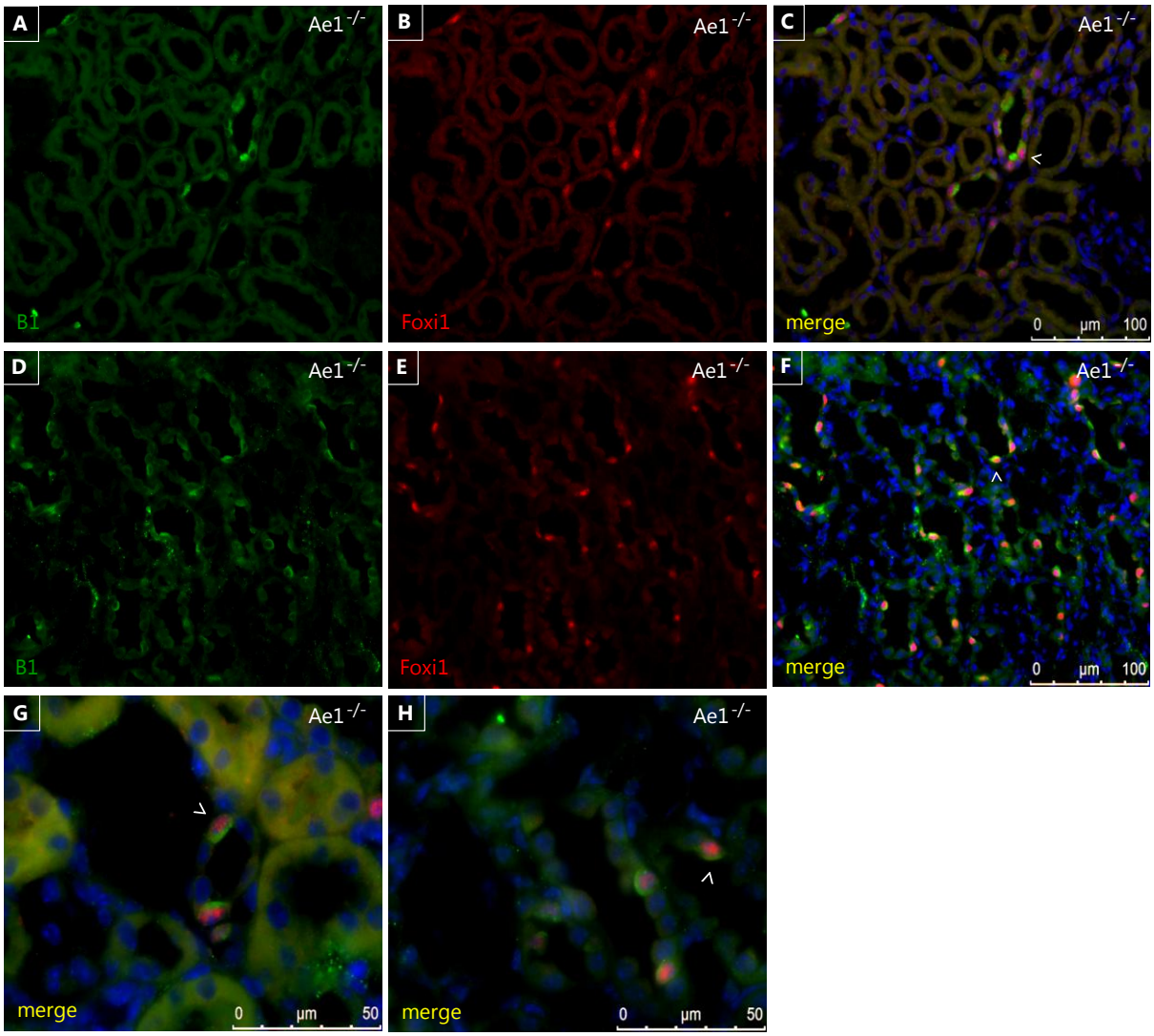

Fig. 10.12 Expression pattern of Foxi1 and B1 expressing cells in kidney of juvenile (P30) Ae1 $^{-/-}$ mouse. **A-C, G)** Renal cortex. **D-F, H)** Renal inner medulla. B1 (B1 subunit of V-ATPase, Atp6v1b1) expressing intercalated cells were frequently present in the renal cortical **(A)** and medullary **(D)** collecting ducts. Nuclear expression pattern of Foxi1 protein was detected in cortical **(B)** and medullary **(E)** tubular structures. Overlay reveals expression of Foxi1 in B1 positive and less frequently in B1 negative cells along the renal collecting ducts **(C, F, G, H)**. Nucleic acid stained with DAPI (blue). arrowhead: B1/Foxi1 positive cell. **A-F)** Magnification 400x. **G,H)** Magnification 1,000x.

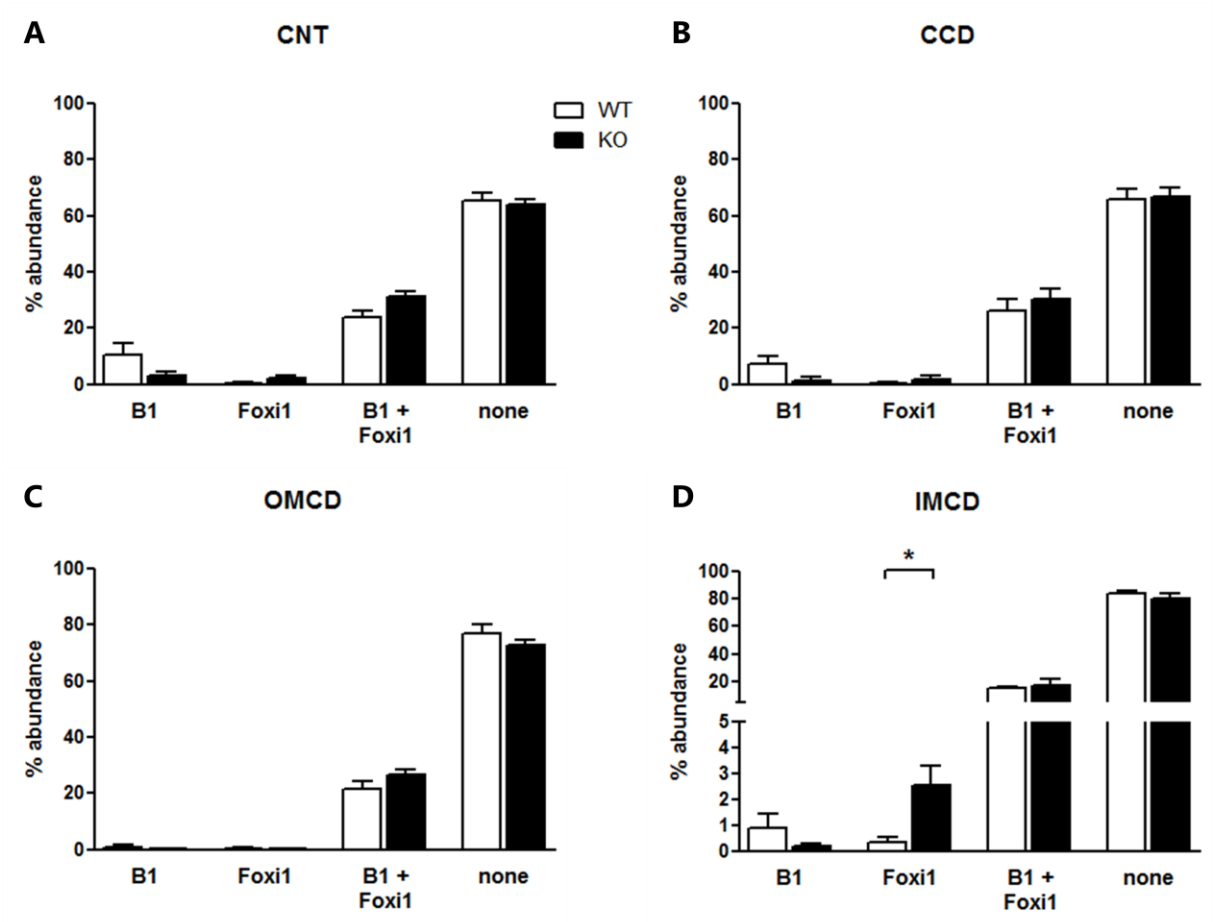

Fig. 10.13 Relative distribution of Foxi1 and B1 subunit of V-ATPase (Atp6v1b1) expressing cells in kidneys of juvenile (P30) Ae1 WT and KO mice. Summary of cell counts assessing the relative abundance of Foxi1 and B1 (B1 subunit of V-ATPase, Atp6v1b1) positive cells in the renal CNT, CCD, OMCD and IMCD of juvenile (P30) Ae1 WT and KO mice. In total, 2,680 cells were counted in WT kidneys (n=4) and 3,489 cells in KO kidneys (n=5). Statistical analysis using Student`s *t*-test. * $p \leq 0.05$, ** $p \leq 0.01$, *** $p \leq 0.001$.

CNT: connecting tubule, CCD: cortical collecting duct, OMCD: outer medullary collecting duct, IMCD: inner medullary collecting duct

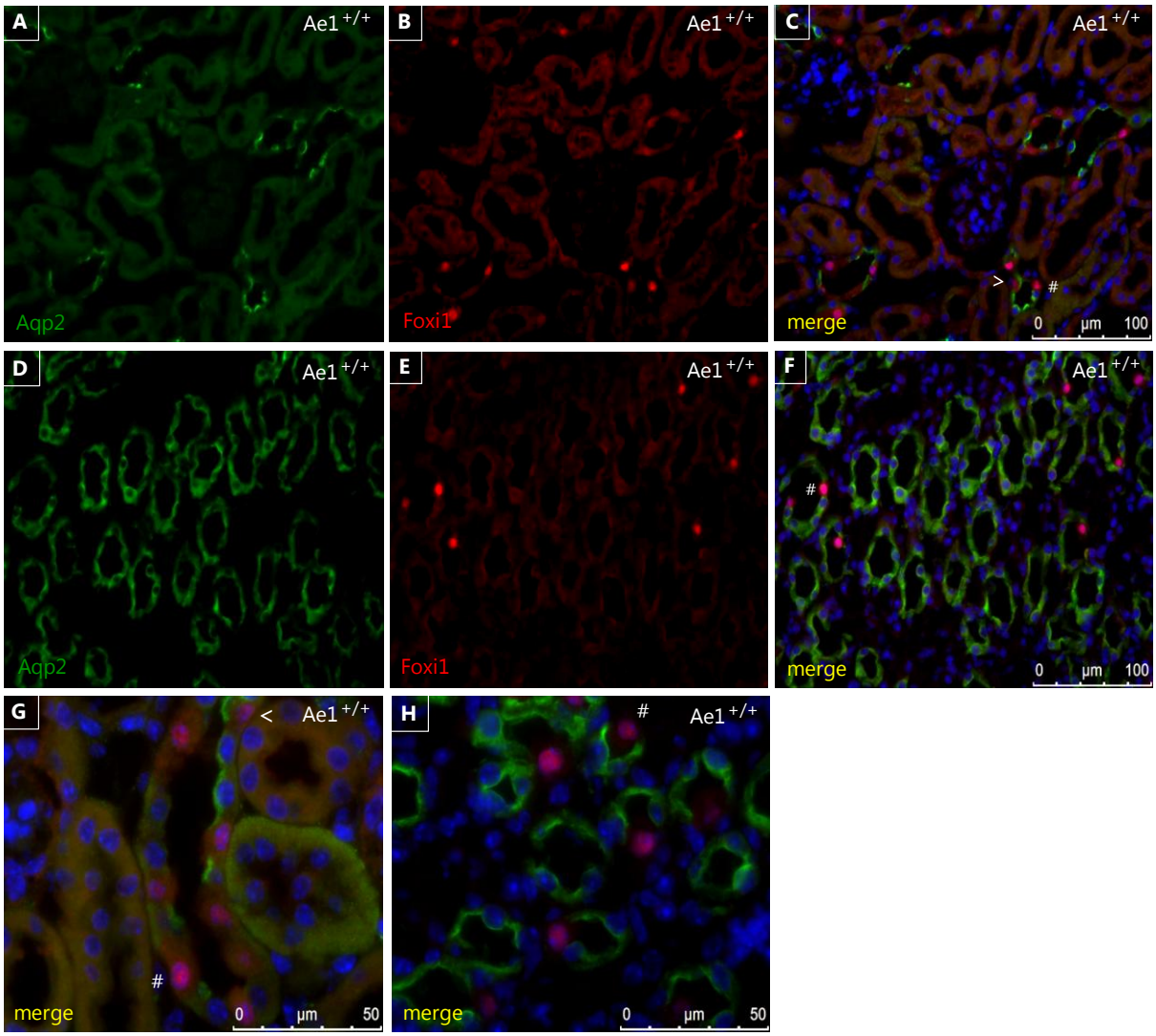

Fig. 10.14 Expression pattern of Foxi1 and Aqp2 expressing cells in kidney of juvenile (P30) Ae1 $^{+/+}$ mouse. **A-C, G)** Renal cortex. **D-F, H)** Renal inner medulla. Principal cells expressing luminal Aqp2 (aquaporin 2) in renal cortical **(A)** and medullary **(D)** collecting ducts. Nuclear expression pattern of Foxi1 protein was detected in cortical **(B)** and medullary **(E)** tubular structures. Overlay reveals predominant expression of Foxi1 in Aqp2 negative and less frequently in Aqp2 positive cells along the renal collecting ducts **(C, F, G, H)**. Nucleic acid stained with DAPI (blue). # Aqp2 negative/Foxi1 positive cell; arrowhead: Aqp2/Foxi1 positive cell. **A-F)** Magnification 400x. **G, H)** Magnification 1,000x.

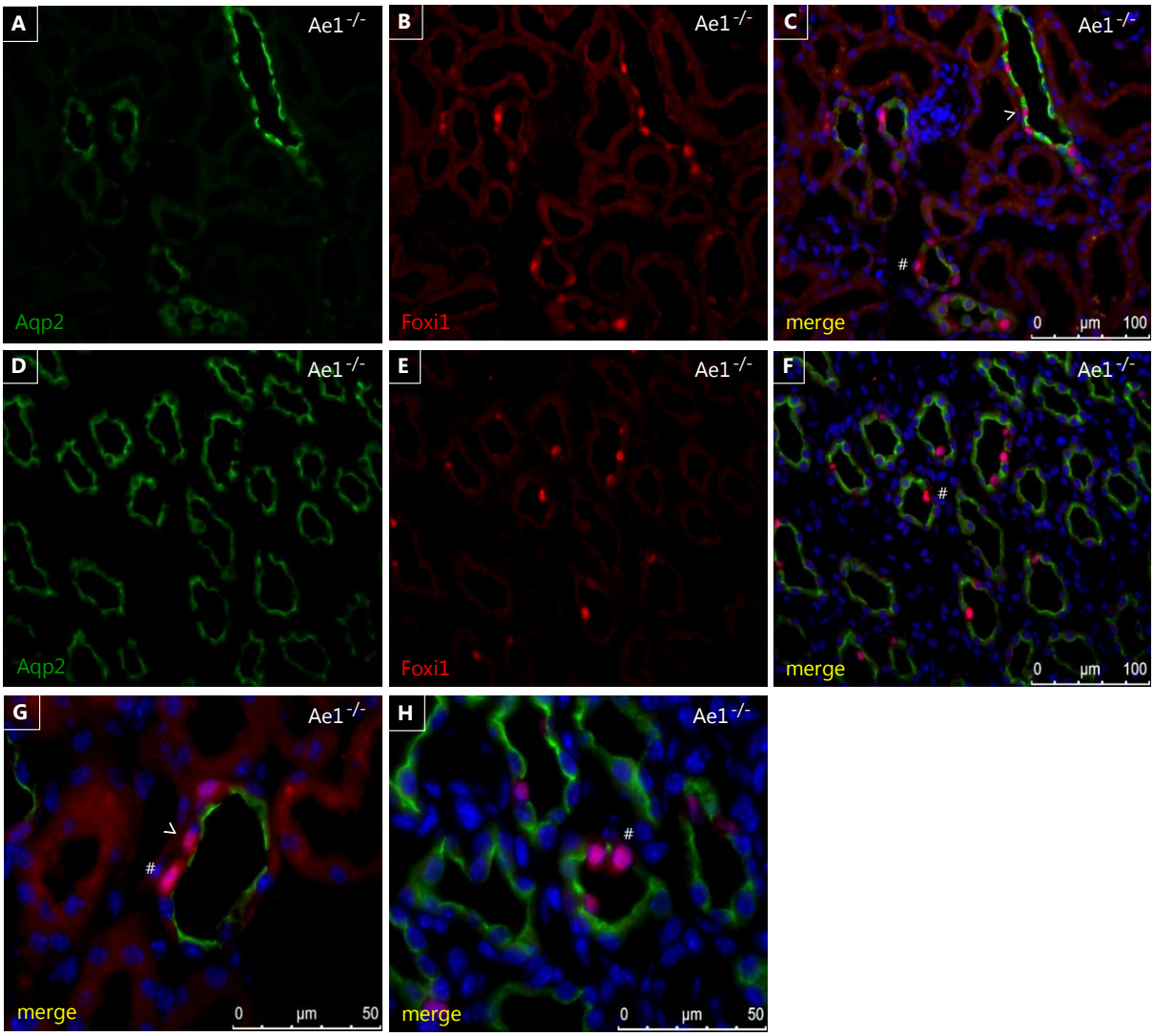

Fig. 10.15 Expression pattern of Foxi1 and Aqp2 expressing cells in kidney of juvenile (P30) Ae1 $^{-/-}$ mouse. **A-C, G)** Renal cortex. **D-F, H)** Renal inner medulla. Principal cells expressing luminal Aqp2 (aquaporin 2) in renal cortical **(A)** and medullary **(D)** collecting ducts. Nuclear expression pattern of Foxi1 protein was detected in cortical **(B)** and medullary **(E)** tubular structures. Overlay reveals predominant expression of Foxi1 in Aqp2 negative and less frequently in Aqp2 positive cells along the renal collecting ducts **(C, F, G, H)**. Nucleic acid stained with DAPI (blue). #: Aqp2 negative/Foxi1 positive cell. arrowhead: Aqp2/Foxi1 positive cell. **A-F)** Magnification 400x. **G, H)** Magnification 1,000x.

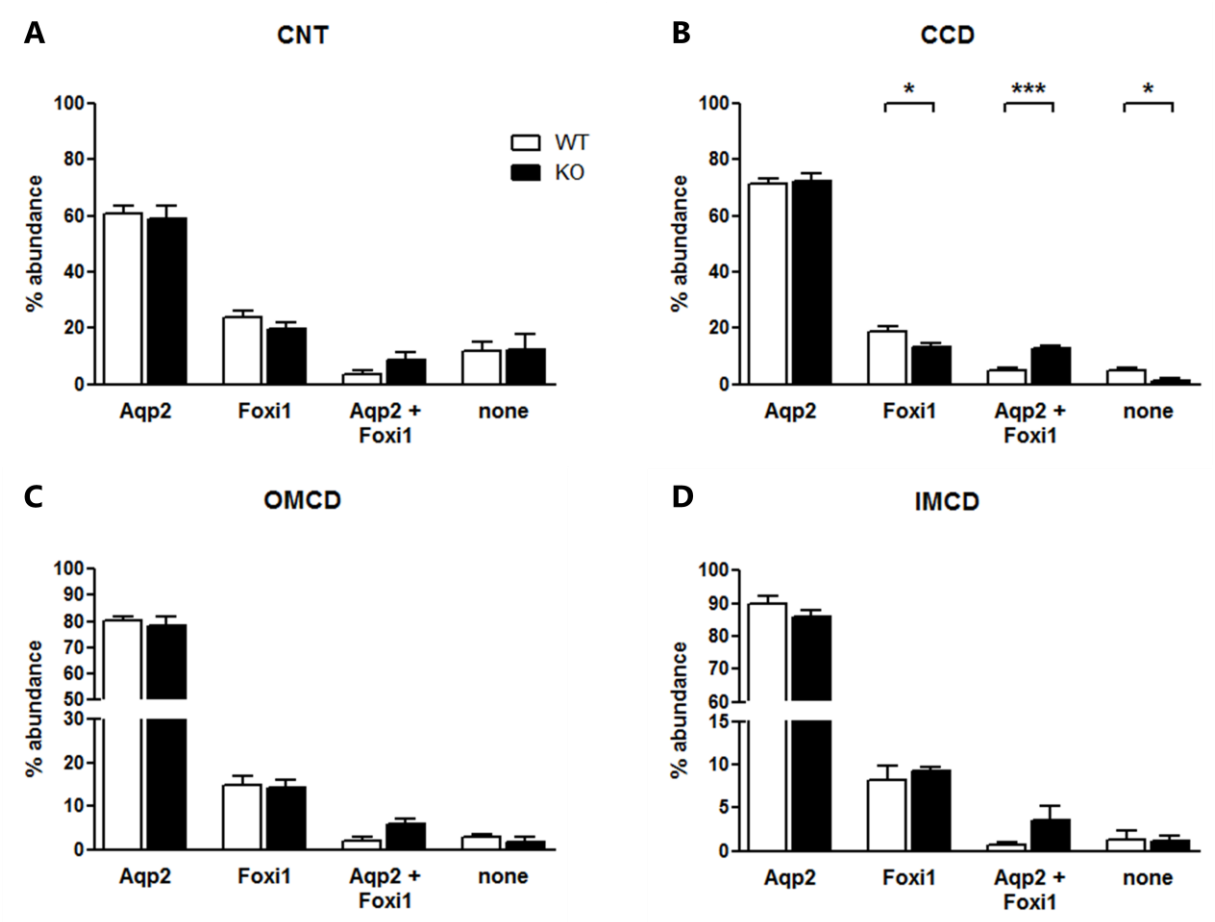

Fig. 10.16 Relative distribution of Foxi1 and Aqp2 expressing cells in kidneys of juvenile (P30) Ae1 WT and KO mice. Summary of cell counts assessing the relative abundance of Foxi1 and Aqp2 (aquaporin 2) positive cells in the renal CNT, CCD, OMCD and IMCD of juvenile (P30) Ae1 WT and KO mice. In total, 4,403 cells were counted in WT kidneys (n=5) and 5,243 cells in KO kidneys (n=5). Statistical analysis using Student`s *t*-test. * $p \leq 0.05$, ** $p \leq 0.01$, *** $p \leq 0.001$.

CNT: connecting tubule, CCD: cortical collecting duct, OMCD: outer medullary collecting duct, IMCD: inner medullary collecting duct

The expression of Cp2l1 was reported to change in accordance with the maturation of the developing nephron and CD system (Fig. 2.12) [90]. In adult mouse kidney, Cp2l1 expression was reported in parts of the DCT, CNT, CCD, and OMCD (Fig. 2.12). However, the cell types expressing Cp2l1 were not further characterized in this study [90]. In the present study, Cp2l1 expression was assessed in P30 kidneys and consistent with previous reports occassionally detected in cells of the DCT, CNT, CCD, and OMCD. Additionally, Cp2l1 was present in cells of the TAL and IMCD. In order to determine the cell type harbouring nucleic Cp2l1, coimmunostainings using the principal cell marker Aqp2 were performed. Interestingly, Cp2l1 was occasionally expressed in Aqp2 positive tubules of the renal cortex and medulla of P30 Ae1 WT (Fig. 10.17) and KO (Fig. 10.18). Moreover, Cp2l1 expression was detected in principal cells ($Aqp2^{+}$) and manifestations of intercalated cells ($Aqp2^{-}$) along the distal tubule. Strikingly, Cp2l1 was found to be present in virtually all nuclei of the IMCD in P30 WT kidneys (Fig. 10.17E, F, H), whereas the nuclear localization was completely absent in IMCDs of P30 Ae1 KO kidney (Fig. 10.18E, F, H). Moreover, instead of the expected nuclear pattern, the signal for Cp2l1 was now detected on the luminal cell membrane of certain cells, but not in all. However, detailed quantification using distinct CD markers are necessary to further analyze the expression pattern of Cp2l1. Furthermore, while analyzing the immunofluorescent images of Cp2l1, the relative signal intensity for Cp2l1, particularly in the renal cortex, appeared stronger in Ae1 deficient kidneys compared to WT (Fig. 10.17B, 10.18B). However, at present immunoblotting of Cp2l1 to assess the relative protein abundance was not successful due to technical reasons.

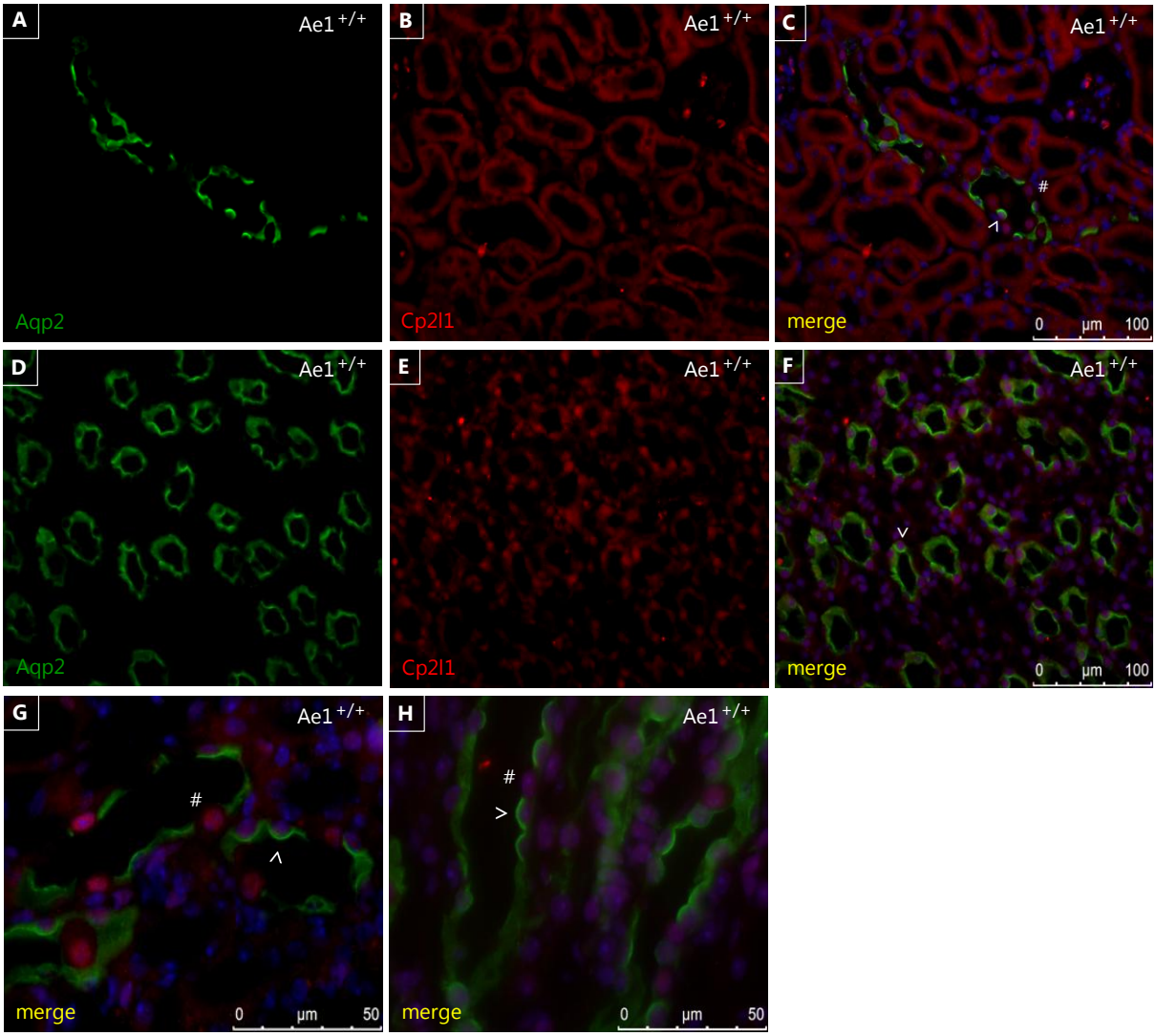

Fig. 10.17 Expression pattern of Cp2l1 and Aqp2 expressing cells in kidney of juvenile (P30) Ae1 $^{+/+}$ mouse. **A-C, G)** Renal cortex**. D-F, H)** Renal inner medulla. Principal cells expressing luminal Aqp2 (aquaporin 2) in renal cortical **(A)** and medullary **(D)** collecting ducts. Nuclear expression pattern of Cp2l1 protein was detected in cortical **(B)** and predominantly medullary **(E)** tubular structures. Overlay reveals expression of Cp2l1 in Aqp2 positive and negative cells along the renal collecting ducts **(C, F, G, H)**. Nucleic acid stained with DAPI (blue). # Aqp2 negative/Cp2l1 positive cell; arrowhead: Aqp2/Cp2l1 positive cell. **A-F)** Magnification 400x. **G, H)** Magnification 1,000x.

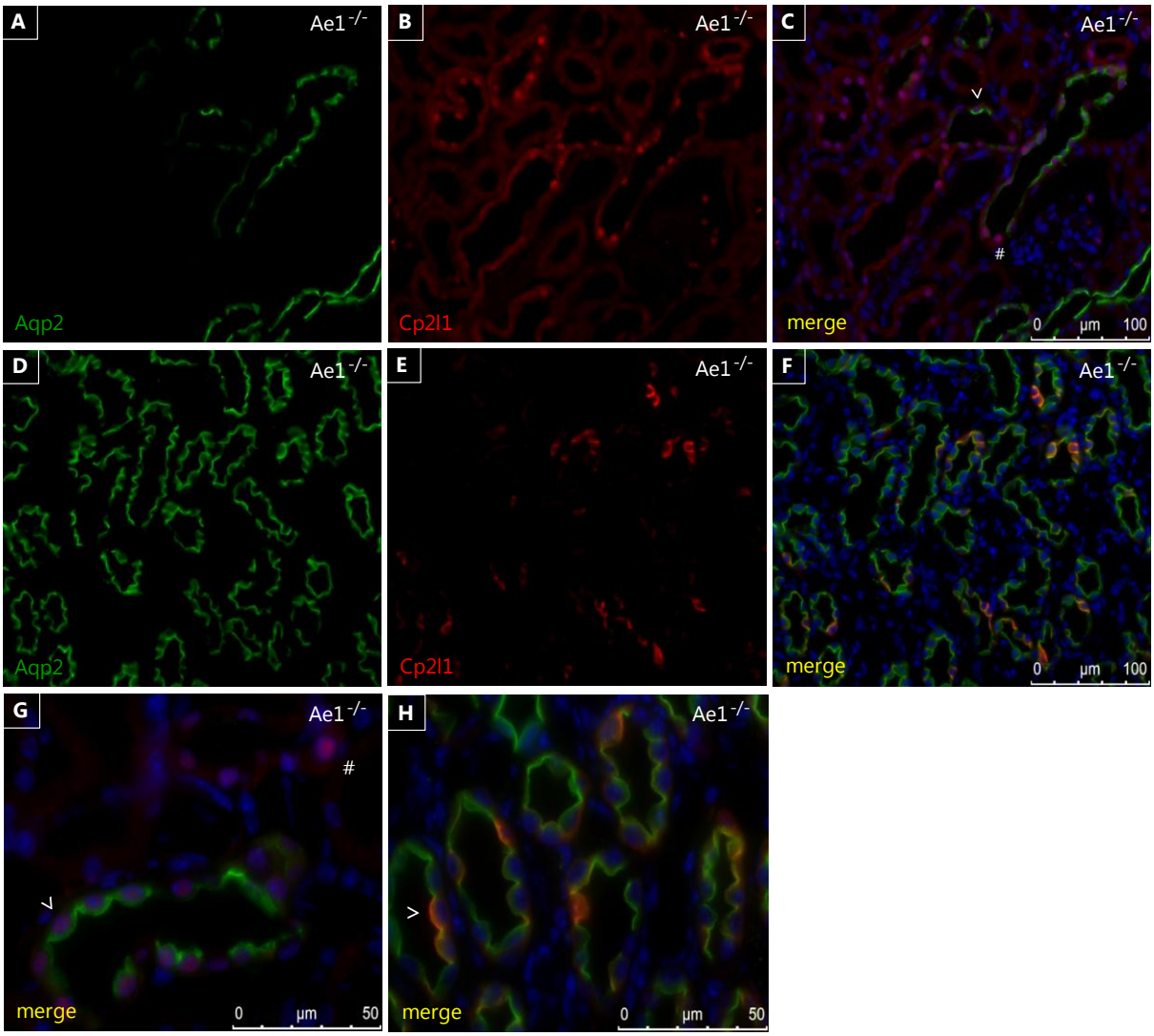

Fig. 10.18 Expression pattern of Cp2l1 and Aqp2 expressing cells in kidney of juvenile (P30) Ae1 -/- mouse. **A-C, G)** Renal cortex**. D-F, H)** Renal inner medulla. Principal cells expressing luminal Aqp2 (aquaporin 2) in renal cortical **(A)** and medullary **(D)** collecting ducts. Nuclear expression pattern of Cp2l1 protein was detected in cortical tubular structures **(B)**, while a cell membrane associated and exclusively extranuclear signal for Cp2l1 was detected in inner medullary tubules **(E)**. Overlay reveals expression of Cp2l1 in Aqp2 positive and negative cells along the renal collecting ducts **(C, F, G, H)**. Nucleic acid stained with DAPI (blue). # Aqp2 negative/Cp2l1 positive cell; arrowhead: Aqp2/Cp2l1 positive cell. **A-F)** Magnification 400x. **G, H)** Magnification 1,000x.

10.1.3 Pendrin is normally expressed in embryonic Ae1 deficient kidney

Kidney sections of 18 days old Ae1 WT and KO embryos were costained with Aqp2 and pendrin (Fig. 10.19), as well as Aqp2 and the a4 and B1 subunits of V-ATPase (data not shown). Despite the intriguing abnormal presence of pendrin in the inner medulla of mature (P30 and P84) Ae1 deficient kidneys (Fig. 10.2 and 10.7), pendrin expression in embryonic kidneys (E18) appeared normal (Fig. 10.19). However, the analyzed tubules might be rather derived from the renal cortex, where normal Pds expression was also preserved in Ae1 deficient mature kidneys. Therefore, analysis of the embryonic inner medullary region seems inevitable. However, mRNA expression studies of Ae1 deficient kidneys at different time points of life suggest a late onset (after postnatal day 3, P3) of abnormal expression of acid-base related transporters and signalling molecules in Ae1 KO kidney (Fig. 10.20).

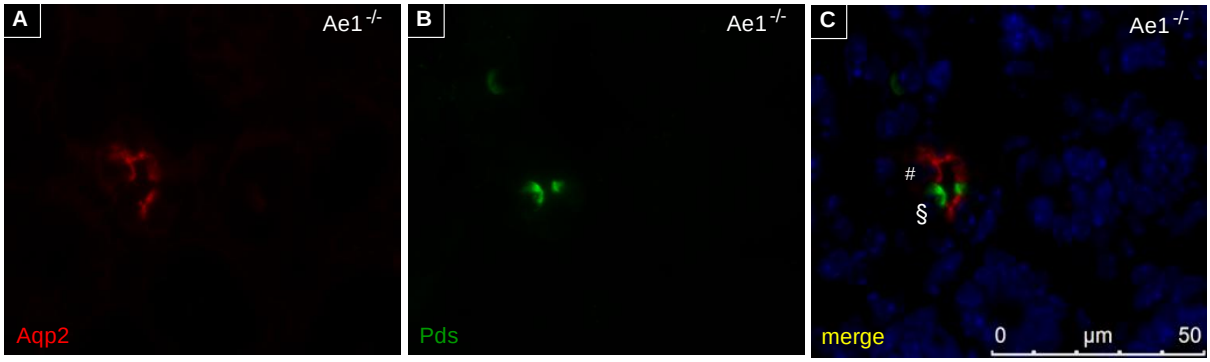

Fig. 10.19 Expression pattern of Aqp2 and Pds expressing cells in embryonic kidney (E18) of Ae1 $^{-/-}$ mouse. **A)** Principal cells are identified by luminal Aqp2 (aquaporin 2) expression. **B)** Pds (pendrin) expression identifies type B-intercalated cells. **C)** merge. Nucleic acid stained with DAPI (blue). # Aqp2 positive/Pds negative cell; § Aqp2 negative/Pds positive cell. Magnification 1,000x.

10.1.4 Ae1 deficiency causes late dysregulation of transcription factors

In order to address the question, whether Ae1 deficiency affects the proper expression of genes regulating CD differentiation, mRNA expression levels of candidate genes were compared at different time points of life (E18, P3, P30, P84) and between Ae1 $^{+/+}$, Ae1 $^{+/-}$ and Ae1 $^{-/-}$ kidneys. According to chapter 2.7 and 5.2.2, *Foxi1*, *Cp2l1*, *Klf4*, *Bdkrb2,* and *Gdf15* are implicated in terminal differentiation of renal CD epithelium. Furthermore, the renal expression of the acid-base regulatory transporters *Ae1*, *Pds*, *Rhcg* and *B1 subunit of V-ATPase* were investigated because of the known complication of dRTA in Ae1 deficiency. The results obtained by qRT-RT-PCR are presented in Fig. 10.20. Interestingly, a difference in the mRNA levels of any gene tested between the Ae1 genotypes was not observed in embryonic kidneys. Moreover, dysregulation of mRNA expression of some candidate genes tested was observed only after postnatal day 3 (P3). As expected and in agreement with the development of dRTA, mRNA of *Pds* and *B1* were significantly downregulated in adult Ae1 KO kidneys (P84). Surprisingly, there was no difference in mRNA abundance of *Foxi1* or *Cp2l1* in Ae1 deficient kidneys at any time point of life examined. However, it is of note, that mRNA levels of regulatory molecules involved in p53 mediated signalling pathways, namely *Gdf15*, *Klf4* and *Bdkrb2*, were significantly upregulated in Ae1 KO kidneys after postnatal day 3 (P3).

Tab. 10.20 Summary of relative mRNA abundance of genes involved in renal collecting duct differentiation in Ae1 mutant kidney. The relative mRNA abundance of several target genes was assessed in male Ae1 mutant mice at four different time points of life. n= 4-8 animals per genotype and age. Gene expression levels were normalized to *Hprt* expression and calculated in percentage (chapter 9.6). E18: embryonic day 18, P3: postnatal day 3, P30: postnatal day 30, P84: postnatal day 84. Statistical analysis using one way ANOVA and Tukey post-test. * indicating significant difference compared to $Ae1^{+/+}$; # indicating significant difference compared to $Ae1^{+/-}$. */# $p \leq 0.05$, **/## $p \leq 0.01$, ***/### $p \leq 0.001$

		% *Ae1*	% *Pds*	% *Rhcg*	% *B1*	% *Foxi*	% *Cp2l1*	% *Gdf15*	% *Klf4*	% *Bdkrb2*
E18	***Ae1*** $^{+/+}$	100.0 ± 33.6	100.0 ± 11.2	100.0 ± 6.8	100.0 ± 14.7	100.0 ± 7.1	100.0 ± 8.8	100.0 ± 16.8	100.0 ± 12.0	100.0 ± 11.6
	Ae1 $^{+/-}$	171.9 ± 17.8	94.0 ± 14.3	87.1 ± 11.5	81.0 ± 16.4	104.2 ± 7.4	98.0 ± 11.8	92.5 ± 25.9	100.8 ± 6.9	106.3 ± 28.9
	Ae1 $^{-/-}$	1.4 ± 0.5 * ##	95.9 ± 14.2	93.2 ± 7.1	78.6 ± 14.2	114.8 ± 8.7	101.6 ± 11.8	112.3 ± 17.2	109.7 ± 6.8	157.7 ± 26.3
P3	***Ae1*** $^{+/+}$	100.0 ± 23.6	100.0 ± 40.6	100.0 ± 18.6	100.0 ± 6.8	100.0 ± 5.3	100.0 ± 8.1	100.0 ± 12.3	100.0 ± 3.7	100.0 ± 23.1
	Ae1 $^{+/-}$	54.6 ± 17.3	70.9 ± 10.5	125.2 ± 9.4	97.6 ± 6.7	98.7 ± 4.7	110.0 ± 6.1	107.7 ± 9.2	98.4 ± 8.9	140.8 ± 14.0
	Ae1 $^{-/-}$	0.1 ± 0.0 *	28.1 ± 5.7	78.9 ± 20.9	90.2 ± 8.9	77.5 ± 13.5	82.0 ± 12.8	119.7 ± 18.6	144.5 ± 18.5 #	169.4 ± 24.5
P30	***Ae1*** $^{+/+}$	100.0 ± 22.6	100.0 ± 15.7	100.0 ± 23.2	100.0 ± 14.5	100.0 ± 23.0	100.0 ± 27.5	100.0 ± 9.5	100.0 ± 15.6	100.0 ± 24.4
	Ae1 $^{+/-}$	25.8 ± 1.7 **	50.6 ± 3.7 **	62.9 ± 3.1	71.5 ± 7.6	94.0 ± 12.8	74.6 ± 9.6	85.9 ± 7.2	83.5 ± 8.2	92.4 ± 24.4
	Ae1 $^{-/-}$	0.3 ± 0.3 ***	78.7 ± 4.3	100.2 ± 15.9	110.8 ± 13.2	164.1 ± 54.5	123.8 ± 26.3	165.9 ± 23.3 * ##	270.1 ± 73.7 * #	309.2 ± 73.0 * #
P84	***Ae1*** $^{+/+}$	100.0 ± 16.6	100.0 ± 12.5	100.0 ± 8.9	100.0 ± 10.4	100.0 ± 13.3	100.0 ± 3.9	100.0 ± 11.7	100.0 ± 6.1	100.0 ± 11.9
	Ae1 $^{+/-}$	53.3 ± 8.5 *	127.8 ± 6.7	134.6 ± 4.1	105.9 ± 3.2	111.6 ± 5.3	106.9 ± 8.3	76.9 ± 4.8	86.1 ± 3.6	87.1 ± 13.7
	Ae1 $^{-/-}$	0.6 ± 0.4 *** #	72.5 ± 3.5 ##	99.7 ± 20.4	71.5 ± 5.4 #	121.6 ± 9.7	112.1 ± 15.2	201.2 ± 17.6 *** ###	214.7 ± 25.7 *** ###	200.3 ± 54.7 #

The extra-cellular matrix protein hensin (Dmbt1) was reported to be crucial for renal intercalated cell differentiation and interconversion (chapter 2.7.5). Since we observed an abnormal expression of Pds in the inner medulla of Ae1 deficient mice, we aimed to investigate mRNA expression levels of *hensin*. Surprisingly, we could not detect *hensin* mRNA in the mouse kidney at any time point of life (Fig. 10.21). Additionally, *hensin* was not detected in cDNA of the immortalized mouse inner medullary collecting duct cell line IMCD3. However, the primer pair used to detect *hensin* produced the expected product with cDNA obtained from mouse jejunum, confirming specificity and feasibility of the assay. Similar results were obtained using the Taqman gene expression assay from Applied Biosystems for mouse *Dmbt1* (Mm00455996_1m*) (data not shown). In order to test, whether mouse strain specific differences may lead to the unexpected absence of *hensin* in C57/Bl6 mouse kidney, total mRNA was extracted from 129SvEv wild-type mouse kidney and the cDNA synthesized was tested (data not shown). Again, we could not detect a RT-RT-PCR primer product for *hensin*. Since a lack of detectable mRNA certainly bears the absence of a related protein product, we have to conclude that *hensin* is not expressed in the kidneys of the mouse strains tested. This is in contrast to the recent report of [99], which was discussed in more detail in chapter 2.7.5.

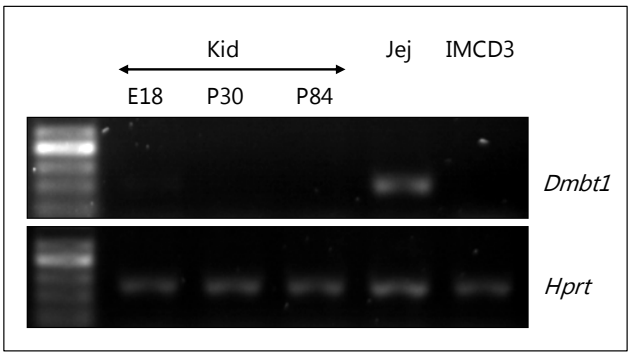

Fig. 10.21 Lack of detectable hensin (Dmbt1) mRNA in mouse kidney. **Top)** qRT-PCR using *hensin* specific primer was performed on kidney cDNA from embryonic (E18), juvenile (P30) and adult (P84) mice, and cDNA obtained from mouse inner medullary collecting duct cell line (IMCD3). The PCR product was loaded on an Agarosegel and visualized under UV-light. *Hensin* is reported to be highly expressed in the intestine and consistently the expected PCR product was obtained in cDNA of mouse jejunum (Jej). **Bottom)** The housekeeping gene *Hprt* was used for additional control.

Since *Gdf15* mRNA was significantly upregulated in mature Ae1 KO mice (P30 and P84) compared to WT, the protein abundance was assessed by immunoblotting (Fig. 10.22, 10.23). As illustrated in Fig. 5.2, the Gdf15 precursor peptide undergoes extensive cellular processing, resulting in the biologically active and secreted mature Gdf15 dimer, which is reported to migrate at approximately 30 kDa in electrophoretic SDS-PAGE [181, 225]. Immunoblotting for Gdf15 on cytosolic fractions of P30 and P84 kidneys revealed significant downregulation of the secreted mature Gdf15 dimer, in $Ae1^{+/-}$ kidney compared to $Ae1^{+/+}$ (Fig. 10.22C, 10.23C), while a probably immature propeptide was not altered [225]. However, the mild decrease in Gdf15 protein abundance in $Ae1^{-/-}$ kidneys did not reach significant difference. Cytosolic fractions of mouse liver and placenta homogenates, respectively, were included for positive control (data not shown). Interestingly, the upper 50 kDa band of Gdf15 was exclusively present in the liver, while the lower 32 kDa band of Gdf15 was only detected in placenta samples (data not shown). Thus, a further proof of the molecular identity of the detected Gdf15 related bands in kidney derived samples is requested. In any case, the quality of the Gdf15 immunoblots is not satisfying and needs to be improved.

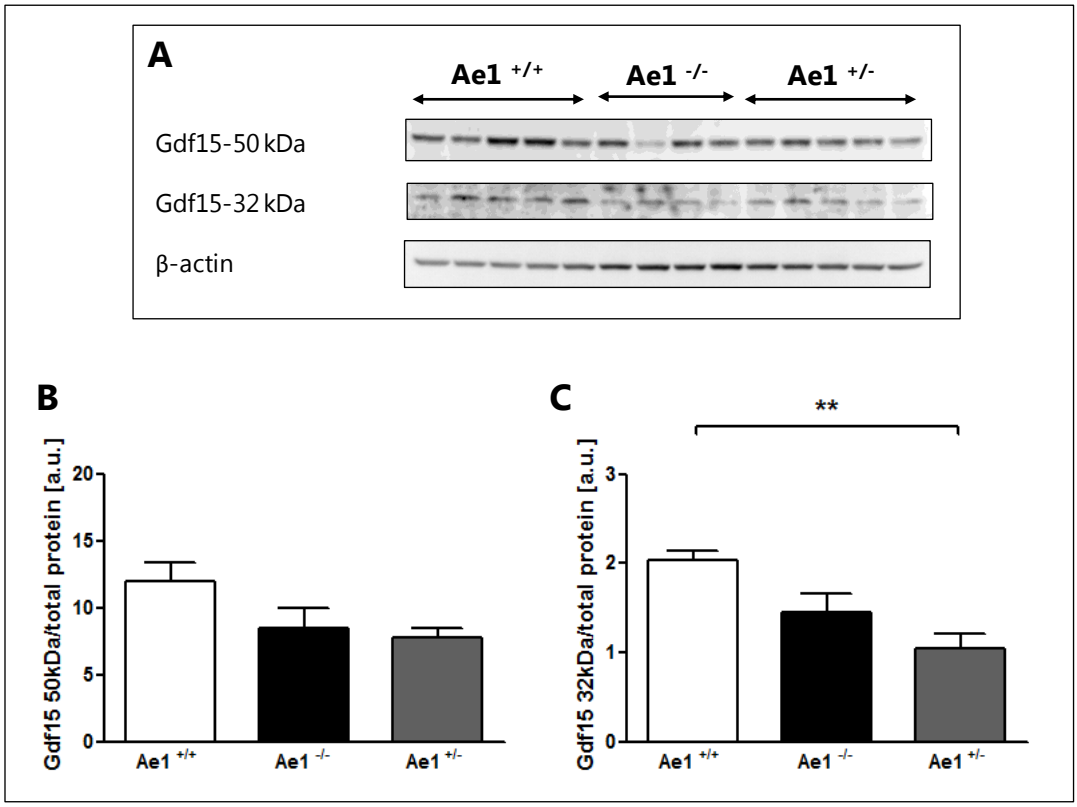

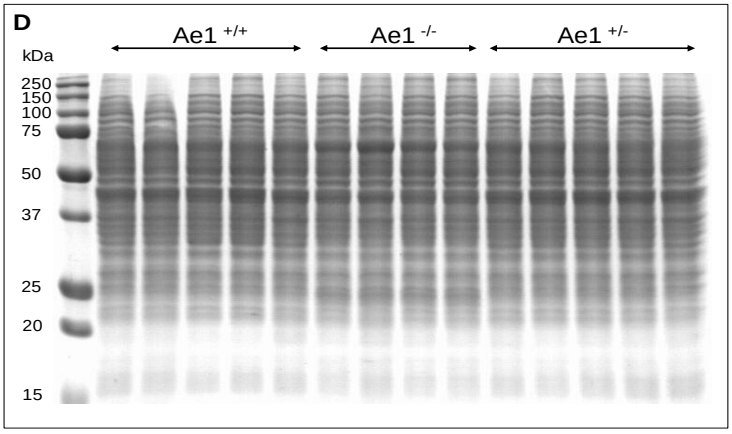

Fig. 10.22 Protein abundance of Gdf15 in P84 Ae1 mutant kidneys. Representative western blot (**A**) for Gdf15 (growth differentiation factor 15) in cytosolic fractions of P84 $Ae1^{+/+}$, $Ae1^{-/-}$ and $Ae1^{+/-}$ kidneys. Two Gdf15 related bands were detected, at 50 kDa and 32 kDa, respectively, probably corresponding to immature propeptide and mature dimer. The relative protein abundance of β-actin was signifcantly higher in $Ae1^{-/-}$ kidneys, despite loading of equal protein amounts and was therefore not considered for normalization. **B, C**) Densitometry of respective Gdf15 signal intensities, normalized to Coomassie Blue staining of duplicate SDS-PAGE gel (**D**). Statistic analysis using one way ANOVA and Tukey post-test. * $p \leq 0.05$, ** $p \leq 0.01$, *** $p \leq 0.001$.

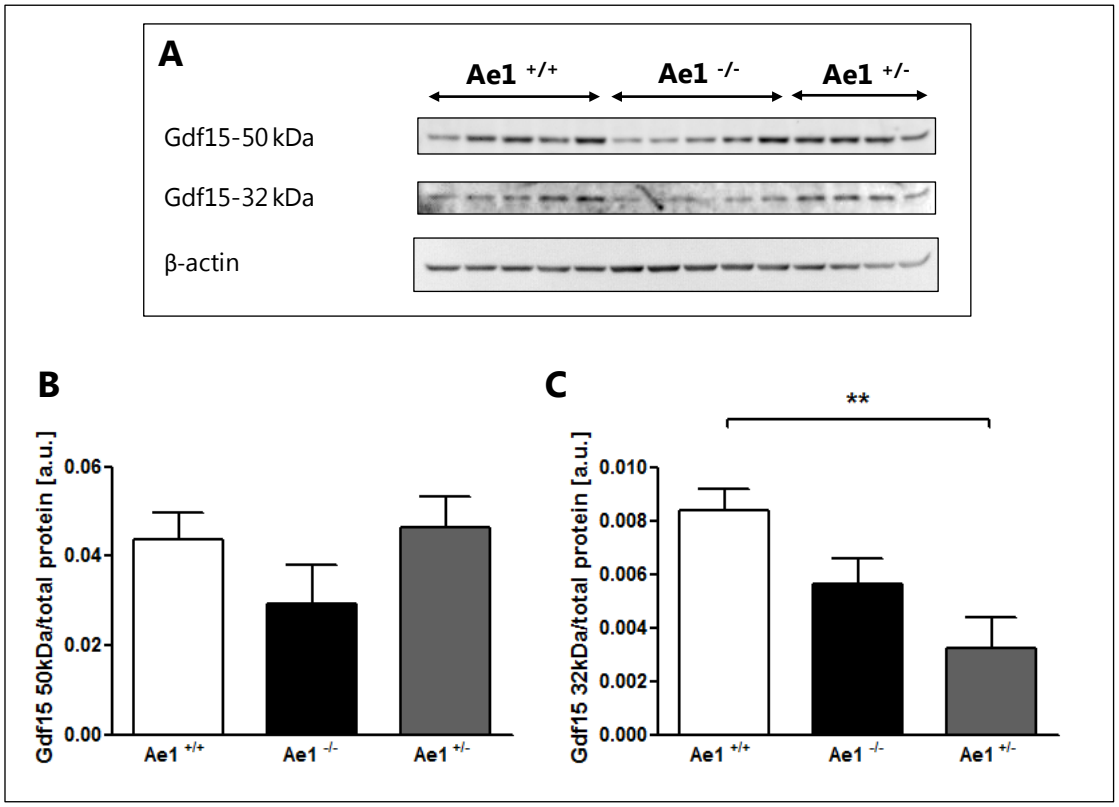

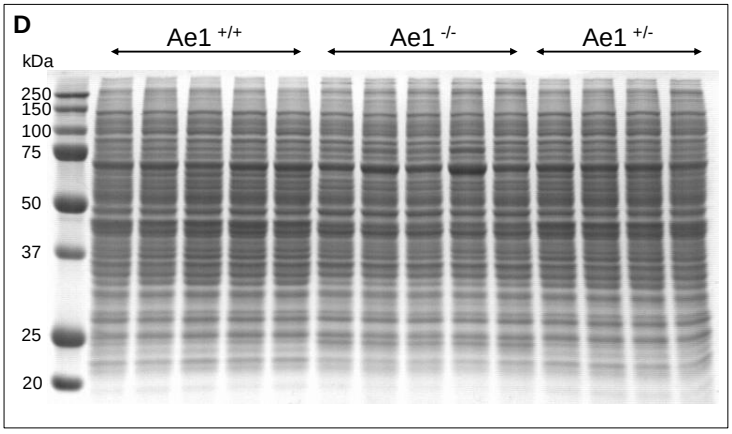

Fig. 10.23 Protein abundance of Gdf15 in P30 Ae1 mutant kidneys. Representative western blot (**A**) for Gdf15 (growth differentiation factor 15) in cytosolic fractions of P30 $Ae1^{+/+}$, $Ae1^{-/-}$ and $Ae1^{+/-}$ kidneys. Two Gdf15 related bands were detected, at 50 kDa and 32 kDa, respectively, probably corresponding to immature propeptide and mature dimer. The relative protein abundance of β-actin was signifcantly higher in $Ae1^{-/-}$ kidneys, despite loading of equal protein amounts and was therefore not considered for normalization. **B, C**) Densitometry of respective Gdf15 signal intensities, normalized to Coomassie Blue staining of duplicate SDS-PAGE gel (**D**). Statistic analysis using one way ANOVA and Tukey post-test. * $p \leq 0.05$, ** $p \leq 0.01$, *** $p \leq 0.001$.

10.2 Renal adaptation to chronic metabolic acidosis

10.2.1 Metabolic parameters

As described in chapter 5.2, acid-base disturbances are known to induce several adaptive responses in the kidney, including a cellular remodelling of the CD epithelium. Therefore, a possible impact on induced chronic metabolic acidosis, lasting for 8 weeks, was investigated and finally compared with observations in Ae1 deficiency. Metabolic parameters of experimental mice (P84) are summarized in Tab. 10.24 and confirmed the expected adaptation to metabolic acidosis induced by addition of NH_4Cl to the food. The health status of the animals was tightly monitored during the experimental procedure by subjective observations (appearance of fur, eyes and activity). Furthermore, adolescence of the acidotic (NH_4Cl) animals seemed normal, since the bodyweight was unaffected by the unusual diet. The daily water intake and respective urinary output was increased in acidotic animals as previously reported [219]. The increased blood plasma chloride levels as well as the increased secretion of urinary NH_3/NH_4^+ reflected the chronic oral uptake of NH_4Cl with the food in acidotic mice. The increased renal secretion of acid equivalents to the urine, indicated by the lowered urinary pH and increased urinary NH_3/NH_4^+ excretion, completely compensated the induced metabolic acidosis. Therefore, blood pH, pCO_2 and HCO_3^- concentrations, as well as the Anion Gap were normal in NH_4Cl loaded mice compared to Control.

Tab. 10.24 Metabolic and urine parameters of Control and 8 weeks NH_4Cl loaded C57/Bl6 (P84) mice. Statistical analysis using Student`s *t*-test (n = 10 per group).

* $p \leq 0.05$, ** $p \leq 0.01$, *** $p \leq 0.001$.

	Control	**NH_4Cl**
Bodyweight (g)	26.16 ± 0.55	25.10 ± 0.36
H_2O Intake (g/g BW)	0.18 ± 0.01	0.26 ± 0.01 ***
Food Intake (g/g BW)	0.17 ± 0.01	0.16 ± 0.01
Stool (g/g BW)	0.04 ± 0.00	0.04 ± 0.00
Urine (g/g BW)	0.04 ± 0.01	0.09 ± 0.01 ***
Blood		
pH	7.35 ± 0.02	7.39 ± 0.07
$_pCO_2$ (mmHG)	45.86 ± 2.46	45.20 ± 2.91
$_pO_2$ (mmHG)	34.94 ± 0.88	41.63 ± 2.17
HCO_3^- (mM)	24.52 ± 0.71	22.96 ± 1.54
Na^+ (mM)	144.60 ± 0.98	146.20 ± 0.37
K^+ (mM)	4.02 ± 0.21	3.98 ± 0.07
Cl^- (mM)	107.00 ± 0.84	110.60 ± 1.25 *
Ca^{++} (mM)	1.15 ± 0.08	1.04 ± 0.06
Hematocrit (%)	45.26 ± 0.40	47.12 ± 1.61
Anion Gap	13.16 ± 1.41	12.60 ± 0.30
Urine		
Creatinine (mg/dl)	32.08 ± 2.38	16.38 ± 1.08 ***
pH	5.83 ± 0.02	5.46 ± 0.01 ***
HCO_3^- (mM)/Crea (mg/dl)	0.008 ± 0.0009	0.005 ± 0.0005 *
NH_3/NH_4^+ (mM)/Crea (mg/dl)	2.05 ± 0.14	26.98 ± 0.63 ***

10.2.2 Renal expression pattern of acid-base transporters during chronic metabolic acidosis

The renal expression pattern of Pds, V-ATPase (represented by a4 and B1 subunit) and Ae1 was assessed by immunofluorescence and the relative abundance of individually labelled cells of Control and NH_4Cl treated mice were compared (Fig. 10.25 to 10.28). Furthermore, the relative protein abundance of the afore-mentioned transporters, as well as Gdf15 and Foxi1, was determined by immunoblotting (Fig. 10.29 to 10.34). Finally, the relative mRNA abundance of candidate genes expressed in kidneys was compared between Control and 8 weeks NH_4Cl treated mice and Ae1 mutant mice, respectively (Fig. 10.35, 10.36).

The obtained results clearly show the renal compensation of the chronic oral acid load in treated C57/Bl6 mice. Moreover, the adaptive responses of the kidney to chronic metabolic acidosis are significantly different to the observations made in Ae1 deficiency.

As expected and shown in Fig. 10.25, the relative abundance of Pds expressing type B-IC decreased significantly upon chronic oral acid loading. However, this adaptation was totally accounted by alterations of the relative cell number in the renal CCD, since the abundance of Pds expressing type B-ICs was not changed in the renal CNT, OMCD or IMCD of NH_4Cl loaded mice compared to Control. The expected decrease of type B-ICs in the renal CCD of acidotic animals was accompanied by an increase of Aqp2 labelled principal cells (Fig. 10.25B). In the renal OMCD, the relative abundance of $Aqp2^+$ cells was reduced in acidotic kidneys, while unlabelled (none) cells increased concomitantly (Fig. 10.25C). A similar, but not yet significantly different trend was observed in renal IMCD of acid loaded mice (Fig. 10.25D). As expected and importantly in contrast to Ae1 deficient mice, Pds expressing cells were not detected at all in the IMCD of chronic NH_4Cl treated animals (Fig. 10.3D, 10.8D, 10.25D).

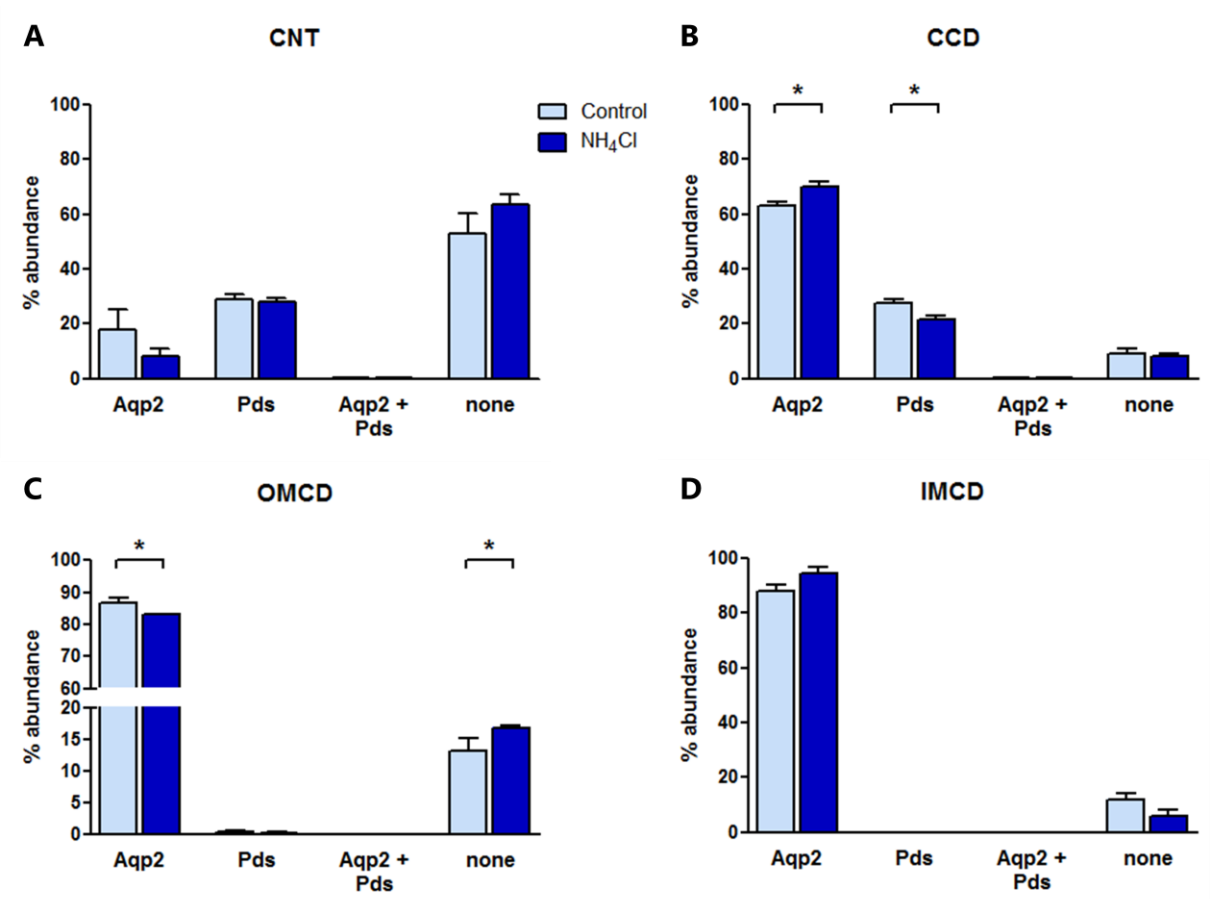

Fig. 10.25 Relative distribution of Aqp2 and Pds expressing cells in kidneys of Control and 8 weeks NH_4Cl treated mice (P84). Summary of cell counts assessing the relative abundance of Aqp2 (aquaporin 2) and Pds (pendrin) positive cells in the renal CNT, CCD, OMCD and IMCD of Control and NH_4Cl treated mice. In total, 7,882 cells were counted in Control kidneys (n=5) and 4,014 cells in NH_4Cl treated kidneys (n=5). Statistical analysis using Student`s *t*-test. * $p \leq 0.05$, ** $p \leq 0.01$, *** $p \leq 0.001$. CNT: connecting tubule, CCD: cortical collecting duct, OMCD: outer medullary collecting duct, IMCD: inner medullary collecting duct

Interestingly, the relative abundance of Ae1 positive ($Ae1^+$) cells remained constant upon chronic NH_4Cl loading (Fig. 10.26). However, similar to the observations made in the Pds staining series (Fig. 10.25B), a significant increase in $Aqp2^+$ cells on the expense of unlabelled (none) cells was present in renal CCD of acid loaded mice (Fig. 10.26B). The unlabelled (none) cells of the Ae1 staining series comprise all types of ICs with the exception of type A-ICs as defined by the respective marker proteins. Therefore, the data suggest that principal cells in the renal CCD increase on the expense of type B-ICs upon chronic acid stimuli. Immunologic detection of the V-ATPase, a more general marker of renal ICs, confirmed the conclusion.

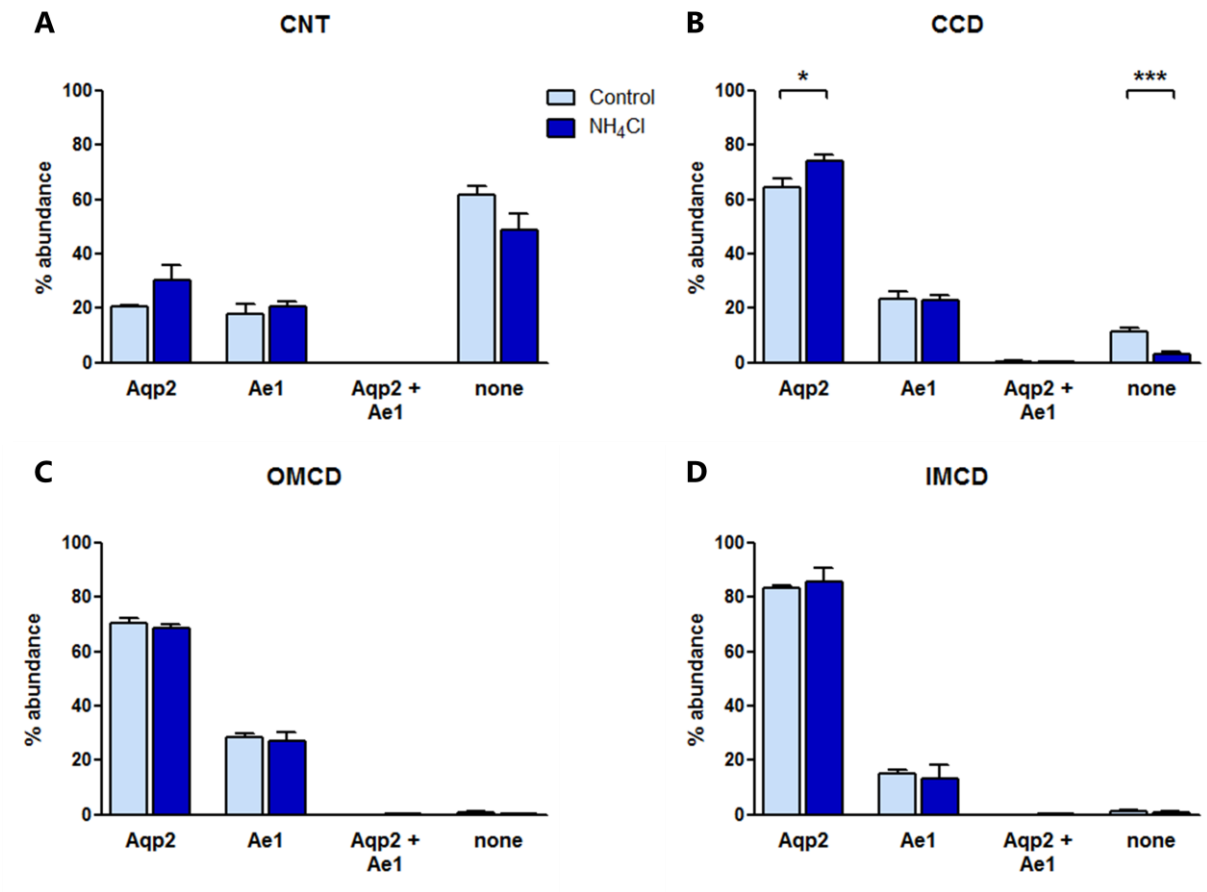

Fig. 10.26 Relative distribution of Aqp2 and Ae1 expressing cells in kidneys of Control and 8 weeks NH_4Cl treated mice (P84). Summary of cell counts assessing the relative abundance of Aqp2 (aquaporin 2) and Ae1 (anion exchanger 1) positive cells in the renal CNT, CCD, OMCD and IMCD of Control and NH_4Cl treated mice. In total, 3,926 cells were counted in Control kidneys (n=5) and 2,913 cells in NH_4Cl treated kidneys (n=5). Statistical analysis using Student`s *t*-test. * $p \leq 0.05$, ** $p \leq 0.01$, *** $p \leq 0.001$.

CNT: connecting tubule, CCD: cortical collecting duct, OMCD: outer medullary collecting duct, IMCD: inner medullary collecting duct

The V-ATPase is composed of distinct subunits (Fig. 5.1) and ubiquitously expressed in different tissues. The a4 subunit of the V-ATPase is specifically expressed in the kidney, while the B1 subunit is only present in renal ICs of the CD system, thus representing a more specific molecular marker. The cellular localization of the V-ATPase differs among renal ICs, matching their function in acid-base regulation. However, the subcellular localization of the V-ATPase within the renal ICs was not further included in the quantitative analysis of the immunologic staining series. Here, cells positive for the a4 ($a4^+$) or B1 ($B1^+$) subunit combine all manifestations of the cellular V-ATPase localization (i.e. apical, cytosolic, basolateral). Comparing the relative abundance of V-ATPase labelled cells in acidotic kidneys, it is of note, that the a4 and B1 subunit of V-ATPase are differentially regulated in distinct parts of the distal tubule (Fig. 10.27, 10.28). This phenomenon was already described during nephrogenesis by Jouret *et al* [29]. The relative abundance of cells positive for the a4 subunit of V-ATPase increased in the renal OMCD of NH_4Cl treated mice, while $Aqp2^+$ decreased (Fig. 10.27C). However, there were no significant differences observed between Control and acidotic kidneys regarding the $a4^+$ or $Aqp2^+$ cell abundance in other distal tubule segments (Fig. 10.27A, B, D). In contrast, the relative abundance of $B1^+$ cells increased significantly in the renal CNT of acidotic mice, maybe to some extent on the expense of unlabelled (none) cells although the reduction did not reach statistical relevance (Fig. 10.28A). However, the renal CNT of mice is a segment, which consists of a variety of distinct and transitory cell types. Hence, it is likely that some less defined cell type expresses the B1 subunit of V-ATPase upon chronic metabolic acidosis. Consistent with observations of the Pds staining series (Fig. 10.25), the relative abundance of $B1^+$ cells of acidotic CCD was decreased and accompanied by a respective increase in $Aqp2^+$ cells (Fig. 10.28B). This observation confirms the previous conclusion that principal cells of the renal CCD increase in abundance, on the expense of type B-ICs upon chronic acid loading. Apart from that, the relative abundance of $B1^+$ cells in OMCD and IMCD was similar in Control and NH_4Cl treated animals (Fig. 10.28C, D).

Notably and in contrast to Ae1 deficiency, Pds expressing cells remained absent in chronic metabolic acidosis. Furthermore, an interconversion of type A-ICs from type B-ICs upon chronic metabolic acidosis is not likely, as the relative abundance of type A-ICs did not change upon prolonged acid load. Instead of, an adaptive increase in PCs of the renal CCD was observed with a concomitant decrease in type B-ICs. However, whether this is a result of proliferation and apoptosis of the respective cell types or from cell type interconversion remains speculative.

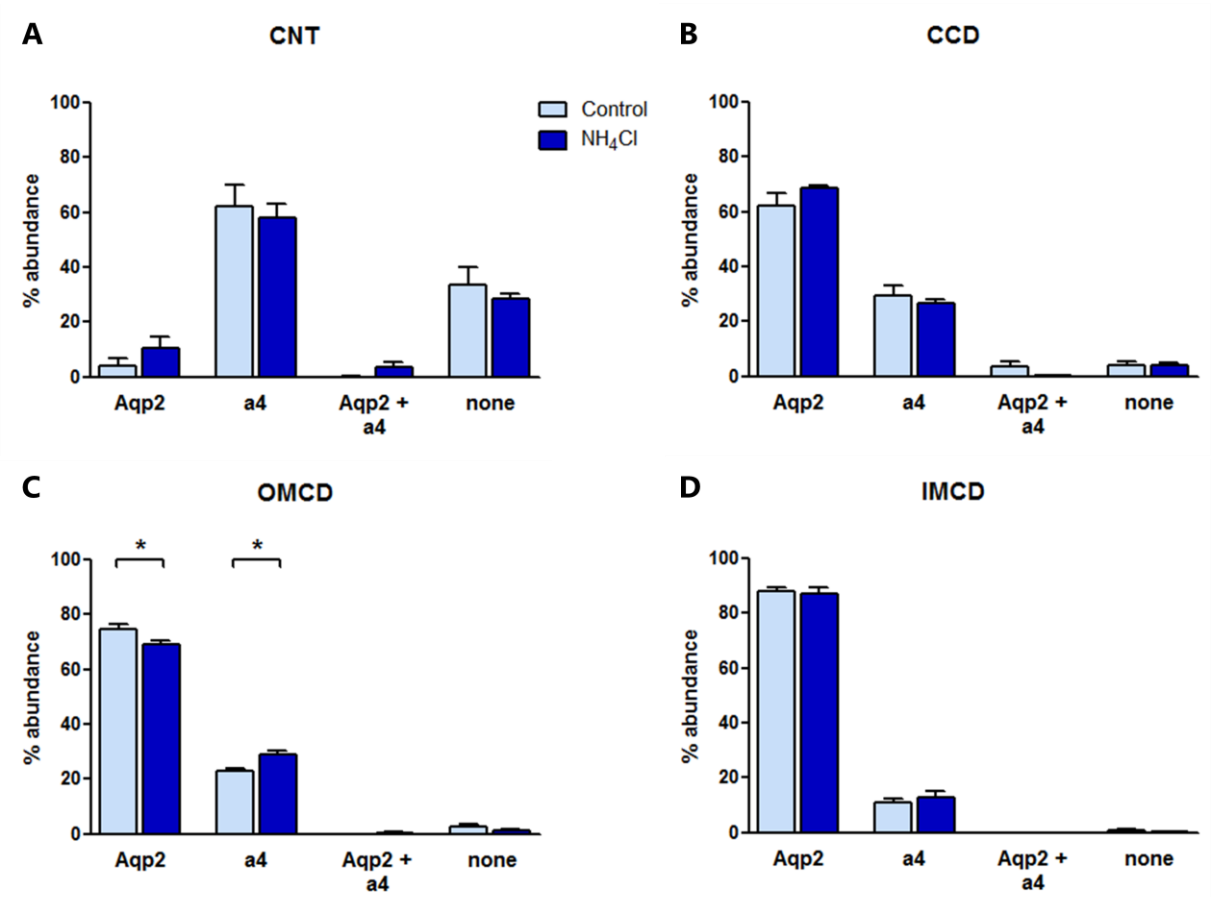

Fig. 10.27 Relative distribution of Aqp2 and a4 expressing cells in kidneys of Control and 8 weeks NH_4Cl treated mice (P84). Summary of cell counts assessing the relative abundance of Aqp2 (aquaporin 2) and a4 (a4 subunit of V-ATPase) positive cells in the renal CNT, CCD, OMCD and IMCD of Control and NH_4Cl treated mice. In total, 5,482 cells were counted in Control kidneys (n=5) and 4,822 cells in NH_4Cl treated kidneys (n=5). Statistical analysis using Student`s *t*-test. * $p \leq 0.05$, ** $p \leq 0.01$, *** $p \leq 0.001$.

CNT: connecting tubule, CCD: cortical collecting duct, OMCD: outer medullary collecting duct, IMCD: inner medullary collecting duct

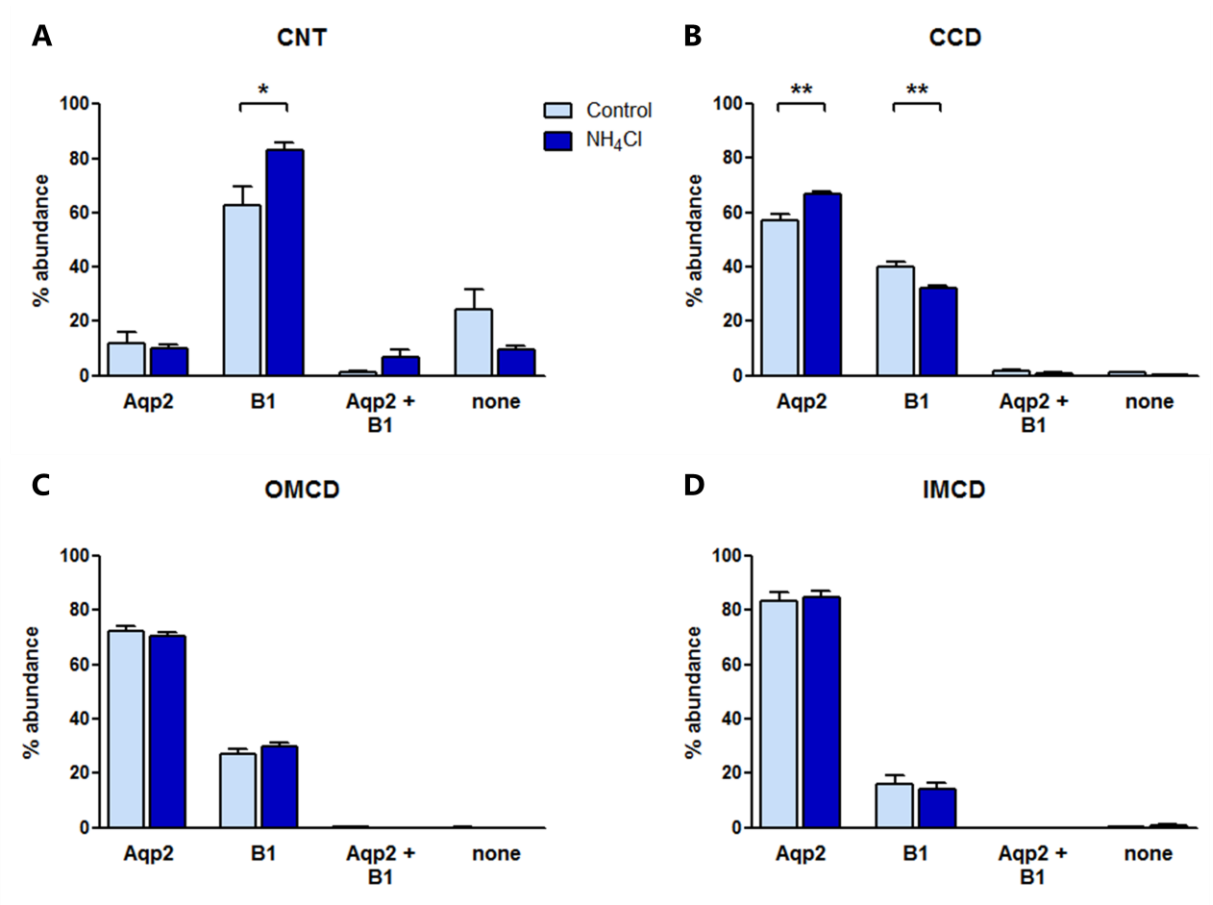

Fig. 10.28 Relative distribution of Aqp2 and B1 expressing cells in kidneys of Control and 8 weeks NH_4Cl treated mice (P84). Summary of cell counts assessing the relative abundance of Aqp2 (aquaporin 2) and B1 (B1 subunit of V-ATPase) positive cells in the renal CNT, CCD, OMCD and IMCD of Control and NH_4Cl treated mice. In total, 4,714 cells were counted in Control kidneys (n=5) and 4,543 cells in NH_4Cl treated kidneys (n=5). Statistical analysis using Student`s *t*-test. * $p \leq 0.05$, ** $p \leq 0.01$, *** $p \leq 0.001$.

CNT: connecting tubule, CCD: cortical collecting duct, OMCD: outer medullary collecting duct, IMCD: inner medullary collecting duct

Immunoblotting of total kidney membrane preparations confirmed the results obtained by immunofluorescent labelling. Again, Aqp2 protein abundance was increased in acidotic kidneys (Fig. 10.29), while Pds abundance was decreased (Fig. 10.30). Moreover, the relative protein abundance of Ae1 and the B1 subunit of V-ATPase did not change upon chronic metabolic acidosis (Fig. 10.31, 10.32).

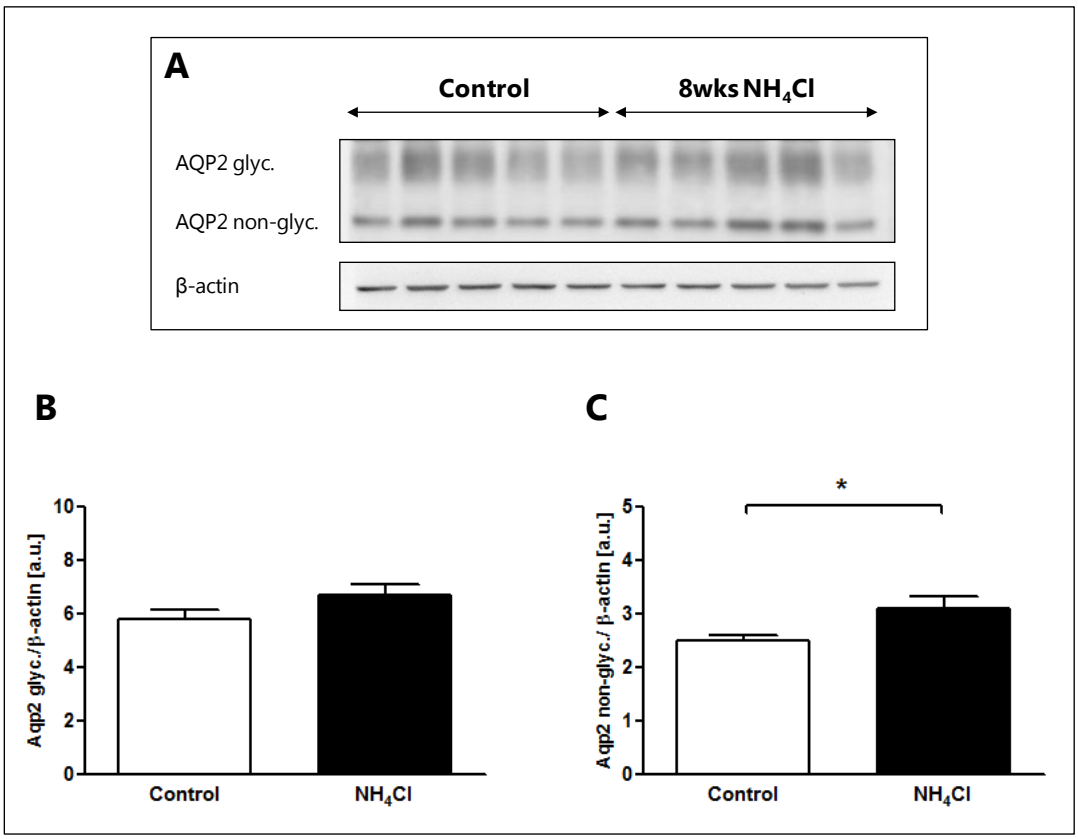

Fig. 10.29 Relative protein abundance of Aqp2 in kidneys of Control and 8 weeks NH_4Cl treated mice (P84). **A**) Representative immunoblot of Aqp2 (aquaporin 2) on total kidney membrane preparation from Control and 8 weeks NH_4Cl treated mice, β-actin served as loading control. **B, C)** Densitometry. Statistical analysis using Student`s *t*-test (n = 5 per group). * $p \leq 0.05$, ** $p \leq 0.01$, *** $p \leq 0.001$.

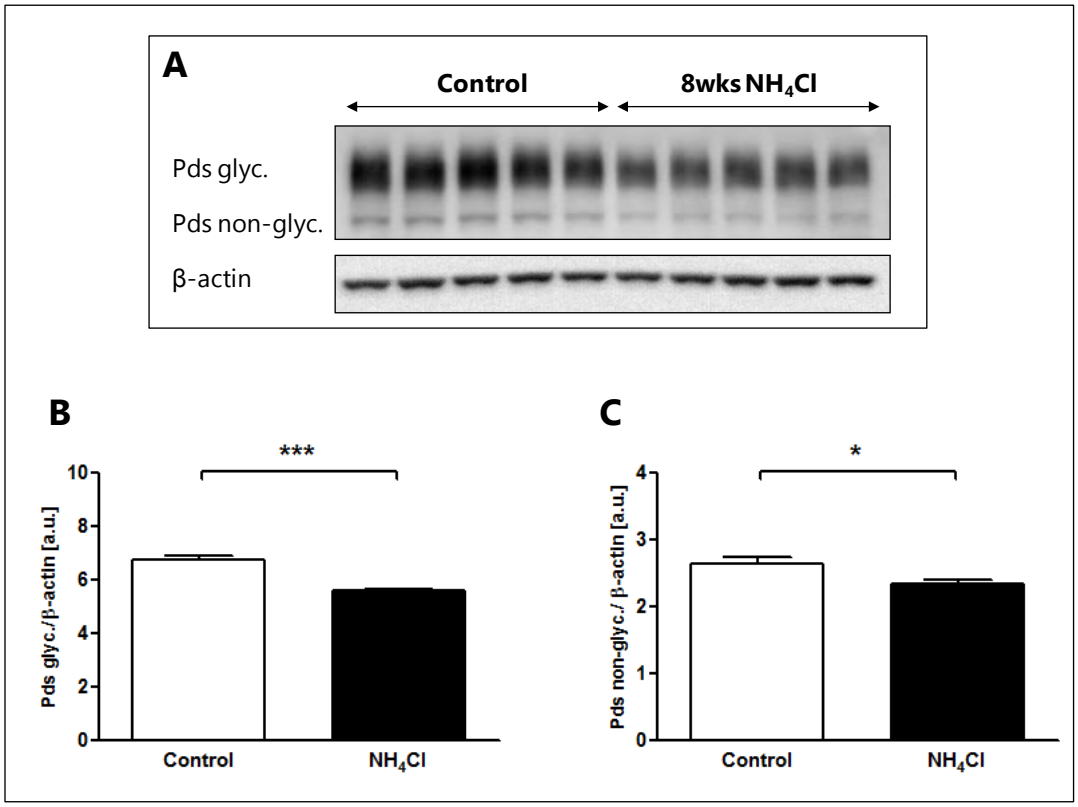

Fig. 10.30 Relative protein abundance of Pds in kidneys of Control and 8 weeks NH_4Cl treated mice (P84). **A**) Representative immunoblot of Pds (pendrin) on total kidney membrane preparation from Control and 8 weeks NH_4Cl treated mice, β-actin served as loading control. **B, C)** Densitometry. Statistical analysis using Student`s *t*-test (n = 5 per group). * $p \leq 0.05$, ** $p \leq 0.01$, *** $p \leq 0.001$.

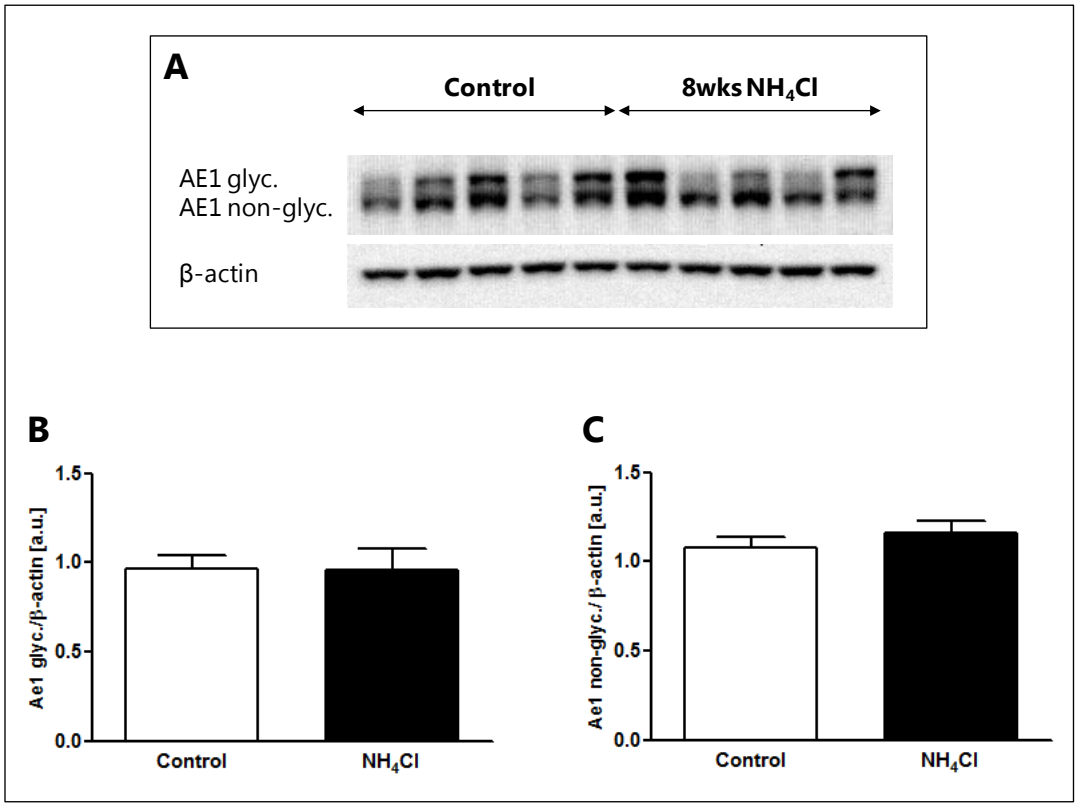

Fig. 10.31 Relative protein abundance of Ae1 in kidneys of Control and 8 weeks NH_4Cl treated mice (P84). **A**) Representative immunoblot of Ae1 (anion exchanger 1) on total kidney membrane preparation from Control and 8 weeks NH_4Cl treated mice, β-actin served as loading control. **B, C)** Densitometry. Statistical analysis using Student`s *t*-test (n = 5 per group). * $p \leq 0.05$, ** $p \leq 0.01$, *** $p \leq 0.001$.

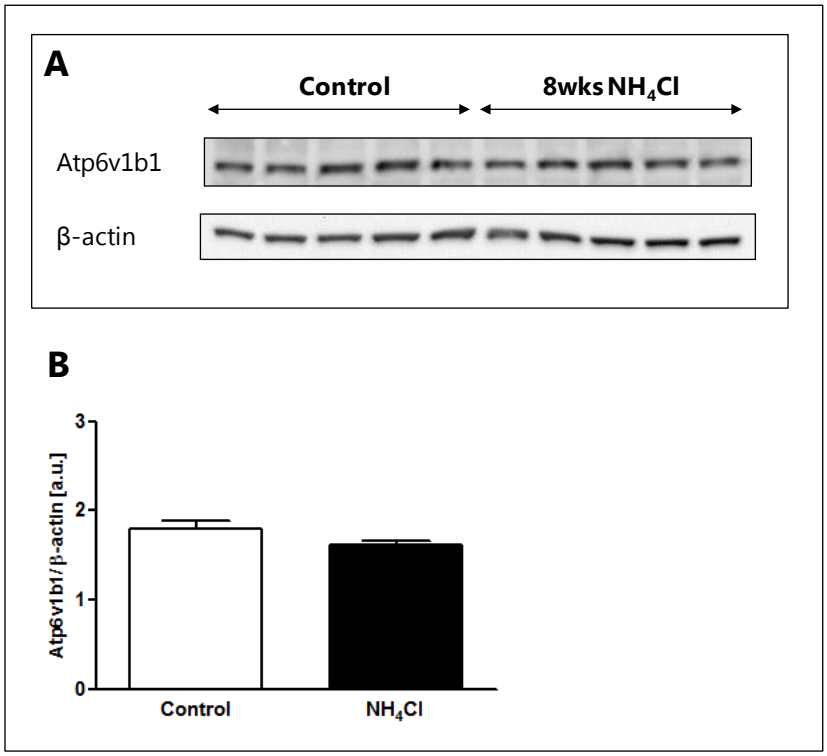

Fig. 10.32 Relative protein abundance of B1 subunit of V-ATPase in kidneys of Control and 8 weeks NH_4Cl treated mice (P84). **A**) Representative immunoblot of B1 subunit of V-ATPase (ATP6v1b1) on total kidney membrane preparation from Control and 8 weeks NH_4Cl treated mice, β-actin served as loading control. **B)** Densitometry. Statistical analysis using Student`s *t*-test (n = 5 per group). * $p \leq 0.05$, ** $p \leq 0.01$, *** $p \leq 0.001$.

In addition to alterations of acid-base transporters, Gdf15 protein abundance was significantly regulated in chronic metabolic acidosis (Fig. 10.33). A supposingly immature propeptide was detected at 50 kDa and found to be significantly downregulated upon chronic acidosis. Consistently, the probably mature secreted dimer of Gdf15 at 32 kDa was significantly upregulated in acidotic kidneys, while *Gdf15* mRNA was not changed (Fig. 10.35J). However, whether the regulated supposingly mature dimer is really present as a secreted signalling peptide of Gdf15 circulating in the blood is not known, since serum levels of Gdf15 were not assessed in Control or acidotic mice. Furthermore, the function of Gdf15 in adaptive responses of the kidney during chronic metabolic acid-base disturbances is not yet resolved. In the early adaptive response of the kidney to metabolic acidosis, Gdf15 was suggested to be involved in the initiation of proliferation (chapter 5.2.2). However, this function seems unlikely in the case of chronic (8 weeks) acidosis, as the initial increase of the proliferation rate might be already terminated and sustained at low comparable rates of Control kidneys. Moreover, Gdf15 is involved in the regulation of cellular processes upon manifold stress stimuli [181]. Hence, a regulatory role of Gdf15 in the kidney of chronic acidotic mice might be rather involved in processes that reduce cellular stress.

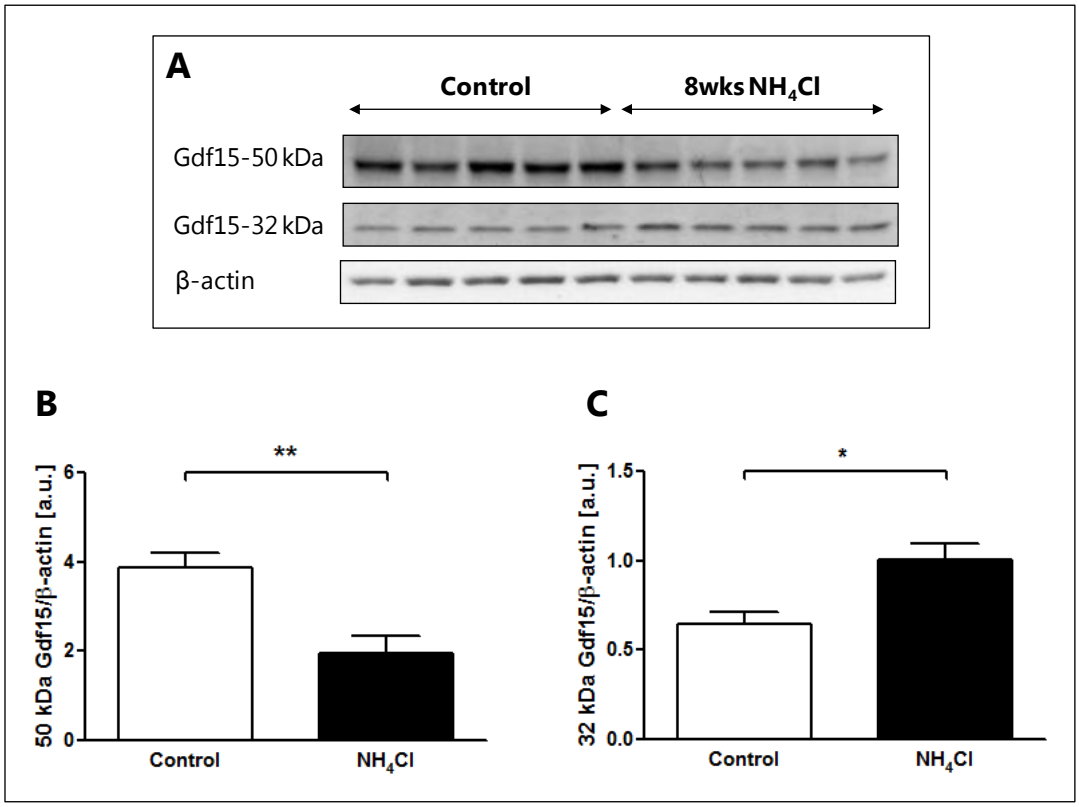

Fig. 10.33 Relative protein abundance of Gdf15 in kidneys of Control and 8 weeks NH_4Cl treated mice (P84). **A**) Representative immunoblot of Gdf15 (growth differentiation factor 15) on cytosolic fractions of total kidney homogenates extracted from Control and 8 weeks NH_4Cl treated mice, β-actin served as loading control. **B, C)** Densitometry. Statistical analysis using Student`s *t*-test (n = 5 per group). * $p \leq 0.05$, ** $p \leq 0.01$, *** $p \leq 0.001$.

In order to assess the relative protein abundance of Foxi1 in Control and acidotic kidneys, immunoblotting of nuclear protein extracts and cytosolic fractions from kidney homogenates were performed. Transiently *Foxi1* transfected Hek293T cells served as a positive control for the pattern of Foxi1 protein and derivates in electrophoretic SDS-PAGE (Fig. 10.34C). Here, three Foxi1 related bands were detected by western blot, of which one matched the expected molecular weight of Foxi1 (41 kDa). The other two Foxi1 related bands were detected at higher molecular weights and are of unknown origin. However, in kidney nuclear extracts all three bands were detected and were found expressed at comparable levels in Control and NH_4Cl treated animals (Fig. 10.34A). Interestingly, Foxi1 immunoblotting on kidney cytosolic fractions of total homogenate showed a distinct pattern (Fig. 10.34B). The lowest band, corresponding to the expected molecular weight was missing. Anyhow, the two higher Foxi1 related bands of unknown origin were present but not regulated upon acid-base disturbance. Future experiments are necessary to solve the character of the Foxi1 related bands detected by immunoblotting. Foxi1 was shown to be capable of remodelling chromatin structures and to remain bound to condensed chromatin during mitosis [226]. However, inactive or premature forms of Foxi1 might also be present outside the nucleus, as indicated by the detection of Foxi1 related proteins with higher molecular weight in the cytosolic fraction of kidney homogenates.

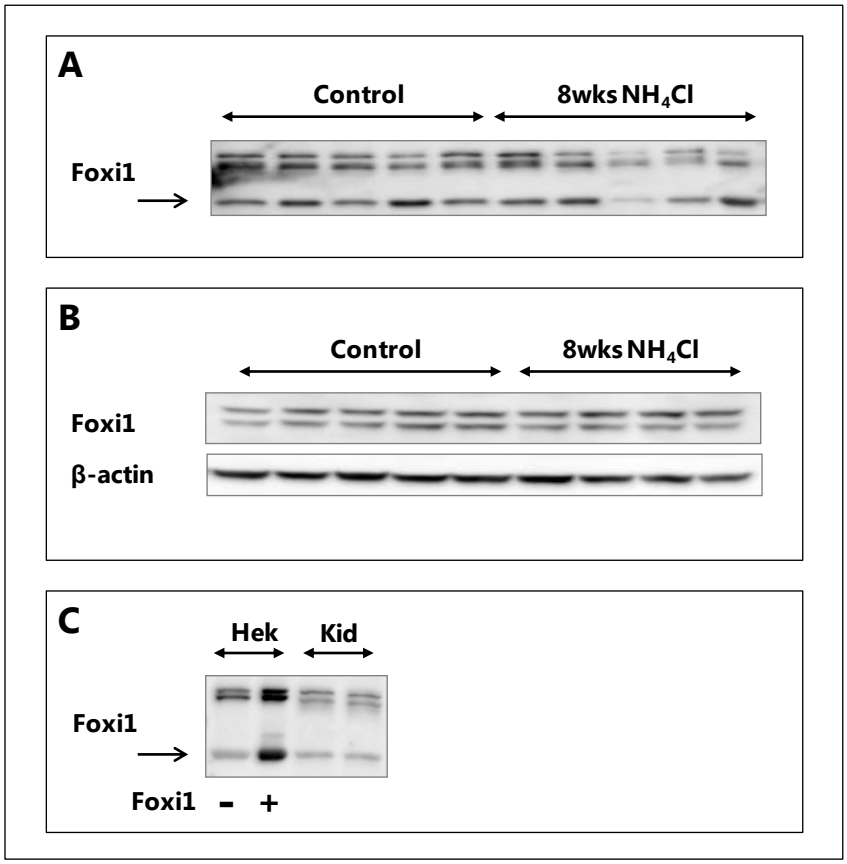

Fig. 10.34 Relative protein abundance of Foxi1 in kidneys of Control and 8 weeks NH_4Cl treated mice (P84). **A-C**) Representative immunoblot of Foxi1 (forkheadbox protein 1). **A)** Nuclear protein extracts from total kidneys of Control and 8 weeks NH_4Cl treated mice. **B)** Cytosolic fractions of total kidney homogenates from Control and 8 weeks NH_4Cl treated mice with β-actin as loading control. **C**) Nuclear protein extracts from untransfected (Foxi1 -) and transiently transfected Hek293T cells (Foxi1 +) and total kidney (Kid) (P30). arrow: indicates expected molecular weight of Foxi1 (41 kDa), only detectable in nuclear protein extracts.

Addressing the question whether chronic acidosis is capable of altering the differentiation of renal IC, total mRNA of Control and NH_4Cl treated mouse kidney was extracted and qRT-PCR was performed for the above introduced candidate genes of acid-base transporters and transcription factors or signalling molecules. Finally, the results were compared with data obtained from Ae1 mutant mouse kidney. The relative mRNA expression levels are presented in bar graphs of Fig. 10.35A-J and a simplified tabular expression of the results is shown in Fig. 10.36. Consistent with the chronic acidosis, relative mRNA levels of *Ae1* (Fig. 10.35A) were upregulated in NH_4Cl loaded mice compared to Control, while *Pds* was downregulated (Fig. 10.35B). Similarly, relative mRNA expression of *Pds* was reduced in Ae1 KO mice. The relative abundance of the *B1 subunit of V-ATPase* was not altered in NH_4Cl loaded animals compared to Control (Fig. 10.35C). However, the *B1 subunit of V-ATPase* was significantly downregulated in Ae1 KO kidneys. Furthermore, *Rhcg* mRNA levels were not changed significantly in chronic metabolic acidosis nor Ae1 related dRTA (Fig. 10.35D). Interestingly, relative *Foxi1* mRNA abundance was not different in NH_4Cl treated mice compared to Control or Ae1 mutant mice (Fig. 10.35E). Strikingly, relative *Cp2l1* mRNA abundance was upregulated in chronic metabolic acidosis but not in Ae1 KO (Fig. 10.35F). Moreover, relative mRNA levels of *Bdkrb2*, *Klf4* and *Gdf15* were significantly upregulated in kidneys Ae1 KO mice compared to WT, but not in kidneys of NH_4Cl loaded mice compared to Control (Fig. 10.35G-J).

Hence, the investigated genes are differentially regulated during chronic metabolic acidosis and Ae1 related dRTA as also shown in the simplified table (Fig. 10.36).

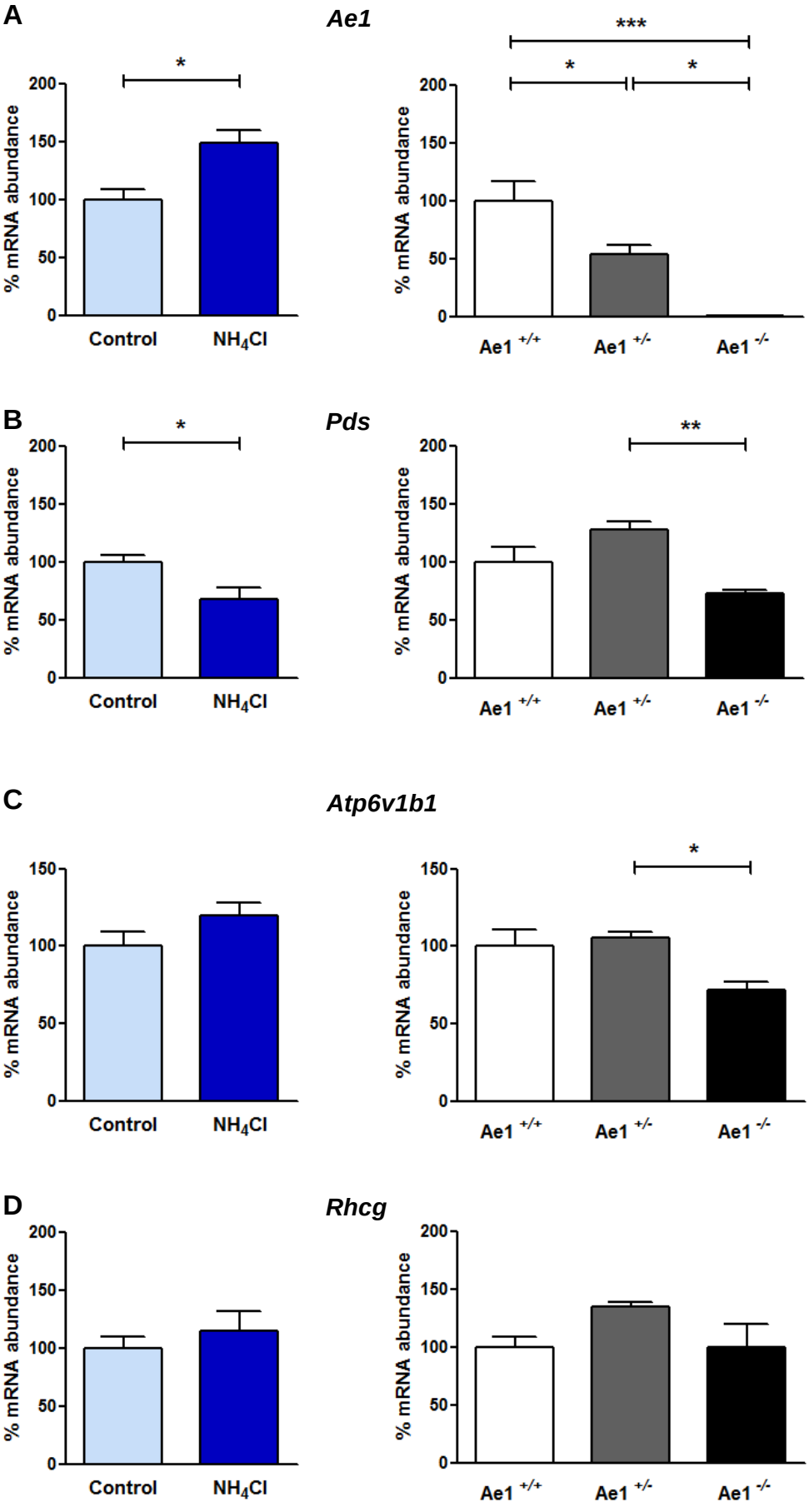
A
Ae1
% mRNA abundance
200
150
100
50
0
*
Control
NH4Cl
***
*
*
Ae1 +/+
Ae1 +/-
Ae1 -/-
B
Pds
**
C
Atp6v1b1
D
Rhcg

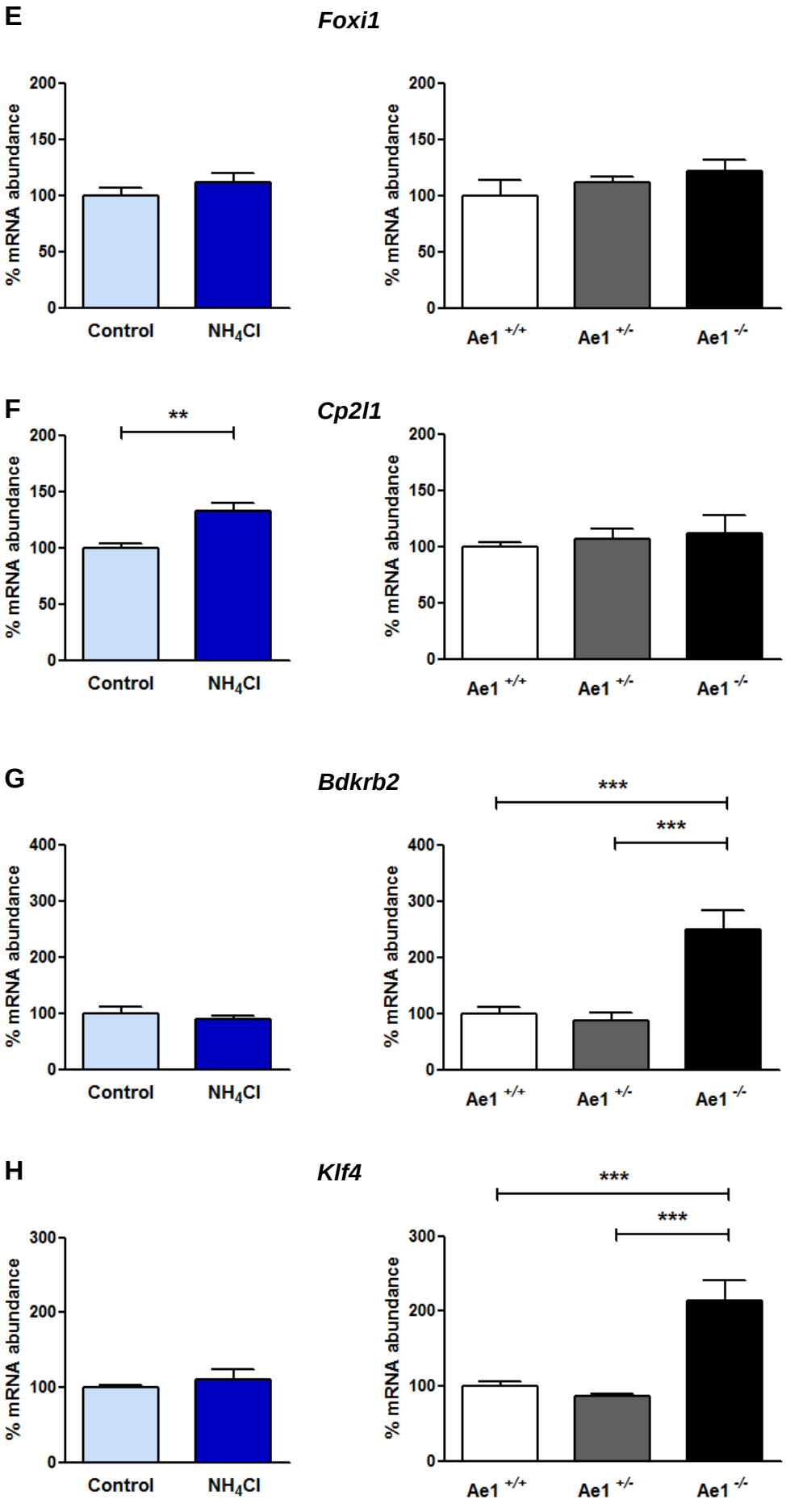
E
Foxi1
% mRNA abundance
200
150
100
50
0
Control
NH4Cl
Ae1 +/+
Ae1 +/-
Ae1 -/-
F
Cp2l1
**
G
Bdkrb2
***
***
H
Klf4
***
***

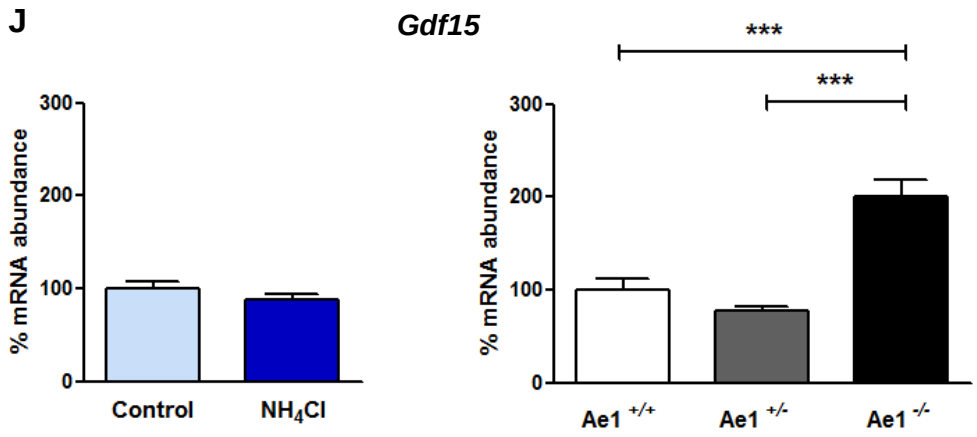

Fig. 10.35 Relative renal mRNA abundance of target genes during chronic metabolic acidosis and dRTA. Left bar graph represents mRNA expression levels in C57/Bl6 Control and NH_4Cl treated mice. Right bar graph shows renal mRNA expression levels of Ae1 mutant mice, respectively. Statistical analysis using Student`s *t*-test (n = 4-5 animals per group). * $p \leq 0.05$, ** $p \leq 0.01$, *** $p \leq 0.001$.

relative change in % mRNA abundance		
gene	**Control vs NH_4Cl**	**Ae1 WT vs KO**
Ae1	↑	↓↓
Pds	↓	↔
Atp6v1b1	↔	↔
Rhcg	↔	↔
Foxi1	↔	↔
Cp2l1	↑↑	↔
Gdf15	↔	↑↑
Klf4	↔	↑↑
Bdkrb2	↔	↔

Fig. 10.36 Summarized results from Fig. 10.35 representing relative changes in mRNA expression levels of NH_4Cl treated mice relative to C57/Bl6 Control and Ae1 KO mice relative to Ae1 WT. ↑ indicating significant upregulation; ↓ indicating significant downregulation; ↔ indicating no difference compared to C57/Bl6 Control, or Ae1 WT respectively.

10.3 Pendrin expression pattern is normal despite incomplete dRTA

Renal Ae1 deficiency in mice and humans leads to distal renal tubular acidosis (dRTA). The previous results proofed that induction of chronic metabolic acid loads by oral application of NH_4Cl is not sufficient to cause the abnormal expression of Pds observed in the inner medulla of Ae1 KO mice. However, possible negative effects on Pds expression in the inner medulla induced by Ae1 related dRTA cannot be excluded by this experimental model. Therefore, the expression pattern of Pds was investigated in mice deficient for the B1 subunit of V-ATPase (B1) or Rhcg. Both mouse models were reported to develop dRTA upon induced acid-base disturbances (chapter 7.1).

In contrast to Ae1 deficient mice, representative photomicrographs of kidneys from B1 and Rhcg deficient mice did not show signs of abnormal Pds expression in cortex or medulla (Fig. 10.37). Hence, Pds expression pattern in the renal inner medulla is normal despite incomplete dRTA. Moreover, Ae1 and the a4 and B1 subunits of V-ATPase were not differentially expressed in kidneys of B1 or Rhcg mutant mice compared to WT (data not shown). However, both mouse models were investigated under basal conditions, where acid-base homeostasis seems compensated despite their renal defects.

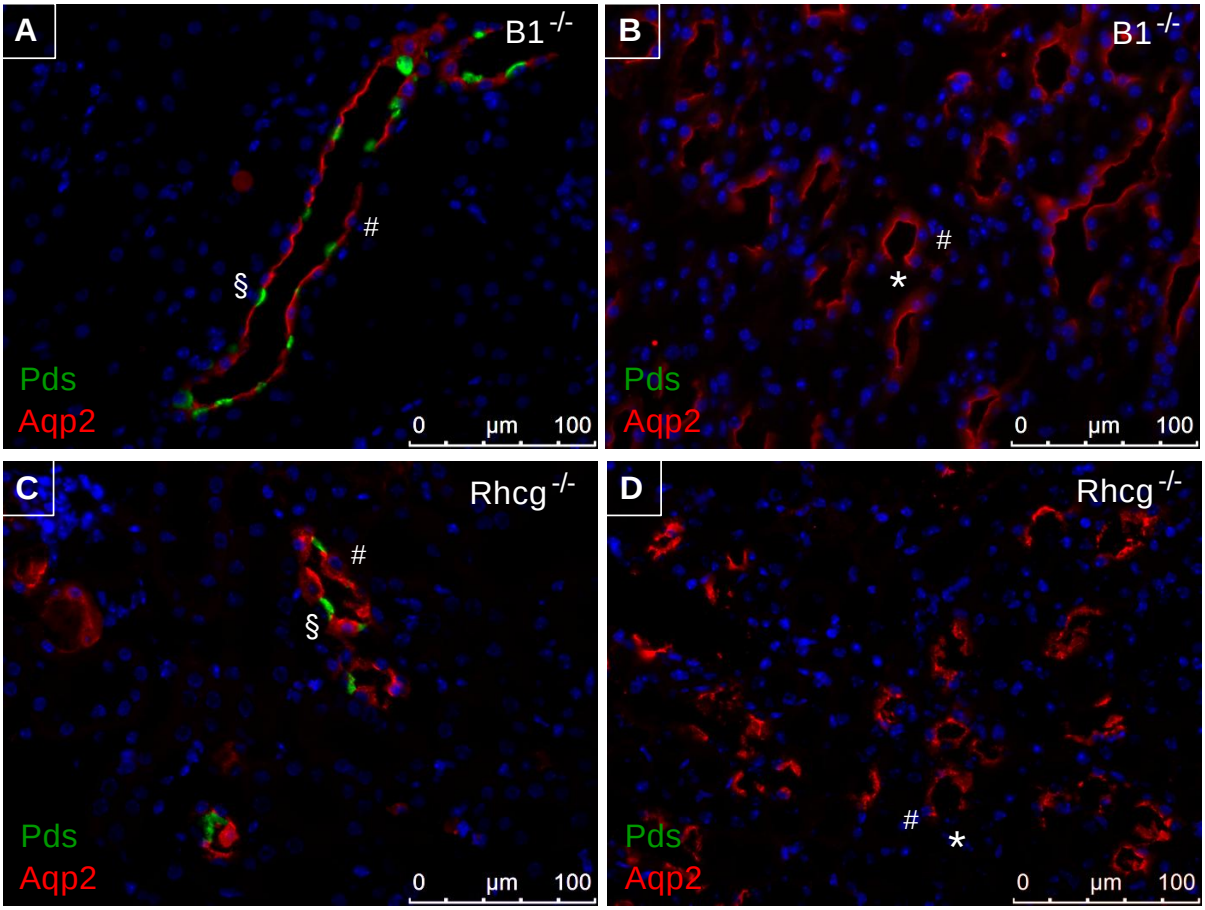

Fig. 10.37 Immunologic localization of Pds in adult (P84) B1$^{-/-}$ and Rhcg$^{-/-}$ mouse kidney. Representative merged photomicrographs from renal cortex (CCD) of B1$^{-/-}$ **(A)** and Rhcg$^{-/-}$ **(C)** mice. Representative merged photomicrographs from renal inner medulla (IMCD) of B1$^{-/-}$ **(B)** and Rhcg$^{-/-}$ **(D)** mice. Individual Aqp2 (aquaporin 2) expression in renal CCD and IMCD identifies principal cells. **A, C)** In the CCD, Pds (pendrin) localizes to the luminal membrane of Aqp2 negative cells, identifying B-ICs. **B, D)** Pds is absent from the mature inner medulla of B1$^{-/-}$ and Rhcg$^{-/-}$ mice (n = 3 per genotype). Nucleic acid is stained with DAPI. § indicating Pds positive cell; # indicating Aqp2 positive cell; * indicating Aqp2/Pds negative cell. Magnification 400x.

10.4 Expression of acid-base transporters in human Control kidney and a case of AE1 related dRTA

In humans, several mutations of AE1 account for the development of primary dRTA (chapter 4.5.1, Tab. 4.2, chapter 6.1.2). However, these patients are rarely biopsied since diagnosis of disease is made from the clinical presentation and genetic analysis. A renal biopsy of a patient with the dominant negative AE1 S613F mutation (kind gift of Dr. R. Unwin, University College of London, UK) was investigated to search for signs of CD cell abnormalities using immunofluorescent markers. As discussed already in detail, under physiologic conditions luminal expression of PDS labels type B-ICs, whereas basolateral presence of AE1 marks type A-ICs (Fig. 10.38A). Similar to mouse and rat kidneys, AQP2 is expressed on the apical cell membrane of principal cells, while the a4 and B1 subunit of V-ATPase is expressed in intercalated cells (Fig. 10.38B, C). Consistent with observations in mouse kidney, human carbonic anhydrase II (CA II) expression was found in AQP2 positive and negative cells of the CNT in Control kidneys and is therefore not considered as a IC cell-specific marker (data not shown).

In a renal biopsy of the above mentioned patient with the dominant negative AE1 mutation S613F a reduced abundance of ICs with a concomitant increased presence of PCs was obvious. Variants of the IC type were detected using AE1, PDS and V-ATPase markers (a4 and B1 subunit) and rarely seen. In contrast, PCs labelled with AQP2 seemed to be the major cell type of the collecting ducts. Furthermore, AE1 immunoreactivity was absent in cells of the connecting tubule and collecting duct in the kidney with AE1 S613F mutation. However as expected, AE1 staining was preserved in erythrocytes (Fig. 10.39B). In addition, PDS positive cells were rarely detected in AE1 S613F renal tissue and PDS seemed to be expressed mostly in the cytosol instead of the apical membrane (Fig. 10.39C). Moreover, few cells coexpressed PDS along with AQP2. Notably, the medullary region was not present in this biopsy as usual. Similarly, the majority of a4 positive cells unusually coexpressed AQP2 (Fig. 10.40). Additionally, B1 immunoreactivity appeared markedly reduced and B1 positive cells were hardly present (Fig. 10.41). However, because of the single case relative

abundance of the labelled cells was not assessed and quantification of relative protein abundance is not possible.

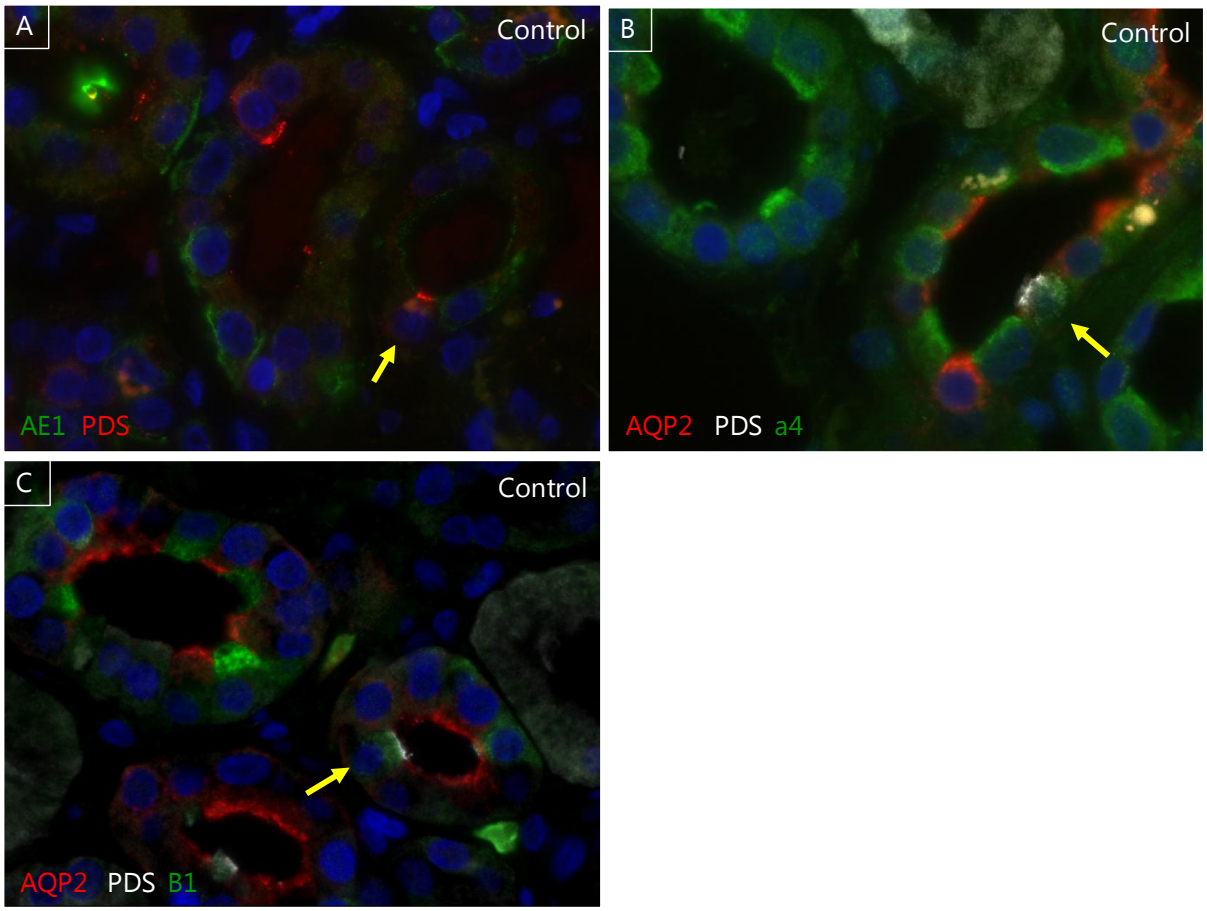

Fig. 10.38 Expression pattern of collecting duct marker proteins in human Control kidney. **A)** AE1 (Anion Exchanger 1) and PDS (Pendrin) are expressed in distinct types of intercalated cells. Basolateral expression of AE1 indicates presence of type A-IC. Apical presence of PDS labels type B-IC (arrow). **B, C)** AQP2 (Aquaporin 2) is exclusively expressed in principal cells. The a4 subunit of V-ATPase is expressed in intercalated cells of the renal collecting duct system and proximal parts of the nephron **(B)**. The B1 subunit of V-ATPase is specifically expressed in renal IC **(C)**. Colocalization of basolateral V-ATPase with luminal PDS confirms type B-IC identity (arrow) **(B)**, while equilateral V-ATPase and PDS expression indicate type non-A/non-B IC phenotype (arrow) **(C)**. Magnification 400x.

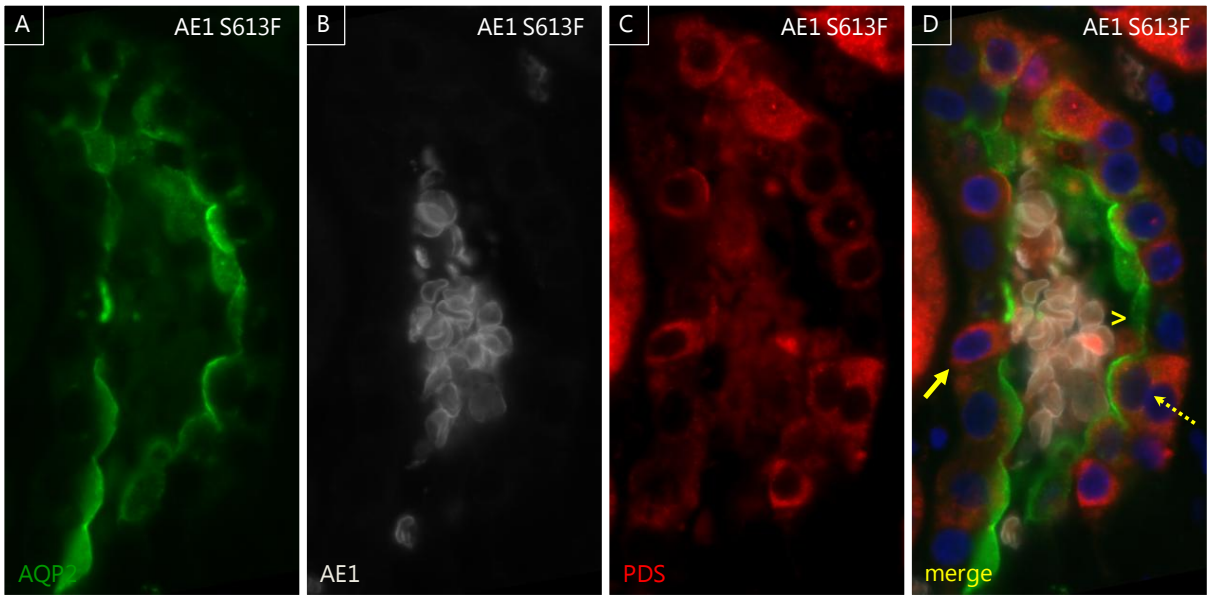

Fig. 10.39 Renal expression pattern of PDS and AQP2 in a case of AE1 S613F. **A)** The majority of cells in the human renal cortex express luminal AQP2 (Aquaporin 2). **B)** Immunoreactivity for AE1 (Anion Exchanger 1) was absent in renal cells of the collecting duct, but is conserved in erythrocytes. **C)** A rather cytosolic expression of PDS (Pendrin) was found in some cells of the renal collecting duct. **D)** merge. Some PDS positive cells remain negative for AQP2 (arrrow), while other PDS positive cells seem to coexpress AQP2 (dashed arrow). arrowhead indicates AQP2 positive/PDS negative cell. Magnification 1,000x.

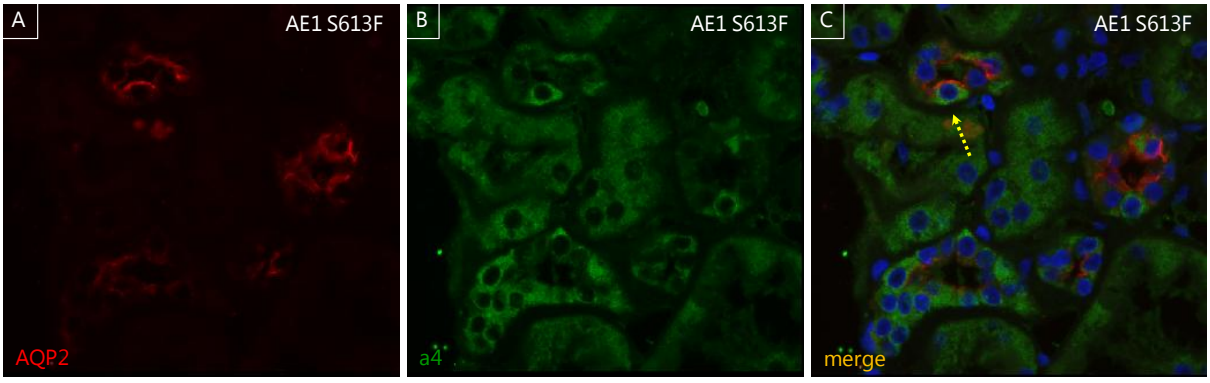

Fig. 10.40 Renal expression pattern of a4 subunit of V-ATPase and AQP2 in a case of AE1 S613F. **A)** Apical AQP2 (Aquaporin 2) is present in the majority of renal collecting duct cells. **B)** The a4 subunit of V-ATPase (a4, ATP6V0A4) is expressed in intercalated cells of the renal collecting ducts and in cells of the proximal nephron. **C)** merge. The majority of a4 positive cells are also positive for AQP2 (dashed arrow). Magnification 400x.

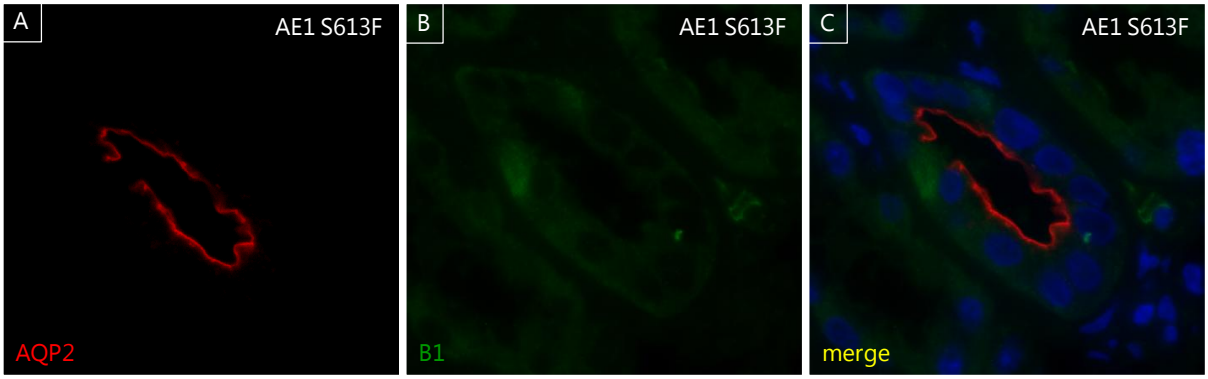

Fig. 10.41 Renal expression pattern of B1 subunit of V-ATPase and AQP2 in a case of AE1 S613F. **A)** Apical AQP2 (Aquaporin 2) is present in the majority of renal collecting duct cells. **B)** The B1 subunit of V-ATPase (B1, ATP6V1B1) is rarely expressed in intercalated cells of the renal collecting ducts. **C)** merge. B1 and AQP2 are expressed in distinct cell types of the renal collecting duct. Magnification 400x.

In another case of primary dRTA related to the dominant negative AE1 R589H mutation (kind gift of Dr. Alper, S.L., Harvard Medical School, Boston, USA) immunofluorescent analysis of the renal CD system failed due to a loss of the renal morphology. Here, chronic nephrocalcinosis and pyelonephritis destroyed the renal tubular structures which were replaced by amorphous fibrotic scars (Fig. 10.42).

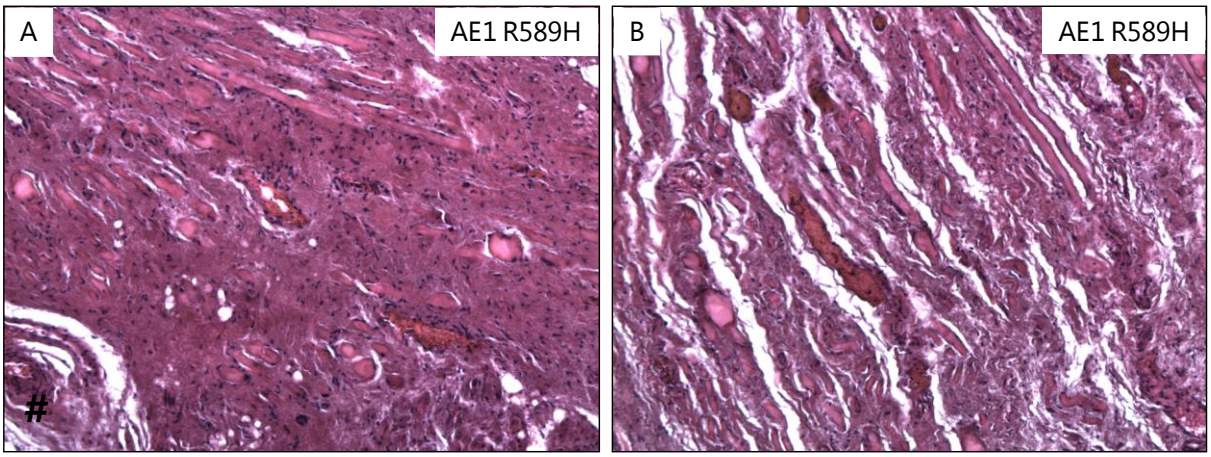

Fig. 10.42 Hematoxylin and Eosin staining of a renal biopsy of a case with AE1 R589H. The kidney morphology shows amorphous fibrotic remodelling and loss of tubular structures due to nephrocalcinosis and recurring pyelonephritis. # indicates fibrotic remains of a glomerulum. Magnification 100x.

11. DISCUSSION

The metanephric mammalian kidney originates from two different primordia, the nephrogenic mesenchymal blastema and the ureteric bud epithelium. The nephrogenic CNT joints the renal CD system to the upstream nephron. The mature renal CD system is the main site of final urinary acidification and according to its functional demands subdivided into the CCD, OMCD and IMCD. However, the renal CNT and CD system are comprised of at least three different cell types, which are unequally distributed (Fig. 2.4). The principal cells (PCs) are the major cell type and involved in systemic electrolyte and water homeostasis. They are interspersed with distinct types of intercalated cells (ICs), which regulate systemic acid-base homeostasis. The two major forms of ICs are the acid secretory type A-ICs and the bicarbonate secretory type B-ICs. In accordance with their function, cells of the renal CD can be distinguished by their ultrastructural appearance and specific marker proteins (Fig. 2.6). In the present study, PCs are identified by the immunologic presence of Aqp2, while both types of ICs are detected by their expression and subcellular localization of the a4 or B1 subunit of V-ATPase. Furthermore, the two major types of IC are distinguished by their expression of Ae1 (type A-ICs) or Pds (type B-ICs).

The Cl^-/HCO_3^- exchanger Ae1 is essentially expressed in erythrocytes and in the kidney exclusively on the basolateral membrane of type A-ICs. In humans, several mutations of the transporter were identified, which either disturb its function in the erythrocyte or the kidney. Consistent with the role of Ae1 in renal type A-ICs, disturbances of Ae1 expression and function in the kidney lead to distal renal tubular acidosis (dRTA), an inability to acidify the urine. However, data of the present study suggest an additional role for Ae1 in the terminal differentiation of the renal CD system, which is most likely beyond its Cl^-/HCO_3^- exchange.

11.1 Loss of Ae1 coincides with the unusual expression of Pds in the renal inner medulla

Despite intensive studies of the early events of nephrogenesis and characterization of the adult kidney, only very little is known about the cellular origin of the different cell types of the renal CD system. Studies of fetal mouse, rat and human kidneys suggest the development of PCs and subtypes of ICs from distinct pools of precursor cells in the renal CNT and MCD (chapter 2.5, Fig. 2.5). Interestingly, subtypes of ICs are not detected in the renal CCD before birth. However, with increasing functional demands of the maturing postnatal kidney, the CD system undergoes continuous remodelling resulting in a distinct segmental pattern. In the adult kidney, type B-ICs are exclusively present in the renal CNT and CCD, while the relative abundance of type A-ICs increases towards the inner medulla with a maximum in the outer medullary region (Fig. 2.4, 2.5).

Surprisingly, immunofluorescent investigation of mature kidneys from juvenile (P30) and adult (P84) Ae1 deficient mice revealed an unusual expression of Pds in cells of the inner medulla (Fig. 10.2, 10.6, 10.7). Moreover, some cells coexpressed Pds along with the PC marker Aqp2. Interestingly, the later observation was confined to the inner medulla of mature Ae1 deficient kidneys, as a normal cellular Pds expression was detected in the mature cortex and in embryonic kidneys.

Only the quantification of immunologically counter-labelled cells in juvenile and adult mouse kidneys revealed some differences concerning the cellular distribution among the genotypes. Consistent with chronic dRTA, the relative abundance of Pds^+ cells in the renal CNT and CCD were significantly reduced, while $Aqp2^+$ cells increased in adult (P84) Ae1 KO kidneys. However, in the renal OMCD of P84 Ae1 KO mice the relative abundance of $Aqp2^+/Pds^+$ coexpressing cells increased, probably on the expense of unlabelled cells. In addition, the relative abundance of Pds^+ and $Aqp2^+/Pds^+$ coexpressing cells in the renal ICMD of P84 Ae1 KO mice increased with a modest decrease in unlabelled cells.

In contrast, Aqp2 and Pds expressing cells in the CNT of juvenile (P30) mouse kidneys were not altered between WT and Ae1 KO mice. Moreover, Pds^+ cells increased in abundance on the expense of unlabelled cells in the CCD and OMCD of P30 Ae1 KO mice. Likewise, Pds^+ and $Aqp2^+/Pds^+$ coexpressing cells in the renal ICMD of P30 Ae1 KO mice increased, while unlabelled cells modestly decreased. Strikingly, the unusual expression of Pds in Ae1 deficient IMCDs is accompanied by a reduced relative abundance of $Aqp2^+$ in P30 mice, while it is paralleled by a reduced abundance of unlabelled cells in P84 kidneys.

The altered cellular expression pattern between P30 and P84 Ae1 KO mice might be a consequence of two circumstances. The juvenile mice just experienced a dietary switch from mother milk to rodent chow, which was shown to provide a strong net alkali load [227]. Consistently, the urinary pH of juvenile mice after weaning from the mother milk was shown to be more alkaline [31]. Hence, the increased need to excrete excess base equivalents from the body might reflect the unexpected increased presence of Pds^+ cells in the CCD and OMCD of P30 Ae1 KO kidney despite early dRTA. It remains speculative, whether this is due to a delayed apoptotic removal of Pds^+ cells from the MCD or an increased proliferation rate of Pds^+ cells. In addition, adult (P84) Ae1 KO mice suffered from chronic dRTA, which affects renal water handling [190, 218]. This might also be the reason for the reduced number of $Aqp2^+$ in the renal CNT of juvenile (P30) WT mice compared to adult (P84) WT animals. Furthermore, an adaptive increase of $Aqp2^+$ cells upon prolonged dRTA might mask the abnormal differentiation of $Aqp2^+$ cells in the renal IMCD, or drive the abnormal differentiation of cells other than $Aqp2^+$. However, in kidneys of juvenile Ae1 KO mice, which might have a less pronounced dRTA, the unusual expression of Pds in the IMCD seems to origin from the abnormal differentiation of cells retaining or acquiring Aqp2 expression.

Consistent with the observations in Ae1 deficient mouse kidney, PDS expression seemed altered in a renal biopsy of a patient with primary dRTA due to the dominant negative AE1 S613F mutation (chapter 10.4). This mutation is known to exclusively affect the expression and functionality of AE1 in renal type A-ICs, but not in erythrocytes. *In vitro* experiments using polarized MDCK cells suggest that the AE1 S613F mutant protein is retained in the ER and thus does not reach the basolateral cell membrane of type A-ICs. Since reticulocytes are not polarized and have different chaperones and trafficking mechanisms than renal epithelial cells, they might circumvent the dominant negative effect of the mutant and escape early ER degradation.

However, a previous investigation of the patient's renal biopsy documented a reduced number of renal ICs and a solely cytosolic expression of AE1 S613F, with a preserved expression in erythrocytes [138]. Similar results were obtained using immunofluorescent molecular CD cell markers in the present study. The abundance of renal ICs (identified by V-ATPase, PDS or AE1) was remarkably low and PCs (identified by AQP2) seemed to comprise the major cell type of the renal CD system. In the present study, AE1 immunoreactivity was only detected in erythrocytes but the accessibility of the renal epitope might have been lost over the years of storage, especially since the original work mentioned a rather weak AE1 signal intensity in renal epithelial cells [138]. Anyway, V-ATPase and PDS expression were detected only in very few cells of the renal CD system and PDS localization appeared to be mostly cytosolic. Notably, the CD section represented on the biopsy were exclusively from the CNT and CCD segment as assessed by the gross morphology of the surrounding tissue and given by the usual technique to take biopsies.

Similarly, a reduced number of renal ICs from the CD system was reported for a case with the dominant negative AE1 R589H mutation [208].

Hence, Ae1 deficiency in mouse and man seems to correlate with abnormal subcellular expression of pendrin and severely reduced number of ICs.

11.2 The type A-IC phenotype is preserved in Ae1 deficient kidneys

In order to further elucidate which CD cell type might be abnormally differentiated in Ae1 KO kidneys, the expression pattern of V-ATPase was examined in P30 mice. The expression pattern of the kidney specific a4 subunit of V-ATPase did not show any significant differences between the genotypes. However, the IC-specific B1 subunit of V-ATPase partially reflected the unusual presence of Pds in the renal MCDs of Ae1 deficient mice. Here, an increased abundance of $B1^+/Aqp2^+$ coexpressing cells was observed in Ae1 KO kidneys, which reached significant difference in the IMCD of P30 mice. In line with the previous observation, $Aqp2^+$ cells of the Ae1 deficient IMCD were simultaneously decreased. Therefore, some Aqp2 expressing cells of the IMCD of Ae1 KO mice might either coexpress Pds ($Aqp2^+/Pds^+$) or B1 ($Aqp2^+/B1^+$) or both ($Aqp2^+/Pds^+/B1^+$), respectively. The unchanged expression pattern of individually $B1^+$ cells in Ae1 deficient kidneys suggests a normal differentiation of the type A-IC phenotype, which certainly represents the major IC subtype in the pool of unlabelled cells. This observation implies that renal Ae1 deficiency does not necessarily result in a loss of type A-ICs, but rather a loss of a proper molecular marker. Unfortunately, no other unequivocal marker of type A-IC is available to date to further confirm maintenance of this cell type. However, the unusual expression pattern of Pds expressing cells in Ae1 KO kidneys might origin from the abnormal differentiation of PCs and affects the type B-IC phenotype or the type non-A/non-B IC variant. However, further experiments are needed to answer this question.

11.3 Foxi1 expression is altered in Ae1 deficient kidneys

Transcription factors of the forkhead box family are involved in early nephrogenesis and terminal differentiation of the renal CD system (chapter 2.7.3). Foxi1 deficient mice were reported to lack molecular markers of renal ICs and consequently develop dRTA [83]. Moreover, the renal CD system of Foxi1 KO mice consists of a single cell type which coexpresses Aqp2 and CaII (Fig. 2.11). Similarly, Foxi1 homologues are required for epidermal ionocyte differentiation in larvae of *Xenopus laevis* and zebrafish (Fig. 2.7, 2.8) [51, 54, 56]. Therefore, the Foxi1 expression pattern was examined in Ae1 deficient kidneys by immunohistochemistry. Previous studies mentioned Foxi1 expression in the murine distal tubule and more precisely in type A-ICs and B-ICs, but not in PCs [82, 83]. However, the preliminary results of the present study reveal a nuclear expression of Foxi1 mainly in $B1^+$ ICs, but also in few $Aqp2^+$ PCs (Fig. 10.11-16). The contrary cellular localization of Foxi1 with previous reports might be due to the distinct experimental approach. Anyhow, quantification of the Foxi1 expression pattern in Ae1 WT and KO kidneys of juvenile mice revealed some interesting differences. The relative abundance of individual $Foxi1^+$ cells was significantly increased in the renal IMCDs of Ae1 KO mice compared to WT. Moreover, a similar amount of $Aqp2^+/Foxi1^+$ cells was increased in IMCDs of Ae1 KO mice, even though it did not reach statistical significance. Furthermore, $Aqp2^+/Foxi1^+$ cells in the CCD of Ae1 deficient kidneys were significantly increased, while the relative abundance of $Foxi1^+$ and unlabelled cells was simultaneously reduced. Similarly, Pds^+ cells were increased in the CCD of Ae1 deficient kidneys on the expense of unlabelled cells, while the relative abundance of $Aqp2^+/B1^+$ tends to increase on the expense of $Aqp2^+$ cells. Likewise, the increase of Pds^+ and $Aqp2^+/Pds^+$ cells in the renal IMCD of Ae1 KO mice on the expense of $Aqp2^+$ cells is paralleled by an increase in $Foxi1^+$ cells. Although the percentage of $Aqp2^+/Foxi1^+$ cells is smaller than the number of cells with unusual Pds and B1 expression, their concomitant appearance is likely related to each other and thus caused by Ae1

deficiency. Moreover, Foxi1 is a known positive transcriptional regulator of the B1 subunit of V-ATPase, Ae1 and Pds [83, 85, 87].

Interestingly, mice with a conditionally disrupted Notch signalling pathway in the renal CD system suffer from nephrogenic diabetes insipidus based on the loss of Aqp2 expressing PCs (chapter 2.7.2) [77]. Additionally, an increased abundance of V-ATPase expressing cells with a concomitant increased mRNA expression of *V-ATPase*, *Ae1*, *Pds* and *Foxi1* was noted. Consistently, a mouse model with a constitutive activation of the Notch signalling pathway in the renal CD system was devoid of molecular markers for ICs and expressed only Apq2 positive PCs (Fig. 2.10). Hence, terminal differentiation of the renal CD cells is regulated by the Notch signalling pathway and Foxi1, but the definite interaction of these transcriptional regulators is not yet elucidated. Studying the expression of the molecular players of the Notch signalling pathway during collecting duct development in WT mice and its regulation in Ae1 KO kidneys would add further important information.

11.4 Cp2l1 expression is altered in Ae1 deficient kidneys

Similar to Foxi1 KO mice and those with disrupted Notch signalling pathway, animals deficient for the transcription factor Cp2l1 are devoid of IC marker in the renal CD system (chapter 2.7.4, Fig. 2.11) [90]. The role of Cp2l1 in the mammalian kidney is only poorly investigated, but studies of the epidermal development of ionocytes in *Xenopus* and zebrafish larvae suggest a regulatory role of Cp2l1 homologues in a Pds expressing ionocyte subtype [51, 57]. Moreover, the transcriptional control of Cp2l1 involves the interaction with the Notch signalling pathway and Foxi transcription factors (Fig. 2.7, 2.8). However, whether this is also true for Cp2l1 in murine kidney cells is not known. Preliminary data from immunologic localization studies on P30 WT mouse kidneys show coexpression of nuclear Cp2l1 mainly with Aqp2 positive and less with Aqp2 negative cells along the renal CD system (Fig, 10.17, 10.18). Apparently, the abundance of Cp2l1 positive cells increases from the CNT towards the inner medulla, where Cp2l1 seems to be expressed in almost every cell. Similarly, the presence of Aqp2 expressing PCs increases from the CNT towards the inner medulla. In addition and in line with a previous report, nuclear Cp2l1 expression is detected in some tubuli of the DCT and TAL [90]. Even though detailed colocalization studies are not yet available, a striking difference in the expression of Cp2l1 was observed in Ae1 deficient kidneys compared to wildtype. The nuclear expression profile of Cp2l1 in inner medullary collecting duct cells was completely absent and moreover appeared to be shifted to the apical membrane in some cells. Whether the altered subcellular localization is related to different activity states of the transcription factor needs to be investigated. However, the loss of Cp2l1 from the nuclei of IMCD cells seems to coincide with the abnormal cell differentiation described upon renal Ae1 deficiency.

11.5 Late onset of Ae1 related abnormal differentiation of renal IMCD

Although Pds expressing cells in kidneys of Ae1 deficient embryos seemed to be preserved, an abnormal regulation of transporters and transcription factors involved in CD cell function and specificity cannot be ruled out. Therefore, mRNA expression levels were compared at different developmental ages in kidneys of Ae1 mutant mice (Tab. 10.20). Interestingly, alterations of genes implicated in renal acid-base handling (*Ae1*, *Pds*, *B1 subunit of V-ATPase* and *Rhcg*) were not altered before postnatal day 30 (P30). This result supports the afore mentioned impact of a dietary switch from mother milk to rodent chow on systemic acid-base homeostasis and the concomitant mutual reaction with Ae1 related dRTA. Alternatively, it may reflect the completion of postnatal maturation of the kidney which includes the removal of Pds^+ cells from the medulla. Surprisingly, mRNA abundance of *Foxi1* and *Cp2l1* were not different between Ae1 WT and mutant mice at any time point of life investigated, despite the marked changes in the protein expression pattern. However, gene expression does not necessarily correlate with protein abundance or activity. On the other hand, genes suggested to be involved in the p53 signalling cascade and probably developmental fate of renal CD cells (*Gdf15, Klf4* and *Bdkrb2*) were steadily upregulated in Ae1 KO mice after postnatal day 3 (P3).

Together with the immunofluorescent analysis of molecular IC markers, the data suggest a late onset of Ae1 related abnormal terminal differentiation of renal CD cells which might be mutually affected by systemic or renal acid-base dysregulation. However, the impact of dRTA seems to be confined to the renal CCD of adult (P84) mouse kidneys, where Pds expressing cells were reduced and Aqp2 positive PCs increased. In addition, the loss of cellular Ae1 expression seems to induce the abnormal differentiation of $Aqp2^+/Pds^+$ coexpressing cells, particularly in the renal IMCD. Similarly, a late onset of IC depletion was reported in CaII deficient mice (chapter 2.7.6, Fig. 2.15) [103].

11.6 Chronic metabolic acidosis induces adaptive remodelling of the distal renal tubule but does not affect terminal differentiation of renal CD cells

Disturbances in systemic acid-base homeostasis are known to induce adaptive responses of the kidney, including a remodelling of the renal tubule (chapter 5). Furthermore, some inherited or acquired defects of renal acid-base transport go along with renal tubular acidosis. Ae1 deficient individuals develop chronic dRTA and accordingly Pds expressing type B-IC were markedly reduced in adult (P84) Ae1 KO mice. Similarly, ICs in the renal CNT and CCD of patients with AE1 related primary dRTA appeared smaller in size and reduced in their abundance. In order to investigate the impact of chronic acid-base disturbance on the terminal differentiation of the renal CD system, immunofluorescent analysis and mRNA expression levels were performed on kidneys of mice with induced chronic metabolic acidosis for 8 weeks. As expected and consistent with the observations in P84 Ae1 deficient mice, kidneys of chronically acid loaded mice showed a reduced abundance of Pds expressing type B-ICs in the CCD, while $Aqp2^+$ cells increased. However and in contrast to P84 Ae1 KO mice, the relative abundance of $Aqp2^+$ cells decreased in the renal OMCD of acidotic animals, while unlabelled cells increased concomitantly. Likewise in contrast to Ae1 deficient kidneys, CD cells coexpressing markers of ICs and PCs respectively were not detected in NH_4Cl treated mouse kidneys. Co-immunolabelling using further molecular markers for distinct types of ICs (V-ATPase subunits and Ae1), confirmed the increase of Aqp2 expressing PCs on the expense of Pds^+ type B-ICs in the renal CCD of acidotic mice (Fig. 10.25 to 10.28). In addition, assessment of the relative protein abundance of Aqp2, Pds, Ae1 and B1 subunit of V-ATPase by western blotting revealed comparable results (Fig. 10.29 to 10.32). The relative protein abundance of Aqp2 was increased in NH_4Cl treated kidneys compared to Control, while Pds abundance was significantly reduced. Furthermore and expected, the relative abundance of Ae1 and the B1 subunit of V-ATPase was not altered upon chronic acid loading.

Finally, the renal mRNA expression pattern of acid-base transporters and transcriptional regulators was compared between NH_4Cl loaded mice and Ae1 deficient mice (Fig. 10.35, 10.36). As illustrated in the simplified table of Fig. 10.36, chronic metabolic acidosis induces a completely distinct adaptive regulation of acid-base transporters and transcriptional regulators compared to Ae1 related dRTA. Consistent with previous observations, NH_4Cl treatment induces an upregulation of *Ae1* mRNA levels with a concomitant downregulation of *Pds* mRNA. In contrast, *Pds* mRNA expression levels are not different in kidneys of Ae1 WT and KO mice. Interestingly and likewise in contrast to Ae1 KO mice, renal *Cp2l1* mRNA expression was significantly upregulated in NH_4Cl treated mice compared to Control. Moreover, *Gdf15* and *Klf4* mRNA expression was significantly upregulated in Ae1 deficient kidneys compared to Ae1 WT, while the transcription of target genes of the p53 signalling pathway were not different in Control and NH_4Cl loaded mice.

Furthermore, western blotting of Gdf15 showed significant downregulation of a probably premature variant, while the supposingly secreted and molecularly active form of Gdf15 is significantly upregulated in NH_4Cl treated mouse kidney (Fig. 10.33). In contrast, Gdf15 related variants appeared not regulated in Ae1 deficient mice. Whether the secreted active signalling peptide of Gdf15 is also represented and regulated in the blood of the mice remains speculative. Gdf15 is a multivariant molecule and involved in several distinct cellular responses. Gdf15 has been reported, together with p53 and PI3/Akt/mTOR signalling cascade, to be involved in the early proliferation of particularly type A-ICs upon induced metabolic acidosis [146]. The present study is the first one that shows the protein pattern of renal Gdf15 detected on western blot, since previous studies were based on mRNA expression. More strikingly, our study suggests for the first time a role for Gdf15 in renal adaptation during chronic acid-base disturbance. Cell proliferation events are rather unlikely in the compensated late phase of chronic acidosis. Hence, Gdf15 might rather play a role in reducing the cellular stress induced by prolonged acidity and may promote anti-apoptotic actions. Such anti-apoptotic actions might be necessary to maintain

the unusual high abundance of Aqp2 expressing PCs in the CCD of acidotic kidneys. Similarly, pro-apoptotic actions of Gdf15 could be necessary to mediate or maintain the reduced presence of Pds expressing type B-ICs in acidotic renal CCDs. However, further experiments investigating the nature of Gdf15 and the related molecular variants detected in the kidney are necessary to determine its precise role in acid-base disturbances.

Foxi1 mRNA expression levels were not altered in chronic metabolic acidosis or dRTA. Anyhow, quantification of labelled cells by immunofluorescence revealed differences in the cellular distribution of Foxi1 in Ae1 KO kidneys compared to WT. Detection of Foxi1 by western blot on kidney samples derived from NH_4Cl loaded and Control mice, demonstrated the presence of distinct Foxi1 related bands which differed markedly in size (Fig. 10.34). Even though the Foxi1 related bands did not appear to be regulated upon acid-base disturbance, their discovery is meaningful not at least because they are detected for the first time. In nuclear protein extracts, three Foxi1 related bands were detected, of which only one corresponds to the expected molecular weight. In contrast, the expected Foxi1 band was absent in cytosolic fractions of the respective kidney samples, while the two Foxi1 related bands of higher molecular weight were present. This finding may suggest, that the Foxi1 variant with the expected molecular weight is the transcriptionally active monomer and therefore present in the nuclear protein fraction but not in the cytosol. Likewise the two Foxi1 related bands of higher molecular weight might be distinct homomultimers or heteromultimers which translocate from the cytosol into the nucleus upon activation or inactivation. Again, further experiments are necessary to proof this idea and characterize the signalling network of Foxi1 in renal CD cells in detail. In addition, immunofluorescent analysis and quantification of the Foxi1 expression pattern for kidneys of Control and NH_4Cl treated mice are missing.

However, altogether the data presented in this study suggest, that prolonged metabolic acidosis induces alterations of the cellular composition of the renal CD system which favour the renal excretion of excess acid along with increased water retention, but does not alter the distinction between differentiated CD cell types.

11.7 Terminal differentiation of renal CD cells is not affected by incomplete dRTA

Inherited dRTA is characterized by the inability to acidify the urine and hence a primary renal defect. In contrast, induced metabolic acidosis in mouse models is a forced disturbance mediated by artificial oral acid loads. Therefore, the two acid-base disturbances might somehow result in different renal adaptive responses and are difficult to compare. Thus, two more distinct transgenic mouse models were examined for the impact of renal acid-base disturbance on CD cell differentiation. Mice deficient for the B1 subunit of V-ATPase, as well as mice lacking Rhcg were shown to develop dRTA when challenged with increased acid loads [114, 215]. Because these mice do not show symptoms of dRTA under basal conditions, adaptive mechanisms such as altered CD cell composition, might be activated and compensate the obvious renal defect.

Despite incomplete dRTA and in contrast to Ae1 deficiency, both mouse models did not show any signs of abnormal expression of Pds, Ae1, a4 and B1 subunits of V-ATPase when investigated by immunofluorescence (Fig. 10.37).

Likewise, Pds deficient mice were not reported to suffer from abnormal CD cell differentiation, despite their severe renal defect [213].

Therefore, our data suggest that the loss of Ae1 protein in the kidney affects the terminal differentiation of cells in the renal IMCD, inducing an abnormal of expression of Pds and moreover a coexpression of Pds and Aqp2 independently of the acid-base disturbance.

11.8 Hensin is not expressed in mouse renal tissue

Over the past two decades, the extracellular matrix protein hensin was continuously suggested to play a crucial role in the terminal differentiation of renal CD cells and recently a hensin deficient mouse model was reported to develop dRTA [99, 100]. Accordingly, we set out to investigate a possible dysregulation of hensin in Ae1 deficient mouse kidney. However, in the present study we failed to detect mRNA expression of *hensin* in premature and mature kidneys of mice (Fig. 10.21).

Hensin was originally discovered *in vitro*, in immortalized cells derived from IMCDs of rabbit kidney. Furthermore, *in vitro* experiments using this cell model suggested a role for hensin in the transdifferentiation of type B-ICs to type A-ICs and *vice versa*. In this experimental protocol, a mixed population of rabbit IMCD cells was cultured with different initial density, which seemed to affect and alter the identity of cells (A-IC or B-IC). Hensin was discovered and reported to mediate the molecular switch that determines the differentiation of cells and thus their identity as type A-ICs or B-ICs. However, in a similar cell line derived from renal mouse IMCDs neither *hensin* mRNA was detected nor mRNA of *Ae1*, *Pds* and *V-ATPase* (data not shown), suggesting that the cell population did not contain any cells resembling the phenotype of type A-ICs or type B-ICs. Anyhow, we repeated the experimental protocol as denoted in the original publications, but were still unable to detect any mRNA for molecular IC markers and *hensin* in mouse IMCD3 cells (data not shown). The repetitive negative result is consistent with the known technical limitation of cultured renal CD derived cells, which immediately lose the phenotypic characteristics of ICs and dedifferentiate *in vitro*. However, species differences might explain the opposing results from *in vitro* studies, since the renal CD system of rabbits is slightly different compared to that of mouse, rat or human.

Notably and in spite of the reported phenotype of the renal CD specific hensin KO mouse and its supposingly crucial role in renal IC differentiation, hensin expression has never been shown in renal tissue of mice. In addition, the data presenting the phenotype of the hensin KO mice are not convincing and raise reasonable doubts on the existence and impact of hensin, at least in mouse kidney.

11.8 Ae1 expression is required to maintain terminal differentiation of renal CD cells

The origin of individual cell types of the renal collecting ducts is not yet entirely proven. But some studies suggest that principal cells and types of intercalated cells origin from the same precursor population, simultaneously in the renal CNT and the inner medullary region [18, 25, 27]. In addition, the transcriptional network and other regulatory signalling molecules involved in terminal differentiation of the renal CDs are only poorly understood. Although some molecules were identified in distinct model organisms, the interaction of the distinct signalling pathways and their cellular localization in mouse kidney is still unknown. Therefore, it is very difficult to get a clear picture of the necessary events and key molecules of renal terminal differentiation and to put all the different information together in the right context. Especially, since it needs to account for the complexity of the cellular events in distinct renal cell populations, the putative interaction of different cell types and signalling networks, and the different systemic and cellular functional demands the maturing kidney is requested to fulfil.

However, the present study provides some new findings regarding a novel and unusual role of Ae1 in the terminal differentiation of renal CD cells, which is most likely beyond Cl^-/HCO_3^- exchange. Ae1 expression in the murine kidney might be a key molecule that triggers the maintenance of terminal differentiation of CD cells. Our findings offer interesting possibilities to fill some of the open gaps of our knowledge and to put important pieces of the puzzle into place. Moreover, we show for the first time the cellular localization of the transcription factors Foxi1 and Cp2l1 in the murine kidney. Furthermore, we provide data indicating a local dysregulation of Foxi1 and Cp2l1 upon renal Ae1 deficiency.

Based on the work by other research groups the following hypothetical model is suggested, summarizing the possible role of some key regulatory molecules in the terminal differentiation of renal CD cells (Fig. 11.1). The cell cycle and transcriptional regulator p53 is expressed in the differentiating zone of the late embryonic kidney and was suggested to influence cell lineage differentiation (chapter 2.7.1, Fig. 2.9). p53 was found to interact with other transcriptional regulators, like Klf4 and Bdkrb2 and to regulate the transcription of renal function genes, such as Aqp2 and Na^+/K^+-ATPase [65]. Recently, the Notch signalling pathway was elegantly shown to determine the cell lineage of renal PC and ICs in the mouse [77]. It is not directly proven for the kidney, but in other tissues p53 family members can modulate the activity of Notch, suggesting a crosstalk of both pathways during terminal CD differentiation [74]. Constitutive activation of the Notch signalling cascade drives the expression of PCs in the absence of ICs. Whether another key regulator is intermediately necessary is not known. On the other hand, constitutive inactivation of Notch leads to the loss of PCs and favours the expression of molecular IC markers, such as V-ATPase, Ae1 and Pds. Furthermore, *Foxi1* mRNA expression levels were significantly increased, suggesting a regulatory interaction of the Notch signalling cascade with Foxi1. Accordingly, Foxi1 mediates the transcriptional activation of molecular IC markers. These observations were also made in epidermal ionocyte

differentiation of *Xenopus laevis* and zebrafish larvae suggesting a well conserved signalling pathway (Fig. 2.7, 2.8) [51, 54].

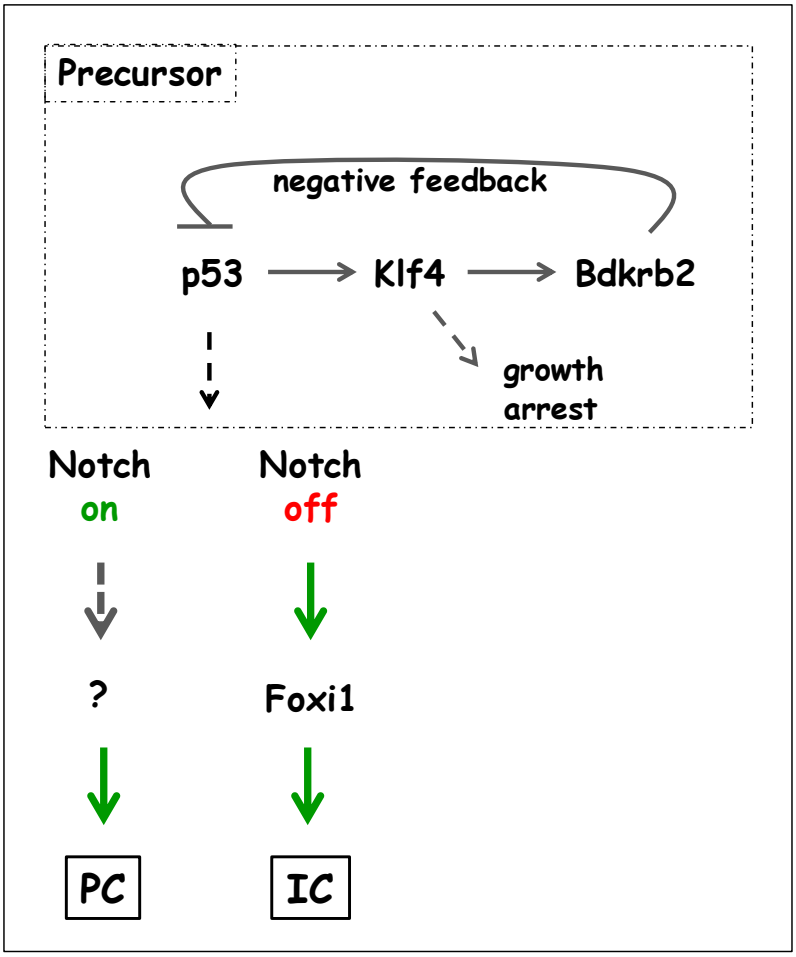

Fig. 11.1 Proposed model of CD cell lineage decision in mouse kidney. Principal cells (PCs) and intercalated cells (ICs) may develop from a common renal precursor. As suggested by El-Dahr, S. and colleagues [66], the cell cycle and transcriptional regulator p53 initiates developmental cell differentiation and requires the interaction with Klf4 and Bdkrb2 (Fig. 2.9). Furthermore, p53 may regulate the Notch signalling pathway promoting cell lineage decisions. The activity of Notch determines the later CD cell type. Constitutive activation of Notch favours the differentiation of PCs in the absence of ICs, while inactivated Notch leads to the differentiation of ICs in the absence of PCs [77]. Whether another transcriptional regulator is involved in the differentiation of PCs is not yet known. However, Foxi1 is essentially involved in the terminal differentiation of the IC phenotype [83].

In the murine kidney, loss of the transcription factors Foxi1 and Cp2l1 goes along with the loss of *Ae1*, *Pds* and *V-ATPase* [83, 90]. Moreover, Foxi1 was directly shown to be a transcriptional regulator of *V-ATPase*, *Pds* and *Ae1* [85, 86]. However, whether Foxi1 and Cp2l1 are only expressed in the developing kidney or also during adulthood had not been known and shown in the present study. Moreover, the CD cell type expressing Foxi1 and Cp2l1 was uncertain and has been analyzed to some extent in this work. The present study shows for the first time, that Foxi1 and Cp2l1 are expressed in distinct CD cell populations of the mature mouse kidney. As suggested previously, Foxi1 expression was mainly found in V-ATPase expressing ICs along the renal CD system. This is consistent with its role as a transcriptional regulator of specific IC transporters. However, we found that Cp2l1 expression colocalized mostly with Aqp2 expressing principal cells. This is surprising, since Cp2l1 deficiency also correlates with the loss of molecular IC markers, rather suggesting its expression in the same locus than its target genes. However, Cp2l1 is an unusual member of the grainyhead family, because it acts as a transcriptional repressor. Interestingly, observations in the epidermis of amphibians suggest an interaction of Notch, Foxi1 and Cp2l1 (Fig. 2.7, 2.8). Hence, Cp2l1 in the mouse kidney might be the proposed intermediate regulator in the cell lineage differentiation of PCs, similar to Foxi1 in the IC lineage (Fig. 11.1). Accordingly, Cp2l1 might modulate the activity of Notch in adjacent cells, which results in the activation of Foxi1 and thus differentiation of IC phenotype. The expression pattern of both transcription factors, Foxi1 and Cp2l1, was altered in Ae1 deficient mature kidneys as already discussed. These observations suggest that Foxi1, Cp2l1 and Ae1 somehow interact together in renal CD cells, particularly in the inner medulla. A negative regulation by some unknown molecule or a negative autoregulation of Cp2l1 might be necessary in murine kidney, similarly to observations made in zebrafish epidermal development (Fig. 2.8). Accordingly, the loss of nucleic Cp2l1 in some cells of Ae1 deficient renal IMCDs might prohibit a repression of Aqp2 or might prevent a negative regulation of Foxi1 which promotes the expression of Pds in these cells. Consequently, Foxi1 positive cells were more abundant in Ae1 deficient renal IMCDs (Fig. 10.13D, 10.16D)

leading to the unusual coexpression of Aqp2 and Pds. However, a definite proof is pending and further investigations are necessary.

With respect to our investigations of incomplete dRTA mouse models, the induced chronic metabolic acidosis model and the fact that Pds KO mice do not have abnormally differentiated CD cells, we can conclude that the presence of Ae1 protein is required in the terminal cell differentiation. Respectively, reports by others and our immunofluorescence data from patients with dRTA related AE1 mutations suggest that the proper expression and subcellular localization of the protein is primarily required and not its anion exchanger activity. Moreover, the very preliminary human data suggest that the findings from the mouse model may be transferable to the human situation.

Ae1 is known to form multi-protein complexes in the erythrocyte, which is essential for the cytoskeletal integrity and transport function (chapter 6.1.2) [186]. Similarly, the kidney specific variant of Ae1 is suggested to interact directly or indirectly with distinct proteins, such as ILK (integrin-linked kinase) and Glyceraldehyde 3-phosphate dehydrogenase (GAPDH) [228-230]. Moreover, Ae1 was shown to form a transport metabolon together with CaII in erythrocytes and the kidney enhancing the transport activity [197]. Likewise, the Ae1-CaII transport metabolon might generate a local cellular pH microenvironment that influences the activity of vicinal regulatory proteins thereby triggering signalling pathways [231].

Deficiency of CaII results in the depletion of ICs from the renal CD system with a late onset in the mature mouse kidney (chapter 2.7.6) [101, 103]. Consistently, pharmacologic inhibition of CaII with acetazolamide reduces the abundance of ICs and alters their morphology [104]. Interestingly, the CD system of Foxi1 deficient mice did not only lack ICs, but consisted of a single cell type which coexpressed Aqp2 and CaII (Fig. 2.11) [83]. Indeed we also report here that CaII expression appears normal in Aqp2 expressing cells of the CNT and early CCD of mouse and human kidney (data not shown). But we did not find CaII and Aqp2 coexpressing cells in the OMCD and

IMCD. However, the observation in Foxi1 KO mice implicates that the restrictive expression of CaII to ICs of the MCD segments is somehow influenced by Foxi1, even though CAII is not a direct transcriptional target of Foxi1. Hence, Foxi1 might interact with another regulatory molecule or a signalling pathway to mediate a cross talk between subpopulations of CD cells and indirectly suppress the expression of CaII in $Aqp2^{+}$ principal cells.

Fox factors were reported to unusually interact with proteins other than transcription factors [232]. Hence, Foxi1 might unusually interact with a multi-protein complex of Ae1 or with Ae1 directly. This speculated interaction could be necessary to maintain or conduct terminal cell differentiation of renal ICs, at least in the mature kidney. A proposed model integrating this speculation and a possible role of the transcriptional repressor Cp2l1 in renal CD differentiation is depicted in Fig. 11.2. In the developing mouse kidney the expression of Pds is observed much later than that of V-ATPase and Ae1 (Fig. 2.5). Hence, type B-ICs develop after type A-ICs. Neither an interconversion of IC phenotypes is proven, nor the question for a common precursor of ICs. However, the presence of a certain type of IC might influence the identity of a neighbouring cell, maybe by paracrine signalling pathways, such as Notch mediated lateral inhibition. This could explain why type B-ICs appear after type A-ICs and our observations of abnormally differentiated CD cells in the absence of renal Ae1. A regulatory feedback of Foxi1 with Ae1 or a multi-protein complex of Ae1 might be required to initiate Pds expression in adjacent cells. The reciprocal signal of a possible Foxi1-Ae1 interaction could induce another unknown factor or again Foxi1, which modulates the expression of Pds in neighbouring cells. A multi-protein Ae1 complex or Ae1 itself might also directly repress the expression of Ae1 in adjacent cells by another unknown signalling cascade, thus providing an autoregulatory mechanism that simultaneously maintains the identity of the effector cell. Similarly, a putative crosstalk of Foxi1 and Cp2l1 might be necessary to repress the expression of CaII in principal cells of the renal MCD, while CaII is strongly expressed in adjacent ICs.

Consistently, the frequency of Cp2l1 expressing cells seemed to increase from the renal cortex towards the inner medulla.

However, with respect to the different signalling cascades that appear to be involved in CD differentiation, the sequential activation of autocrine and paracrine actions seems inevitable. Moreover, this would allow a controlled, rapid and locally organized response to functional demands of the mature kidney.

Embryonic terminal differentiation of the CD cells might nevertheless require additional or different signalling pathways. During embryonic kidney development two populations of precursor cells seem to exist in the CNT and inner medulla, which give rise to types of ICs and PCs. However, the renal CNT origins from the nephrogenic mesenchyme, while the CDs derive from the ureteric bud epithelium. Hence, it is not surprising, that the unusual differentiation of Pds and Aqp2 coexpressing cells was confined to the renal inner medulla. It might well be, that other transcriptional networks and regulators are present in the CNT compared to the renal inner medulla as they derive from different primordia. On the other hand, the urinary composition is constantly modified along the CD system and the compostion is different in the CNT and IMCD. Similarly, the interstitial pH is more acidic and the oxygen supply is lower in the inner medulla compared to the renal CNT. Hence, the different functional demands and external stimuli in the renal CNT and inner medulla might influence the interaction of signalling networks and the behaviour of individual molecules.

However, much more work needs to be done to investigate all the different aspects mentioned and to answer all the open questions left.

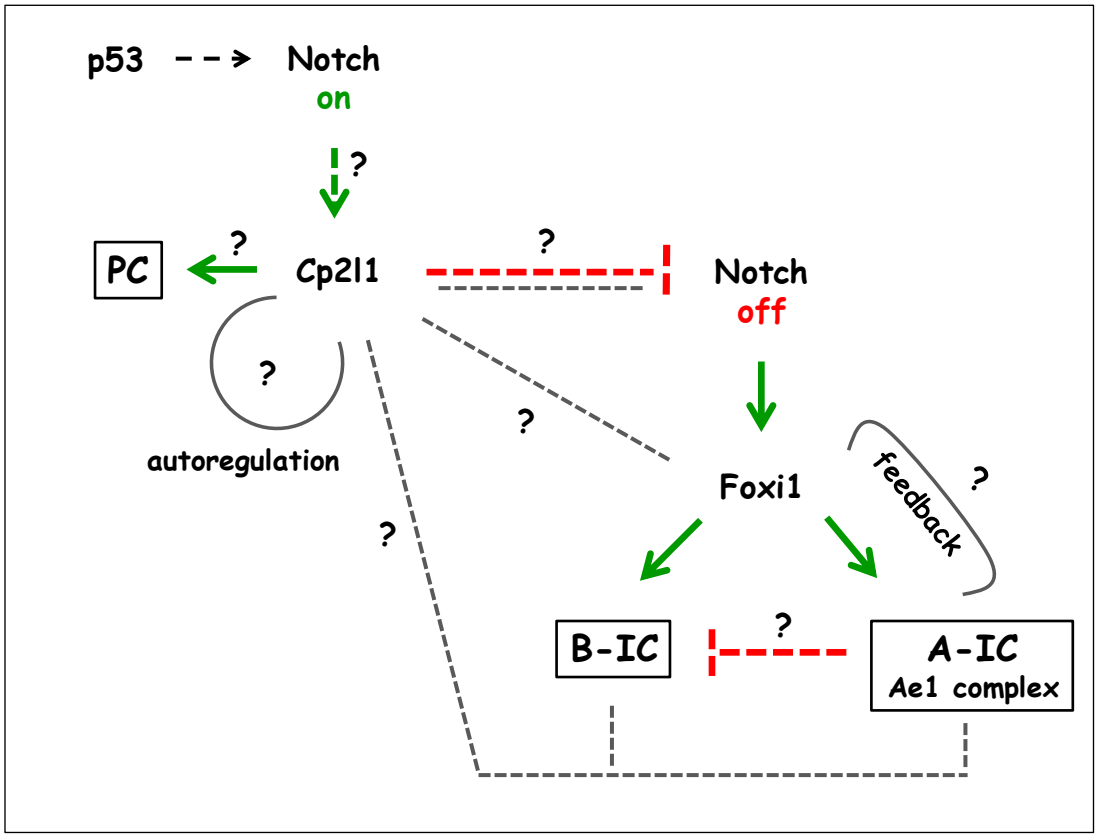

Fig. 11.2 Proposed model of renal CD differentiation in mouse. Notch activity might be modulated by p53 in precursor or terminally differentiated cells. Activated Notch interacts with Cp2l1 and promotes the differentiation of PCs. The transcriptional repressor Cp2l1 inactivates Notch signalling in adjacent cells. Repression of Notch leads to activation of Foxi1, which promotes the differentiation of ICs. Interaction of Foxi1 or another transcriptional regulator with Ae1 or an Ae1 related multi-protein complex induces a feedback loop that drives the differentiation of type B-ICs and maintains the type A-IC phenotype. Cp2l1 might be negatively autoregulated or interacts reciprocally with inactivated Notch, Foxi1, or signalling molecules of differentiated CD cells.

12. FUTURE PERSPECTIVES

The present study provides some new and interesting data that suggest a potential role of Ae1 or an Ae1 based multi-protein complex in the terminal differentiation of renal CD cells apart from Cl^-/HCO_3^- exchange. However, further investigations are necessary to establish the speculated role of Ae1 and to characterize the nature of a potential Ae1 related multi-protein complex. In addition, the localization and regulatory role of the transcription factors Foxi1 and Cp2l1 in mouse renal ICs, integrative to data from invertebrate model organisms, raise some new aspects that need further investigation. Respectively, the following experimental approaches are suggestive for future studies:

- Since little is known about potential regulatory pathways and signalling molecules involved in terminal CD cell differentiation, RNA microarray analysis of mature kidneys from Ae1 WT and KO animals could be useful to identify more candidate genes and to further investigate the different signalling pathways (p53, Notch, PI3/Akt/mTOR). Consistently, the mRNA expression of the transcription factors *Gdf15*, *Klf4* and *Bdkrb2*, probably involved in p53 regulated signalling pathway, were already shown to be upregulated in Ae1 deficient mature kidneys.
- Likewise, the protein expression levels, posttranslational modifications, as well as the cellular localization of p53, Gdf15, Klf4 and Bdkrb2 within the kidney of Ae1 WT and KO animals are important to further investigate their role in terminal IC differentiation.
- In the present study, Gdf15 protein abundance was altered in chronic acid loaded mouse kidneys. However, the cellular localization of Gdf15 in the kidney as well as the relevance of the different Gdf15 forms (propeptide, mature and secreted peptide) are not yet known and need to be characterized.

- Good evidence from transgenic mice suggests the Notch signalling pathway critical for CD cell differentiation. Hence, the signalling cascade should be analyzed in Ae1 deficient kidneys with respect to our proposed model (Fig. 11.2). In addition, investigation of Ae1, Foxi1 and Cp2l1 in transgenic Notch mouse models (i.e. Notch deficiency, constitutive activated Notch) would be helpful to further establish their function and proposed interaction in renal IC differentiation.
- A number of Ae1 interacting proteins, critical for cytoskleletal integrity and trafficking events, were already identified in erythrocytes. However, the situation is less clear for the kidney specific Ae1 isoform, since the majority of identified interacting erythroidal proteins do not exist in both tissues simultaneously. Moreover, the kAe1 isoform lacks a portion of the interactive N-terminal domain. Therefore and to proof the hypothesis of an Ae1 based multi-protein complex involved in terminal IC differentiation, a profound analysis of potential interactive partners would be helpful. Technically, several experimental approaches might be applicable such as yeast-two hybrid screening, co-immunoprecipitations or pull down assays with subsequent mass spectrometry analysis.
- Identification of upstream triggers for signalling cascades involved in remodelling of the collecting duct in response to altered electrolyte or acid-base status

- Unfortunately, cultured cells of the renal CD system tend to lose specific protein expression like Ae1, Pds, V-ATPase and dedifferentiate immediately when cultured *in vitro*. Interestingly, the present study revealed the endogenous expression of Foxi1 in untransfected Hek293T cells (Fig. 10.34C). In addition, Bounoure L, Bourgeois S, and Wagner CA noted the presence of the *B1* subunit of *V-ATPase* in these cells (unpublished observation). Therefore, Hek293T cells might be a useful model to study the suggested interaction of Ae1 with putative signalling pathways of terminal cell differentiation. In addition, they could be useful to study a possible interaction of the distinct signalling pathways, i.e. by applying pharmacologic inhibitors of the Notch signalling cascade or siRNA mediated gene silencing. Moreover, two MDCK subtypes were reported with features resembling renal PCs and ICs, respectively [233]. A detailed analysis should investigate their suitability as a model for terminal CD cell differentiation, as well. Alternatively, transfection of cells with transcription factors of interest could provide important information about possible inductive signals (i.e. acid-base, electrolyte composition), posttranslational modifications and activity, interactions with other molecules, their subcellular localization and targeting, as well as suggested interactions with other signalling cascades. Last but not least, the terminal differentiation of renal CD cells might be studied by in *in vitro* cultures of mouse embryonic stem cells or metanephric mesenchyme and ureteric bud derived progenitor cells [234, 235].

- The present study provides novel data on Foxi1 and Cp2l1 expression in the mature mouse kidney. Anyhow, these data are preliminary and detailed colocalization studies are necessary to further analyze the expressing cell populations with respect to the distinct CD segments. Furthermore, the cellular distribution and abundance of Foxi1 and Cp2l1 in Ae1 deficient kidneys and acid loaded kidneys needs to be determined. Moreover, immunoblot of Foxi1 on kidney nuclear protein extracts and cytosolic protein fractions suggest multimeric presence of Foxi1 in the distinct cellular compartments. Analysis of the nature and regulatory relevance of these potential Foxi1 manifestations would be necessary to understand the function of Foxi1 in terminal cell differentiation. In addition, a potential interaction of Foxi1 and Cp2l1 needs to be examined and characterized. Consistently, expression of Foxi1 in Cp2l1 deficient kidneys and Cp2l1 expression in Foxi1 deficient kidneys would be useful. Furthermore, the Notch signalling cascade should be analyzed in Foxi1 and Cp2l1 deficient animals.
- In order to definitely exclude dRTA related effects on terminal renal IC differentiation mice deficient for either the B1 subunit of V-ATPase or Rhcg were analyzed in the present study. However, the analysis was performed under standard laboratory conditions where these animals display an incomplete form of dRTA. Therefore, a repetitive investigation of kidneys from transgenic animals receiving a chronic oral acid load *a priori* would give more substantiated results.

REFERENCES

1. Boron, W.F. and E.L. Boulpaep, *Medical physiology a cellular and molecular approaoch*. Updated ed. 2005, Philadelphia, Pa.: Elsevier Saunders. 1319 S.

2. Davidson, A.J., *Mouse kidney development.* 2008.

3. Horster, M., et al., *Epithelial nephrogenesis.* Pflügers Archiv European Journal of Physiology, 1997. **434**(6): p. 647-660.

4. Horster, M.F., G.S. Braun, and S.M. Huber, *Embryonic Renal Epithelia: Induction, Nephrogenesis, and Cell Differentiation.* Physiol Rev, 1999. **79**(4): p. 1157-1191.

5. Davies, J.A., *Morphogenesis of the Metanephric Kidney.* TheScientificWorldJOURNAL, 2002. **2**: p. 1937-1950.

6. Kuure, S., R. Vuolteenaho, and S. Vainio, *Kidney morphogenesis: cellular and molecular regulation.* Mech Dev, 2000. **92**(1): p. 31-45.

7. Dressler, G.R., *The Cellular Basis of Kidney Development.* Annual Review of Cell and Developmental Biology, 2006. **22**(1): p. 509-529.

8. Bridgewater, D. and N.D. Rosenblum, *Stimulatory and inhibitory signaling molecules that regulate renal branching morphogenesis.* Pediatr Nephrol, 2009. **24**(9): p. 1611-9.

9. Davies, J.A., *The Kidney Development Database*. 2012, http://golgi.ana.ed.ac.uk/kidhome.html

10. Rosenblum, N.D., *Developmental biology of the human kidney.* Semin Fetal Neonatal Med, 2008. **13**(3): p. 125-32.

11. Meyer, T.N., et al., *Spatiotemporal regulation of morphogenetic molecules during in vitro branching of the isolated ureteric bud: toward a model of branching through budding in the developing kidney.* Developmental Biology, 2004. **275**(1): p. 44-67.

12. Piscione, T.D. and N.D. Rosenblum, *The molecular control of renal branching morphogenesis: current knowledge and emerging insights.* Differentiation, 2002. **70**(6): p. 227-246.

13. Bates, C.M., *Transcriptional control of renal collecting duct development.* American Journal of Physiology - Renal Physiology, 2005. **288**(5): p. F897-F898.

14. McMahon, A.P., et al., *GUDMAP: The Genitourinary Developmental Molecular Anatomy Project.* Journal of the American Society of Nephrology, 2008. **19**(4): p. 667-671.

15. Kloth, S., et al., *Histochemical markers reveal an unexpected heterogeneous composition of the renal embryonic collecting duct epithelium.* Kidney Int, 1993. **44**(3): p. 527-36.

16. Zhu, L. and A.I. Skoultchi, *Coordinating cell proliferation and differentiation.* Current opinion in genetics & development, 2001. **11**(1): p. 91-7.

17. Seldin, D.W. and G. Giebisch, *The Kidney Physiology and Pathophysiology*. 2000, Lippincott Williams & Wilkins. p. 587-654.

18. Kim, J., C.C. Tisher, and K.M. Madsen, *Differentiation of intercalated cells in developing rat kidney: an immunohistochemical study.* Am J Physiol, 1994. **266**(6 Pt 2): p. F977-90.

19. Capasso, G., *A crucial nephron segment in acid-base and electrolyte transport: the connecting tubule.* Kidney Int, 2006. **70**(10): p. 1674-6.

20. Brown, D., J. Roth, and L. Orci, *Lectin-gold cytochemistry reveals intercalated cell heterogeneity along rat kidney collecting ducts.* Am J Physiol, 1985. **248**(3 Pt 1): p. C348-56.

21. Biner, H.L., et al., *Human cortical distal nephron: distribution of electrolyte and water transport pathways.* J Am Soc Nephrol, 2002. **13**(4): p. 836-47.

22. Bastani, B., *Immunocytochemical localization of the vacuolar H(+)-ATPase pump in the kidney.* Histol Histopathol, 1997. **12**(3): p. 769-79.

23. Emmons, C. and I. Kurtz, *Functional characterization of three intercalated cell subtypes in the rabbit outer cortical collecting duct.* J Clin Invest, 1994. **93**(1): p. 417-23.

24. Emmons, C. and I. Kurtz, *H+/base transport pathways in the cortical collecting duct.* Exp Nephrol, 1993. **1**(6): p. 325-33.

25. Song, H.-K., et al., *Origin and Fate of Pendrin-Positive Intercalated Cells in Developing Mouse Kidney.* Journal of the American Society of Nephrology, 2007. **18**(10): p. 2672-2682.

26. Evan, A.P., et al., *Postnatal maturation of rabbit renal collecting duct. II. Morphological observations.* Am J Physiol, 1991. **261**(1 Pt 2): p. F91-107.

27. Hiatt, M.J., et al., *Remodeling of the fetal collecting duct epithelium.* Am J Pathol, 2010. **176**(2): p. 630-7.

28. Narbaitz, R., D. Vandorpe, and D.Z. Levine, *Differentiation of renal intercalated cells in fetal and postnatal rats.* Anat Embryol (Berl), 1991. **183**(4): p. 353-61.

29. Jouret, F., et al., *Ubiquitous and kidney-specific subunits of vacuolar H+-ATPase are differentially expressed during nephrogenesis.* J Am Soc Nephrol, 2005. **16**(11): p. 3235-46.

30. Holthofer, H., *Ontogeny of cell type-specific enzyme reactivities in kidney collecting ducts.* Pediatr Res, 1987. **22**(5): p. 504-8.

31. Bonnici, B. and C. Wagner, *Postnatal expression of transport proteins involved in acid–base transport in mouse kidney.* Pflügers Archiv European Journal of Physiology, 2004. **448**(1): p. 16-28.

32. Kim, J., et al., *Role of apoptotic and nonapoptotic cell death in removal of intercalated cells from developing rat kidney.* Am J Physiol, 1996. **270**(4 Pt 2): p. F575-92.

33. Wagner, C.A., et al., *The anion exchanger pendrin (SLC26A4) and renal acid-base homeostasis.* Cell Physiol Biochem, 2011. **28**(3): p. 497-504.

34. Nielsen, S., et al., *Physiology and Pathophysiology of Renal Aquaporins.* Journal of the American Society of Nephrology, 1999. **10**(3): p. 647-663.

35. Nielsen, S., et al., *Aquaporins in the kidney: from molecules to medicine.* Physiol Rev, 2002. **82**(1): p. 205-44.

36. Madsen, K.M. and C.C. Tisher, *Structural-functional relationship along the distal nephron.* Am J Physiol, 1986. **250**(6 Pt 3): p. F1-15.

37. Verlander, J.W., K.M. Madsen, and C.C. Tisher, *Structural and functional features of proton and bicarbonate transport in the rat collecting duct.* Semin Nephrol, 1991. **11**(4): p. 465-77.

38. Schuster, V.L., *Organization of collecting duct intercalated cells.* Kidney Int, 1990. **38**(4): p. 668-672.

39. Clapp, W.L., et al., *Intercalated cells of the rat inner medullary collecting duct.* Kidney Int, 1987. **31**(5): p. 1080-7.

40. Schuster, V.L., *Function and regulation of collecting duct intercalated cells.* Annu Rev Physiol, 1993. **55**: p. 267-88.

41. Matsumoto, T., G. Fejes-Toth, and G.J. Schwartz, *Postnatal differentiation of rabbit collecting duct intercalated cells.* Pediatr Res, 1996. **39**(1): p. 1-12.

42. Teng-umnuay, P., et al., *Identification of distinct subpopulations of intercalated cells in the mouse collecting duct.* J Am Soc Nephrol, 1996. **7**(2): p. 260-74.

43. Wagner, S., et al., *Immunochemical characterization of a band 3-like anion exchanger in collecting duct of human kidney.* Am J Physiol, 1987. **253**(2 Pt 2): p. F213-21.

44. Brown, D., S. Hirsch, and S. Gluck, *Localization of a proton-pumping ATPase in rat kidney.* J Clin Invest, 1988. **82**(6): p. 2114-26.

45. Drenckhahn, D. and C. Merte, *Restriction of the human kidney band 3-like anion exchanger to specialized subdomains of the basolateral plasma membrane of intercalated cells.* Eur J Cell Biol, 1987. **45**(1): p. 107-15.

46. Wall, S.M., et al., *Localization of pendrin in mouse kidney.* Am J Physiol Renal Physiol, 2003. **284**(1): p. F229-41.

47. Kim, Y.-H., et al., *Immunocytochemical localization of pendrin in intercalated cell subtypes in rat and mouse kidney.* American Journal of Physiology - Renal Physiology, 2002. **283**(4): p. F744-F754.

48. Wall, S.M., *Recent advances in our understanding of intercalated cells.* Curr Opin Nephrol Hypertens, 2005. **14**(5): p. 480-4.

49. Pozzi, A. and R. Zent, *Integrins, extracellular matrix, and terminal differentiation of renal epithelial cells.* Journal of the American Society of Nephrology : JASN, 2008. **19**(6): p. 1043-4.

50. Drummond, I.A. and A.J. Davidson, *Zebrafish kidney development.* Methods in cell biology, 2010. **100**: p. 233-60.

51. Quigley, I.K., J.L. Stubbs, and C. Kintner, *Specification of ion transport cells in the Xenopus larval skin.* Development, 2011. **138**(4): p. 705-714.

52. Chang, W.J. and P.P. Hwang, *Development of zebrafish epidermis.* Birth defects research. Part C, Embryo today : reviews, 2011. **93**(3): p. 205-14.

53. Dubaissi, E. and N. Papalopulu, *Embryonic frog epidermis: a model for the study of cell-cell interactions in the development of mucociliary disease.* Disease Models & Mechanisms, 2011. **4**(2): p. 179-192.

54. Janicke, M., T.J. Carney, and M. Hammerschmidt, *Foxi3 transcription factors and Notch signaling control the formation of skin ionocytes from epidermal precursors of the zebrafish embryo.* Dev Biol, 2007. **307**(2): p. 258-71.

55. Hsiao, C.D., et al., *A positive regulatory loop between foxi3a and foxi3b is essential for specification and differentiation of zebrafish epidermal ionocytes.* PLoS ONE, 2007. **2**(3): p. e302.

56. Esaki, M., et al., *Mechanism of development of ionocytes rich in vacuolar-type H(+)-ATPase in the skin of zebrafish larvae.* Developmental Biology, 2009. **329**(1): p. 116-29.

57. Janicke, M., B. Renisch, and M. Hammerschmidt, *Zebrafish grainyhead-like1 is a common marker of different non-keratinocyte epidermal cell lineages, which segregate from each other in a Foxi3-dependent manner.* Int J Dev Biol, 2010. **54**(5): p. 837-50.

58. Almog, N. and V. Rotter, *Involvement of p53 in cell differentiation and development.* Biochimica et Biophysica Acta (BBA) - Reviews on Cancer, 1997. **1333**(1): p. F1-F27.

59. Vousden, K.H., *p53: death star.* Cell, 2000. **103**(5): p. 691-4.

60. Schmid, P., et al., *Expression of p53 during mouse embryogenesis.* Development, 1991. **113**(3): p. 857-65.

61. Saifudeen, Z., S. Dipp, and S.S. El-Dahr, *A role for p53 in terminal epithelial cell differentiation.* J Clin Invest, 2002. **109**(8): p. 1021-30.

62. Hilliard, S., et al., *Tight regulation of p53 activity by Mdm2 is required for ureteric bud growth and branching.* Developmental Biology, 2011. **353**(2): p. 354-66.

63. Aboudehen, K., et al., *Mechanisms of p53 Activation and Physiological Relevance in the Developing Kidney.* American journal of physiology. Renal physiology, 2012.

64. Saifudeen, Z., et al., *The bradykinin type 2 receptor is a target for p53-mediated transcriptional activation.* J Biol Chem, 2000. **275**(20): p. 15557-62.

65. Saifudeen, Z., et al., *Combinatorial control of the bradykinin B2 receptor promoter by p53, CREB, KLF-4, and CBP: implications for terminal nephron differentiation.* American journal of physiology. Renal physiology, 2005. **288**(5): p. F899-909.

66. El-Dahr, S.S., K. Aboudehen, and Z. Saifudeen, *Transcriptional control of terminal nephron differentiation.* Am J Physiol Renal Physiol, 2008. **294**(6): p. F1273-8.

67. Semaan, S.J., Y. Li, and R.W. Nickells, *A single nucleotide polymorphism in the Bax gene promoter affects transcription and influences retinal ganglion cell death.* ASN neuro, 2010. **2**(2): p. e00032.

68. El-Dahr, S.S., *Ontogeny of the intrarenal kallikrein-kinin system: proposed role in renal development.* Microscopy research and technique, 1997. **39**(3): p. 222-32.

69. El-Dahr, S.S., et al., *Ontogeny of bradykinin B2 receptors in the rat kidney: implications for segmental nephron maturation.* Kidney Int, 1997. **51**(3): p. 739-49.

70. El-Dahr, S.S., et al., *Bradykinin B2 null mice are prone to renal dysplasia: gene-environment interactions in kidney development.* Physiol Genomics, 2000. **3**(3): p. 121-31.

71. Fan, H., J. Stefkova, and S.S. El-Dahr, *Susceptibility to metanephric apoptosis in bradykinin B2 receptor null mice via the p53-Bax pathway.* American journal of physiology. Renal physiology, 2006. **291**(3): p. F670-82.

72. El-Dahr, S.S., K. Aboudehen, and S. Dipp, *Bradykinin B2 receptor null mice harboring a Ser23-to-Ala substitution in the p53 gene are protected from renal dysgenesis.* American Journal of Physiology - Renal Physiology, 2008. **295**(5): p. F1404-F1413.

73. Saifudeen, Z., et al., *Spatiotemporal Switch from ΔNp73 to TAp73 Isoforms during Nephrogenesis.* Journal of Biological Chemistry, 2005. **280**(24): p. 23094-23102.

74. Sasaki, Y., et al., *The p53 family member genes are involved in the Notch signal pathway.* J Biol Chem, 2002. **277**(1): p. 719-24.

75. Bray, S.J., *Notch signalling: a simple pathway becomes complex.* Nat Rev Mol Cell Biol, 2006. **7**(9): p. 678-689.

76. Sirin, Y. and K. Susztak, *Notch in the kidney: development and disease*. The Journal of pathology, 2012. **226**(2): p. 394-403.

77. Jeong, H.W., et al., *Inactivation of Notch signaling in the renal collecting duct causes nephrogenic diabetes insipidus in mice.* J Clin Invest, 2009. **119**(11): p. 3290-300.

78. Koo, B.K., et al., *An obligatory role of mind bomb-1 in notch signaling of mammalian development.* PLoS ONE, 2007. **2**(11): p. e1221.

79. Ma, M. and Y.-J. Jiang, *Jagged2a-Notch Signaling Mediates Cell Fate Choice in the Zebrafish Pronephric Duct.* PLoS Genet, 2007. **3**(1): p. e18.

80. Jackson, B.C., et al., *Update of human and mouse forkhead box (FOX) gene families.* Hum Genomics, 2010. **4**(5): p. 345-52.

81. Hannenhalli, S. and K.H. Kaestner, *The evolution of Fox genes and their role in development and disease*. Nat Rev Genet, 2009. **10**(4): p. 233-240.

82. Overdier, D.G., et al., *The winged helix transcriptional activator HFH-3 is expressed in the distal tubules of embryonic and adult mouse kidney.* J Biol Chem, 1997. **272**(21): p. 13725-30.

83. Blomqvist, S.R., et al., *Distal renal tubular acidosis in mice that lack the forkhead transcription factor Foxi1.* J Clin Invest, 2004. **113**(11): p. 1560-70.

84. Hulander, M., et al., *The winged helix transcription factor Fkh10 is required for normal development of the inner ear.* Nat Genet, 1998. **20**(4): p. 374-6.

85. Vidarsson, H., et al., *The forkhead transcription factor Foxi1 is a master regulator of vacuolar H-ATPase proton pump subunits in the inner ear, kidney and epididymis.* PLoS ONE, 2009. **4**(2): p. e4471.

86. Blomqvist, S.R., et al., *Epididymal expression of the forkhead transcription factor Foxi1 is required for male fertility.* Embo J, 2006. **25**(17): p. 4131-4141.

87. Kurth, I., et al., *The forkhead transcription factor Foxi1 directly activates the AE4 promoter.* Biochem J, 2006. **393**(Pt 1): p. 277-83.

88. Veljkovic, J. and U. Hansen, *Lineage-specific and ubiquitous biological roles of the mammalian transcription factor LSF.* Gene, 2004. **343**(1): p. 23-40.

89. Rodda, S., et al., *CRTR-1, a developmentally regulated transcriptional repressor related to the CP2 family of transcription factors.* J Biol Chem, 2001. **276**(5): p. 3324-32.

90. Yamaguchi, Y., S. Yonemura, and S. Takada, *Grainyhead-related transcription factor is required for duct maturation in the salivary gland and the kidney of the mouse.* Development, 2006. **133**(23): p. 4737-48.

91. Schwartz, G.J., *Plasticity of Intercalated Cell Polarity: Effect of Metabolic Acidosis.* Nephron Physiol, 2001. **87**(4): p. 304-313.

92. Schwartz, G.J., et al., *Acid incubation reverses the polarity of intercalated cell transporters, an effect mediated by hensin.* J Clin Invest, 2002. **109**(1): p. 89-99.

93. Takito, J., C. Hikita, and Q. Al-Awqati, *Hensin, a new collecting duct protein involved in the in vitro plasticity of intercalated cell polarity.* J Clin Invest, 1996. **98**(10): p. 2324-31.

94. De Lisle, R.C., et al., *Effects of Muclin (Dmbt1) deficiency on the gastrointestinal system.* American journal of physiology. Gastrointestinal and liver physiology, 2008. **294**(3): p. G717-27.

95. Hikita, C., et al., *Induction of terminal differentiation in epithelial cells requires polymerization of hensin by galectin 3.* The Journal of cell biology, 2000. **151**(6): p. 1235-46.

96. Schwaderer, A.L., et al., *Galectin-3 expression is induced in renal beta-intercalated cells during metabolic acidosis.* Am J Physiol Renal Physiol, 2006. **290**(1): p. F148-58.

97. Vijayakumar, S., et al., *Differentiation of columnar epithelia: the hensin pathway.* J Cell Sci, 2006. **119**(Pt 23): p. 4797-801.

98. Vijayakumar, S., et al., *Role of integrins in the assembly and function of hensin in intercalated cells.* J Am Soc Nephrol, 2008. **19**(6): p. 1079-91.

99. Gao, X., et al., *Deletion of hensin/DMBT1 blocks conversion of β- to α-intercalated cells and induces distal renal tubular acidosis.* Proceedings of the National Academy of Sciences, 2010. **107**(50): p. 21872-21877.

100. Al-Awqati, Q. and X.B. Gao, *Differentiation of intercalated cells in the kidney.* Physiology, 2011. **26**(4): p. 266-72.

101. Breton, S., et al., *Depletion of intercalated cells from collecting ducts of carbonic anhydrase II-deficient (CAR2 null) mice.* American Journal of Physiology - Renal Physiology, 1995. **269**(6): p. F761-F774.

102. Sun, X., M. Soleimani, and S. Petrovic, *Decreased expression of Slc26a4 (Pendrin) and Slc26a7 in the kidneys of carbonic anhydrase II-deficient mice.* Cell Physiol Biochem, 2008. **21**(1-3): p. 95-108.

103. Brion, L.P., C. Suarez, and P. Saenger, *Postnatal disappearance of type A intercalated cells in carbonic anhydrase II-deficient mice.* Pediatr Nephrol, 2001. **16**(6): p. 477-81.

104. Bagnis, C., et al., *Remodeling the cellular profile of collecting ducts by chronic carbonic anhydrase inhibition.* American Journal of Physiology - Renal Physiology, 2001. **280**(3): p. F437-F448.

105. Boron, W.F., *Acid-Base Transport by the Renal Proximal Tubule.* Journal of the American Society of Nephrology, 2006. **17**(9): p. 2368-2382.

106. Preisig, P.A. and R.J. Alpern, *Basolateral membrane H-OH-HCO3 transport in the proximal tubule.* American Journal of Physiology - Renal Physiology, 1989. **256**(5): p. F751-F765.

107. Capasso, G., et al., *Bicarbonate transport along the loop of Henle: molecular mechanisms and regulation.* J Nephrol, 2002. **15 Suppl 5**: p. S88-96.

108. de Mello-Aires, M. and G. Malnic, *Distal tubule bicarbonate transport.* J Nephrol, 2002. **15 Suppl 5**: p. S97-111.

109. Weiner, I.D. and J.W. Verlander, *Role of NH3 and NH4+ transporters in renal acid-base transport.* American Journal of Physiology - Renal Physiology, 2011. **300**(1): p. F11-F23.

110. McGivan, J.D. and C.I. Bungard, *The transport of glutamine into mammalian cells.* Front Biosci, 2007. **12**: p. 874-82.

111. Yip, K.P. and I. Kurtz, *NH3 permeability of principal cells and intercalated cells measured by confocal fluorescence imaging.* American Journal of Physiology - Renal Physiology, 1995. **269**(4): p. F545-F550.

112. Quentin, F., et al., *RhBG and RhCG, the putative ammonia transporters, are expressed in the same cells in the distal nephron.* J Am Soc Nephrol, 2003. **14**(3): p. 545-54.

113. Eladari, D., et al., *Expression of RhCG, a New Putative NH3/NH4+ Transporter, along the Rat Nephron.* Journal of the American Society of Nephrology, 2002. **13**(8): p. 1999-2008.

114. Biver, S., et al., *A role for Rhesus factor Rhcg in renal ammonium excretion and male fertility.* Nature, 2008. **456**(7220): p. 339-343.

115. Hamm, L.L. and E.E. Simon, *Roles and mechanisms of urinary buffer excretion.* American Journal of Physiology - Renal Physiology, 1987. **253**(4): p. F595-F605.

116. Wagner, C.A. and J.P. Geibel, *Acid-base transport in the collecting duct.* J Nephrol, 2002. **15 Suppl 5**: p. S112-27.

117. Wagner, C.A., et al., *Renal acid-base transport: old and new players.* Nephron Physiol, 2006. **103**(1): p. p1-6.

118. Kraut, J.A. and N.E. Madias, *Serum Anion Gap: Its Uses and Limitations in Clinical Medicine.* Clinical Journal of the American Society of Nephrology, 2007. **2**(1): p. 162-174.

119. Graham, T. *Acid Base Online Tutorial*. 2006; Available from: http://fitsweb.uchc.edu/student/selectives/TimurGraham/Acid_Base_Physiology.html.

120. Madias, N.E., *Renal acidification responses to respiratory acid-base disorders.* J Nephrol, 2010. **23 Suppl 16**: p. S85-91.

121. Madias, N.E. and H.J. Adrogue, *Cross-talk between two organs: how the kidney responds to disruption of acid-base balance by the lung.* Nephron Physiol, 2003. **93**(3): p. p61-6.

122. Kraut, J.A. and N.E. Madias, *Metabolic acidosis: pathophysiology, diagnosis and management.* Nat Rev Nephrol, 2010. **6**(5): p. 274-85.

123. Jacobson, H.R. and D.W. Seldin, *On the generation, maintenance, and correction of metabolic alkalosis.* American Journal of Physiology - Renal Physiology, 1983. **245**(4): p. F425-F432.

124. Gennari, F.J. and J.J. Cohen, *Renal tubular acidosis.* Annu Rev Med, 1978. **29**: p. 521-41.

125. Unwin, R.J. and G. Capasso, *The renal tubular acidoses.* JRSM, 2001. **94**(5): p. 221-225.

126. Karet, F.E., *Inherited Distal Renal Tubular Acidosis.* Journal of the American Society of Nephrology, 2002. **13**(8): p. 2178-2184.

127. Alper, S.L., *Genetic diseases of acid-base transporters.* Annu Rev Physiol, 2002. **64**: p. 899-923.

128. Karet, F.E., *Disorders of water and acid-base homeostasis.* Nephron Physiol, 2011. **118**(1): p. p28-34.

129. Bruce, L.J., et al., *Familial distal renal tubular acidosis is associated with mutations in the red cell anion exchanger (Band 3, AE1) gene.* J Clin Invest, 1997. **100**(7): p. 1693-707.

130. Karet, F.E., et al., *Mutations in the chloride-bicarbonate exchanger gene AE1 cause autosomal dominant but not autosomal recessive distal renal tubular acidosis.* Proc Natl Acad Sci U S A, 1998. **95**(11): p. 6337-42.

131. Smith, A.N., et al., *Mutations in ATP6N1B, encoding a new kidney vacuolar proton pump 116-kD subunit, cause recessive distal renal tubular acidosis with preserved hearing.* Nat Genet, 2000. **26**(1): p. 71-5.

132. Batlle, D., et al., *Hereditary distal renal tubular acidosis: new understandings.* Annu Rev Med, 2001. **52**: p. 471-84.

133. Stehberger, P.A., et al., *Localization and regulation of the ATP6V0A4 (a4) vacuolar H+-ATPase subunit defective in an inherited form of distal renal tubular acidosis.* J Am Soc Nephrol, 2003. **14**(12): p. 3027-38.

134. Yang, Q., et al., *Vacuolar H+ -ATPase B1 subunit mutations that cause inherited distal renal tubular acidosis affect proton pump assembly and trafficking in inner medullary collecting duct cells.* J Am Soc Nephrol, 2006. **17**(7): p. 1858-66.

135. Cohen, E.P., et al., *Absence of H(+)-ATPase in cortical collecting tubules of a patient with Sjogren's syndrome and distal renal tubular acidosis.* J Am Soc Nephrol, 1992. **3**(2): p. 264-71.

136. Bastani, B., et al., *Lack of H-ATPase in distal nephron causing hypokalaemic distal RTA in a patient with Sjogren's syndrome.* Nephrol Dial Transplant, 1995. **10**(6): p. 908-9.

137. Han, J.S., et al., *Secretory-Defect Distal Renal Tubular Acidosis Is Associated with Transporter Defect in H+-ATPase and Anion Exchanger-1.* Journal of the American Society of Nephrology, 2002. **13**(6): p. 1425-1432.

138. Walsh, S., et al., *Immunohistochemical comparison of a case of inherited distal renal tubular acidosis (with a unique AE1 mutation) with an acquired case secondary to autoimmune disease.* Nephrol Dial Transplant, 2007. **22**(3): p. 807-12.

139. Shayakul, C. and S.L. Alper, *Inherited renal tubular acidosis.* Curr Opin Nephrol Hypertens, 2000. **9**(5): p. 541-6.

140. Igarashi, T., et al., *Mutations in SLC4A4 cause permanent isolated proximal renal tubular acidosis with ocular abnormalities.* Nat Genet, 1999. **23**(3): p. 264-6.

141. Fry, A.C. and F.E. Karet, *Inherited renal acidoses.* Physiology, 2007. **22**: p. 202-11.

142. Nagai, R., et al., *Renal tubular acidosis and osteopetrosis with carbonic anhydrase II deficiency: pathogenesis of impaired acidification.* Pediatr Nephrol, 1997. **11**(5): p. 633-6.

143. Sly, W.S., et al., *Carbonic anhydrase II deficiency in 12 families with the autosomal recessive syndrome of osteopetrosis with renal tubular acidosis and cerebral calcification.* N Engl J Med, 1985. **313**(3): p. 139-45.

144. Karet, F.E., *Mechanisms in Hyperkalemic Renal Tubular Acidosis.* Journal of the American Society of Nephrology, 2009. **20**(2): p. 251-254.

145. Schwartz, G.J., J. Barasch, and Q. Al-Awqati, *Plasticity of functional epithelial polarity.* Nature, 1985. **318**(6044): p. 368-71.

146. Van Huyen, J.P., et al., *GDF15 triggers homeostatic proliferation of acid-secreting collecting duct cells.* J Am Soc Nephrol, 2008. **19**(10): p. 1965-74.

147. Schwartz, J.H. and E.A. Alexander, *Adaptation of intercalated cells along the collecting duct to systemic acid/base changes.* Kidney Int, 2010. **78**(10): p. 949-951.

148. Welsh-Bacic, D., et al., *Proliferation of Acid-Secretory Cells in the Kidney during Adaptive Remodelling of the Collecting Duct.* PLoS ONE, 2011. **6**(10): p. e25240.

149. Harris, P.J., *Regulation of proximal tubule function by angiotensin.* Clin Exp Pharmacol Physiol, 1992. **19**(4): p. 213-22.

150. Laghmani, K., et al., *Endothelin-1/endothelin-B receptor-mediated increases in NHE3 activity in chronic metabolic acidosis.* J Clin Invest, 2001. **107**(12): p. 1563-9.

151. Bichara, M., et al., *Acute metabolic acidosis enhances circulating parathyroid hormone, which contributes to the renal response against acidosis in the rat.* J Clin Invest, 1990. **86**(2): p. 430-443.

152. Krapf, R., et al., *Chronic metabolic acidosis increases the serum concentration of 1,25-dihydroxyvitamin D in humans by stimulating its production rate. Critical role of acidosis-induced renal hypophosphatemia.* J Clin Invest, 1992. **90**(6): p. 2456-2463.

153. Santella, R.N., F.J. Gennari, and D.A. Maddox, *Metabolic acidosis stimulates bicarbonate reabsorption in the early proximal tubule.* Am J Physiol, 1989. **257**(1 Pt 2): p. F35-42.

154. Preisig, P.A. and R.J. Alpern, *Chronic metabolic acidosis causes an adaptation in the apical membrane Na/H antiporter and basolateral membrane Na(HCO3)3 symporter in the rat proximal convoluted tubule.* J Clin Invest, 1988. **82**(4): p. 1445-53.

155. Ambuhl, P.M., et al., *Chronic metabolic acidosis increases NHE3 protein abundance in rat kidney.* Am J Physiol, 1996. **271**(4 Pt 2): p. F917-25.

156. Wu, M.S., et al., *Role of NHE3 in mediating renal brush border Na+-H+ exchange. Adaptation to metabolic acidosis.* J Biol Chem, 1996. **271**(51): p. 32749-52.

157. Laghmani, K., et al., *Chronic metabolic acidosis enhances NHE-3 protein abundance and transport activity in the rat thick ascending limb by increasing NHE-3 mRNA.* J Clin Invest, 1997. **99**(1): p. 24-30.

158. Chan, Y.L. and G. Giebisch, *Relationship between sodium and bicarbonate transport in the rat proximal convoluted tubule.* Am J Physiol, 1981. **240**(3): p. F222-30.

159. Schwartz, G.J. and Q. Al-Awqati, *Regulation of transepithelial H+ transport by exocytosis and endocytosis.* Annu Rev Physiol, 1986. **48**: p. 153-61.

160. Abuladze, N., et al., *Molecular cloning, chromosomal localization, tissue distribution, and functional expression of the human pancreatic sodium bicarbonate cotransporter.* J Biol Chem, 1998. **273**(28): p. 17689-95.

161. Soleimani, M., et al., *Effect of in vitro metabolic acidosis on luminal Na+/H+ exchange and basolateral Na+:HCO3- cotransport in rabbit kidney proximal tubules.* J Clin Invest, 1992. **90**(1): p. 211-8.

162. Soleimani, M., Y.J. Hattabaugh, and G.L. Bizal, *pH sensitivity of the Na+:HCO3- cotransporter in basolateral membrane vesicles isolated from rabbit kidney cortex.* J Biol Chem, 1992. **267**(26): p. 18349-55.

163. Brandes, A., et al., *Adaptive redistribution of NBCe1-A and NBCe1-B in rat kidney proximal tubule and striated ducts of salivary glands during acid-base disturbances.* Am J Physiol Regul Integr Comp Physiol, 2007. **293**(6): p. R2400-11.

164. Dinour, D., et al., *A novel missense mutation in the sodium bicarbonate cotransporter (NBCe1/SLC4A4) causes proximal tubular acidosis and glaucoma through ion transport defects.* J Biol Chem, 2004. **279**(50): p. 52238-46.

165. Horita, S., et al., *Functional analysis of NBC1 mutants associated with proximal renal tubular acidosis and ocular abnormalities.* J Am Soc Nephrol, 2005. **16**(8): p. 2270-8.

166. Tizianello, A., et al., *Renal ammoniagenesis during the adaptation to metabolic acidosis in man.* Contrib Nephrol, 1982. **31**: p. 40-6.

167. Alleyne, G.A., et al., *Glutamine metabolism in metabolic acidosis.* Ciba Found Symp, 1982. **87**: p. 101-19.

168. Biber, J., et al., *Regulation of phosphate transport in proximal tubules.* Pflugers Arch, 2009. **458**(1): p. 39-52.

169. Murer, H. and J. Biber, *Phosphate transport in the kidney.* J Nephrol, 2010. **23 Suppl 16**: p. S145-51.

170. Nowik, M., et al., *Renal phosphaturia during metabolic acidosis revisited: molecular mechanisms for decreased renal phosphate reabsorption.* Pflugers Arch, 2008. **457**(2): p. 539-49.

171. Wagner, C.A., *Metabolic acidosis: new insights from mouse models.* Curr Opin Nephrol Hypertens, 2007. **16**(5): p. 471-6.

172. Wagner, C.A., K.E. Finberg, and S. Breton, *Renal vacuolar H+-ATPase.* Physiol Rev, 2004. **84**: p. 1263-1314.

173. Purkerson, J.M., et al., *Adaptation to metabolic acidosis and its recovery are associated with changes in anion exchanger distribution and expression in the cortical collecting duct.* Kidney Int, 2010. **78**(10): p. 993-1005.

174. Al-Awqati, Q., *Plasticity in epithelial polarity of renal intercalated cells: targeting of the H(+)-ATPase and band 3.* American Journal of Physiology - Cell Physiology, 1996. **270**(6): p. C1571-C1580.

175. Oliver, J.A., et al., *The renal papilla is a niche for adult kidney stem cells.* J Clin Invest, 2004. **114**(6): p. 795-804.

176. Al-Awqati, Q. and J.A. Oliver, *The kidney papilla is a stem cells niche.* Stem cell reviews, 2006. **2**(3): p. 181-4.

177. Reule, S. and S. Gupta, *Kidney regeneration and resident stem cells.* Organogenesis, 2011. **7**(2): p. 135-9.

178. Wehrli, P., et al., *Replication of segment-specific and intercalated cells in the mouse renal collecting system.* Histochem Cell Biol, 2007. **127**(4): p. 389-98.

179. Vogetseder, A., et al., *Tubular cell proliferation in the healthy rat kidney.* Histochem Cell Biol, 2005. **124**(2): p. 97-104.

180. Al-Awqati, Q., et al., *Phenotypic plasticity in the intercalated cell: the hensin pathway.* Am J Physiol, 1998. **275**(2 Pt 2): p. F183-90.

181. Mimeault, M. and S.K. Batra, *Divergent molecular mechanisms underlying the pleiotropic functions of macrophage inhibitory cytokine-1 in cancer.* Journal of cellular physiology, 2010. **224**(3): p. 626-35.

182. Alper, S.L., M.N. Chernova, and A.K. Stewart, *Regulation of Na+-independent Cl-/HCO3-exchangers by pH.* Jop, 2001. **2**(4 Suppl): p. 171-5.

183. Romero, M.F., C.M. Fulton, and W.F. Boron, *The SLC4 family of HCO 3 - transporters.* Pflugers Arch, 2004. **447**(5): p. 495-509.

184. Alper, S.L., *Molecular physiology and genetics of Na+-independent SLC4 anion exchangers.* J Exp Biol, 2009. **212**(11): p. 1672-1683.

185. Jennings, M.L., *Proton fluxes associated with erythrocyte membrane anion exchange.* J Membr Biol, 1976. **28**(2-3): p. 187-205.

186. Cordat, E. and J.R. Casey, *Bicarbonate transport in cell physiology and disease.* Biochem J, 2009. **417**(2): p. 423-39.

187. Alper, S.L., et al., *Differential inhibition of AE1 and AE2 anion exchangers by oxonol dyes and by novel polyaminosterol analogs of the shark antibiotic squalamine.* Biochem Cell Biol, 1998. **76**(5): p. 799-806.

188. Sterling, D. and J.R. Casey, *Transport activity of AE3 chloride/bicarbonate anion-exchange proteins and their regulation by intracellular pH.* Biochem J, 1999. **344 Pt 1**: p. 221-9.

189. Fujinaga, J., F.B. Loiselle, and J.R. Casey, *Transport activity of chimaeric AE2-AE3 chloride/bicarbonate anion exchange proteins.* Biochem J, 2003. **371**(Pt 3): p. 687-96.

190. Stehberger, P.A., et al., *Distal renal tubular acidosis in mice lacking the AE1 (band3) Cl-/HCO3- exchanger (slc4a1).* J Am Soc Nephrol, 2007. **18**(5): p. 1408-18.

191. Shayakul, C. and S.L. Alper, *Defects in processing and trafficking of the AE1 Cl-/HCO3- exchanger associated with inherited distal renal tubular acidosis.* Clin Exp Nephrol, 2004. **8**(1): p. 1-11.

192. Wu, F., et al., *Anion exchanger 1 interacts with nephrin in podocytes.* J Am Soc Nephrol, 2010. **21**(9): p. 1456-67.

193. Dubreuil, R., et al., *The Drosophila Anion Exchanger (DAE) lacks a detectable interaction with the spectrin cytoskeleton.* Journal of Negative Results in BioMedicine, 2010. **9**(1): p. 5.

194. Piermarini, P.M., et al., *A SLC4-like anion exchanger from renal tubules of the mosquito (Aedes aegypti): evidence for a novel role of stellate cells in diuretic fluid secretion.* American Journal of Physiology - Regulatory, Integrative and Comparative Physiology, 2010. **298**(3): p. R642-R660.

195. Zhu, Q., D.W. Lee, and J.R. Casey, *Novel topology in C-terminal region of the human plasma membrane anion exchanger, AE1.* J Biol Chem, 2003. **278**(5): p. 3112-20.

196. Vince, J.W. and R.A. Reithmeier, *Carbonic anhydrase II binds to the carboxyl terminus of human band 3, the erythrocyte C1-/HCO3- exchanger.* J Biol Chem, 1998. **273**(43): p. 28430-7.

197. Sterling, D., R.A.F. Reithmeier, and J.R. Casey, *A Transport Metabolon.* Journal of Biological Chemistry, 2001. **276**(51): p. 47886-47894.

198. Bruce, L.J., et al., *A band 3–based macrocomplex of integral and peripheral proteins in the RBC membrane.* Blood, 2003. **101**(10): p. 4180-4188.

199. Perrotta, S., et al., *The N-terminal 11 amino acids of human erythrocyte band 3 are critical for aldolase binding and protein phosphorylation: implications for band 3 function.* Blood, 2005. **106**(13): p. 4359-4366.

200. Alper, S.L., *Familial renal tubular acidosis.* J Nephrol, 2010. **23 Suppl 16**: p. S57-76.

201. Groves, J.D. and M.J. Tanner, *Glycophorin A facilitates the expression of human band 3-mediated anion transport in Xenopus oocytes.* Journal of Biological Chemistry, 1992. **267**(31): p. 22163-70.

202. Williamson, R.C. and A.M. Toye, *Glycophorin A: Band 3 aid.* Blood Cells Mol Dis, 2008. **41**(1): p. 35-43.

203. Tanphaichitr, V.S., et al., *Novel AE1 mutations in recessive distal renal tubular acidosis. Loss-of-function is rescued by glycophorin A.* J Clin Invest, 1998. **102**(12): p. 2173-2179.

204. Devonald, M.A.J., et al., *Non-polarized targeting of AE1 causes autosomal dominant distal renal tubular acidosis.* Nat Genet, 2003. **33**(2): p. 125-127.

205. Toye, A.M., et al., *Band 3 Walton, a C-terminal deletion associated with distal renal tubular acidosis, is expressed in the red cell membrane but retained internally in kidney cells.* Blood, 2002. **99**(1): p. 342-347.

206. Cordat, E., et al., *Dominant and recessive distal renal tubular acidosis mutations of kidney anion exchanger 1 induce distinct trafficking defects in MDCK cells.* Traffic, 2006. **7**(2): p. 117-28.

207. Jarolim, P., et al., *Autosomal dominant distal renal tubular acidosis is associated in three families with heterozygosity for the R589H mutation in the AE1 (band 3) Cl-/HCO3- exchanger.* J Biol Chem, 1998. **273**(11): p. 6380-8.

208. Shayakul, C., et al., *Characterization of a highly polymorphic marker adjacent to the SLC4A1 gene and of kidney immunostaining in a family with distal renal tubular acidosis.* Nephrology Dialysis Transplantation, 2004. **19**(2): p. 371-379.

209. Mount, D.B. and M.F. Romero, *The SLC26 gene family of multifunctional anion exchangers.* Pflugers Arch, 2004. **447**(5): p. 710-21.

210. Petrovic, S., et al., *SLC26A7: a basolateral Cl-/HCO3- exchanger specific to intercalated cells of the outer medullary collecting duct.* Am J Physiol Renal Physiol, 2004. **286**(1): p. F161-9.

211. Burckhardt, B.C. and G. Burckhardt, *Transport of organic anions across the basolateral membrane of proximal tubule cells.* Rev Physiol Biochem Pharmacol, 2003. **146**: p. 95-158.

212. Kim, Y.H., et al., *Intercalated cell H+/OH- transporter expression is reduced in Slc26a4 null mice.* Am J Physiol Renal Physiol, 2005. **289**(6): p. F1262-72.

213. Amlal, H., et al., *Deletion of the anion exchanger Slc26a4 (pendrin) decreases apical Cl(-)/HCO3(-) exchanger activity and impairs bicarbonate secretion in kidney collecting duct.* American journal of physiology. Cell physiology, 2010. **299**(1): p. C33-41.

214. Karet, F.E., et al., *Mutations in the gene encoding B1 subunit of H+-ATPase cause renal tubular acidosis with sensorineural deafness.* Nat Genet, 1999. **21**(1): p. 84-90.

215. Finberg, K.E., et al., *The B1-subunit of the H(+) ATPase is required for maximal urinary acidification.* Proc Natl Acad Sci U S A, 2005. **102**(38): p. 13616-21.

216. Haldane, J.B., *Experiments on the regulation of the blood's alkalinity: II.* J Physiol, 1921. **55**(3-4): p. 265-75.

217. Nonoguchi, H., et al., *Regulation of aquaporin-2 by metabolic acidosis.* American journal of physiology. Cell physiology, 2004. **287**(3): p. C824; author reply C814-5.

218. Amlal, H., S. Sheriff, and M. Soleimani, *Upregulation of collecting duct aquaporin-2 by metabolic acidosis: role of vasopressin.* American Journal of Physiology-Cell Physiology, 2004. **286**(5): p. C1019-C1030.

219. Nowik, M., et al., *Induction of metabolic acidosis with ammonium chloride (NH4Cl) in mice and rats--species differences and technical considerations.* Cell Physiol Biochem, 2010. **26**(6): p. 1059-72.

220. Peters, L.L., et al., *Anion exchanger 1 (band 3) is required to prevent erythrocyte membrane surface loss but not to form the membrane skeleton.* Cell, 1996. **86**(6): p. 917-27.

221. Seaton, B. and A. Ali, *Simplified manual high performance clinical chemistry methods for developing countries.* Med Lab Sci, 1984. **41**(4): p. 327-36.

222. Nowik, M., et al., *Genome-wide gene expression profiling reveals renal genes regulated during metabolic acidosis.* Physiol Genomics, 2008. **32**(3): p. 322-34.

223. Wybenga, D.R., J. Di Giorgio, and V.J. Pileggi, *Manual and automated methods for urea nitrogen measurement in whole serum.* Clin Chem, 1971. **17**(9): p. 891-5.

224. Taussky, H.H. and E. Shorr, *A microcolorimetric method for the determination of inorganic phosphorus.* J Biol Chem, 1953. **202**(2): p. 675-85.

225. Bootcov, M.R., et al., *MIC-1, a novel macrophage inhibitory cytokine, is a divergent member of the TGF-beta superfamily.* Proc Natl Acad Sci U S A, 1997. **94**(21): p. 11514-9.

226. Yan, J., et al., *The forkhead transcription factor FoxI1 remains bound to condensed mitotic chromosomes and stably remodels chromatin structure.* Mol Cell Biol, 2006. **26**(1): p. 155-68.

227. Lin, S.-H., et al., *Physiological disposal of the potential alkali load in diet of the rat: steps to achieve acid-base balance.* American Journal of Physiology - Renal Physiology, 1998. **274**(6): p. F1037-F1044.

228. Wu, F., T.J. Satchwell, and A.M. Toye, *Anion exchanger 1 in red blood cells and kidney: Band 3's in a pod.* Biochem Cell Biol, 2011. **89**(2): p. 106-14.

229. Su, Y., et al., *Glyceraldehyde 3-phosphate dehydrogenase is required for band 3 (anion exchanger 1) membrane residency in the mammalian kidney.* Am J Physiol Renal Physiol, 2011. **300**(1): p. F157-66.

230. Keskanokwong, T., et al., *Interaction of integrin-linked kinase with the kidney chloride/bicarbonate exchanger, kAE1.* J Biol Chem, 2007. **282**(32): p. 23205-18.

231. Johnson, D.E. and J.R. Casey, *Cytosolic H+ microdomain developed around AE1 during AE1-mediated Cl-/HCO3- exchange.* J Physiol, 2011. **589**(Pt 7): p. 1551-69.

232. Benayoun, B.A., S. Caburet, and R.A. Veitia, *Forkhead transcription factors: key players in health and disease.* Trends Genet, 2011. **27**(6): p. 224-32.

233. Gekle, M., et al., *Characterization of two MDCK-cell subtypes as a model system to study principal cell and intercalated cell properties.* Pflugers Arch, 1994. **428**(2): p. 157-62.

234. Nishikawa, M., et al., *Stepwise renal lineage differentiation of mouse embryonic stem cells tracing in vivo development.* Biochemical and Biophysical Research Communications, 2012. **417**(2): p. 897-902.

235. Velagapudi, C., et al., *Reciprocal Induction of Simple Organogenesis by Mouse Kidney Progenitor Cells in Three-Dimensional Co-Culture.* The American Journal of Pathology, 2012. **180**(2): p. 819-830.

ACKNOWLEDGEMENTS

I would like to thank:

- my supervisor Prof. Carsten A. Wagner, for giving me the opportunity to work in his group and for the support and guidance throughout the years of my Master thesis and current PhD thesis;

- the members of my PhD thesis committee, Prof. Biber, J., Prof. Loffing, J. and Prof. Unwin, for helpful discussion and advices concerning the project;

- Dr. Hernando, N., for helpful discussion and precious advices in scientific and technical issues concerning the project;

- all the people who supported me with their scientific and technical expertise: Edenhofer, I., Ruderisch, N., Nowik, M., Reining, S., Todkar, A., Bourgeois, S., Capuano, P., Mohebbi, N. and Mihailova, M.;

- all current and former colleagues of the Wagner group and the J-floor of the Institute of Physiology for discussions, advices, support and for creating a great working atmosphere.

Furthermore, I would like to thank:

- the European Renal Genome Project "EuReGene" for partial financial support of this project and scientific network;
- the Zurich Center for Integrative Human Physiology "ZIHP" and the Zurich Integrative Rodent Physiology "ZIRP" for providing a scientific and educational network as well as a basic technical infrastructure.

CURRICULUM VITAE

Name:	**Kampik**
First name:	**Nicole Beate**
Date of birth:	15 June, 1978
Nationality:	German
Current address:	Im Loo 37
	8957 Spreitenbach, Switzerland
Phone:	+41-79-548 16 20
e-mail:	nic.kam@access.uzh.ch

Education:

1990 – 1994	Sankt Marien Oberschule, Berlin, Germany Realschulabschluss (secondary school)
2000 – 2003	Peter A. Silbermann Abendgymnasium, Berlin, Germany Allgemeine Hochschulreife (university-entrance diploma)
2003 – 2005	Justus-Liebig-University, Giessen, Germany Studies in Biology, Vordiplom (pre-diploma)
2005 – 2006	University of Zurich, Zurich, Switzerland Bachelor of Science (B.Sc.) in Biology
2006 – 2008	University of Zurich, Institute of Physiology, Kidney and Acid-Base Physiology, Prof. Carsten A. Wagner, Zurich, Switzerland Master of Science (M.Sc.) in Humanbiology Title: "Acute Regulation of the Anion Exchanger 1 (AE1, SLc4a1)"
since 2008	PhD student at the University of Zurich, Institute of Physiology, Kidney and Acid-Base Physiology, Prof. Carsten A. Wagner and Zurich Center for Integrative Human Physiology (ZIHP), Zurich, Switzerland

LIST OF PUBLICATIONS

Wu, F., Saleem, M.A., **Kampik, N.B.**,, Satchwell, T.J., Williamson, R.C., Blattner, S.M., Ni, L., Toth, T., White, G., Young, M.T., Parker, M.D., Alper, S.L., Wagner, C.A. and Toye, A.M. (2010). *"Anion exchanger 1 interacts with nephrin in podocytes."* J Am Soc Nephrol 21(9): 1456-1467.

Kampik, N.B., Nowik, M., Mihailova, M., Eladari, D. and Wagner, C. A. (2010). *"Induction of metabolic acidosis with ammonium chloride (NH_4Cl) in mice and rats - species differences and technical considerations."* Cell Physiol Biochem 26(6): 1059-1072.

Stuiver, M., Lainez, S., Will, C., Terryn, S., Gunzel, D., Debaix, H., Sommer, K., Kopplin, K., Thumfart, J., **Kampik, N.B.**, Querfeld, U., Willnow, T.E., Nemec, V., Wagner, C.A., Hoenderop, J.G., Devuyst, O., Knoers, N.V., Bindels, R.J., Meij I.C. and Muller, D. (2011). *"CNNM2, encoding a basolateral protein required for renal Mg_2^+ handling, is mutated in dominant hypomagnesemia."* Am J Hum Genet 88(3): 333-343.

Winter, C., **Kampik, N.B.**, Vedovelli, L., Rothenberger, F., Paunescu, T.G., Stehberger, P.A., Brown, D., John, H. and Wagner, C.A. (2011). *"Aldosterone stimulates vacuolar H^+-ATPase activity in renal acid-secretory intercalated cells mainly via a protein kinase C dependent pathway."* Am J Physiol Cell Physiol.